Final Report
Submitted to National Institute of Justice, Office of Justice Programs, U.S. Department of Justice

Award No.: 2008-DN-BX-K132

Project Title: Detecting Buried Remains Using Ground-Penetrating Radar

Principal Investigator
John J. Schultz, Ph.D.
Associate Professor,
Department of Anthropology
University of Central Florida
john.schultz@ucf.edu
407-823-2227

Project/Grant Period (Start Date, End Date): 11/01/2008 to 01/31/2012

Abstract

Geophysical techniques, such as ground-penetrating radar (GPR), have been successfully used by law enforcement agencies to locate graves and forensic evidence. However, more controlled research is needed to better understand the applicability of this technology when searching for clandestine graves in various environments and soil types. The purpose of this study was to determine the applicability of GPR for detecting controlled graves. Objectives for this project included determining how different burial scenarios (e.g., wrapping the carcass and placing items over the carcass) are factors in producing a distinctive anomalous response, determining how different GPR imagery options can provide increased visibility of the burials, and comparing GPR imagery between the 500 MHz and 250 MHz antennae. An electromagnetic induction (EMI) meter was also employed to determine the applicability of this technology to locate unmarked graves. Finally, the last objective was to provide basic guidelines for forensic investigators to utilize when conducting buried body searches involving these geophysical tools.

The research design included constructing a grid on secured land in a field area that contained a total of eight graves representing common burial scenarios in Spodosol, a common soil type of Florida. Six burial scenarios contained a pig carcass at a deep (1.00 m) or a shallow (.50 m) depth: a shallow unwrapped pig carcass, a deep unwrapped pig carcass, a deep pig carcass wrapped in a tarp, a deep pig carcass wrapped in a cotton blanket, a deep pig carcass covered with a layer of rocks, and a deep pig carcass covered with a layer of lime. Two blank control graves, one shallow and one deep were also constructed. Graves were monitored with EMI (24 months) and GPR (30 months) using both the 500 and 250 MHz antennae.

Results indicated that the electromagnetic induction meter was not a viable option in the detection of clandestine graves for this soil type, as graves were never detected during the

monitoring period. Conversely, GPR was shown to be a favorable tool for monitoring controlled graves for a 30 month period as many scenarios were still detected at the end of the monitoring period. Of the imagery options available, reflection profiles were the preferred option. Burial scenarios with grave items (rocks, lime, blanket, and tarp) produced a more distinctive response for a longer period of time compared to carcasses not wrapped. However, some months produced poor visibility of the imagery that was somewhat correlated with lower precipitation. Thus, dry soil or low soil moisture resulted in reduced demarcation of the graves. Overall, the 250 MHz antenna results were more favorable than the results of the more commonly used 500 MHz, as the 250 MHz antenna provided increased visibility for large cadavers buried in deep graves while the 500 MHz results were more favorable for the shallow pig scenario. At the same time, detection of the deep blank control grave suggests that clandestine graves can be detected for a longer time period in this soil because the soil disturbance will be detected.

Controlled forensic geophysical research involving GPR has proven to be a valuable resource, and the information gathered from these studies has been applied to forensic casework. The probability of detecting a grave for a longer postmortem interval differs with the soil type and the materials added to the grave with the body. Also, since increased soil moisture may serve to highlight buried features, operators should be cautioned when performing GPR surveys during dry conditions. If time permits, both the 250 MHz and the 500 MHz antennae should be employed; however, if time is limited, the 250 MHz antenna is recommended for searches. Finally, the data should be further processed in the lab, and reflection profiles should be assessed.

Table of Contents

Executive Summary

Description of the Problem

Locating and recovering buried bodies in clandestine graves is a problem that law enforcement agencies are faced with again and again. Forensic anthropologists and archaeologists can contribute to the detection and recovery of clandestine graves and other forensic objects by applying archaeological field skills to the forensic context. For example, geophysical tools, particularly ground-penetrating radar (GPR), is commonly used during searches for clandestine graves. However, the use of such tools and techniques requires extensive training and practice. Law enforcement agencies may not have the resources to procure remote sensing technology nor to train agents in their use; therefore, forensic anthropologists and archaeologists can fill this gap and supply their knowledge and expertise in this area.

In particular, it is common to conduct controlled geophysical research to study the numerous variables that affect grave detection. One of the most useful methods for gaining experience in performing geophysical surveys for buried evidence or features is to set up a controlled research site to monitor and detect the specific items in question for some length of time utilizing euthanized pig carcasses (*Sus scrofa*) as human cadaver proxies. Controlled experiments offer two advantages. First, their results can be used to form guidelines for working with GPR in a variety of different settings. Local environments and soil types can be tested to determine their effect on conducting GPR surveys. Secondly, controlled experimentation offers the chance for users to become familiar with working the GPR equipment and processing data. Therefore, controlled research for this technology should be pursued to understand the applicability of GPR and provide experience to GPR technicians.

A number of gaps with published research indicated a need for long-term grave monitoring, as well as understanding the use of GPR in detecting burials with grave objects distinct from the buried body. In addition, no controlled research was yet been undertaken to appraise the use of GPR in a Spodosol environment. Furthermore, there was a need to compare the applicability of different antennae in locating clandestine graves to identify the best frequency for forensic work, especially between those antennae with higher frequency emissions as compared to those with lower frequency emissions. Moreover, while the electromagnetic induction meter has been presented as a tool to use for clandestine grave searches, there is limited casework and controlled forensic research using this tool. The lack of published material on the use of an electromagnetic induction (EMI) meter to located buried bodies underscores the importance of testing this tool in a controlled setting that monitors real-life forensic scenarios.

Purpose, Goals and Objectives

The primary objective of this research was to test the application of geophysical techniques in the investigation of different burial scenarios and compare different geophysical techniques over a period 30 months. Pig carcasses (*Sus scrofa*) were buried as human proxies in six different burial scenarios, and two control graves without pig carcasses were also constructed to compare the effect of only the disturbed soil of the grave. Two main geophysical techniques were tested: GPR and EMI. The applicability of the electromagnetic induction meter was documented by presenting the data as a contoured map and observing any changes in the succeeding months. GPR imagery data was processed and compared between the 500 and 250 MHz antennae to ascertain the effect of different burial scenarios and the efficacy of detection for each antenna. The effect of interment time on GPR imaging was also investigated. Analyzing

these variables allowed the author to establish guidelines for the use of GPR and EMI in the investigation for clandestine graves.

In summary, the goals and objectives of this project included the following:

1. Provide basic guidelines for forensic investigators for buried body searches involving the use of GPR and EMI.
2. Document the changes in GPR imagery characteristics of bodies buried in a Spodosol soil which result from decomposition and subsequent compaction of the backfill for a period of 30 months.
3. Determine how different burial scenarios (e.g., wrapping the carcass and placing items over the carcass in the grave) are factors in producing a distinctive anomalous response.
4. Determine how advanced GPR 3-D modeling postprocessing software can provide increased visibility of the burials.
5. Compare GPR imagery data between the 500 MHz and 250 MHz antennae.
6. Document the changes in apparent conductivity, expressed on a conductivity map, from bodies buried in a Spodosol soil which result from decomposition and subsequent compaction of the backfill for a 24 month time period.

Research Design

The field site used for this controlled research project was located on the University of Central Florida's main campus property, in the Arboretum. The field site is located within property maintained by the Civil Engineering Division of the University of Central Florida's College of Engineering and Computer Science, referred to as the Geotechnical Engineering Test Site. The test site was secured with a six foot locked fence. The soil at the research site is classified as a Spodosol that contained sandy soil horizons and a spodic horizon (accumulation of organic matter, aluminum oxide, and possibly iron oxide). The test site was secured with a 6 foot locked fence. The ground for the site was relatively flat, and a small portion without trees or brush was mowed and maintained to create a permanent research grid of 11 m by 22 m. Permanent non-metal markers were placed at the corners of the grid so the exact position of the survey transects could be duplicated each time geophysical data was collected.

A total of eight graves were monitored. Six pig carcasses (*Sus scrofa*) were buried at regular intervals throughout the grid in a variety of burial scenarios as well as two control graves; it was important to include these control pits to test the geophysical response of only the disturbed soil. Testing responses from the control graves would determine if forensic investigators could detect the distinctions between a grave with a buried component (the pig proxies and various grave objects) or simple disturbed soil. The euthanized pig carcasses were buried during January of 2009. The eight graves include the following scenarios:

1. A blank control grave consisting of only disturbed backfill (approximately 1. 00 m deep) to determine the geophysical response to disturbed soil only.
2. A blank control grave consisting of only disturbed backfill (approximately 0.50 m deep) to determine the geophysical response to disturbed soil only.
3. A pig carcass buried without additional grave objects at a depth of approximately 0.50 m.
4. A pig carcass buried without additional grave objects at a depth of approximately 1.00 m.
5. A pig carcass buried wrapped in a vinyl tarpaulin at a depth of approximately 1.00 m.
6. A pig carcass buried wrapped in a cotton blanket at a depth of approximately 1.00 m.
7. A pig carcass buried underneath a layer of lime (calcium hydroxide) at a depth of approximately 1.00 m.
8. A pig carcass buried underneath a layer of rocks at a depth of approximately 1.00 m.

Grid data collection was performed monthly for a 30 month monitoring period using a Mala RAMAC X3M GPR unit, with 500 MHz and 250 MHz antenna. Data was collected using transect spacing of 0.25 m in both a west-east direction and a north-south direction. The final phase of this research was the processing of the data collected in the field to create two imagery options: reflection profiles and horizontal, or time, slices. Two software programs were used for postprocessing: REFLEXW (Version 6.0.5) for presenting reflection profiles and GPR-SLICE (Version 7) for presenting horizontal slices. Reflection profiles represent length and depth and are the individual grid transects. Horizontal slices are planview representation of the grid at

different depths. The grid data are welded together in the GPR program to create a three-dimensional cube. The cube can then be cut in a variety of planes to view the features, with the horizontal slice being the most common.

All of the grave scenarios were scored each month using the reflection profiles and horizontal slices. The response for each grave was scored on a four point scale: None, Poor, Good, and Excellent. A score of None demonstrated no discernible response. A grave scored as Poor showed a slightly discernible response that may not have been visible at the time of the actual geophysical survey. A score of Good indicated a grave that would most likely be discernible during a geophysical survey. Finally, a grave scored as Excellent demonstrated a clearly visible response. When determining how many months of the collection period the grave was discernible, only graves with scores of Excellent and Good were considered as visible for that month.

Conductivity data collection was performed using a Geonics EM 38 electromagnetic induction meter. Measurements were recorded using an Allegro CX handheld data logger to store the data collected from the field. The grid data collection was performed at the end of every month for a total of 24 months. Geophysical data was collected with a transect spacing of 0.25 m in a west-east direction. The final phase of this research was the processing of the data into a suitable format using a Geonics DAT 38W computer program and then the data was displayed as a contour map using Golden Software Surfer 8 (Version 8.4). A contour map image uses the X and Y coordinates and the value of the conductivity measurements, represented as Z, to map out the site wherein it is employed. The closer two lines are together on the map, the greater the apparent conductivity of the buried feature.

Precipitation data provided by National Climatic Data Center was utilized as a proxy to infer soil moisture and was obtained for the closest recorded location to the site, Orlando International Airport.

Findings and Conclusions

Two of the objectives for this project dealt with evaluating the utility of an EMI meter for grave detection. Unfortunately the use of the EMI meter in this soil type and with the pig graves is strongly discouraged since none of the controlled burials were detected over the 24 months of data collection. Starting with Month 1 of data collection, none of the grave scenarios were detected using EMI, and over a 24 month period, data collection showed little variability, and no visible anomalies for any burial scenarios were noted. Unfortunately, this tool is unable to detect buried bodies and the soil disturbances in the tested soil. While this technology has been listed as a possible geophysical tool for forensic applications, pre-survey testing would be needed to determine if the use of this technology is appropriate with the soil of the proposed site. However, if a suspected grave is known to contain a large metal weapon and is buried less than 1 meter in depth, then an EMI meter may be a geophysical search option when searching for a clandestine grave because large metal items should be easily detected at shallow depths.

Detection of a clandestine grave can be due to a number of variables such as the body, items added to a grave, soil disturbance, and a combination of these variables. In addition, it is important to process the data after collection as this task may increase the visibility of features that may not be visible in the field. This research investigated multiple variables to discern which variables affect detection of graves in central Florida when buried in a Spodosol. At the same time, imagery options must be considered. In the examined soil and for the scenarios tested,

reflection profiles provided the best GPR imagery for extended periods of interment with the controlled graves. Even though the horizontal time slices provide a 2-D plan view by slicing a 3-D cube pseudo-image of the research site, detection of the controlled graves was more likely for a longer period using the reflection profiles, which are commonly used to make in-field assessment. There was overall poor visibility of the graves using both the 500 and 250 MHz horizontal time slice data, as graves were barely distinguishable.

In terms of antenna selection, this study provided surprising results. While the 500 MHz antenna is a common choice for forensic applications because it provides a favorable compromise between depth of penetration and vertical visibility, the 250 MHz was a better option with the soil type tested as more salient reflections were easier to discern on the reflection profile. In addition, five out of eight controlled grave scenarios were visible for more months with 250 MHz antenna compared to the 500 MHz data. Conversely, the higher detail of the 500 MHz antenna results in more clutter and less discernible features because the increased detail may not detect the burial feature as one large feature. Rather, individual features of the grave may be detected resulting in less salient features. Interestingly, the shallow pig burial was visible more often with the 500 MHz antenna compared to the 250 MHz antenna. This result suggests that the 500 MHz antenna may be a better option for detecting shallow features (less than 0.50 m), while the 250 MHz antenna is a better option for detecting deeper features (greater than 0.50 m).

When considering the effect of burial scenario on GPR grave detection, it is also important to consider the visibility of the scenarios over the monitoring period on the reflection profiles. Using the 250 MHz antenna, the most visible grave was the deep grave with a layer of rocks, which was visible for 27 out of 30 months. This was followed by the scenarios with the

grave items such as a cadaver wrapped in a tarpaulin and the cadaver with a layer of rocks. All three of these scenarios were more visible than just the buried deep cadaver and the cadaver wrapped in a blanket. The rocks and lime provided a larger contrasting area in the grave than just the carcass. At the same time, the cadaver wrapped in a tarpaulin more than likely trapped more moisture in the grave making the grave more conducive, and thus, more visible.

The response for the blank controlled graves differed. While the shallow control grave was visible for 1 month with the 500 MHz antenna and zero months with the 250 MHz, the deep control grave was visible for 22 months with the 500 MHz antenna and 18 months with the 250 MHz. Since the soil profile of the shallow graves primarily consisted of sand horizons with the spodic horizon below the graves, these results are not surprising as a soil disturbance of controlled graves in sandy soil horizons in central Florida may not be detected. Conversely, there was a surprise with the visibility scores of the deep control hole for 24 out of 30 months. However, the soil profile at the research site for the deep graves consisted of a spodic horizon. Since the composition of the spodic horizon contrasts with the generally homogenous sandy soil horizons, a soil disruption of this horizon is more likely to be detected.

While it was possible to discern a number of controlled graves after 30 months of interment, processing and moisture differences affected the visibility of the graves when using the reflection profiles. Over time, the processing required more gain to increase the visibility and therefore the detection of the graves. Moisture trends were noted by comparing the total monthly rainfall with the visibility score of the graves. A general trend of increased precipitation (i.e. soil moisture) produced an increased visibility score when viewing the reflection profile. For example, this pattern of grave visibility was evident when viewing Month 21 for the 250 MHz reflection profile. During Month 21, the total monthly rainfall was 0 inches compared to

5.67 inches for Month 20 and 1.67 inches for Month 22. When the visibility data is compared to the moisture data, month 21 had decreased visibility compared to Months 20 and 22.

A number of guidelines for geophysical surveys are recommended when performing surveys for clandestine graves. Out of all of the available geophysical equipment, GPR is the best option for locating clandestine graves (Dupras et al., 2006; France et al., 1992; France et al., 1997). Operators should have forensic experience when evaluating whether a search can be performed, setting up a grid, performing the survey, and processing and interpreting the data.

Investigators should determine as much information about the burial prior, if possible, to performing a geophysical search. For example, it would be useful to know the depth and size of the burial, if the body was wrapped with any materials, if any debris was placed over the body, and if any metal was placed in the grave. In addition, the search site should be inspected to determine if GPR will be suitable as a search tool. Ground-penetrating radar is best utilized in a flat-field setting of short grass with the limited presence of trees and brush in order to minimize the masking effect of a root system. The presence of subsurface features such as tree roots, buried debris, cobbles, or buried pipes may result in false positives that can obscure the response from the body or grave. Therefore, a plan of the area with any pipes marked should be obtained prior to the search. Also, soil type is a factor to consider. Prior knowledge of a search site will allow the GPR technician to formulate plausible predictions to law enforcement concerning the likelihood of a successful search.

Prior to collecting GPR data, a grid should be constructed to ensure grave detection but not spaced far enough apart where a forensic target would be missed. If time allows, a transect spacing of 0.25 m is an optimal spacing for a forensic search (Dionne et al., 2010; Pomfret, 2006). Furthermore, the survey should be performed in orthogonal directions and utilization of

both antennae, is recommended if there are no time constraints. Additionally, if there are time constraints preventing the use of both antennae, pre-survey testing can be performed to determine which antenna is more suitable to the local soils.

If the visibility of the field data (i.e. reflection profiles) is discernible, a preliminary assessment can be made in the field. At the same time, after all of the grid data has been collected in the field, it should be brought back to the office for processing and for further analysis using both the reflection profiles and horizontal slices. Doing so may allow the GPR technician to discern anomalies that were not visible in the field before the data was processed. The last task of a survey is to ground truth, or use some invasive field technique, when checking the areas that produced anomalies. The GPR operator should be able to evaluate which anomalies need to be checked first. If all of the anomalies are checked and no evidence of a clandestine burial is detected, the GPR operator must decide if the area has been cleared. If it is not possible to clear the area, then other more invasive search methods may have to be implemented.

I. Introduction

Statement of Problem

Locating and recovering buried bodies in clandestine graves is a problem that law enforcement agencies are faced with again and again. Forensic anthropologists and archaeologists can contribute to the detection and recovery of clandestine graves and other forensic evidence by applying field skills and methods used in an archaeological context to the forensic context (Dupras et al., 2006; Schultz, 2007). An example of this contribution is the growing application of geophysical methods in the attempt to detect clandestine graves at the request of law enforcement agencies (Mellett, 1992; Davenport, 2001a; Dupras et al., 2006; Schultz, 2007; Ruffell et al., 2009). However, the use of such tools and techniques requires extensive training and practice. Law enforcement agencies may not have the resources to procure geophysical and remote sensing technology nor to train agents in their use; therefore, forensic anthropologists and archaeologists familiar with these tools can fill this gap and supply their knowledge and expertise in this area. In particular, it is common to conduct controlled geophysical research to study the various factors that affect grave detection (e.g., France et al., 1992; Strongman, 1992; France et al., 1997; Freeland et al., 2003; Schultz et al., 2006; Schultz, 2008; Schultz and Martin, 2011).

The primary objective of this research was to test the application of two geophysical techniques in the investigation of different burial scenarios and compare these methods over a period of 30 months. Pig carcasses (*Sus scrofa*) were buried as human proxies in six different burial scenarios, and two control graves without pig carcasses were also constructed to compare the effect of only the disturbed soil of the grave. Two main geophysical techniques were tested: ground-penetrating radar (GPR) and electromagnetic induction (EMI). The applicability of the

EMI meter was documented by processing the data as a contoured map and observing any changes in values or spatial patterns of the succeeding months. GPR imagery data were processed and compared between the 500 and 250 MHz antennae to ascertain the effect of different burial scenarios and the efficacy of detection for each antenna. The effect of interment time on GPR imaging was also investigated. Analyzing these variables allowed the author to establish guidelines for the use of GPR and EMI in the investigation for clandestine graves.

In summary, the goals and objectives of this project included the following:

1. Provide basic guidelines for forensic investigators for buried body searches involving the use of GPR and an EMI meter.
2. Document the changes in GPR imagery characteristics of bodies buried in a Spodosol soil which result from their decomposition and the subsequent compaction of the backfill for a period of 30 months.
3. Determine how different burial scenarios (e.g., wrapping the carcass and placing items over the carcass in the grave) are factors in producing a distinctive anomalous response.
4. Determine how advanced GPR 3-D modeling postprocessing software can provide increased visibility of the burials and remains.
5. Compare GPR imagery data between the 500 and 250 MHz antennae.
6. Document the changes in apparent conductivity, expressed on a conductivity map, from bodies buried in a Spodosol soil which result from decomposition and subsequent compaction of the backfill for a 24 month time period.

Literature Citations and Review

Ground-Penetrating Radar

Forensic geoscience is a discipline that studies the interaction of human remains and the earth's subsurface layers. It is "…concerned with the application of geological and wider environmental science information and methods to investigations which may come before a court of law" (Pye and Croft, 2004:1). Geoscientists use a variety of techniques on the subsurface of the earth that can either be invasive or noninvasive (Killam, 2004; Dupras et al., 2006). Invasive methods include any techniques that disturb the ground, and these techniques also have a higher likelihood of destroying evidence (Davenport, 2001a; Killam, 2004; Dupras et al., 2006). Such techniques include probing, shoveling, or using any earth-moving equipment to displace soil. Conversely, noninvasive techniques do not disturb soil and allow researchers to investigate the subsurface with much less risk of destroying evidence (Davenport, 2001a; Killam, 2004; Dupras et al., 2006). Geophysical techniques such as GPR fall into the latter category and are an excellent method of locating clandestine graves without disturbing the ground and associated evidence. In addition, the use of geophysical techniques may allow suspected areas to be thoroughly searched without the laborious process of actively digging through the subsurface of a large area.

One of the most useful methods for gaining experience in performing geophysical surveys for buried evidence or features is to set up a controlled research site to monitor and detect the specific items in question for some length of time. Since operator experience is a major limiting factor when using geophysical technologies, controlled studies not only provide operators with experience in a known setting that is invaluable when they perform real-life searches, these studies also provide operators with the knowledge of the limitations and

applicability of using different geophysical tools for varying situations. Proponents of using geophysical surveys for archaeological contexts have stressed the importance of controlled research to develop techniques and approaches that increase the effectiveness of geophysical surveys (Schurr, 1997; Isaacson et al., 1999). This has resulted in the construction of controlled archaeological test sites to provide training and research in archaeogeophysics (e.g., Isaacson et al., 1999) and forensic geophysics (e.g., France et al., 1992; Strongman, 1992; France et al., 1997; Freeland et al., 2003; Schultz et al., 2006; Pringle et al. 2008; Schultz, 2008; Novo et al., 2011; Schultz and Martin, 2011).

Controlled experiments offer two advantages. First, the results can be used to form guidelines for working with GPR in a variety of different settings. Local environments and soil types can be tested to determine their effect on conducting GPR surveys. To ensure the best application of GPR, controlled forensic research, in which GPR is tested on controlled burials for a long-term period of time, must be funded and pursued. In the published literature showcasing controlled research of GPR, there has been limited work using human cadavers (Freeland et al., 2003) due to the difficulty of procuring and performing research with human remains. Instead, the majority of studies utilize euthanized pig carcasses (*Sus scrofa*), as human cadaver proxies (e.g., France et al., 1992; Strongman, 1992; France et al., 1997; Freeland et al., 2003; Schultz et al., 2006; Schultz, 2008; Schultz and Martin, 2011). Table 1 provides an overview of the studies that involved controlled forensic research with GPR.

The group NecroSearch, which comprises the practitioners of numerous disciplines, popularized the use of GPR for forensic applications through controlled research. NecroSearch explored a multidisciplinary approach to clandestine grave detection, including fields such as botany, geophysics, entomology, and geology (France et al., 1992). The group determined that

GPR was the best geophysical tool to employ for locating clandestine graves in a forensic context. Subsequently, other examples of controlled research with GPR have followed. As previously mentioned, most of the studies involved using pig carcasses as proxies for human cadavers, the one exception occurring in a study by Freeland et al. (2003) where a single human cadaver was used. Most controlled studies use 'standard' burials; that is, the burials were composed of bodies without any accompanying grave goods. Soil type has been one of the variables studied; it was shown that clayey soil consistently provided poor depth of GPR exploration and clarity of reflected signals (Freeland et al., 2003) while sandy soil provides greater exploration depths and clarity of reflected signals (Schultz et al., 2006; Schultz, 2008) for graves detected.

Table 1: Examples of controlled research using GPR in a forensic context

Study	Location	Antenna	Cadaver Type	Depth	Results
France et al., 1992	Colorado	300 and 900 MHz	6 pigs	50.8-78.7 cm	-GPR was most effective geophysical tool used -Calibration needed prior to data collection.
Strongman, 1992	British Columbia, Canada	500 MHz	1 bear, 2 goats	N/A	-Burials were able to be detected after 5 years -Testing adult versus juvenile carcasses
Freeland et al., 2003	Tennessee	400 and 900 MHz	1 human cadaver	60 cm	-400 MHz antenna detected grave -900 MHz was unable to penetrate clay past 30 cm. -Clay was not conducive to GPR work
Schultz et al., 2006	Florida	500 MHz	12 large pigs	6 at 0.50-0.60 m, 6 at 1.00-1.1m	-Cadavers in sand were easily detected. -Skeletonization did not significantly affect detection. -Cadavers in clay were increasingly difficult to find with decomposition.
Schultz, 2008	Florida	500 MHz	12 small pigs	6 at 0.50-0.60 m 6 at 1.00-1.10 m	-Difficulties in locating small cadavers in sand once skeletonized -Deep graves were detected for a longer period.

While a number of controlled studies have performed grave monitoring for nearly 2 years (Schultz et al., 2006; Schultz, 2008), there is a need for longer-term grave monitoring in excess of 2 years. Controlled research must also explore the use of GPR in detecting burials with grave objects distinct from the buried body. In addition, no controlled research has yet been undertaken to appraise the use of GPR in a Spodosol environment. Furthermore, there is also a need to compare the applicability of different antennae in locating clandestine graves to identify the most efficient frequency for forensic work, especially between the standard frequency

antenna commonly used (400-500 MHz) compared to a lower frequency antenna (250 MHz) (Table 1).

Electromagnetic Induction

While a number of references dealing with forensic geophysics include an EMI meter as a possible tool for searches (France et al., 1992; France et al., 1997; Killam, 2004; Dupras et al., 2006; Davenport, 2001a; Davenport, 2001b), there is only one published case study on the use of an EMI meter used in conjunction with GPR to locate a body that had been buried for several years (Nobes, 2000). The lack of published material on the successful use of an EMI meter to locate buried bodies underscores the importance of testing this tool in a controlled setting that monitors real-life forensic scenarios. Thus, information may be provided to law enforcement agencies with the proper guidelines and discussions on potentials and limitations of this methodology for a forensic search.

II. Materials and Methods

The field site used for this controlled research project was on the University of Central Florida's main campus in Orlando, Florida. The field site was specifically located within the Arboretum at the Geotechnical Engineering Test Site which is maintained by the Civil Engineering Division of the University of Central Florida's College of Engineering and Computer Science (Figure 1). The test site was secured with a locked 6 foot locked fence. The ground for the site was relatively flat, and a small portion without trees or brush was mowed and maintained to create a permanent research grid of 11 m by 22 m. Permanent non-metal markers were placed at the corners of the grid so the exact position of the survey transects could be duplicated each time geophysical data was collected.

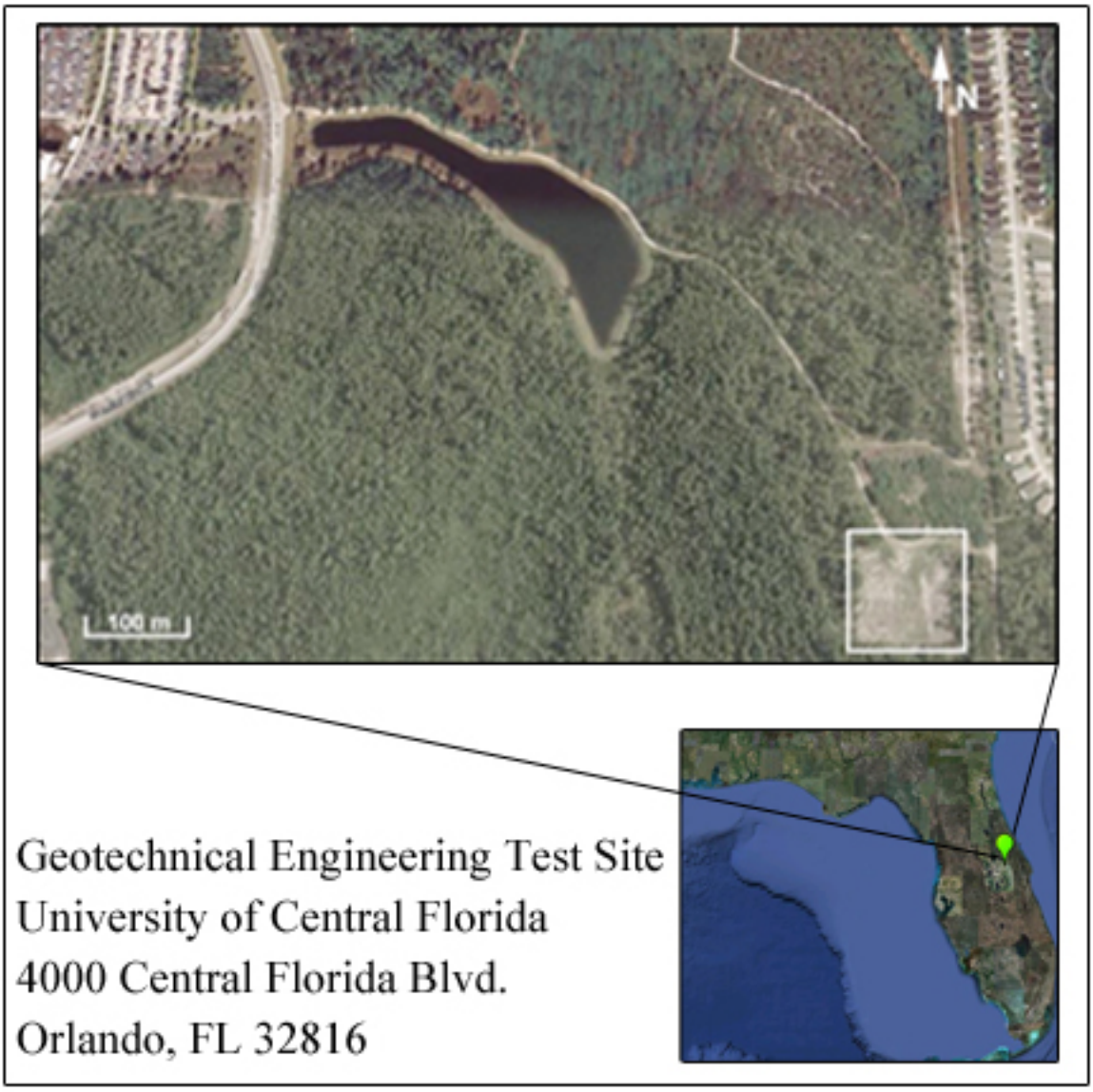

Figure 1: The Geotechnical Engineering Test Site located in the white box in the Arboretum on the northeast side of the University Central Florida campus.

The soil at the research site is Spodosol and classified as a Pomello series. A spodic horizon is an alluvial horizon consisting of an accumulation of organic matter, aluminum oxide, and there can also be iron oxide (Brady and Weil, 2002**).** While there was variation of the soil profile at the site, the middle of the grid displayed five soil horizons. The following soil profile was described from the pit of Grave 2B. The surface soil horizon (A) was encountered at 0 to

~40 cm with a light gray color (Munsell soil chart color: 10YR 7/2) and consists of fine sand. The subsurface soil horizon (E) was encountered at a depth of ~40 cm to ~55 cm with a gray color (Munsell soil chart color: 10YR 5/1) and consists of fine sand. The first subsurface soil horizon (Bh1 horizon) was encountered at a depth of ~55 cm to ~70 cm with a black color (Munsell soil chart color: 10YR 2/1) and consists of fine sand. The second subsurface soil horizon (Bh2 horizon) was encountered at a depth of ~70 cm to ~80 cm with a dark reddish brown color (Munsell soil chart color: 5YR 3/3) and consists of fine sand. The last horizon, the parent material (C), was encountered at a depth of ~80 cm with a pale brown color (Munsell soil chart color: 10YR 6/4) and consists of fine sand. The spodic horizon for this soil begins at approximately 55 cm. The major difference between the soil horizon at the site and the published representative Pomello series from a different area of the county is a shallower depth of the spodic horizon beginning at 17.75 cm (Doolittle and Schellentrager, 1989).

A total of eight graves were constructed in two rows within the research grid (Figure 2 and Figure 3). Two graves represented control graves without a carcass to test the geophysical response of only the disturbed soil. Testing responses from the control pits is important to determine which component of the grave is detected such as the carcass and burial items, disturbed soil, or all three. The other six graves contained a pig carcass (*Sus scrofa*) and represented a variety of burial scenarios (Table 2 and Figure 3). The euthanized pig carcasses were buried in January of 2009 after sustaining gunshot wounds to the head with .22 caliber handgun. The eight graves included the following scenarios (Table 2 and Figure 3):

1. A blank control grave consisting of only disturbed backfill (approximately 1. 00 m) to determine the geophysical response to disturbed soil only.
2. A blank control grave consisting of only disturbed backfill (approximately 0.50 m) to determine the geophysical response to disturbed soil only.
3. A pig carcass buried without additional grave objects at an approximate depth of 0.50 m.

4. A pig carcass buried without additional grave objects at an approximate depth of 1.00 m.
5. A pig carcass buried wrapped in a vinyl tarpaulin at an approximate depth of 1.00 m.
6. A pig carcass buried wrapped in a cotton blanket at an approximate depth of 1.00 m.
7. A pig carcass buried underneath a layer of lime (calcium hydroxide) at an approximate a depth of 1.00 m.
8. A pig carcass buried underneath a layer of rocks at an approximate depth of 1.00 m.

The pig carcasses were placed into the burial pits on their right sides, with their heads towards the north wall and their back is parallel and facing the east wall. Figure 2 shows the location of the burials within the research grid, and Figure 3 includes images of each scenario prior to refilling the graves.

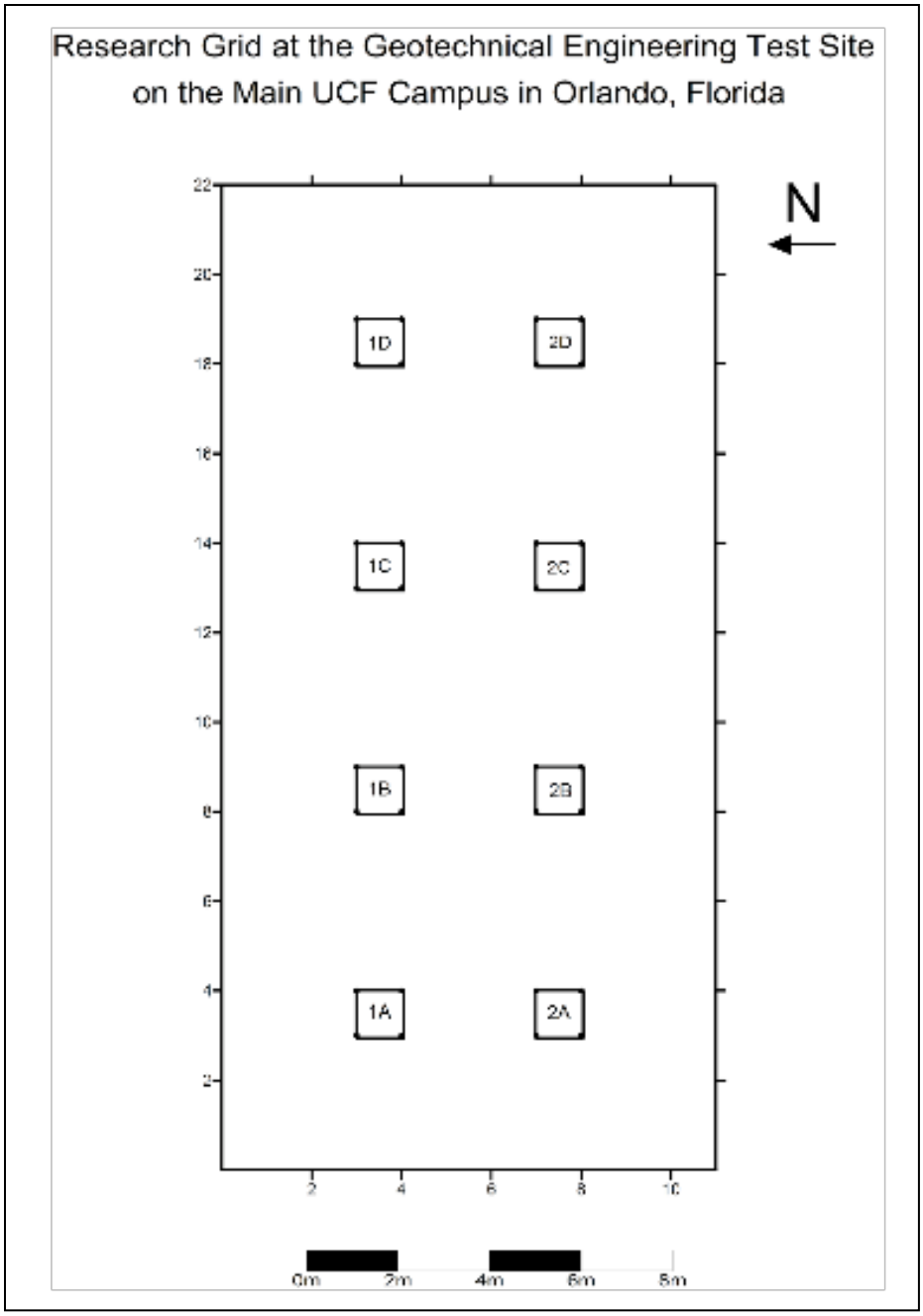

Figure 2: Diagram of research site grid with eight graves arranged in two rows

Table 2: Detailed grave information for each of the burial scenarios

Grid Location	Burial Date	Depth of Unit (below surface)	Scenario	Weight of Pig (lbs)
1A	1/30/2009	0.50 m	Shallow pig grave	90
1B	1/30/2009	1.00 m	Deep pig grave	100
1C	1/30/2009	1.00 m	Deep grave with layer of rocks covering pig	90
1D	1/30/2009	1.00 m	Deep grave with pig wrapped in tarpaulin	98
2A	1/26/2009	0.50 m	Shallow control hole	N/A
2B	1/30/2009	1.00 m	Deep control hole	N/A
2C	1/30/2009	1.00 m	Deep grave with layer of lime covering pig	95
2D	1/30/2009	1.00 m	Deep grave with pig wrapped in blanket	97
Calibration Unit (outside grid)	1/9/2009	1.00 m	Rebar hole	

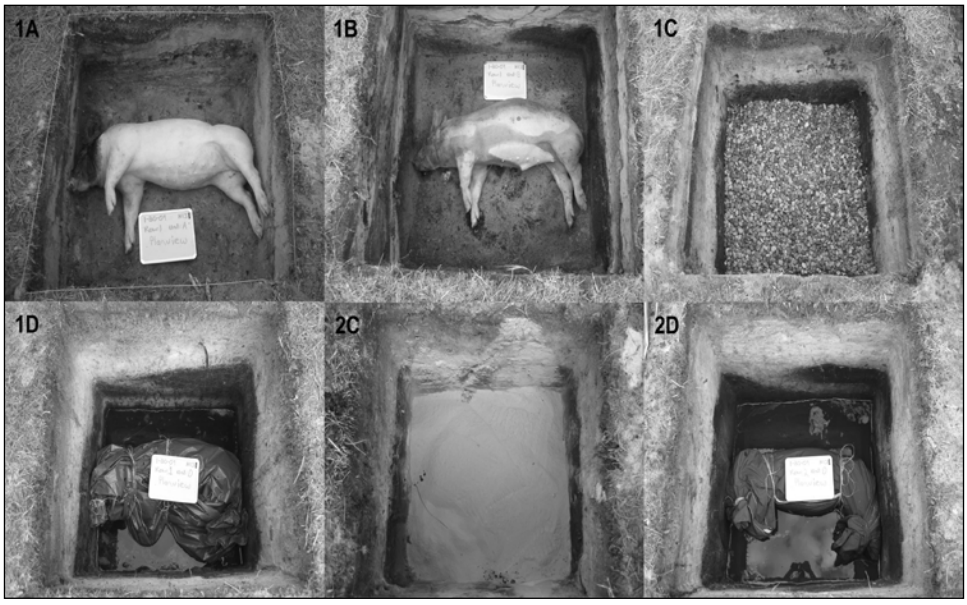

Figure 3: Images of six controlled graves with pig carcasses prior to refilling the graves. Note dark horizon (spodic horizon) at the bottom of the grave shaft

Ground-penetrating Radar

There are generally three main components of a standard GPR unit used for forensics and archaeology (Figure 4): the antenna (which both transmits and receives electromagnetic waves), the control unit, and the monitor which displays results in real time. The GPR unit generates radar waves, "a form of electromagnetic energy" (Conyers, 2004:23), that permeate the subsurface. When the electromagnetic waves encounter an object in the subsurface, a resulting reflected wave will occur that will be received by the receiving portion of the antenna. However, the amplitude of the returning wave- that is, the strength of the returning signal- is directly dependent on the contrast in dielectric permittivity between adjoining two materials (Ruffell, 2005). A stronger contrast between two horizons, or a strong contrast between a feature and the surrounding soil, will result in a stronger reflection.

The antenna frequency represents the center at which its radar waves are generated by the antenna (Reynolds, 1997). Antenna frequency emissions range from 10 MHz to 1.5 GHz

(Watters and Hunter, 2004). The choice of antenna frequency has a direct relationship with depth of penetration and vertical visibility. In short, the lower the frequency, the deeper the electromagnetic wave will project with decreased visibility of smaller features. Conversely, the higher the frequency, the shallower the electromagnetic wave will project with increased detail of subsurface features. According to Conyers and Goodman (1997), a 10 to 120 MHz antenna may display results up to 50 meters deep, while a 900 MHz antenna can only display results less than a meter deep, but with an increased visibility (Schultz, 2007). Therefore, a happy medium is often found with a 400 to 500 MHz antenna for forensic and archaeological applications (Dupras et al., 2006; Schultz, 2007).

Grid data collection was performed monthly for a 30 month monitoring period using a cart-mounted Mala RAMAC X3M GPR unit, with 500 MHz and 250 MHz antenna (Figure 5). Separate surveys were conducted with each antenna. Data was collected using transect spacing of 0.25 m in both a west-east (Figure 6) direction and a north-south direction (Figure 7). Additionally, the GPR unit was calibrated for accurate depth measurements that may be affected by changes in soil moisture. A buried object at a specific depth is used for calibration to determine the sensitivity of the instrument and can allow wave velocity, and thus depth, to be more accurately calculated within the soil (Strongman, 1992; Conyers and Cameron, 1998; Conyers, 2004; Martin, 2010). Prior to data collection, the GPR unit was calibrated using a metal bar that was pounded into the ground horizontally at a depth of 1.00 m, a method suggested by Conyers (2004). The calibration test unit was located 2.00 m away from the east end of the grid (Table 2). The data were collected over the test unit and the velocity of radar pulse propagation was adjusted until the depth of the metal bar was read at the correct depth on the reflection profile at 1.00 m.

The final phase of this research was the processing of the data gathered in the field. Two imagery options were used: reflection profiles and horizontal time slices. REFLEXW (Version 6.0.5) was used to process raw reflection profiles which represent single transect data and provides the data in two dimensions: depth and distance. All of the reflection profiles were processed with the same parameters and filters. Processing procedures for the reflection profiles using REFLEXW included subtract mean/dewow, static correction, manual Y gain, background filter, and bandpass frequency filter. The only processing procedure that differed was the addition of gain. While more gain was required overtime to increase the visibility of the graves, all of the profiles were reprocessed and double-checked to ensure that gain settings were appropriate for visibility.

Horizontal slices were created using the software program GPR-SLICE (Version 7). All of the horizontal slices were processed with the same parameters and filters. Processing procedures for the horizontal slices using GPR-SLICE included gain, static correction, boxcar filter, bandpass filter, background filter, and autogain. Horizontal slices, also referred to in the literature as Z-slices or time slices, are planview representations of the grid. The software allows all of the reflection profiles to be welded together into a 3-D cube by interpolating the space between the transects. The cube can then be cut at different depths and presented as individual horizontal slices that represent the grid at different depth intervals. Each horizontal slice represents the amalgamation of both the X and Y orientation's data. Each image represents an approximate depth around 0.85 to 1.00 m for deep graves and 0.50 to 0.60 m for shallow graves.

All of the grave scenarios were scored each month using the reflection profiles and horizontal slices. The response for each grave was scored on a four point scale: None, Poor, Good, and Excellent (Figure 4). A score of None demonstrated no discernible response. A

grave scored as Poor showed a slightly discernible response that may not have been visible during an actual geophysical survey. A score of Good indicated a grave that would most likely be discernible in the field during a geophysical survey. Finally, a grave scored as Excellent demonstrated a clearly visible response. When determining how many months of the collection period the grave was discernible, only graves with scores of Excellent and Good were considered as visible for that month.

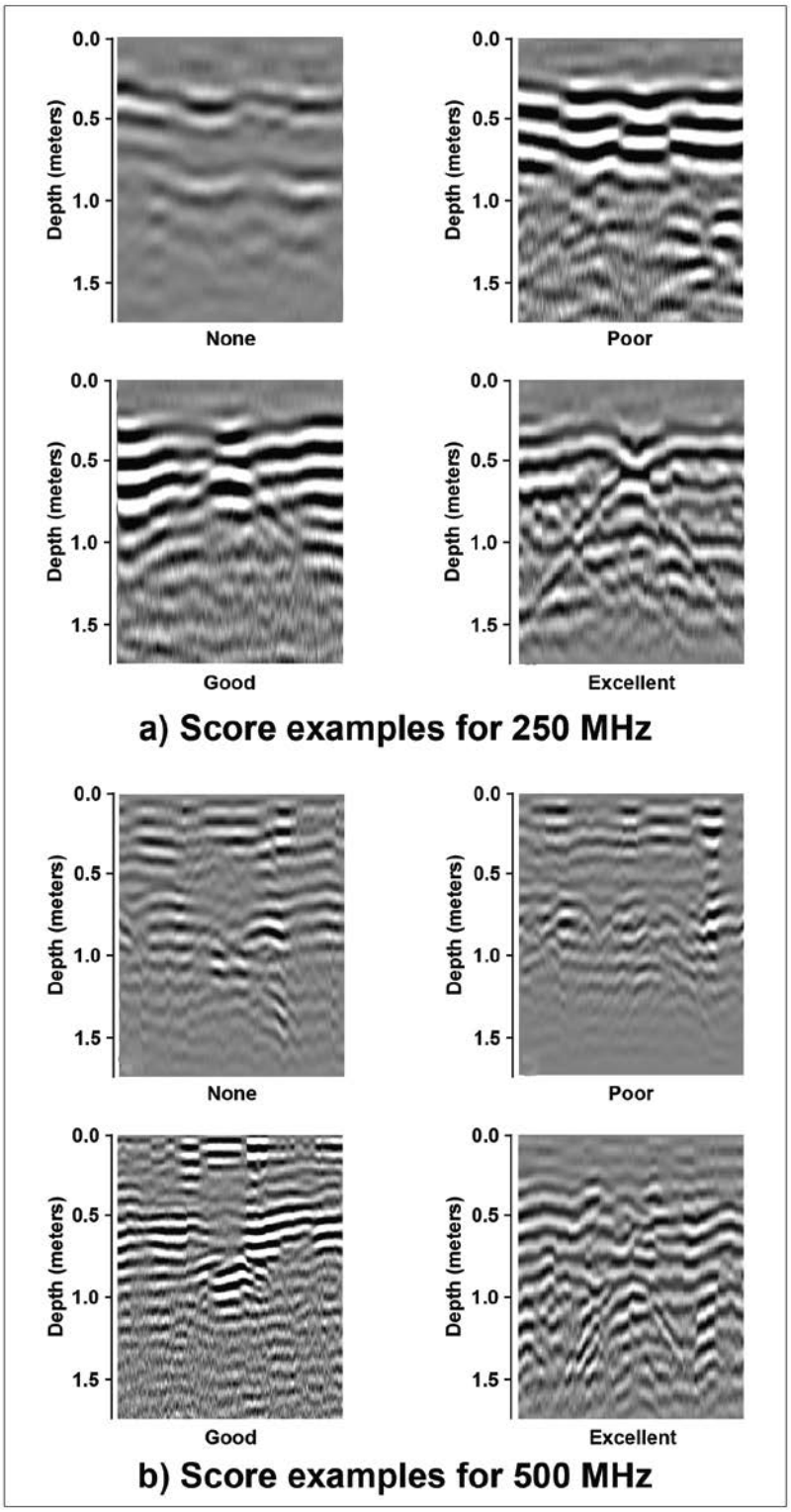

Figure 4: Score examples for the used for the 250 MHz antenna (a) and the 500 MHz antenna (b) reflection profiles

Figure 5: Operation of cart-mounted GPR Unit with built-in survey wheel by William Hawkins with three main components labeled: monitor, control unit, and antenna

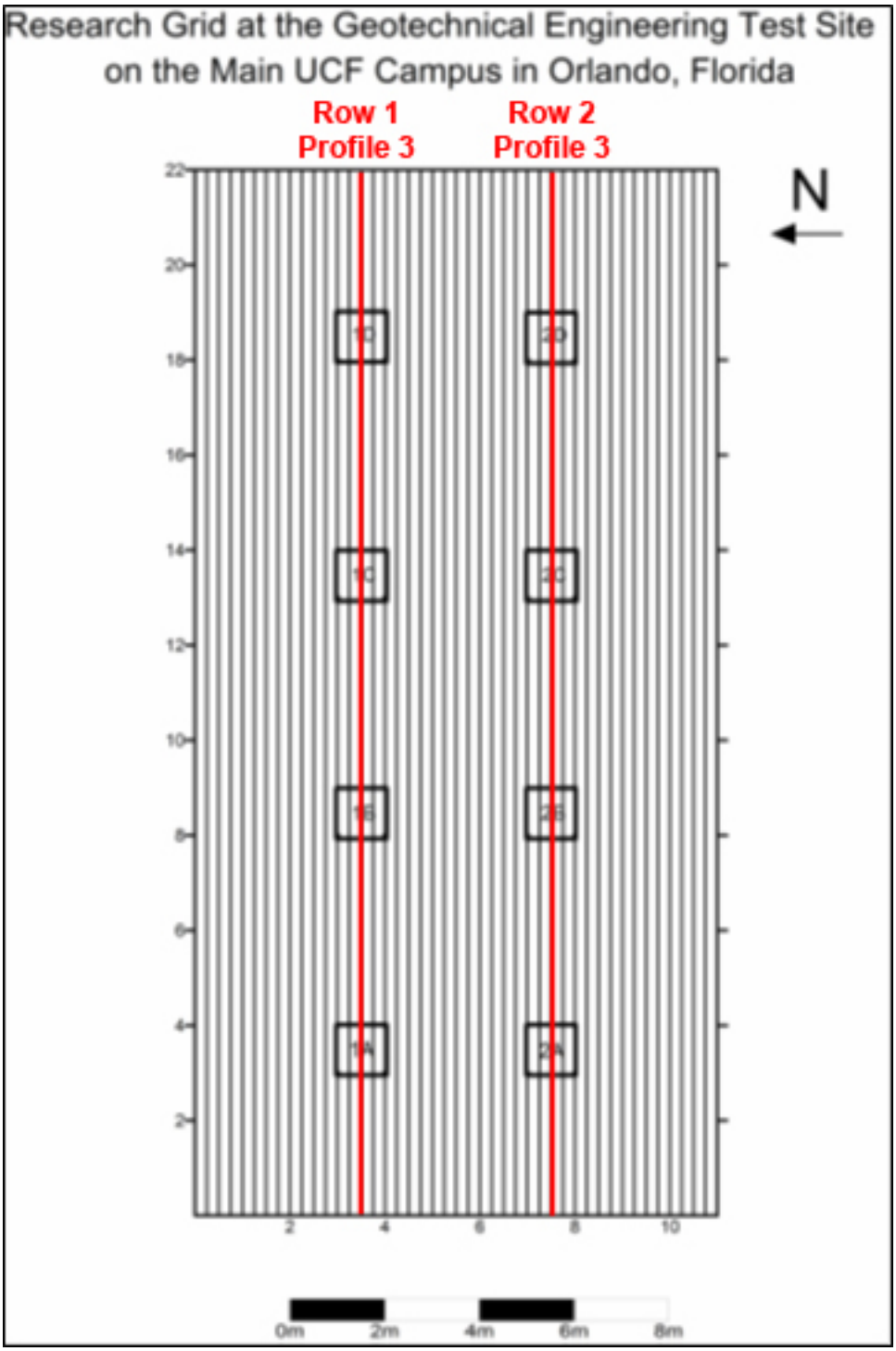

Figure 6: Diagram of geophysical research site grid with 0.25 m transects and Profile 3 of Rows 1-4 highlighted (west-east direction)

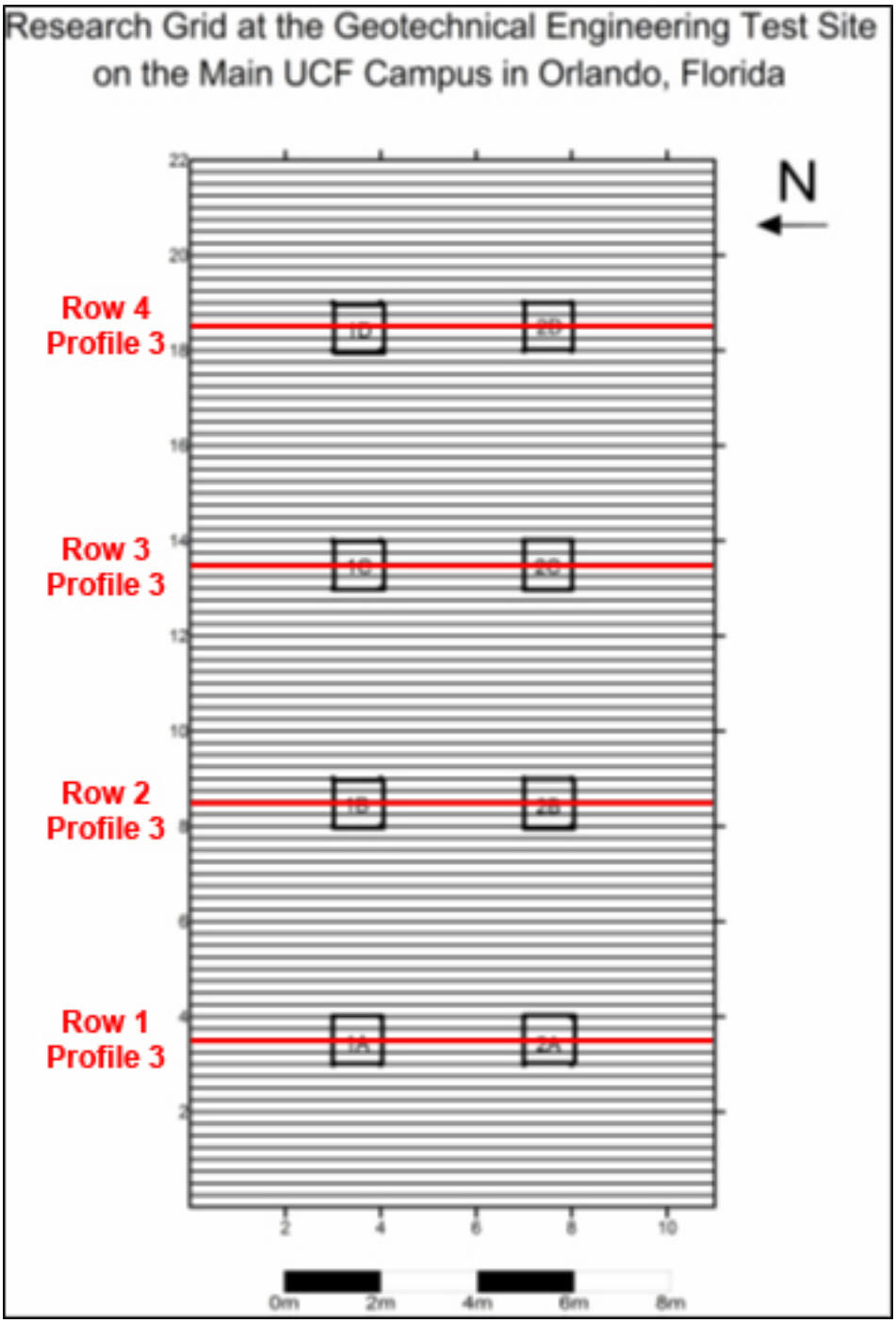

Figure 7: Diagram of the geophysical research site grid with 0.25 m transects and Profile 3 of Rows 1-4 highlighted (north-south direction)

Electromagnetic Induction

Though there are numerous models of EMI meters, the conventional technology used by both forensic anthropologists and archaeologists is the horizontal loop (or slingram) EMI meter that can be operated by a single individual and houses both the transmitter and receiver coils (Dupras et al., 2006). The horizontal loop model can be employed either horizontally, where the instrument is laid on its side on the ground, or vertically for greater depth, where the instrument is held upright (Clay, 2005). The EMI meter is composed of two main components: the transmitter and the receiver coils. The transmitter coil emits an electromagnetic wave into the subsurface. When the electromagnetic wave travels through the subsurface and encounter conductors such as a metal object, secondary eddy currents will be produced and received by the receiver. The receiver identifies changes in EM wavelength that are the direct response of changes in apparent conductivity (Bevan, 1983; Clay, 2005). In this research, the vertical mode was used in order to document changes at a greater depth.

Data collection was performed by operating the EMI meter, a Geonics EM38-RT with an Allegro CX handheld data logger to store the data collected from the field (Figure 8). The vertical dipole (vertical orientation of the instrument) that was used for this research is best for detecting conductivity differences at greater depths than with the horizontal dipole, which is used for conductivity differences near the surface (Reynolds, 1997). The EMI meter measures ground conductivity in millisiemens per meter (mS/m) which will increase with a better conductor (Killam, 2004). Conversely, negative values will be read if the EMI meter is in close proximity to a conductive object because of the geometry between metallic objects and the transmitting and receiving of coils (Ward, 1990). The EMI meter was calibrated throughout data collection by

choosing a small area with outside of the designated research grid known to be without burials or metal.

The grid data collection was performed at the end of every month for a total of 24 months. Apparent conductivity data was collected with a transect spacing of 0.25 m in an west-east direction (Figure 6). The final phase of this research was the processing of the data gathered in the field. Per protocols established by Martin (2010), conductivity measurements were recorded with a hand-held Allegro CX Field computer that connects to the conductivity meter; the data collected was then transferred back to a desktop computer from the field computer. Apparent conductivity data was processed and formatted using the DAT38W computer software to display the information using Golden Software Surfer 8 (Version 8.4) as a contour map image. A contour map image uses the X and Y coordinates and the value of the apparent conductivity measurements, represented as Z, to map out the site wherein it is employed. The closer two lines are together on the map, the greater the conductivity of that area.

Figure 8: Operation of EMI meter in vertical dipole orientation by Michael Martin

Soil Moisture Data

Precipitation data provided by National Climatic Data Center (NCDC) of the National Oceanic and Atmospheric Administration (NOAA) was utilized as a proxy to infer increases and decreases in soil moisture. Precipitation and temperature information was obtained for the closest recorded location to the site, Orlando International Airport, approximately 22 kilometers from the research site. The data obtained can be found at http://www4.ncdc.noaa.gov/cgi-win/wwcgi.dll?wwDI~StnSrch~StnID~20004451. This allowed daily maximum temperature,

daily mean temperature, average monthly temperature, monthly maximum temperature, and daily rainfall for the 30 months of data collection.

III. Results

Electromagnetic Induction

All images from the processed data are located in Appendix A. Prior to the burial of the pigs within the grid, conductivity measurements were recorded in order to compare with the measurements once the pig carcasses were buried (Figure 9a). The preburial contour map shows a number of unknown conductivity anomalies throughout the grid. The overlay map showing the locations of the burials shows no conductivity anomalies at any of the grave locations (Figure 9a), although there is conductivity anomaly near the northeast corner of Grave 2B.

After the pig carcasses had been buried for one month, the conductivity map resembles the preburial grid in a number of ways. First, each of the unknown reflection features present in the preburial grid are also present in the research grid at Month 1. There are no new reflection features present after the first month of burial that were not present when the electromagnetic induction data collected for the preburial grid. Further, when the overlay map is placed on top of the contour map for Month 1, there are no conductivity anomalies present within the location of any of the eight burials (Figure 9b). Both control pits containing only disturbed soil, as well as the six burials containing a pig carcass and the associated artifacts show no conductivity anomalies that may suggest burial detection. Thus, both the preburial conductivity map (Figure 9a) and the conductivity map at Month 1 of burial are notably similar (Figure 9b).

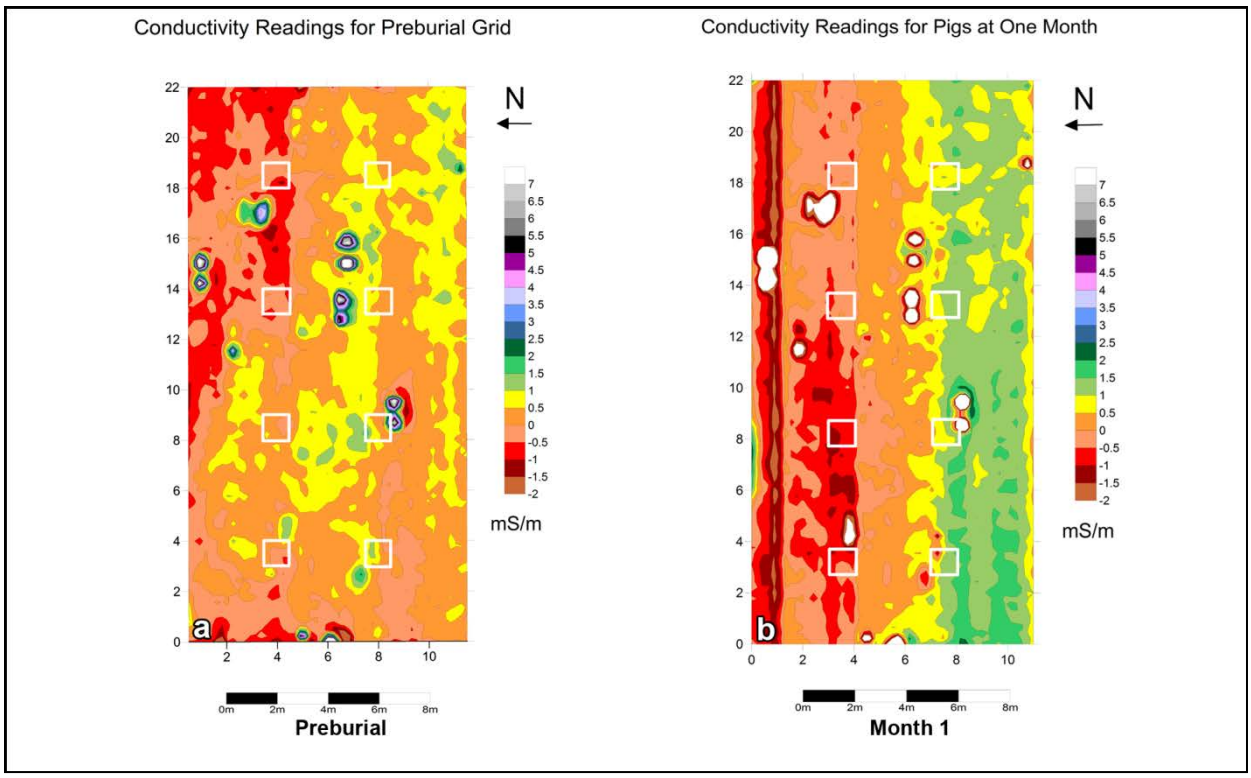

Figure 9: Electromagnetic Induction readings for the grid at Preburial (a) and Month 1 (b)

When analyzing the electromagnetic induction results for the remainder of the 24 months of data collection, the results are very similar to both the preburial grid and the Month 1 grid as none of the burials were detected for the entire monitoring period. The conductivity monitoring was terminated at Month 24.

Ground-Penetrating Radar

500 MHz Antenna Reflection Profiles

Transect data (west-east direction) was collected over each of the two rows of burials and consisted of five transects at a 0.25 m spacing. As illustrated, the five grave transects collected by the 500 MHz antenna for Row 1 at Month 1 are presented below with the Spodic horizon,

which is located approximately between 0.50 and 0.90 m, labeled (Figure 10a-e). Profile 1 (Figure 10a) represents the north side of the burial pit and Profile 5 (Figure 10e) represents the south side of the burial pit, the middlemost profile, Profile 3 (Figure 10c), represents the transect that was collected over the approximate center of the grave and the center of the pig carcass. It became apparent that the middlemost profile (Figure 10c) represented the most visible profile for all of the graves. Since the middlemost profile provided the highest visibility for the grave scenarios, only this profile was scored for visibility and is presented in this report for all reflection profiles. The middle reflection profiles for the monthly 500 MHz data are located in Appendix B.

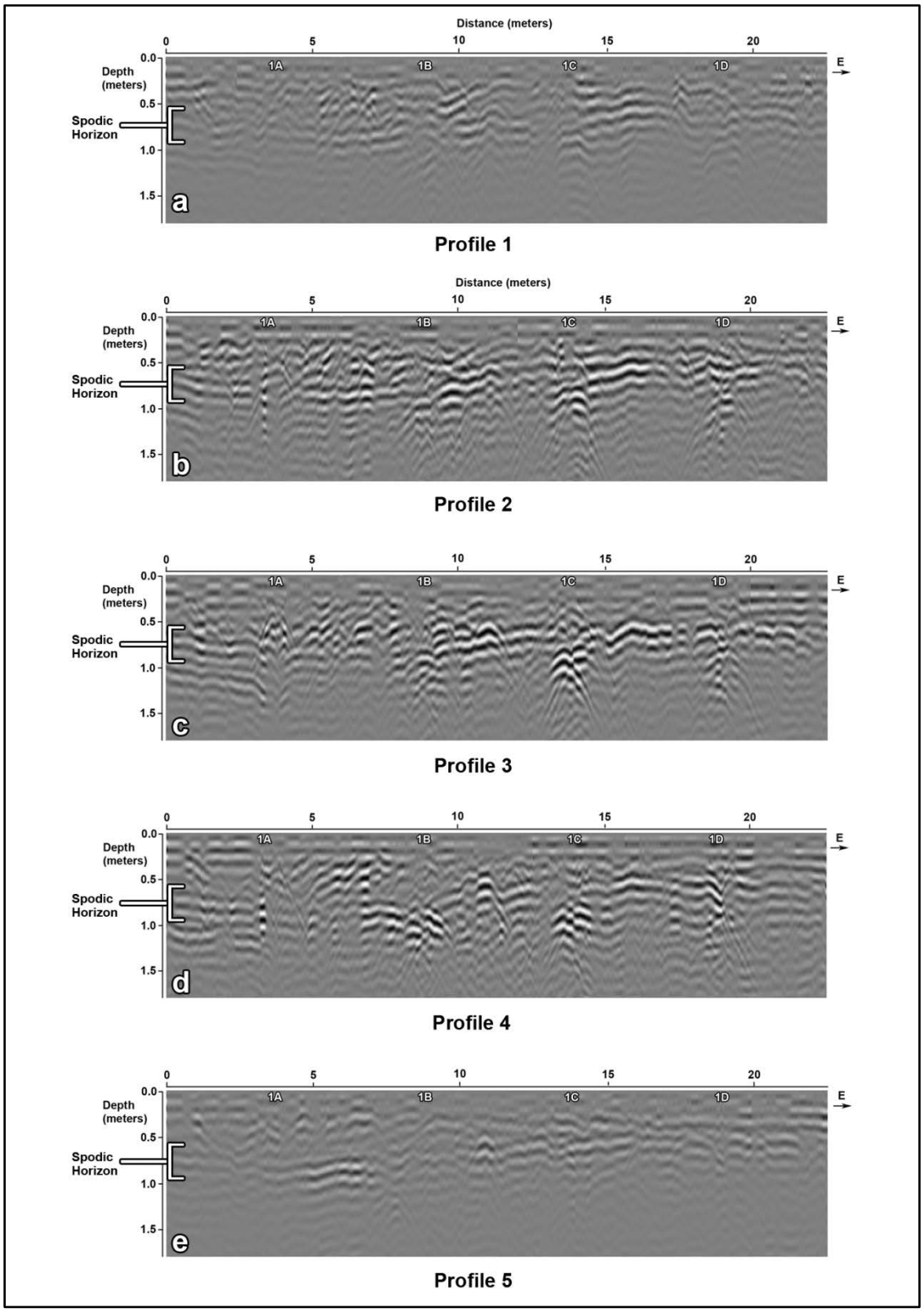

Figure 10: Reflection profiles collected with the 500 MHz antenna of Row 1 at Month 1

Row 1 Reflection Profile Data

A summary of all recorded responses throughout the 30 month data collection period is found below in Table 3. Grave 1A, the shallow pig grave, was visible for 22 of the 30 months of data collection. This grave produced a stronger visibility response during the first year of data collection, with scores of Excellent in Months 4 through 8 and Month 11. Visibility responses decreased for the remainder of the project, but were still somewhat visible to Month 30. The deep pig grave, Grave 1B, produced weaker results than the shallow pig grave (Grave 1A) with 14 visible months during the 30 months of data collection. Unlike Grave 1A, this grave produced scores of None for three consecutive months (Months 10 to 12). The visibility of Grave 1B steadily declined during the second year of data collection, but became slightly more visible for the last 5 months. Grave 1C was the deep grave with layer of rocks covering the pig. This grave produced the most visibility when compared to the other graves, with the most frequent scoring of Excellent, particularly at the beginning of data collection (Months 3 to 9). Furthermore, Grave 1C exhibited the strongest response for Months 4 to 6 and 26 of the 30 months producing visible response. Visibility decreased during the warmer months of 2010 (Months 13 to 21), but produced more responsive results again toward the end of the project (Months 22 to 30). The deep grave with the pig wrapped in tarpaulin, Grave 1D, produced infrequent visibility responses through the duration of the project and was visible for 18 of the 30 months of data collection. No distinguishable pattern could be determined among the visibility scores for this grave as the response for this grave was assigned scores of either Poor or Good.

Row 2 Reflection Profile Data

A summary of all recorded responses throughout the 30 month data collection period is found below in Table 3. Grave 2A, the shallow control grave, demonstrated the weakest response using the 500 MHz antenna with no visible months for the 30 months of data collection. The only response other than None exhibited by this grave was during Month 27, with a visibility score of Poor. The deep control grave, Grave 2B, produced more visible results than the shallow control grave, with 5 months of visibility. A majority of the scores for this grave were Poor or None, with an occasional Good (Months 18, 22, 23, and 28) and one Excellent (Month 25). The Good and Excellent scores are more prevalent in the last eight months of the project. Grave 2C, the deep grave with a layer of lime covering the pig, was visible for 15 of the 30 months of data collection, but was not visible for eight consecutive months (Months 6 to 13). This scenario was moderately discernible for the rest of the project, oscillating between scores of Good and Poor. This grave was somewhat visible for Months 22 and 23, but for a majority of the data collection the grave exhibited Good visibility. Similar to Grave 2C, the deep grave with the pig wrapped in a blanket (Grave 2D) also was not visible for a long period of time (Months 6 to 12) and yielded inconsistent results with visibility for only 14 of 30 months. Grave 2D also exhibited scores of Good and Poor for the remainder of the project and was visible for the last seven months of data collection (Months 24-30).

Table 3: Monthly imagery scores for each burial scenario based on reflection profiles using the 500 MHz antenna

	Burial Scenario							
Month	**1A**	**1B**	**1C**	**1D**	**2A**	**2B**	**2C**	**2D**
1	Good	Poor	Excellent	Poor	None	None	Good	None
2	Good	Good	Good	Poor	None	Poor	Poor	Poor
3	Poor	Good	Excellent	Poor	None	Poor	Poor	Poor
4	Excellent	Excellent	Excellent	Good	None	Poor	Good	Good
5	Excellent	Excellent	Excellent	Excellent	None	Poor	Excellent	Good
6	Excellent	Good	Excellent	Good	None	None	None	None
7	Excellent	Good	Excellent	Poor	None	None	None	None
8	Excellent	Poor	Excellent	Poor	None	None	None	None
9	Good	Poor	Excellent	Poor	None	Poor	None	None
10	Good	None	Good	Good	None	None	None	None
11	Excellent	None	Excellent	None	None	Poor	None	None
12	Good	None	Good	None	None	None	None	None
13	Good	Poor	Poor	Excellent	None	Poor	Poor	Good
14	Poor	Good	Good	Good	None	None	Good	Poor
15	Poor	Good	Poor	Good	None	Poor	Poor	Good
16	Poor	Poor	Poor	Poor	None	Poor	Good	Good
17	Good	Poor	Good	Good	None	Poor	Good	Poor
18	Poor	None	Good	Good	None	Good	Good	Poor
19	Good	Good	Good	Good	None	Poor	Good	Good
20	Good	Poor	Good	Poor	None	Poor	Poor	Poor
21	Good	Poor	Good	Poor	None	Poor	Poor	Poor
22	Poor	Poor	Good	Poor	None	Good	Good	Good
23	Poor	Poor	Good	Good	None	Good	Good	Poor
24	Good	Good	Good	Good	None	None	Good	Good
25	Good	Poor	Good	Good	None	Excellent	Good	Good
26	Good	Good	Excellent	Good	None	Poor	Good	Good
27	Good	Poor	Good	Good	None	None	Poor	Good
28	Good	Good	Poor	Good	Poor	Good	Good	Good
29	Poor	Good	Good	Good	None	Poor	Good	Good
30	Good	Good	Good	Good	None	None	Poor	Good

500 MHz Horizontal Time Slices

Horizontal slice imagery collected with the 500 MHz antenna and displayed with the software program GPR-SLICE (Version 7) can be found in Appendix C.

Row 1 Horizontal Slice Data

A summary of all recorded responses throughout the 30 month data collection period is found below in Table 4. Grave 1A, the shallow pig grave, was not visible using horizontal slices for the entire project and was not visible for the 30 months of data collection. Similar to Grave 1A, the deep pig grave, Grave 1B, did not produce visible results and was only visible for 4 out of 30 months of the data collection period, making it the least visible of the graves besides the control graves. The grave was clearly visible at the beginning of the project but the response became indistinguishable after Month 6. The deep grave with a layer of rocks covering the pig, Grave 1C, produced the most favorable results for both rows when compared to the other graves with 9 out of 30 visible months. This grave was clearly visible from the beginning of the project until Month 18, when it became less discernable. For the remainder of the project, the visibility scores were inconsistent, ranging from Excellent to None. Grave 1D was the deep grave with the pig wrapped in tarpaulin. This grave was not as distinguishable as Grave 1C with 14 out of 30 visible months, but was still visible at the beginning of the project. At Month 17, the grave became indiscernible, with scores of Poor and None for the remainder of the project.

Row 2 Horizontal Slice Data

A summary of all recorded responses throughout the 30 month data collection period is found below in Table 4. Grave 2A served as the shallow control grave and could not be detected

using horizontal slice data for the entire project. The deep control grave, Grave 2B, was slightly more responsive than the shallow control grave, with an occasional score of Excellent (Months 14, 15, 17, and 20). For most of the project Grave 2B produced no response or was barely visible, with only 6 out of 30 months of visible results. The deep grave with a layer of lime covering the pig, Grave 2C, was not visible for most of the project and only demonstrated 8 out of 30 months of visible data. However, this was the most visible grave for Row 2. Grave 2D was the deep grave with the pig wrapped in a blanket. This grave was not visible after Month 8 and was only visible for 3 of the 30 months of data collection.

Table 4: Monthly imagery scores for each burial scenario based on horizontal time slices using the 500 MHz antenna

	Burial Scenario							
Month	**1A**	**1B**	**1C**	**1D**	**2A**	**2B**	**2C**	**2D**
1	None	Excellent	Excellent	Good	None	Poor	Good	None
2	None	Good	Excellent	Poor	None	None	Good	None
3	None	None	Excellent	Good	None	None	Poor	None
4	None	Good	Excellent	Excellent	None	Good	Excellent	Excellent
5	None	Good	Excellent	Excellent	None	None	Excellent	Good
6	None	None	Excellent	Good	None	None	None	Good
7	None	None	Excellent	Good	None	None	Good	Poor
8	None	None	Excellent	Excellent	None	None	None	Poor
9	None	None	Excellent	Excellent	None	None	None	None
10	None	None	Excellent	Excellent	None	None	Good	None
11	None	None	Excellent	Excellent	None	None	None	None
12	None	None	Excellent	Poor	None	None	None	None
13	None	None	Good	Good	None	Poor	None	None
14	None	Poor	Excellent	Excellent	None	Excellent	Good	None
15	None	None	Excellent	Good	None	Excellent	Excellent	None
16	None	None	Excellent	Excellent	None	None	Poor	Poor
17	None	None	Excellent	Poor	None	Excellent	None	None
18	Poor	None	Poor	Poor	None	None	Poor	None
19	None	None	Poor	None	None	Good	None	None
20	None	None	Excellent	Poor	None	Excellent	None	None
21	None	None	None	None	None	None	None	None
22	None	None	Poor	None	None	None	None	None
23	None	None	None	None	None	None	None	None
24	None	None	Poor	None	None	Poor	None	None
25	None	None	None	None	None	None	None	None
26	None	None	Good	Poor	None	None	None	None
27	None	None	None	None	None	None	None	None
28	None	None	None	None	None	None	None	None
29	None	None	None	None	None	None	None	None
30	None	None	None	None	None	None	None	None

250 MHz Antenna Reflection Profiles

Transect data (west-east direction) was collected over each of the two rows of burials and consisted of five transects at a 0.25 m spacing. As illustrated, the five grave transects collected by the 250 MHz antenna for Row 1 at Month 1 are presented below with the Spodic horizon,

which is located approximately between 0.50 and 0.90 m, labeled (Figure 11a-e). Profile 1 (Figure 11a) represents the north side of the burial pit and Profile 5 (Figure 11e) represents the south side of the burial pit, the middlemost profile, Profile 3 (Figure 11c), represents the transect that was collected over the approximate center of the grave and the center of the pig carcass. It became apparent that the middlemost profile (Figure 11c) represented the most visible profile for all of the graves. Since the middlemost profile provided the highest visibility for the grave scenarios, only this profile was scored for visibility and is presented in this report for all reflection profiles. The middle reflection profiles for the monthly 250 MHz data are located in Appendix D.

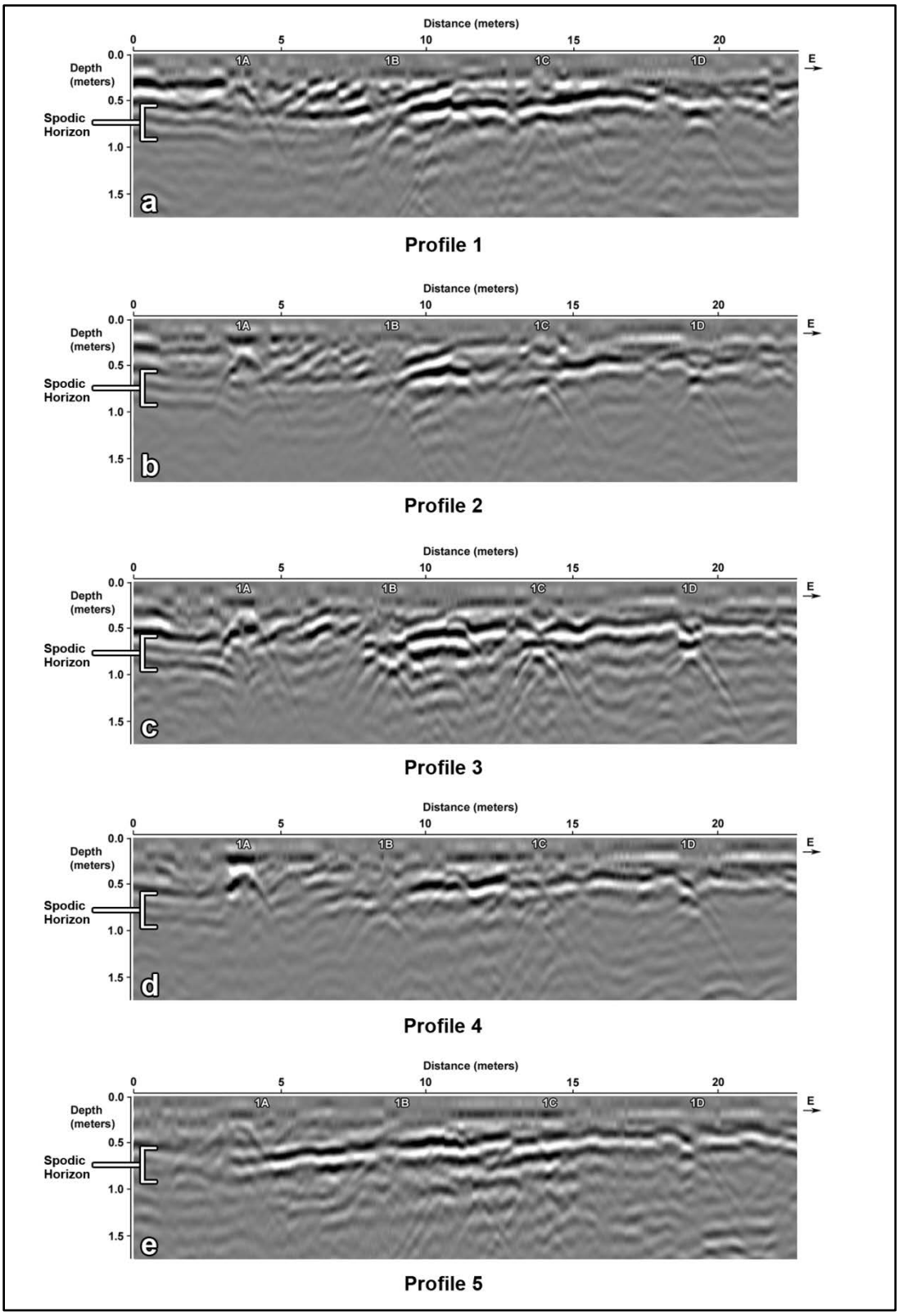

Figure 11: Refection profiles using the 250 MHz antenna for Row 1 at Month 1

Row 1 Reflection Profile Data

A summary of all recorded responses throughout the 30 month data collection period is found below in Table 5. Grave 1A, the shallow pig grave, showed a discernible response throughout the majority of the 30 months, with scores of Excellent and Good for 18 of the 30 months. The visibility of the reflection profile for this grave started somewhat strong but fluctuated during the first two years of collection. The last six months of visibility for the grave were not as favorable, with the visibility scores vacillating between Poor and Good. The reflection profile visibility of Grave 1B, the deep pig grave, oscillated greatly throughout the two and a half years of data collection and was visible for 20 of the 30 months of data collection. There is no discernible pattern that can be applied to this grave, as visibility scoring ranges from None to Excellent from Month 1 to Month 30. No clear decrease or increase in distinguishability exists when considering the visibility of the reflection profiles for this grave. Grave 1C was the deep grave with a layer of rocks covering the pig. The visibility of Grave 1C produced more favorable results than Graves 1A and 1B, with 28 of 30 visible months of data collection. Visibility for this grave was scored as Excellent through the duration of data collection except in Months 1, 2, 3, 21, and 30. Also, Grave 1C received a Poor score only twice (Months 3 and 21) and never received a score of None. This grave also showed the best response compared to all of the graves at its apex (top of the hyperbola) from Months 4 to 8 and at Month 12. The deep grave with the pig wrapped in tarpaulin, Grave 1D, showed results similar to Grave 1C with 27 of 30 months of visibility. A majority of the scores were Excellent, with only two weakened responses of Poor (Months 3 and 21) and one score of None (Month 2). This grave kept relatively strong visibility throughout the duration of data collection.

Row 2 Reflection Profile Data

A summary of all recorded responses throughout the 30 month data collection period is found below in Table 5. Grave 2A, the shallow control grave, exhibited the weakest response to the GPR unit when compared to the other graves. A majority of the visibility scores yielded a score of None. Grave 2A did not produce a clearly discernible response until Month 19. Furthermore, Month 19 was the only month to show a visibility score higher than Poor, with a score of Good. Grave 2B was the other control hole but with a depth of 1.00 m. This grave yielded moderate visibility, with steady visibility scores of mostly Good. However, sporadically, scores of None (Months 3, 20, and 27) and Poor (Months 26 and 28) would be produced. Overall, this grave was visible for 24 out of 30 months of data collection. Grave 2C, the deep grave with a layer of lime covering the pig, showed visibility similar to Grave 2B with 25 months of visibility. A score of None was only produced once (Month 12) and a score of Poor was only produced at the end of the 30 months (Months 27, 28, and 30) and at Month 18. Grave 2D, a deep grave with the pig wrapped in a blanket, started with unfavorable results for the first three months, but produced a score of Excellent for eight consecutive months (Months 4-11). The duration of the project yielded mostly Excellent and Good scores with 23 months of visibility. Like Grave 2C, less favorable scores of Poor (Months 1, 12, 20, 21, and 28) and None (Months 2 and 3) were produced throughout data collection.

Table 5: Monthly imagery scores for each burial scenario based on reflection profiles using the 250 MHz antenna

	Burial Scenario							
Month	**1A**	**1B**	**1C**	**1D**	**2A**	**2B**	**2C**	**2D**
1	Good	Poor	Good	Good	None	Good	Good	Poor
2	Good	Good	Good	None	None	Good	Good	None
3	Poor	Poor	Poor	Poor	None	None	Good	None
4	Excellent	Excellent	Excellent	Excellent	None	Good	Excellent	Excellent
5	Excellent	Excellent	Excellent	Excellent	None	Good	Excellent	Excellent
6	Excellent	Excellent	Excellent	Excellent	None	Good	Excellent	Excellent
7	Excellent	Excellent	Excellent	Excellent	None	Good	Excellent	Excellent
8	Excellent	Excellent	Excellent	Excellent	None	Good	Excellent	Excellent
9	Good	Good	Excellent	Excellent	None	Good	Good	Excellent
10	None	Poor	Excellent	Excellent	None	Excellent	Excellent	Excellent
11	Poor	None	Excellent	Excellent	None	Excellent	Good	Excellent
12	Poor	None	Excellent	Good	None	Good	None	Poor
13	Poor	Excellent	Excellent	Excellent	None	Excellent	Excellent	Excellent
14	Good	Excellent	Excellent	Excellent	None	Excellent	Excellent	Excellent
15	Good	Excellent	Excellent	Excellent	None	Good	Excellent	Excellent
16	Poor	Poor	Excellent	Excellent	Poor	Excellent	Excellent	Excellent
17	Poor	Good	Excellent	Excellent	None	Good	Good	Excellent
18	Poor	Good	Excellent	Good	None	Good	Poor	Good
19	Excellent	Excellent	Excellent	Excellent	Good	Good	Excellent	Excellent
20	Excellent	Excellent	Excellent	Excellent	None	None	Good	Poor
21	Poor	Poor	Poor	Poor	None	Good	Good	Poor
22	Poor	Good	Excellent	Excellent	None	None	Excellent	Good
23	Poor	Poor	Excellent	Excellent	None	Good	Excellent	Excellent
24	Good	Poor	Excellent	Good	None	Excellent	Excellent	Excellent
25	Good	Poor	Excellent	Excellent	Poor	Excellent	Excellent	Excellent
26	Good	Excellent	Excellent	Excellent	Poor	Poor	Good	Good
27	Poor	Good	Excellent	Good	None	None	Poor	Good
28	Good	Excellent	Excellent	Good	None	Poor	Poor	Poor
29	Good	Excellent	Excellent	Good	Poor	Excellent	Excellent	Excellent
30	Good	Excellent	Good	Excellent	None	Good	Poor	Excellent

250 MHz Horizontal Time Slices

Horizontal slice imagery collected with the 250 MHz antenna and displayed with the software program GPR-SLICE (Version 7) can be found in Appendix E.

Row 1 Horizontal Slice Data

A summary of all recorded responses throughout the 30 month data collection period is found below in Table 6. The shallow pig grave, Grave 1A, produced unfavorable results and was only visible for 2 of the 30 months of data collection. Grave 1B, the deep pig grave, was only visible for 9 of 30 months of data collection. However, after the first year of data collection, Grave 1B became indiscernible for the remainder of data collection, except during Months 14 and 19. Grave 1C, the deep grave with a layer of rocks covering the pig, was clearly visible for the first 16 months of the project. However, the visibility of the grave decreased after Month 16 and became nonexistent starting with Month 27. This grave produced the most favorable results with 19 out of 30 months of visibility. Grave 1D was the deep grave with the pig wrapped in tarpaulin. This grave produced similar results to Grave 1C, but became less visible beginning at Month 16. Grave 1D was clearly discernible for most of the first 15 months but became less discernible after Month 15 and became indiscernible after Month 15 except for Months 25 and 26. Overall the grave demonstrated 14 visible months out of the 30 months of data collection.

Row 2 Horizontal Slice Data

A summary of all recorded responses throughout the 30 month data collection period is found below in Table 6. Similar to the horizontal slice results from Row 1, Row 2 the shallow control grave, Grave 2A, was not visible for the entire project. For a majority of the project, Grave 2B, the deep control grave, was not visible except in Months 11, 13, 14, 15, 17, and 19. After Month 19, the grave no longer could be seen on a horizontal slice except in Month 26. Overall, the deep control gave was only visible for 7 of 30 months of data collection. Grave 2C,

the deep grave with the pig covered in a layer of lime, was only visible for 8 out of 30 months, with the visibility occurring primarily in the first year of data collection. Finally, the deep grave with the pig wrapped in a blanket, Grave 2D, started with barely visible results for Months 1 and 2, but became visible with Months 4 to 8. During Months 9 to 12 the grave became less visible, but picked up for Months 13 to 15. After Month 15, Grave 2D was not visible except during Month 26. This grave showed 10 months of visibility for the 30 month data collection period primarily during the first year, providing the most visible grave for Row 2.

Table 6: Monthly imagery scores for each burial scenario based on horizontal time slices using the 250 MHz antenna

Burial Scenario								
Month	**1A**	**1B**	**1C**	**1D**	**2A**	**2B**	**2C**	**2D**
1	None	Poor	Good	Good	None	None	Good	Poor
2	Good	Good	Excellent	Poor	None	Poor	Poor	Poor
3	Good	Good	Good	Good	Poor	Poor	Poor	Good
4	None	Excellent	Excellent	Excellent	None	None	Excellent	Excellent
5	None	Good	Good	Good	None	None	Good	Good
6	None	Excellent	Excellent	Excellent	None	None	Excellent	Excellent
7	None	Excellent	Excellent	Excellent	None	None	Excellent	Excellent
8	None	Good	Excellent	Excellent	None	None	Excellent	Excellent
9	None	None	Excellent	Excellent	None	None	None	Poor
10	None	None	Excellent	Excellent	None	None	None	Poor
11	None	None	Good	Poor	None	Good	None	Poor
12	None	None	Good	Poor	None	None	None	Poor
13	None	None	Excellent	Excellent	None	Good	Poor	Excellent
14	None	Excellent	Excellent	Good	None	Good	Good	Good
15	None	Poor	Excellent	Excellent	None	Excellent	None	Good
16	None	None	Good	Poor	None	None	None	Poor
17	None	None	Poor	Poor	None	Excellent	None	Poor
18	None	None	Poor	Poor	None	None	None	Poor
19	None	Poor	Excellent	Poor	None	Good	None	Poor
20	None	None	Poor	Poor	None	None	None	Poor
21	None	None	None	None	None	None	None	None
22	None	None	None	None	None	None	None	None
23	None	None	None	None	None	None	None	None
24	None	None	Poor	Poor	None	None	None	Poor
25	None	None	Good	Good	None	None	None	None
26	None	Excellent	Excellent	Excellent	None	Excellent	Good	Excellent
27	None	None	None	None	None	None	None	None
28	None	None	None	None	None	None	None	None
29	None	None	None	None	None	None	None	None
30	None	None	None	None	None	None	None	None

IV. Conclusions

Discussion of Findings

Electromagnetic Induction

One of the objectives (Objective 6) for this project dealt with evaluating the utility of an electromagnetic induction meter for grave detection. Unfortunately, the use of the electromagnetic induction meter in this soil type and with the pig graves is strongly discouraged since none of the controlled burials were detected over the 24 months of data collection. Starting Month 1 of data collection, none of the grave scenarios were detected, and over a 24 month period, data collection showed little variability and no visible conductivity for any burial scenario. A number of publications (Killam, 2004; France et al., 1992; France et al., 1997, Davenport 2001a; Davenport 2001b; Dupras et al., 2006; Dionne et al., 2011) list the electromagnetic induction meter as a possible geophysical tool for forensic applications. However, pre-survey testing would be needed to determine if the use of this technology is appropriate for detecting soil disturbances at the proposed site. Unfortunately, while an EMI meter has been used successfully for detecting a clandestine grave in conjunction with GPR (Nobes, 2000), this tool was unable to detect disturbances in the sandy soils at the test site. However, as Dionne et al. (2011) has shown with controlled research, the EMI meter is an excellent tool for detecting buried metallic objects. If a suspected grave is known to contain a large metal weapon and is buried less than a meter in depth, then an EMI meter may be a geophysical search option when searching for a clandestine grave.

Ground-Penetrating Radar

Detection of a forensic grave can be due to a number of variables such as the body, items added to a grave, soil disturbance, or a combination of these grave variables. In addition, it is important to process the data after collection, as this task may increase the visibility of features that may not be visible on raw radar profiles examined in the field. This research investigated multiple variables to discern which variables affect the detection of graves in central Florida when buried in a Spodosol. At the same time, imagery options must be considered. In terms of imagery options, reflection profiles provided the best GPR imagery for extended periods of interment with the controlled graves (Objective 4). Even though the horizontal slices provide a 2-D plan view by slicing a 3-D cube of the research site, detection of the controlled graves occurred more frequently and for a longer period using the reflection profiles. This is not surprising since the reflection profiles are commonly used to make in-field assessments when performing a survey (Dupras et al., 2006; Schultz, 2007; Schultz, 2008). There was overall poor visibility of the graves using both the 500 MHz (Figure 12) and 250 MHz (Figure 13) horizontal slice data as graves were poorly detected over the second half of grave monitoring.

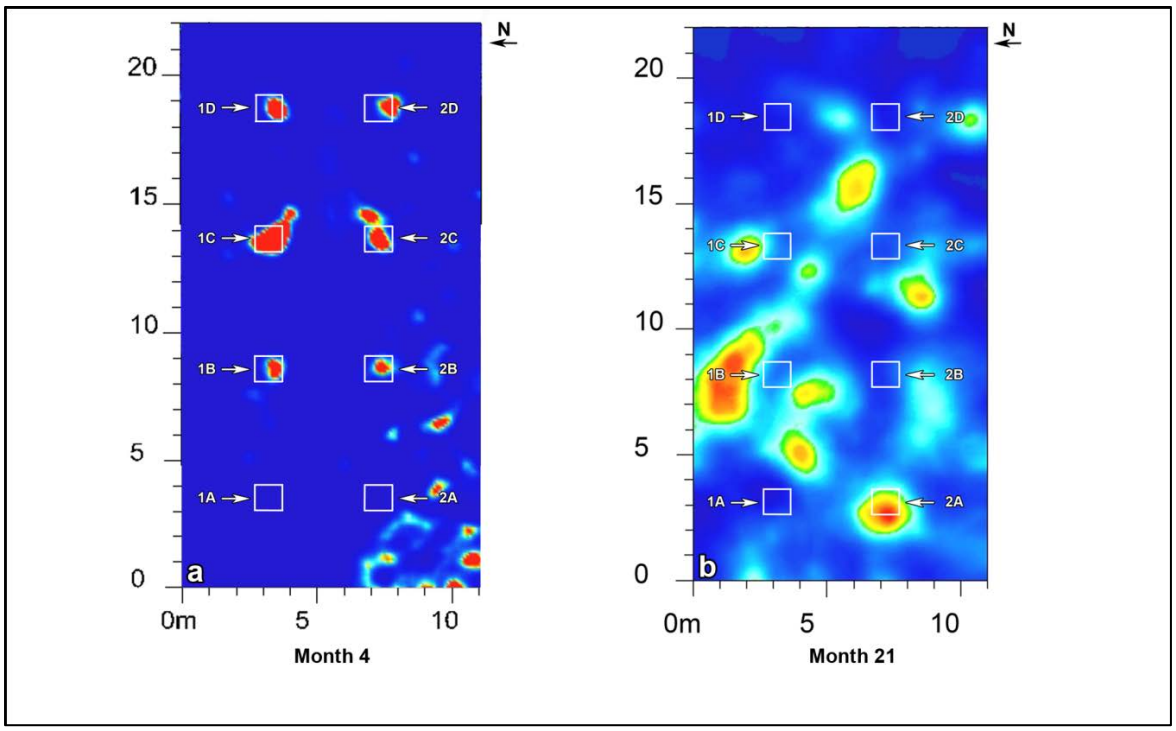

Figure 12: Horizontal slice data using the 500 MHz antenna showing detection of deep graves during Month 4 (a) and no detection of graves during Month 21 (b) at a depth of 0.85 to 1.00 m.

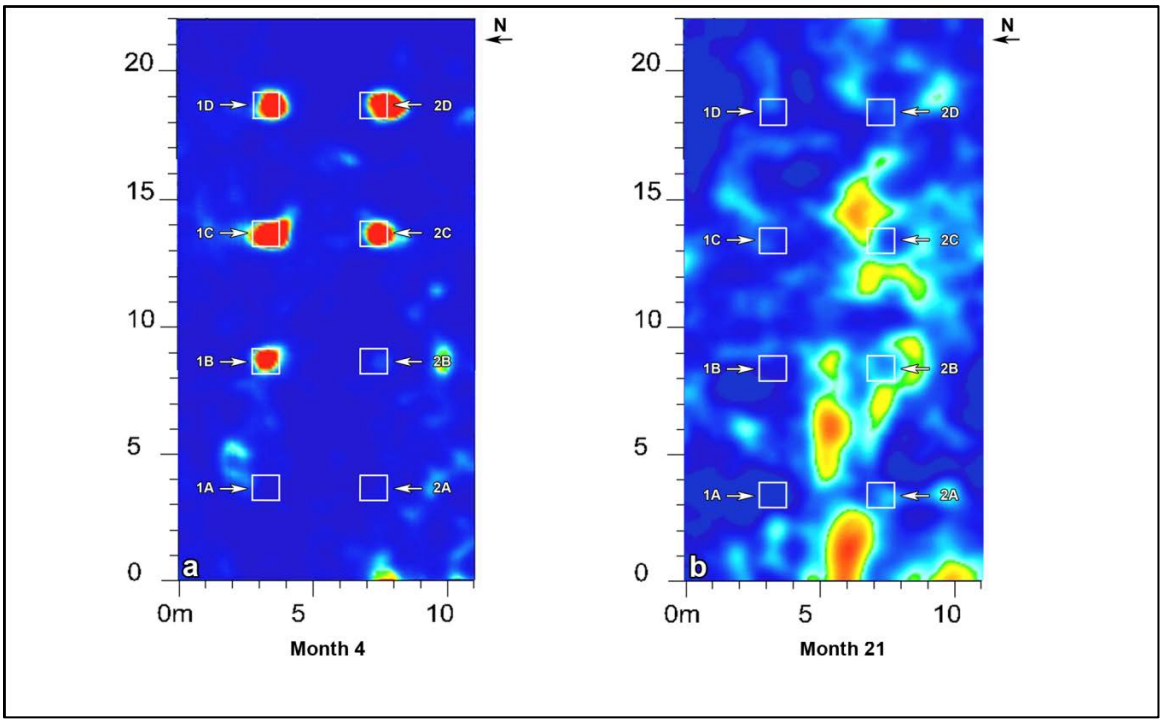

Figure 13: Horizontal slice results using the 250 MHz antenna showing detection of deep graves during Month 4 (a) and no detection of graves during Month 21(b) at a depth of 0.85 to 1.00 m.

In terms of antenna selection (Objective 5), this study provided surprising results. In the sandy soils examined in this study, the 500 MHz antenna generally provides a favorable compromise between depth of penetration and vertical visibility making it a favorable choice for most controlled studies and forensic cases (Dupras et al., 2006; Schultz et al., 2006; Schultz, 2007; Schultz, 2008). However, a lower frequency antenna may be a better option for soils that limit penetration of the EM wave such as soils with a high clay content. As preliminary results of this study first reported (Schultz and Martin, 2011) the 250 MHz may be a better option with this soil type tested as this antenna produced more salient reflections that were easier to discern on the reflection profile for the duration of the study (Tables 7 and 8; Figure 13). The reflections produced by the 250 MHz antenna (Figure 14a) are more noticeable, compared to the 500 MHz (Figure 14b) antenna, since features are detected as larger prominent reflections with less clutter and the Spodic horizon is more discernible (Schultz and Martin, 2011). Conversely, the higher detail of the 500 MHz antenna results in more clutter and less discernable features because the increased detail may not detect the burial feature as one large reflection. Rather, individual features of the grave may be detected resulting in less salient features. However, the shallow pig burial (Grave 1A) was visible more often with the 500 MHz antenna when compared to the 250 MHz antenna. This is not surprising, as the 500 MHz antenna has a higher resolution and a faster clear time from the strong surface pulse, thus resulting in more discernible shallow profiles. Therefore, the 500 MHz antenna should be a better option for detecting shallow features (less than 0.50 m), while the 250 MHz antenna is a better option for detecting deeper features.

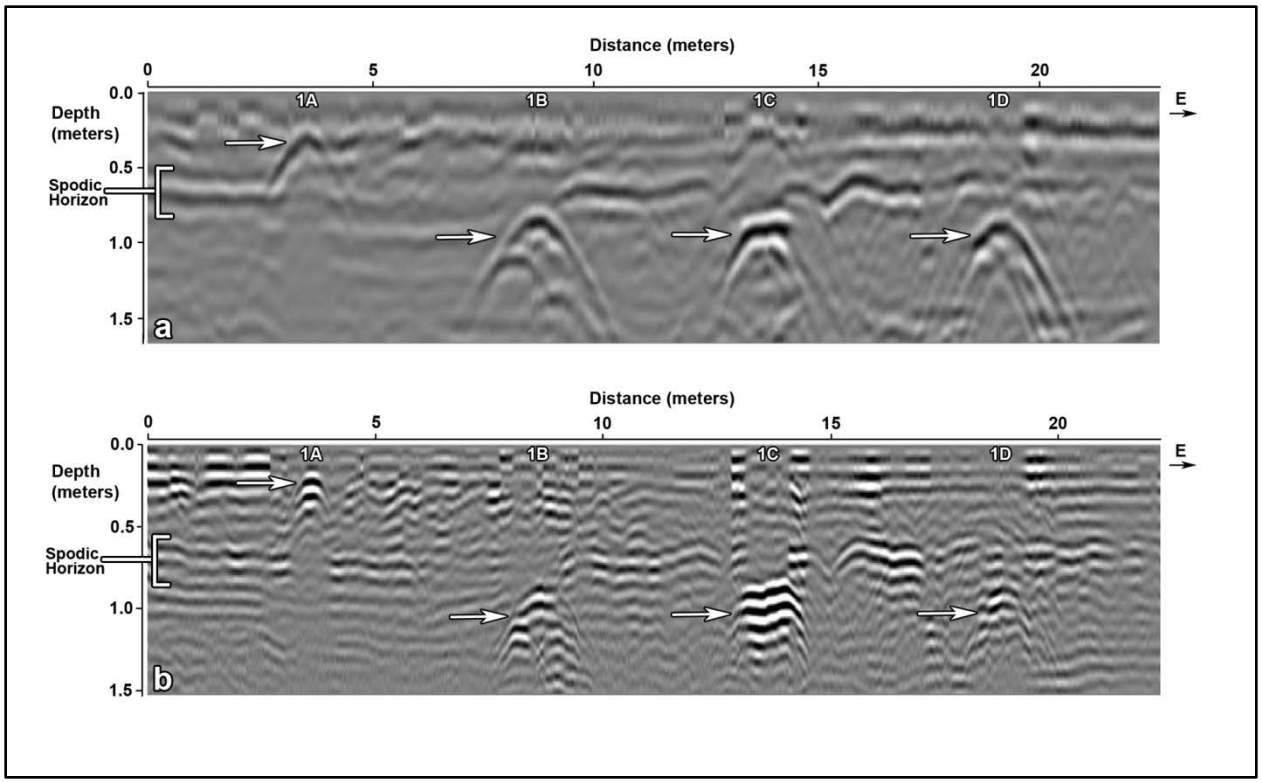

Figure 14: Comparison of reflection profiles of 250 MHz (a) and 500 MHz (b) antennae for Month 4 showing increased visibility of grave reflections with the 250 MHz data

Table 7: Summary of results for the 500 MHz antenna using reflection profiles

Grave	Scenario	*Visible Months	Comment
1A	Shallow pig grave	22	Stronger visibility response for first year
1B	Deep pig grave	1	Visibility declines during second year
1C	Deep grave with layer of rocks covering pig	26	Produced the best response
1D	Deep grave with pig wrapped in tarpaulin	18	No distinguishable pattern could be determined
2A	Shallow control hole	1	Demonstrated the weakest response with only one month of visibility
2B	Deep control hole	5	Increased visibility for the last 8 months
2C	Deep grave with layer of lime covering pig	15	Moderate visibility
2D	Deep grave with pig wrapped in blanket	14	Moderate visibility

**Visible months are months with reflection profiles scored as Good or Excellent*

Table 8: Summary of results for the 250 MHz antenna using reflection profiles

Grave	Scenario	*Visible Months	Comment
1A	Shallow pig grave	18	Visibility started strong but fluctuated for first 24 months
1B	Deep pig grave	20	Fluctuated for 30 months
1C	Deep grave with layer of rocks covering pig	28	Produced the best response
1D	Deep grave with pig wrapped in tarpaulin	27	Relatively strong visibility throughout the monitoring period
2A	Shallow control hole	0	Produced the weakest response
2B	Deep control hole	24	Moderate visibility with sporadic indiscernible months
2C	Deep grave with layer of lime covering pig	25	Moderate visibility
2D	Deep grave with pig wrapped in blanket	23	Moderate visibility with a decrease in visibility after the first 11 months

**Visible months are months with reflection profiles scored as Good or Excellent*

When considering the effect of burial scenario on GPR grave detection (Objectives 2 and 3), it is also important to consider the visibility of the scenarios over the monitoring period when using the 250 MHz and the reflection profiles (Tables 7 and 8; Figures 15-22). Refer to Figures 15 through 22 which provide a series of six reflection profile images for each scenario to show how the visibility of the graves change over time. The most visible grave was the deep grave with a layer of rocks (Grave 1C) for 28 out of 30 months using the 250 MHz antenna. This was followed by the scenarios with the grave items such as a pig carcass wrapped in a tarp (Grave 1D) and a pig carcass with a layer of lime (Grave 2C). All three of these scenarios were more visible than just the deep buried pig carcass (Grave 1B) and the pig carcass wrapped in a blanket (Grave 2D). The rocks and lime provided a larger contrasting area in the grave than just the carcass. At the same time, the pig carcass with the tarp more than likely trapped more moisture in the grave, making the grave more conductive, and, thus, more visible.

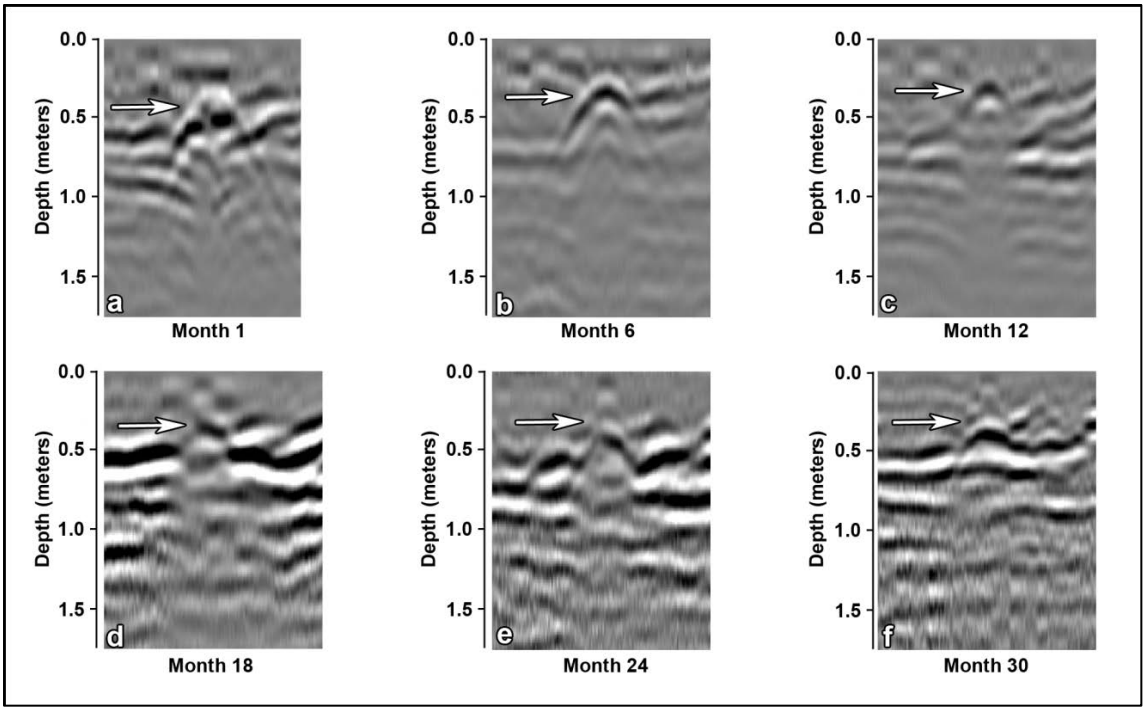

Figure 15: Reflection profiles collected with the 250 MHz antenna of Grave 1A for Months 1, 6, 12, 18, 24, and 30

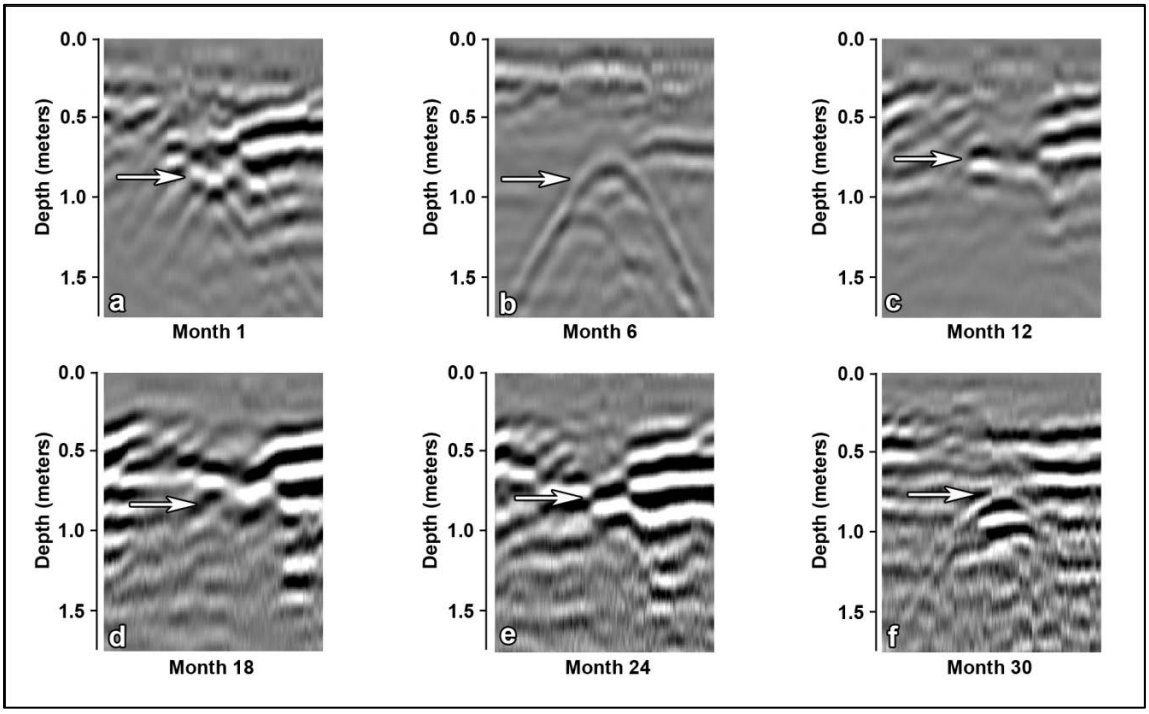

Figure 16: Reflection profiles collected with the 250 MHz antenna of Grave 1B for Months 1, 6, 12, 18, 24, and 30.

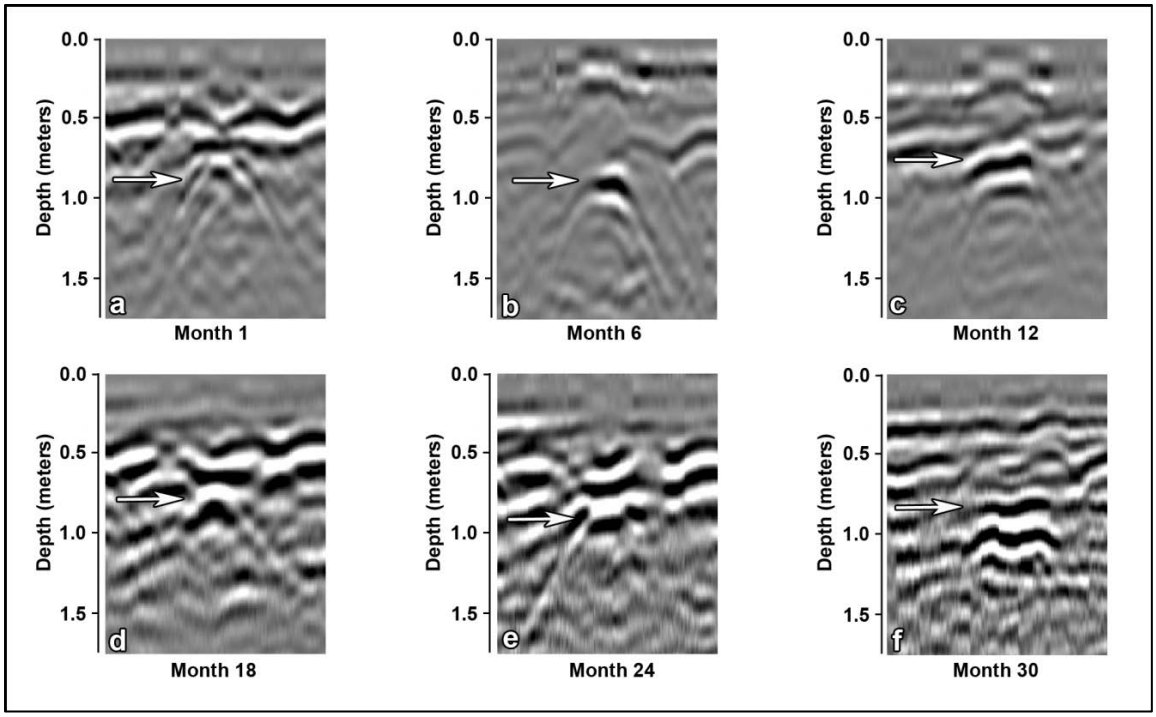

Figure 17: Reflection profiles collected with the 250 MHz antenna of Grave 1C for Months 1, 6, 12, 18, 24, and 30.

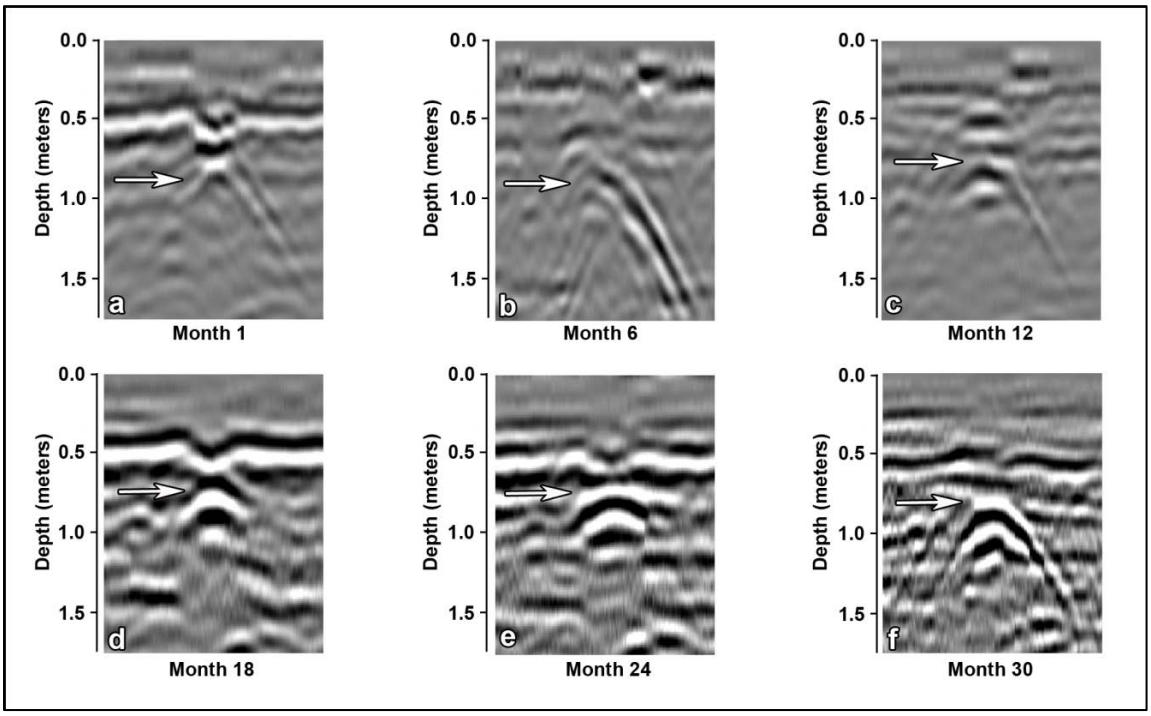

Figure 18: Reflection profiles collected with the 250 MHz antenna of Grave 1D for Months 1, 6, 12, 18, 24, and 30.

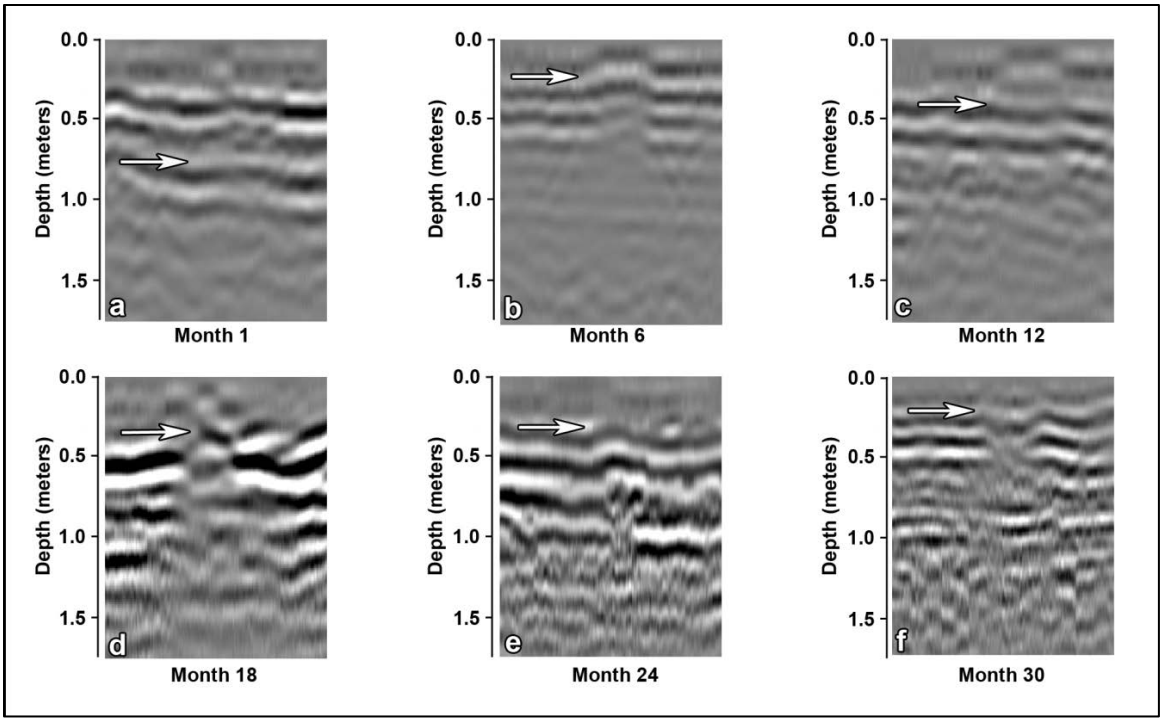

Figure 19: Reflection profiles collected with the 250 MHz antenna of Grave 2A for Months 1, 6, 12, 18, 24, and 30.

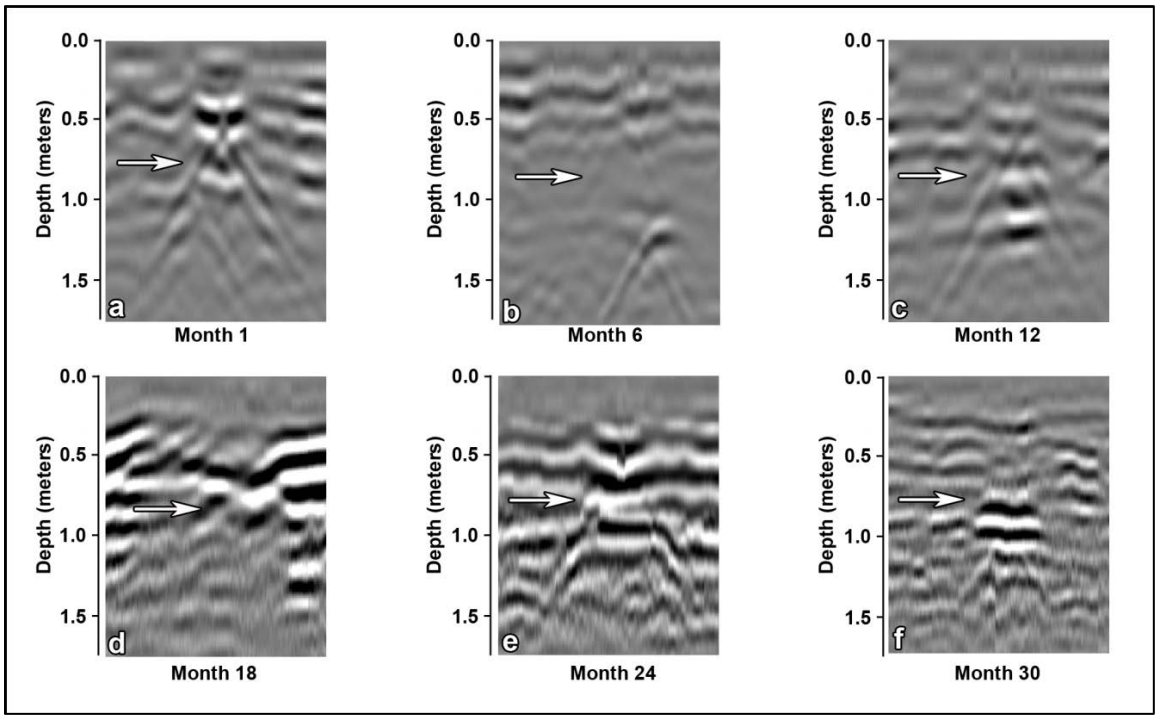

Figure 20: Reflection profiles collected with the 250 MHz antenna of Grave 2B for Months 1, 6, 12, 18, 24, and 30.

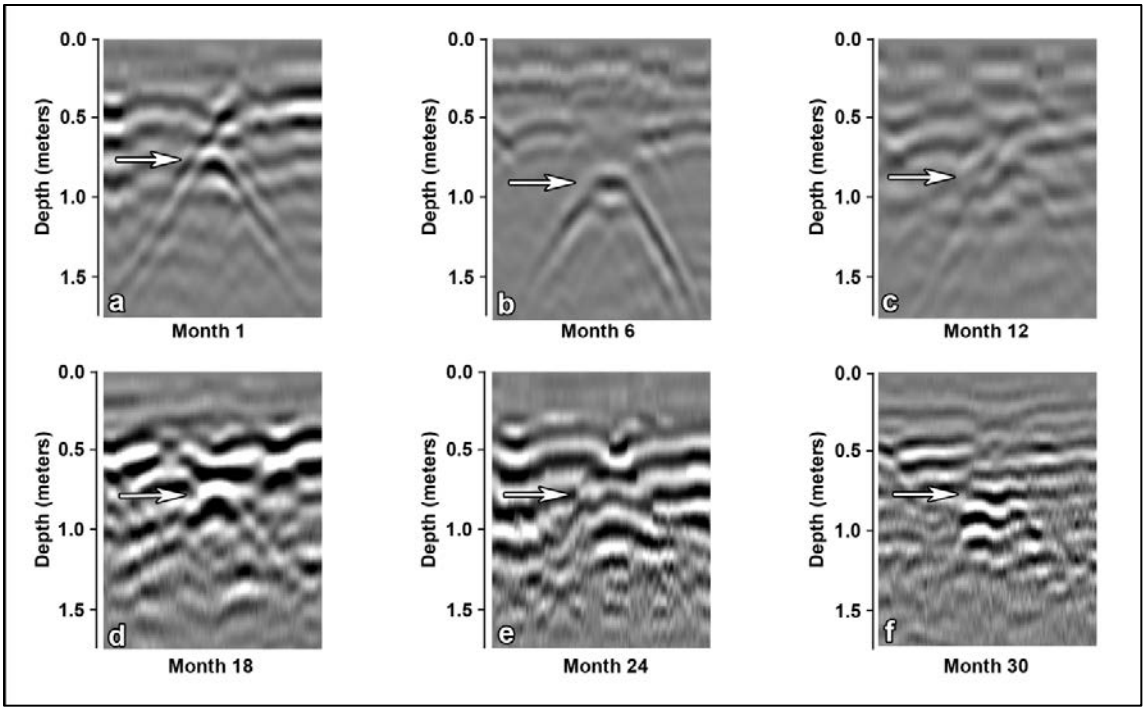

Figure 21: Reflection profiles collected with the 250 MHz antenna of Grave 2C for Months 1, 6, 12, 18, 24, and 30.

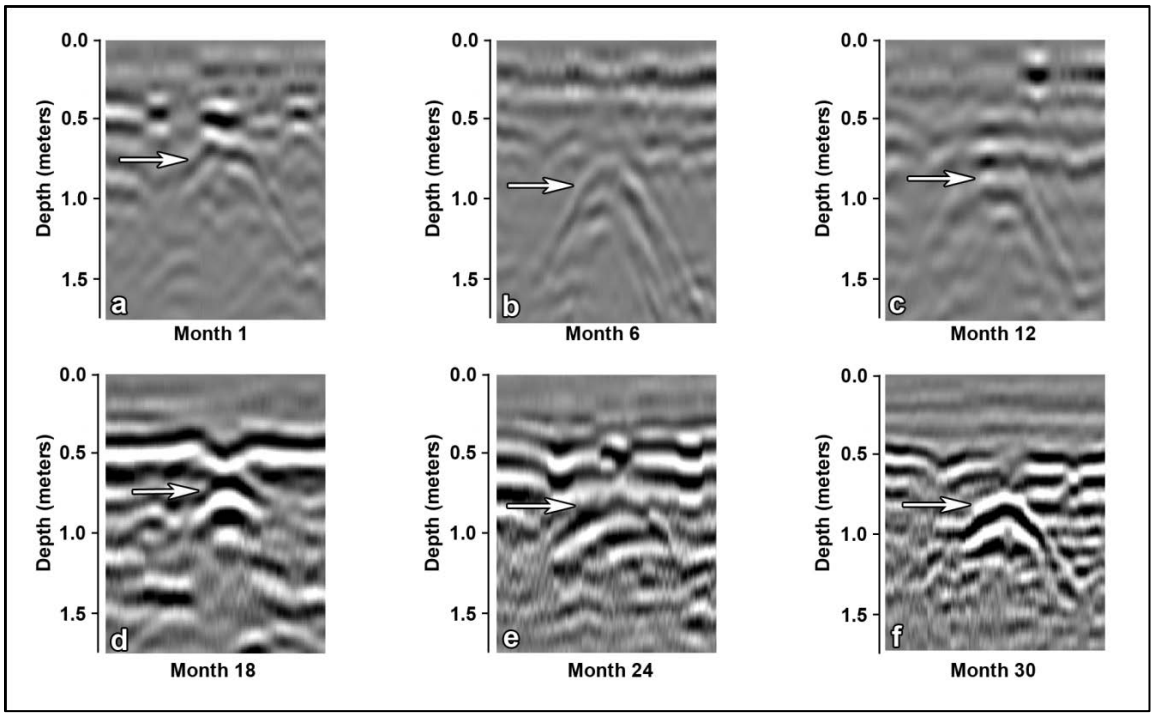

Figure 22: Reflection profiles collected with the 250 MHz antenna of Grave 2D for Months 1, 6, 12, 18, 24, and 30.

The response for the blank controlled graves differed. For example, there was an apparent visibility difference between the shallow control grave (Grave 2A) and the shallow pig grave (Grave 1A). While the control grave (Grave 2A) was only visible for 1 month with the 500 MHz antenna and 0 months with the 250 MHz, the shallow pig grave (Grave 1A) was visible for 22 months with the 500 MHz antenna and 18 months with the 250 MHz antenna. These results clearly indicate that the shallow pig grave (Grave 1A) was being detected because of the buried pig carcass remains and not the disturbed soil of the grave. Since the soil profile of the shallow graves primarily consisted of sand horizons, these results are not surprising as previous research has shown that the soil disturbance of controlled graves in sandy soil horizons in central Florida are generally not detected (Schultz et al., 2006; Schultz, 2008). While the soil profile consisted of a spodic horizon, it was at a depth below the shallow graves and, thus, was not disrupted. As a result, the backfill of the grave was generally not detected over the course of the study because of the low conductivity of the fairly homogeneous sandy soils, even with compaction over the monitoring period.

Conversely, there were unexpected results with the visibility of the deep control grave (Grave 2B) for 24 out of 30 months. The compaction of the backfill during the monitoring period did not necessarily lead to a grave response. However, the soil profile at the research site for the deep graves consisted of a spodic horizon which is an alluvial horizon consisting of an accumulation of organic matter, aluminum oxide, and possibly iron oxide (Brady and Weil, 2002). Since composition of the spodic horizon contrasted with the generally homogenous sandy soil horizons, the soil disruption of the spodic horizon was detected.

Length of interment and moisture trends for the graves was a consideration for visibility. While it was possible to discern a number of graves after 30 months of interment, additional

processing was needed and moisture differences also affected the visibility of the graves when using the reflection profiles. Over time, increased gain was required to increase the visibility, as the response from the graves decreased (Figure 23). Moisture trends were determined by comparing the total monthly precipitation with the visibility score of the graves. A general trend of increased moisture produced increased visibility. For example, over the 3 months of data collection using the 250 MHz with decreased moisture there was reduced visibility of graves as no graves were scored as Excellent, and the majority of graves were scored as Poor. By Month 4, the total monthly rainfall increased (Table 9) resulting in seven out eight visibility scores of Excellent for the 250 MHz (Table 5). The same trend was also observed with the 500 MHz data using the reflection profiles (Tables 3 and 10). Furthermore, another example of increased moisture producing increased visibility is with Month 21 for the 250 MHz reflection profile data. During Month 21, the total monthly rainfall was 0 inches compared to 5.67 inches for Month 20 and 1.67 inches for month 22 (Table 9). When the visibility data (Table 5) is compared to the moisture data (Table 9), Month 21 (Figure 24b) had decreased visibility compared to the Months 20 (Figure 24a) and 22 (Figure 24c). Only two out of eight graves were visible for Month 21 as scores of Good. Conversely, five out of eight graves, with five Excellent scores, were visible for Month 20, and five out of eight graves were visible for Month 22.

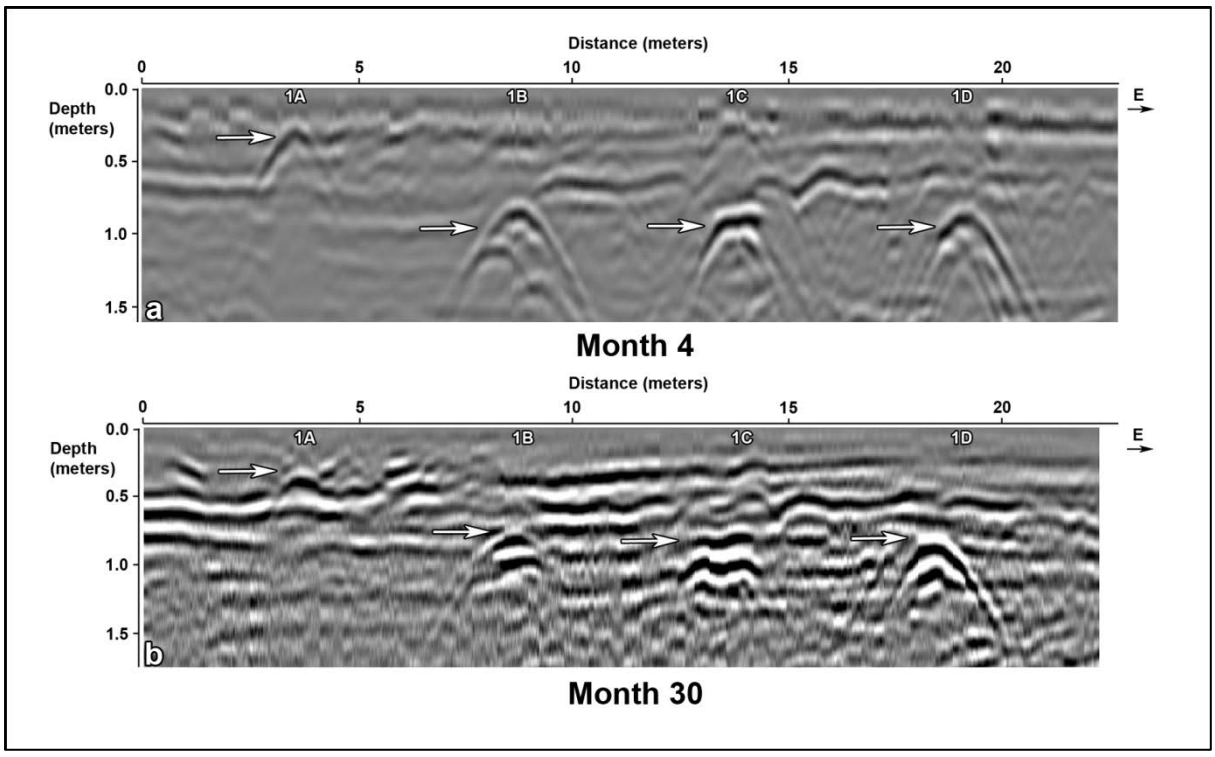

Figure 23: Reflection profiles collected with the 250 MHz antenna for Months 4 (a) and 30 (b) displaying the need for increased gain for later months (e.g. Month 30) to view the grave reflections

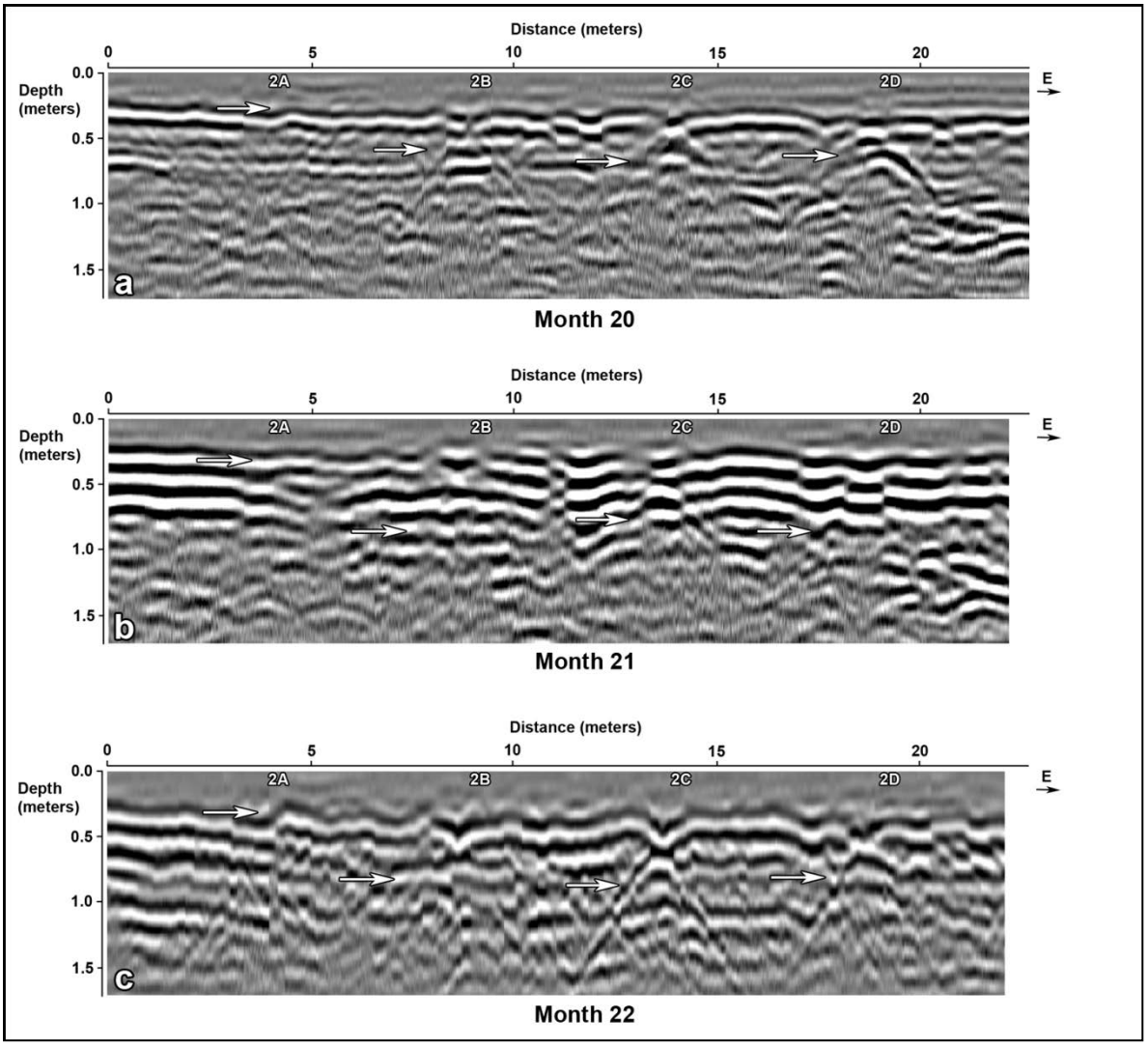

Figure 24: Reflection profiles collected with the 250 MHz antenna for Months 20, 21, and 22 showing a decreased response for Month 21 that correlated with lower precipitation.

Table 9: Temperature and precipitation data from the NOAA correlated to 250 MHz antenna data collection dates

Month	Daily Maximum Temp (°C)	Daily Mean Temp (°C)	Avg Monthly Temp (°C)	Highest Temp of Month (°C)	ADD* (°C)	Daily Rainfall (in)	Total Monthly Rainfall (in)
1	22.22	14.44	15.83	29.44	781.11	0.00	0.62
2	32.78	25.00	19.72	32.22	2177.78	0.00	0.48
3	30.00	23.33	410.83	32.78	3288.89	0.00	1.01
4	31.67	26.67	25.44	36.11	4765.00	0.00	14.56
5	32.78	28.89	27.78	36.11	5960.00	0.00	8.05
6	33.33	27.78	27.78	34.44	7281.11	0.00	6.05
7	33.89	28.33	28.50	35.00	8858.33	0.36	4.74
8	33.33	27.22	27.50	33.89	10180.56	0.00	4.58
9	33.33	27.78	25.22	35.00	11473.33	0.00	2.85
10	26.11	19.44	20.78	30.56	12755.56	0.00	1.00
11	11.67	6.11	17.67	29.44	13949.44	0.00	5.39
12	16.11	12.78	12.44	28.33	14761.11	0.00	3.53
13	21.67	12.78	12.61	24.44	15646.11	0.00	4.35
14	25.00	17.22	16.06	26.67	16668.89	0.00	8.87
15	24.44	19.44	21.72	31.11	17778.89	0.00	4.73
16	32.78	27.78	26.11	33.33	19223.33	0.66	3.00
17	33.89	30.00	28.56	37.22	20571.67	0.00	3.23
18	36.11	31.67	28.89	36.67	22068.89	0.00	4.26
19	31.67	28.33	28.83	36.11	23472.78	0.01	5.62
20	27.78	25.00	27.67	35.00	24886.11	0.00	5.67
21	32.78	27.22	23.50	33.33	26046.67	0.00	0.00
22	26.67	23.33	19.83	30.00	27260.56	0.06	1.68
23	21.67	16.11	11.11	25.00	28313.33	0.00	0.78
24	25.00	18.33	15.22	27.22	29231.11	0.00	5.92
25	26.11	20.56	18.94	31.11	30341.11	0.00	0.25
26	26.11	20.00	20.56	33.33	31492.22	0.00	5.74
27	30.00	22.78	24.28	35.00	32680.56	0.00	0.65
28	28.33	24.44	25.72	35.56	34115.00	0.42	2.10
29	30.00	26.67	28.11	37.22	35453.33	1.36	7.34
30	33.89	29.44	28.11	35.00	37035.56	0.02	9.11

* ADD stands for Accumulated Degree Days

Table 10: Temperature and precipitation data from the NOAA correlated to 500 MHz antenna data collection dates

Month	Daily Maximum Temp (°C)	Daily Mean Temp (°C)	Avg Monthly Temp (°C)	Highest Temp of Month (°C)	ADD* (°C)	Daily Rainfall (in)	Total Monthly Rainfall (in)
1	22.22	14.44	15.83	29.44	781.11	0.00	0.62
2	32.78	25.00	19.72	32.22	2177.78	0.00	0.48
3	30.00	23.33	410.83	32.78	3165.00	0.00	1.01
4	31.11	26.11	25.44	36.11	4720.56	0.00	14.56
5	32.78	28.89	27.78	36.11	5913.33	0.01	8.05
6	31.67	27.22	27.78	34.44	7235.56	0.00	6.05
7	33.33	28.89	28.50	35.00	8766.11	0.00	4.74
8	31.67	26.67	27.50	33.89	10135.56	0.00	4.58
9	31.67	27.22	25.22	35.00	11427.78	0.00	2.85
10	25.56	18.33	20.78	30.56	12718.33	0.00	1.00
11	8.33	5.00	17.67	29.44	13926.67	0.00	5.39
12	17.22	13.33	12.44	28.33	14792.22	0.62	3.53
13	18.33	11.67	12.61	24.44	15615.56	0.00	4.35
14	22.78	17.22	16.06	26.67	16633.89	0.00	8.87
15	28.89	23.89	21.72	31.11	17701.11	0.55	4.73
16	33.33	27.78	26.11	33.33	19268.89	0.00	3.00
17	35.56	30.00	28.56	37.22	20476.67	0.04	3.23
18	35.56	30.00	28.89	36.67	21923.33	1.63	4.26
19	32.78	28.89	28.83	36.11	23426.11	0.00	5.62
20	30.00	25.00	27.67	35.00	24843.33	0.00	5.67
21	33.33	27.22	23.50	33.33	26001.67	0.00	0.00
22	29.44	23.89	19.83	30.00	27302.22	0.00	1.68
23	26.11	21.11	11.11	25.00	28279.44	0.01	0.78
24	27.78	20.56	15.22	27.22	29269.44	0.00	5.92
25	26.67	21.11	18.94	31.11	30302.78	0.11	0.25
26	31.11	25.00	20.56	33.33	31416.67	0.26	5.74
27	35.00	29.44	24.28	35.00	32640.00	0.00	0.65
28	31.67	26.11	25.72	35.56	34158.89	0.00	2.10
29	31.11	27.22	28.11	37.22	35498.33	0.63	7.34
30	35.00	29.44	28.78	35.00	36988.33	0.02	9.11

* ADD stands for Accumulated Degree Days

Implications for Policy and Practice

A number of guidelines (Objective 1) are suggested when performing a geophysical search for clandestine graves that should be implemented as standard practice. Out of all of the available geophysical equipment, GPR is generally the best option for locating clandestine graves. Operator experience should be of paramount importance when using this equipment. Operators should have forensic experience when evaluating whether a search can be performed, setting up a grid, performing the survey, and processing and interpreting the data.

If possible, the investigators should determine as much information about the burial prior to performing a geophysical search. For example, it would be useful to know the depth and size of the burial, if the body was wrapped with any materials, if any debris was placed over the body, and if any metal was placed in the grave. In addition, the search site should be inspected to determine if GPR will be suitable as a search tool. The GPR should be operated over a fairly level surface. Additionally, the presence of subsurface features such as tree roots, buried debris, cobbles, or buried pipes may result in false positives that can obscure the response from the body or grave. Therefore, ground-penetrating radar is best utilized in a field setting of short grass with the limited presence of trees and brush in order to minimize the masking effect of a root system when using the GPR. Also, soil type is a factor to consider. Dry, sandy soil is best for the application of GPR while wet, clayey soils will result in major wave attenuation. Prior knowledge of a search site will allow the GPR technician to formulate plausible predictions to law enforcement about the likelihood of a successful search. While utilization of the GPR is always recommended when the site features are appropriate, the GPR operator should also make sure that law enforcement personnel also understand the limitations of detecting graves for extended postmortem intervals.

Once the site is properly assessed and prepared, a grid must be constructed with transects spaced close enough to ensure grave detection but far enough to allow more efficient operations as well as minimize the amount of time required for a search to be performed. In this research, the GPR unit was operated along transect spacing of 0.25 m apart. This spacing provided an excellent medium between the two previous constraints, allowing human cadaver-sized graves (the pig carcass proxies) to be detected across a set of five transects while minimizing the amount of time needed in the field. Additionally, if the area being surveyed is small enough and if time allows, utilization of multiple antennae operating at high and low frequencies is advised for a broader dataset with which to investigate. If there are time constraints, pre-survey testing can be performed to determine which antenna is more suitable to the local soils.

If subsurface anomalies are discernible on reflection profiles, a preliminary assessment can be made in the field. At the same time, after all of the grid data has been collected in the field, it should be brought back to the office for processing and for further analysis using both the reflection profiles and horizontal slices. Doing so will allow the GPR technician to possibly be able to discern anomalies that were not visible in the field before the data was processed. Showing an anomaly in both a reflection profile and horizontal slice will allow the operator to infer the size and depth of a feature buried in the subsurface.

The last task of a survey is to ground truth, or use some invasive field technique, when checking the areas that produced anomalies. The GPR operator should be able to evaluate which anomalies need to be checked first. If all of the anomalies are checked and no evidence of a clandestine burial is detected, the GPR operator must decide if the area has been cleared of a clandestine burial. If it is not possible to clear the area, then other more invasive search methods may have to be implemented.

Implications for Future Research

Controlled forensic geophysical research involving GPR has proven to be a valuable resource in the last two decades, and the information gathered from these studies has been applied to real-life forensic cases. Controlled research is vital to understand the applicability of using GPR for forensic applications and to understand the various factors that affect detection. In particular, as this research has shown, it is important to understand how long a grave will be detected in various soil types and for extended postmortem intervals. In certain soils, it may not be possible to detect a grave with GPR for short interment periods after decomposition of the body and grave compaction. Results from this research indicate that even under favorable soil conditions, the detection of clandestine graves will vary within short temporal scales. Further studies should be funded that address the long term applicability of GPR for detecting graves in different soils and environments so investigators will have a higher rate of success in their local areas.

V. References

Bevan BW. 1983. Electromagnetics for mapping buried earth features. Journal of Field Archaeology 10(1): 47-54.

Brady NC, Weil RR. 2002. The nature and properties of soil. Upper Saddle River: Prentice Hall.

Clay RB. 2005. Conductivity survey: A survival manual. Cultural Resource Analysts, Inc.

Conyers LB. 2004. Ground-penetrating radar for archaeology. Walnut Creek, CA: AltaMira Press.

Conyers LB, Cameron C. 1998. Ground-Penetrating radar techniques and three-dimensional computer mapping in the American southwest. Journal of Field Archaeology 25(4):417-430.

Conyers LB, Goodman D. 1997. Ground-Penetrating radar: An introduction for archaeologists. Walnut Creek, CA: AltaMira Press.

Davenport CG. 2001a. Remote sensing applications in forensic investigations. Historical Archaeology 35:87-100.

Davenport CG. 2001b. Where is it? Searching for buried bodies and hidden evidence. Church Hill: SportWork.

Dionne CA, Schultz JJ, Murdock RA, Smith SA. 2011. Detecting buried metallic weapons in a controlled setting using a conductivity meter. Forensic Sciences International 2008:18-24

Dionne CA, Wardlaw DK, Schultz JJ. 2010. Delineation and resolution of cemetery graves using geophysical methods. Technical Briefs in Historical Archaeology 5:20-30.

Doolittle JA, Schellentrager G. 1989. Soil survey of Orange County, FL. United States Department of Agriculture, National Cooperative Soil Survey.

Dupras TL, Schultz JJ, Wheeler SM, Willimas LJ. 2006. Forensic recovery of human remains: archaeological approaches. Boca Raton: CRC Press.

France DL, Griffin TJ, Swanburg JG, Lindemann JW, Davenport GC, Trammell V, et al. 1992. A multidisciplinary approach to the detection of clandestine graves. Journal of Forensic Sciences 37:1445-1458.

France DL, Griffin TJ, Swanburg JG, Lindemann JW, Davenport GC, Trammell V, et al. 1997. NecroSearch revisited: further multidisciplinary approaches to the detection of clandestine graves. In: Haglund WD, Sorg MH, editors. Forensic taphonomy: The postmortem fate of human remains. Boca Raton: CRC Press, p 497-509.

Freeland RS, Miller ML, Yoder RE, Koppenjan SK. 2003. Forensic applications of FM-CW and pulse radar. Journal of Environmental & Engineering Geophysics 8:97-103.

Isaacson J, Hollinger RE, Gundrum D, Baird J. 1999. A controlled test site facility in Illinois: training and research in archaeogeophysics. Journal of Field Archaeology 26(2):227-236.

Killam EW. 2004. The detection of human remains, 2nd edition. Springfield, IL: Charles C. Thomas.

Martin M. 2010. Detecting various burial scenarios in a controlled setting using ground-penetrating radar and conductivity. Master's Thesis. Department of Anthropology, University of Central Florida.

Mellett JS. 1992. Location of human remains with ground-penetrating radar. In: Hanninen P, Autio S, editors. Fourth International Conference on Ground Penetrating Radar June 8-13. Rovaniemi, Finland: Geological Survey of Finland, Special Paper 16:359-65.

Nobes DC. 2000. The search for "Yvonne": a case example of the delineation of a grave using near-surface geophysical methods. Journal of Forensic Sciences 45:715-721.

Novo A, Lorenzo H, Rial FI, Solla M. 2011. 3D GPR in forensics: Finding a clandestine grave in a mountainous environment. Forensic Science International 204:134-138.

Pomfret. 2006. Ground-Pentrating radar profile spacing and orientation for subsurface resolution of linear features. Archaeology Prospection 13(2):151-153.

Pye K, Croft DJ. 2004. Forensic geoscience: principles, techniques, and applications. London: Geological Society Special Publications.

Reynolds JM. 1997. An introduction to applied and environmental geophysics. New York: John Willey and Sons, Inc.

Ruffell A. 2005. Searching for the IRA "disappeared": ground-penetrating radar investigation of a churchyard burial site, Northern Ireland. Journal of Forensic Science 50:1430-1435.

Ruffell A, Donnelly C, Carver N, Murphy E, Murray E, McCambridge J. 2009. Suspect burial excavation procedure: a cautionary tale. Forensic Science International 183:11-16.

Schultz JJ. 2007. Using ground-penetrating radar to locate clandestine graves of homicide victims: forming forensic archaeology partnerships with law enforcement. Homicide Studies 11(11):15-29.

Schultz JJ. 2008. Sequential monitoring of burials containing small pig cadavers using ground penetrating radar. Journal of Forensic Sciences 53:279-287.

Schultz JJ, Collins ME, Falsetti AB. 2006. Sequential monitoring of burials containing large pig cadavers using ground-penetrating radar. Journal of Forensic Sciences 51:607-616.

Schultz JJ, Martin MM. 2011. Controlled GPR grave research: Comparison of reflection profiles between 500 and 250 MHz antennae. Forensic Science International 209:64-69.

Schurr MR. 1997. Using the concept of the learning curve to increase productivity of geophysical surveys. Archaeological Prospection 4(2):69-83.

Strongman KB. 1992. Forensic applications of ground-penetrating radar. In: Pilon J, editor. Ground-pentrating radar. Ottowa: Geological Surbey of Canada. Pp 203-211.

Ward GH. 1990. Geotechnical and environmental geophysics. Tulsa: Society of Exploration and Geophysicists.

Watters M, Hunter JR. 2004. Geophysics and burials: field experience and software development. In: Pye K, Croft DJ, editors. Forensic geosciences: principles, techniques, and applications. London: Geological Society. Pp 21-31.

VI. Acknowledgements

I would like to thank Robert K. Banks, Office of Research and Commercialization, WAF facility for logistics obtaining the pig carcasses. Also, thanks to the numerous undergraduate and graduate students for their help in collecting data for this project.

VII. Dissemination of Research Findings

Presentations

Martin MM, Schultz JJ. 2010. Detecting Various Burial Scenarios in a Controlled Setting using Ground- Penetrating Radar. Poster presented at the annual meeting of the American Academy of Forensic Sciences, Seattle, Washington (February).

Hawkins W, Fletcher J, Schultz JJ. 2011. Monitoring the Long-Term Applicability of Ground Penetrating Radar Using Proxy Cadavers. Poster presented at the annual meeting of the American Academy of Forensic Sciences, Chicago (February).

Theses Completed

Michael MM. 2010. *Using GPR to locate controlled grave scenarios*. M.A. Thesis, Department of Anthropology, University of Central Florida. Degree awarded Spring 2010

Hawkins WT. 2011. *Using GPR to locate controlled grave scenarios for long term interments*. M.A. Thesis, Department of Anthropology, University of Central Florida. Degree awarded Spring 2011

Peer Reviewed Journal Article

Schultz JJ, Martin MM. 2011. Controlled GPR Grave Research: Comparison of Reflection Profiles between 500 and 250 MHz Antennae. *Forensic Science International* 209:64-69.

Peer-reviewed Journal Article Submitted

Martin MM, Schultz JJ. Monitoring Controlled Representing Common Burial Scenarios with Ground Penetrating Radar. Submitted to the *Journal of Applied Geophysics*, July 2011.

VIII. Appendices

APPENDIX A: CONDUCTIVITY CONTOUR MAPS PRODUCED FROM ELECTROMAGNETIC INDUCTION

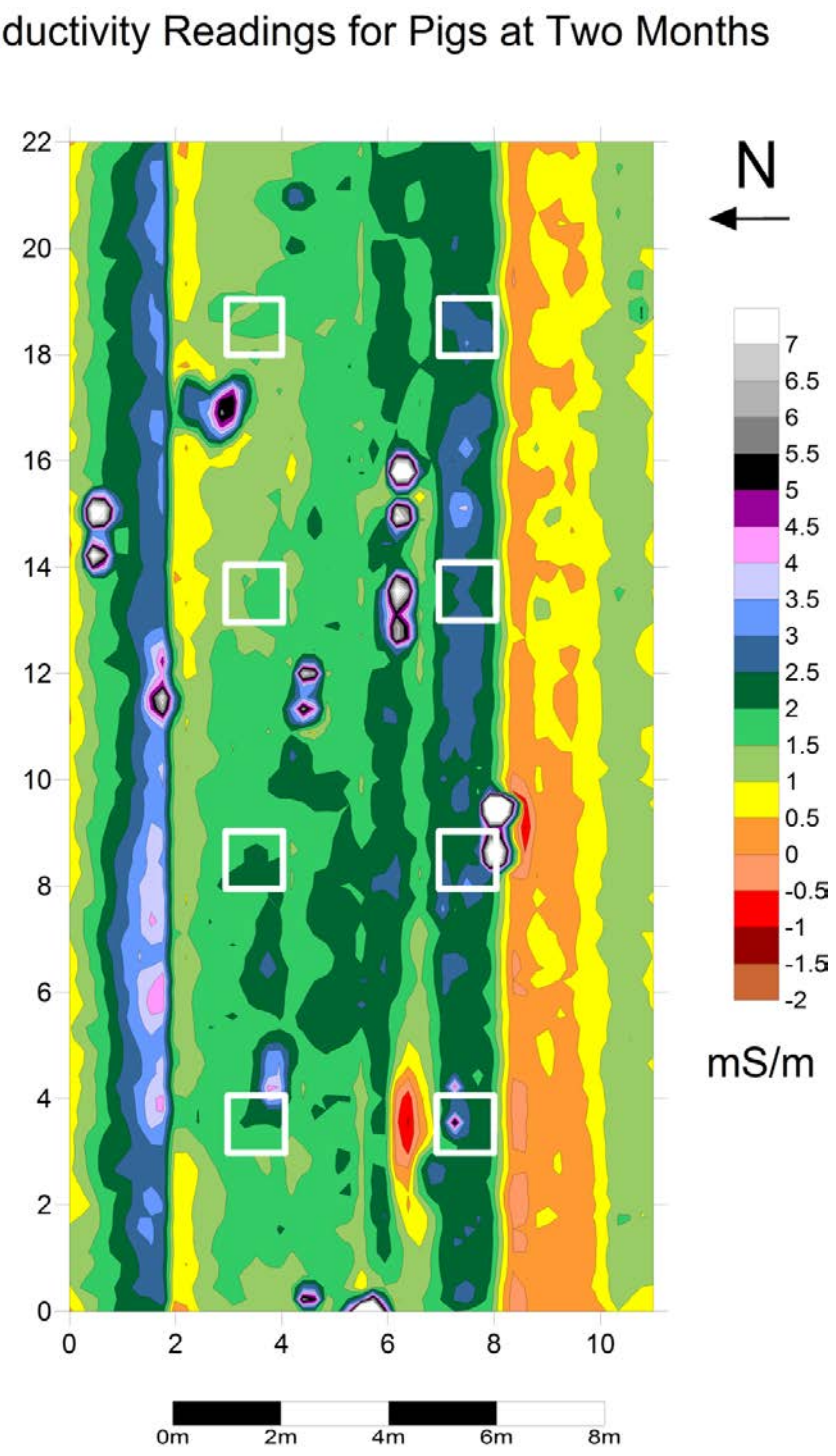

Figure A1: Conductivity map for pigs 2 months after interment

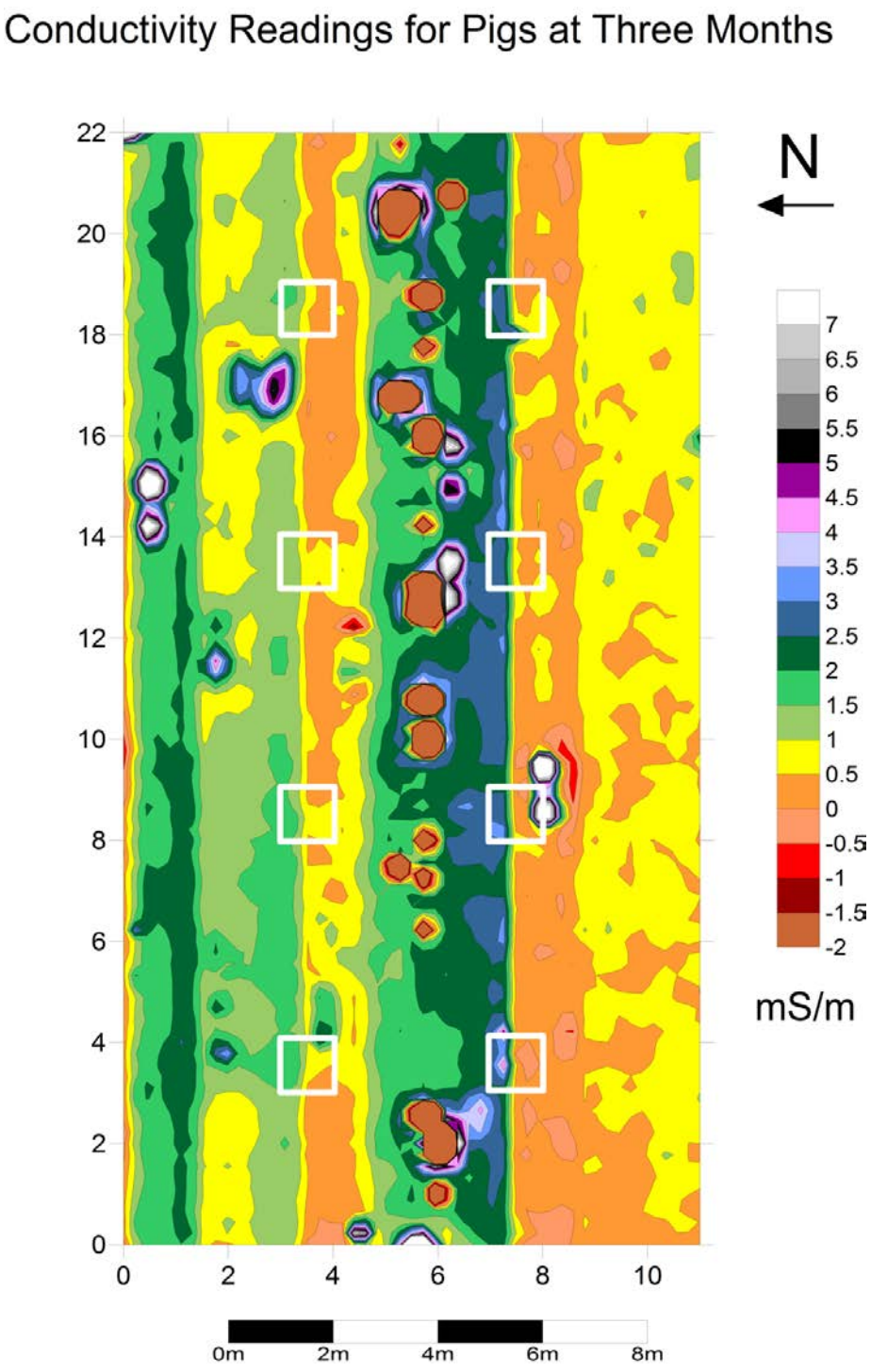

Figure A2: Conductivity map for pigs 3 months after interment

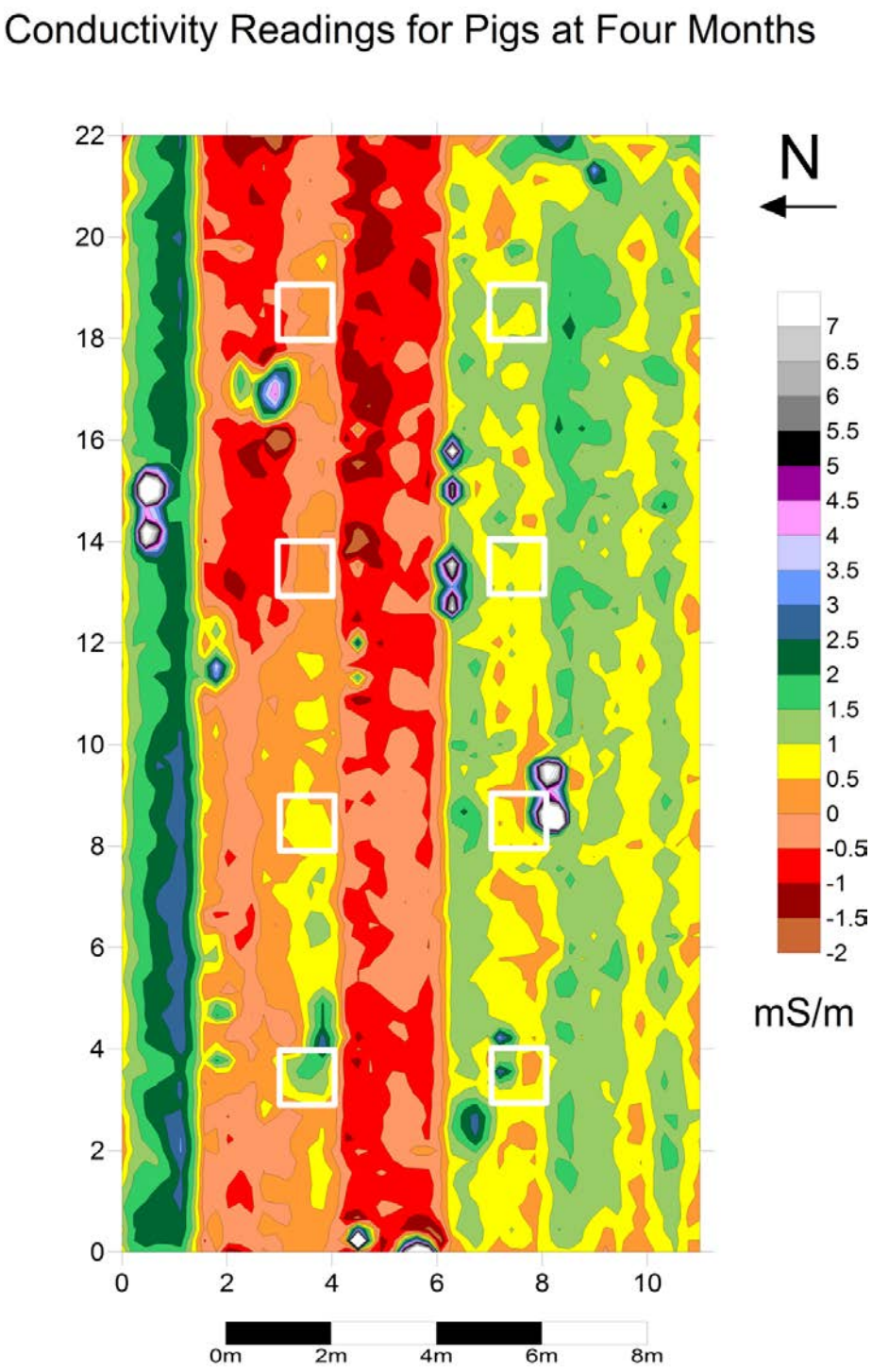

Figure A3: Conductivity map for pigs 4 months after interment

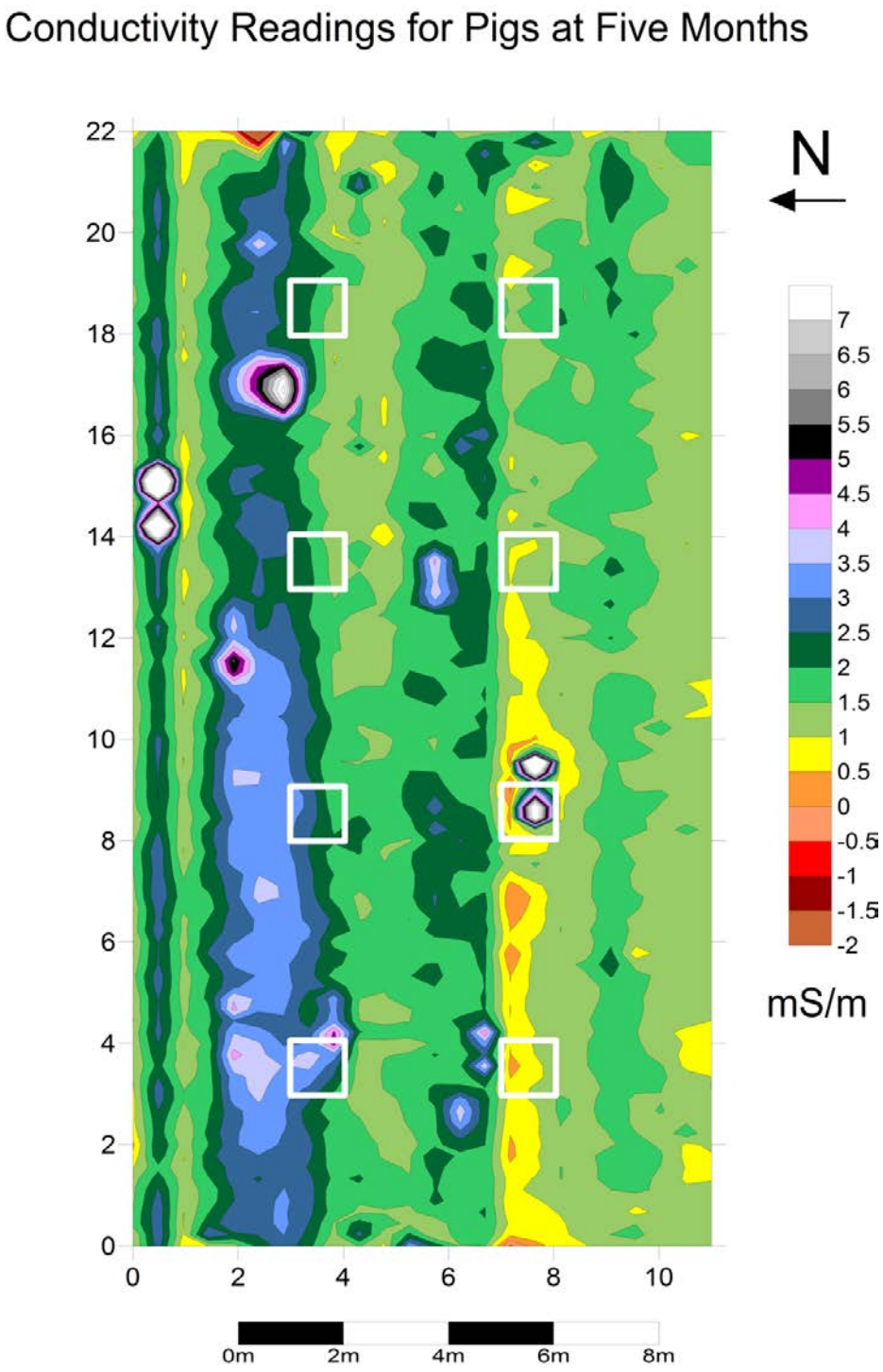

Figure A4: Conductivity map for pigs 5 months after interment

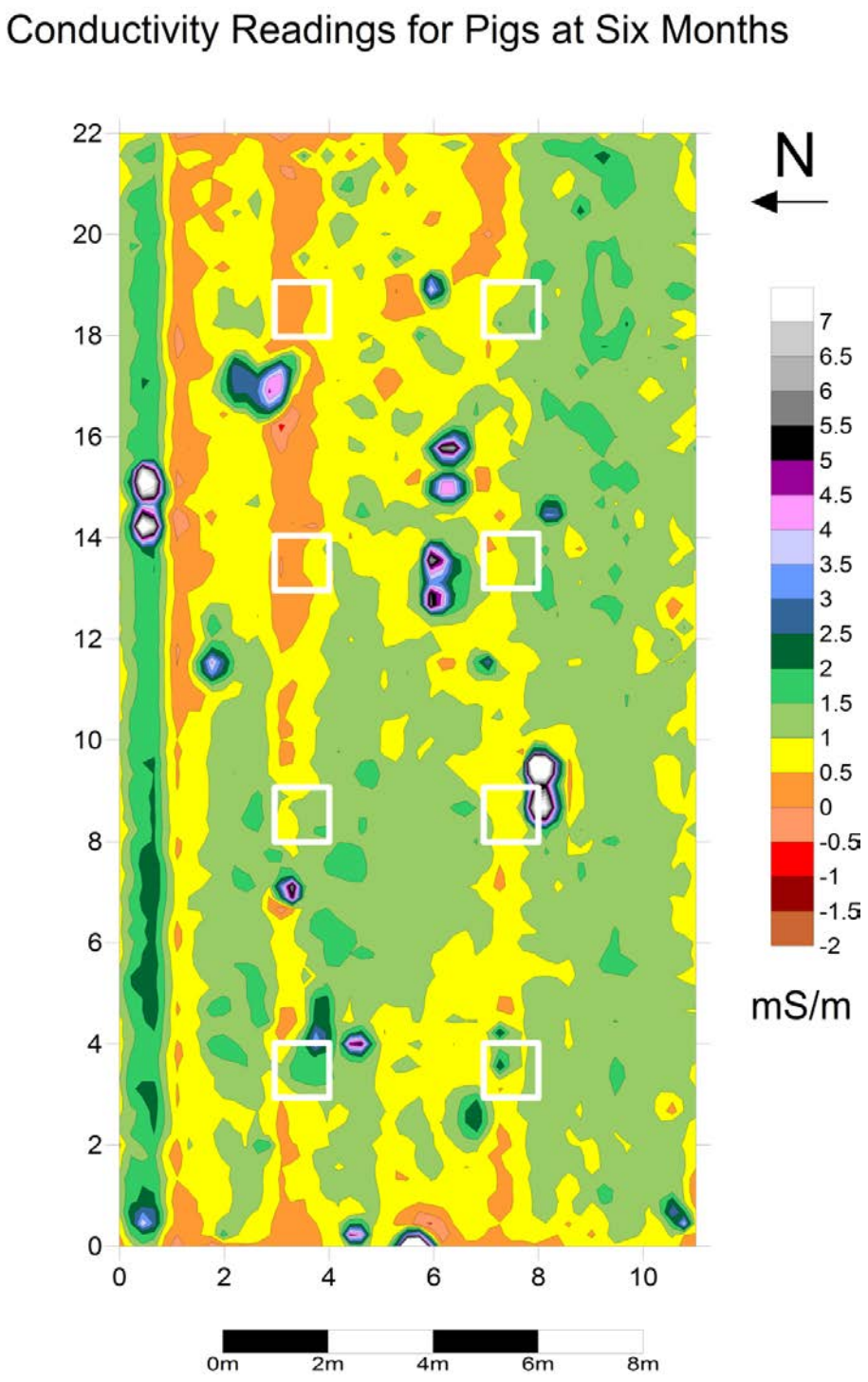

Figure A5: Conductivity map for pigs 6 months after interment

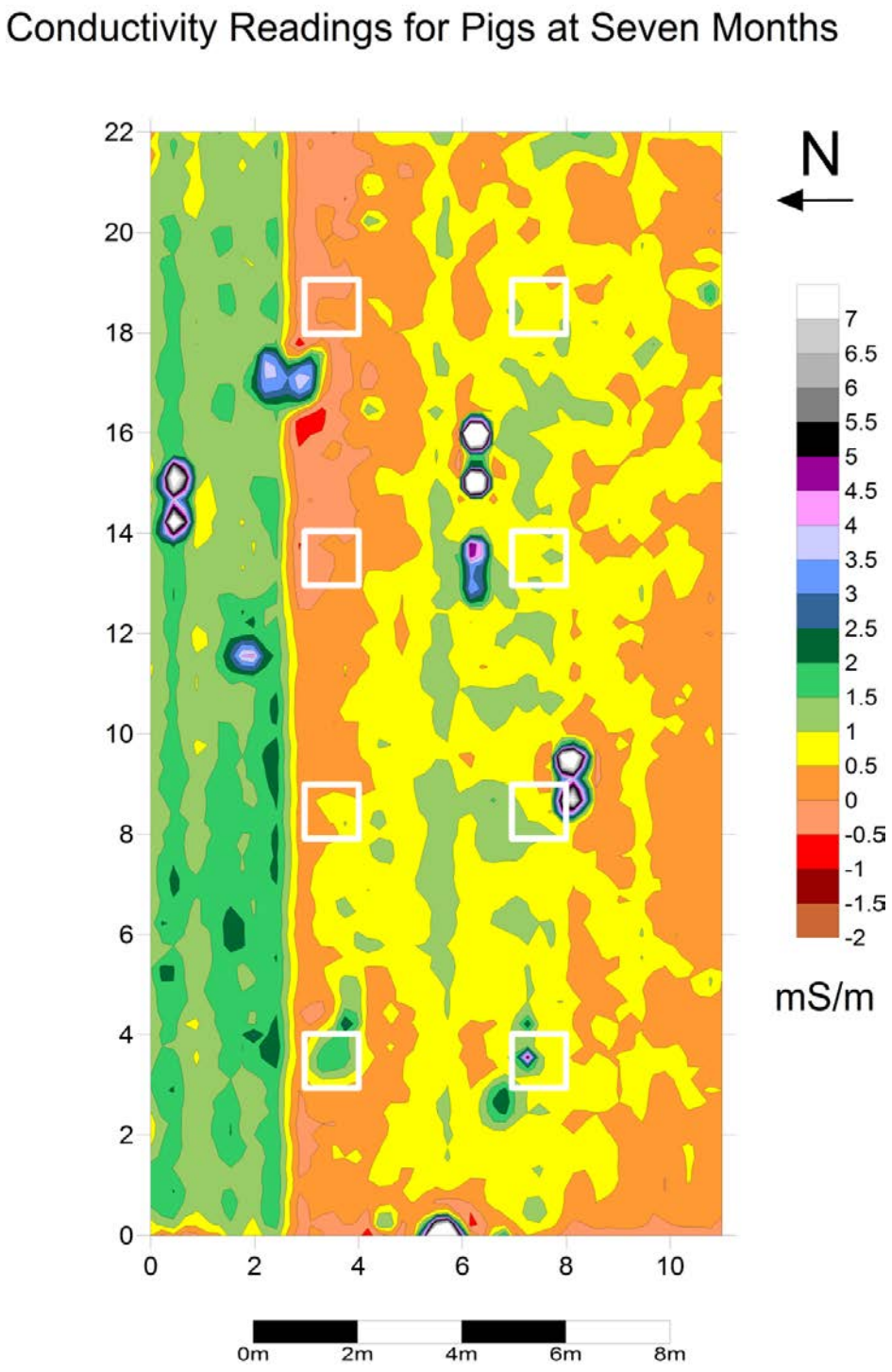

Figure A6: Conductivity map for pigs 7 months after interment

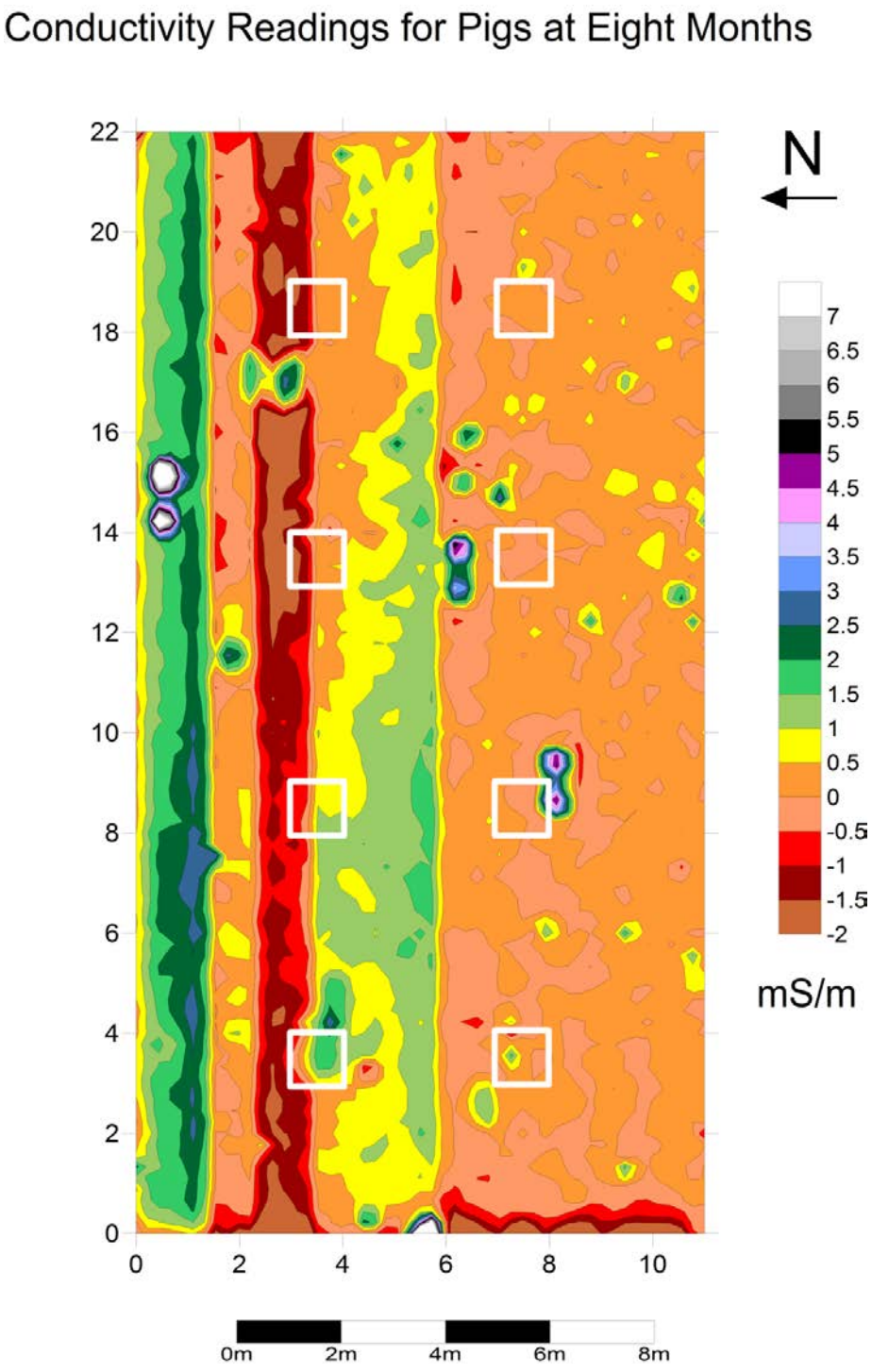

Figure A7: Conductivity map for pigs 8 months after interment

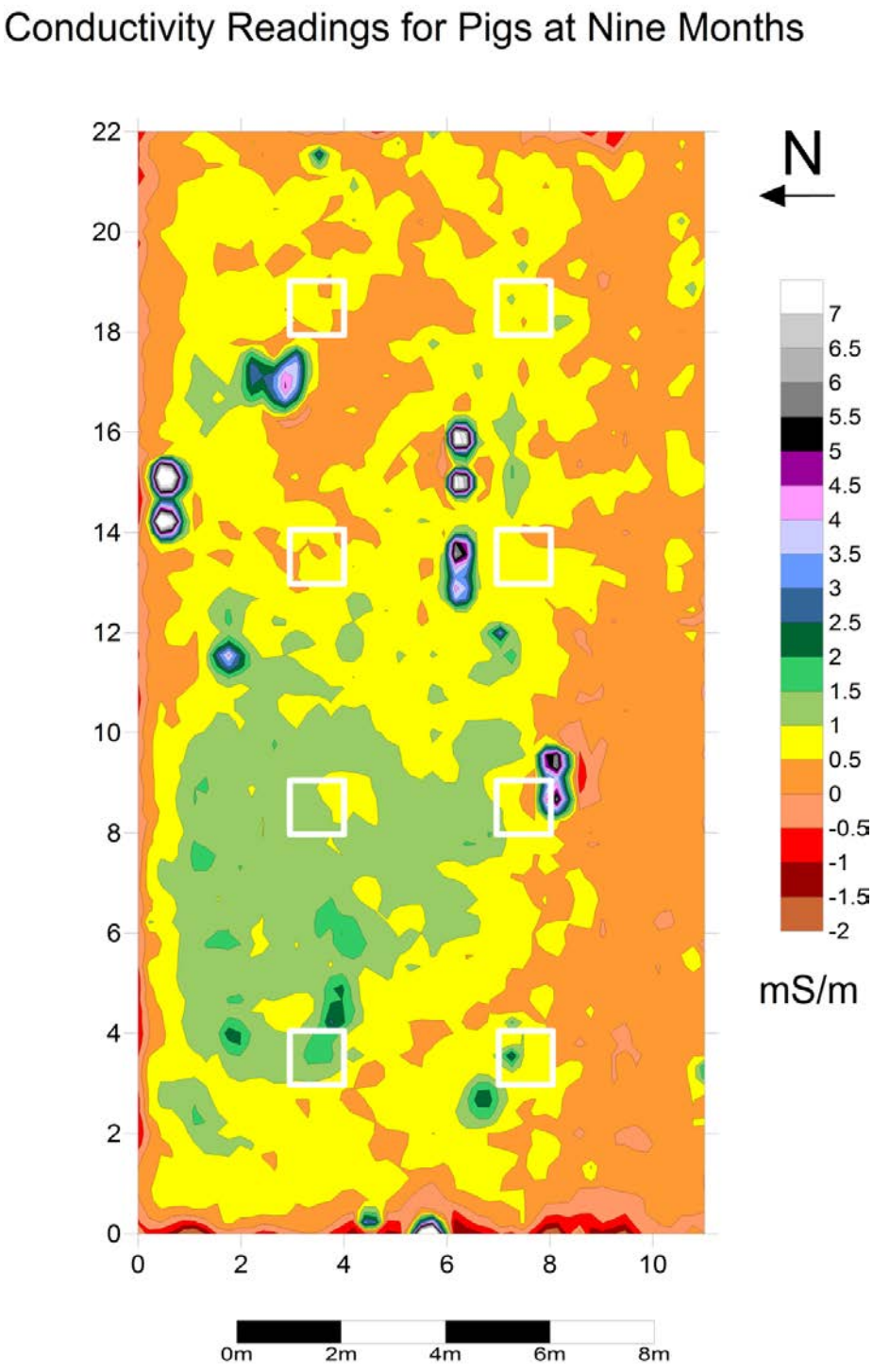

Figure A8: Conductivity map for pigs 9 months after interment

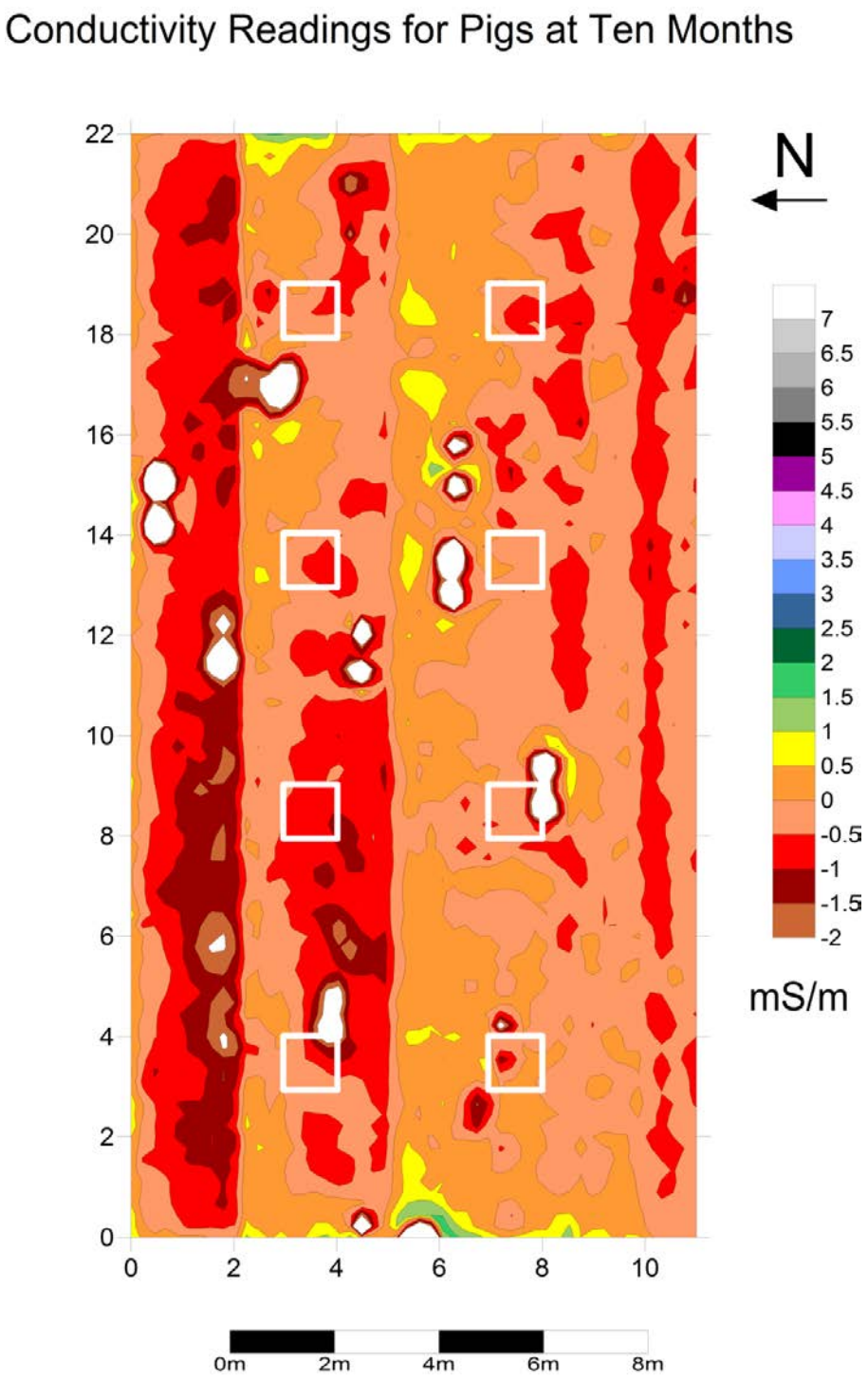

Figure A9: Conductivity map for pigs 10 months after interment

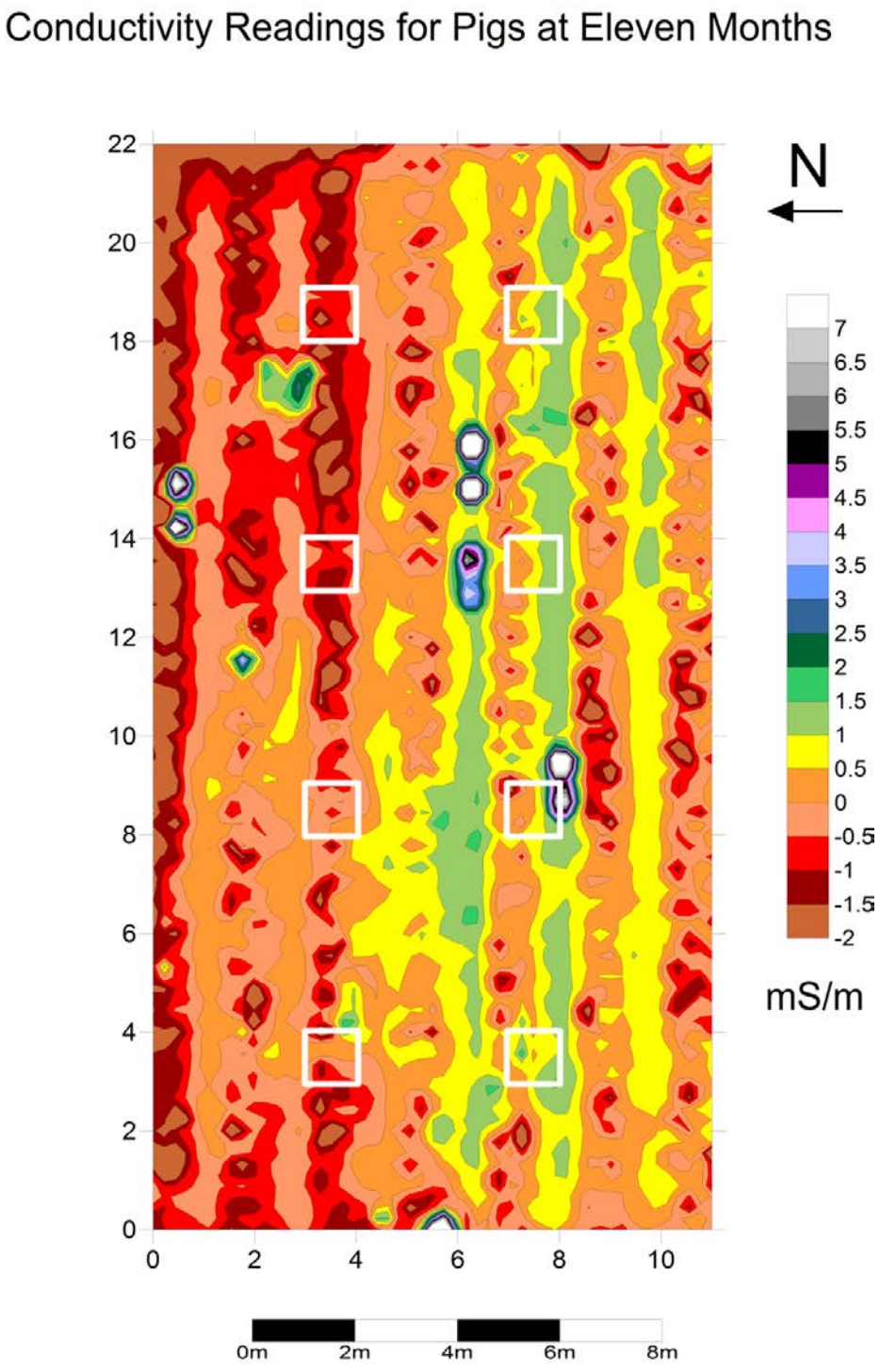

Figure A10: Conductivity map for pigs 11 months after interment

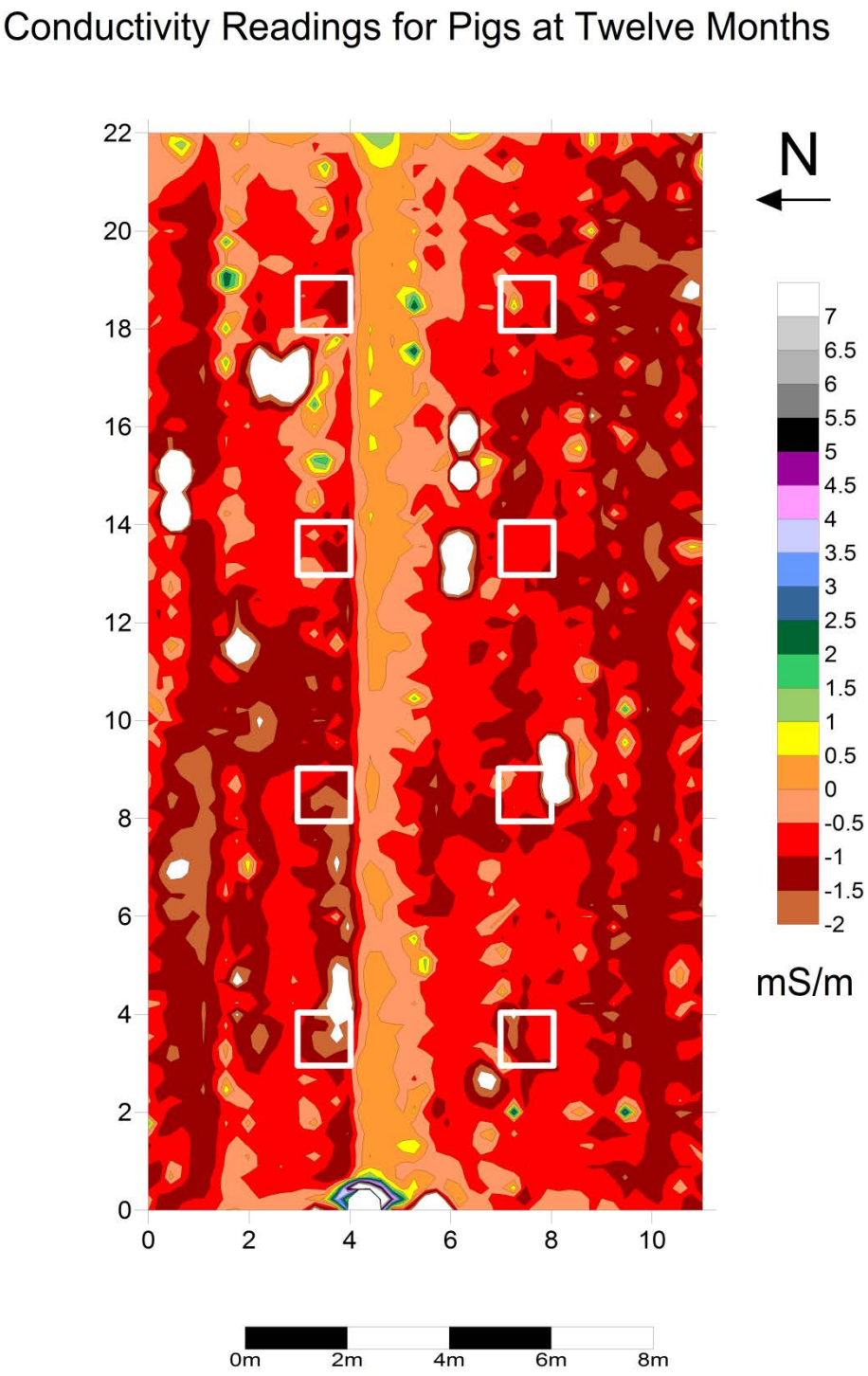

Figure A11: Conductivity map for pigs 12 months after interment

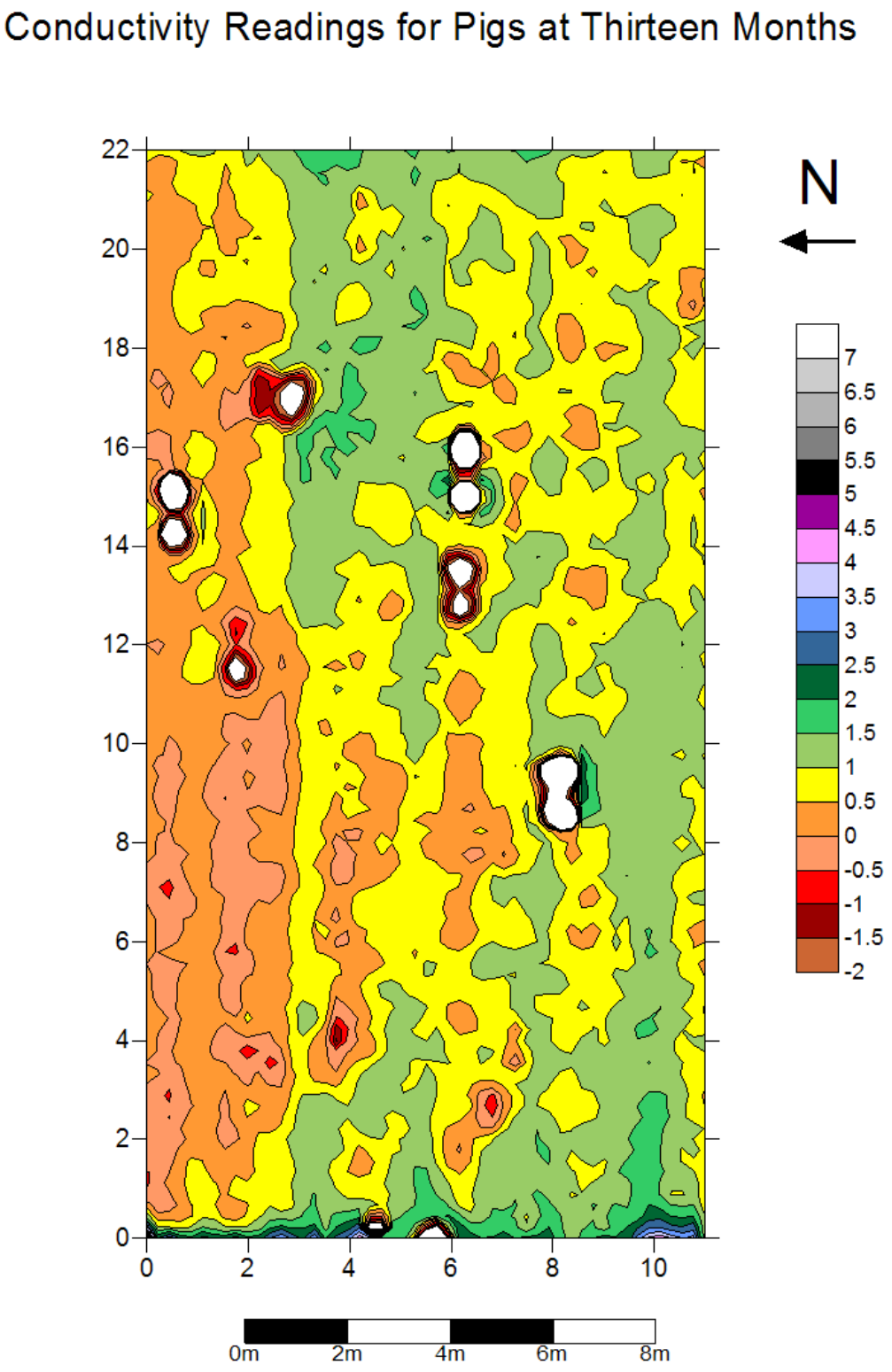

Figure A12: Conductivity map for pigs 13 months after interment

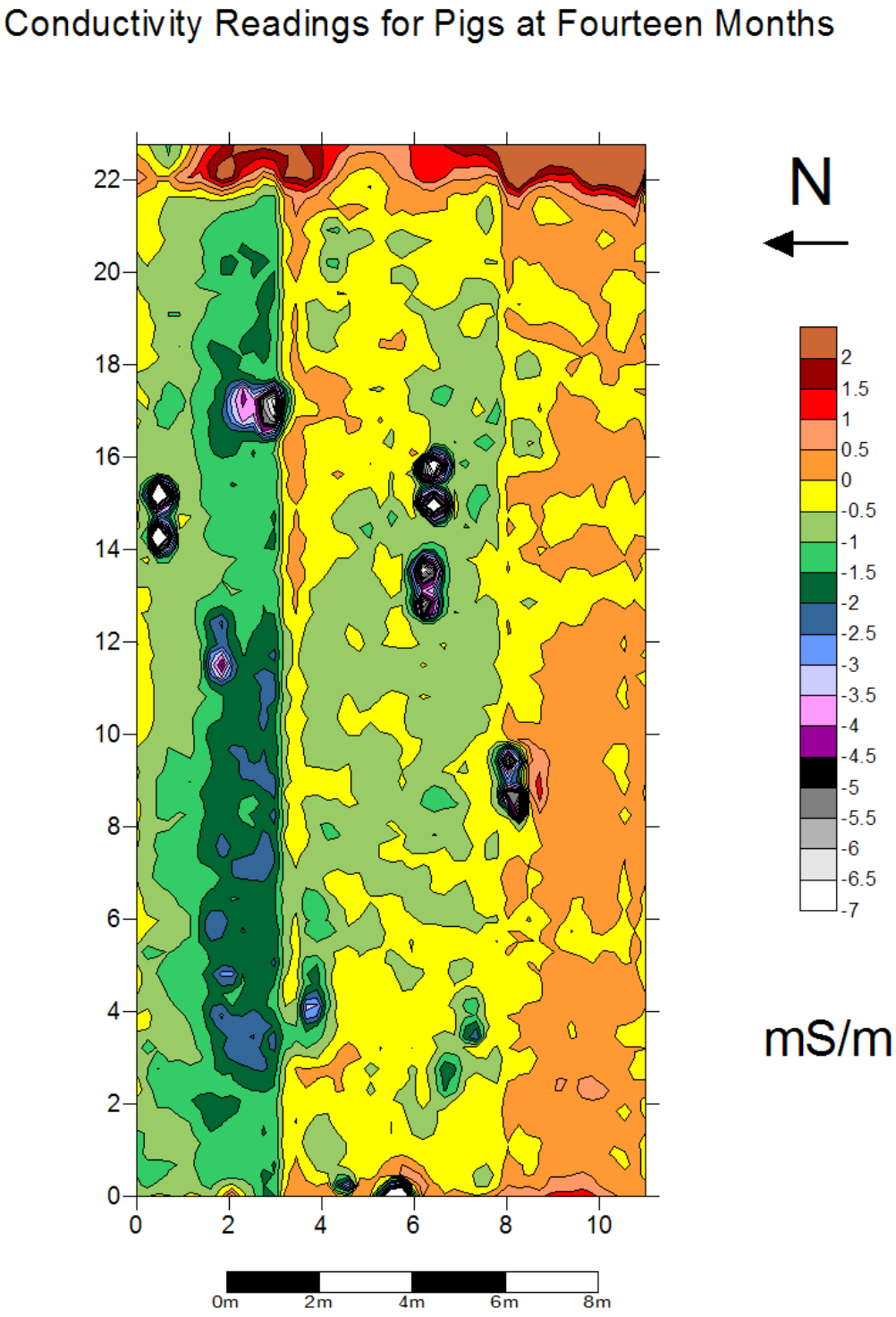

Figure A13: Conductivity map for pigs 14 months after interment

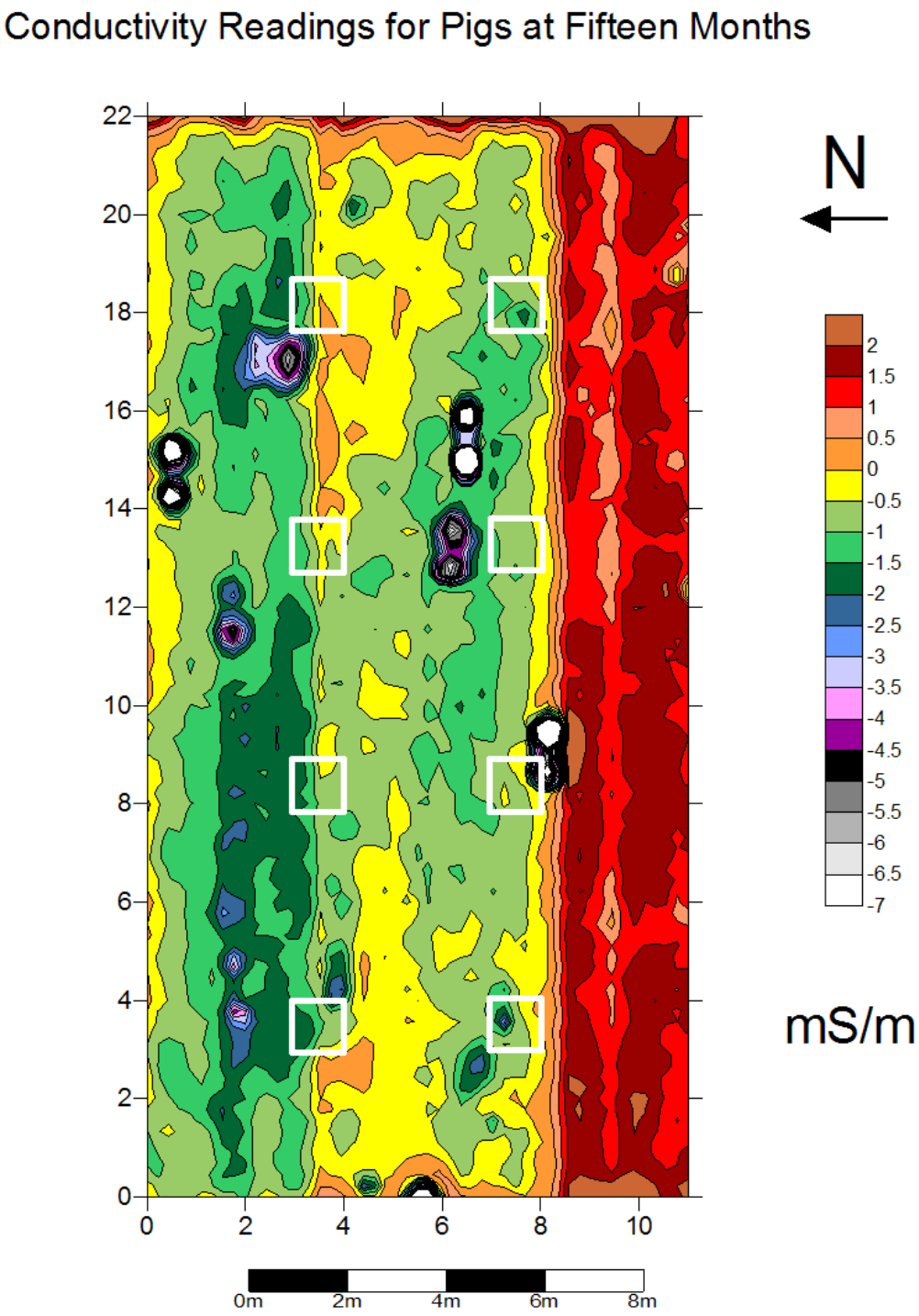

Figure A14: Conductivity map for pigs 15 months after interment

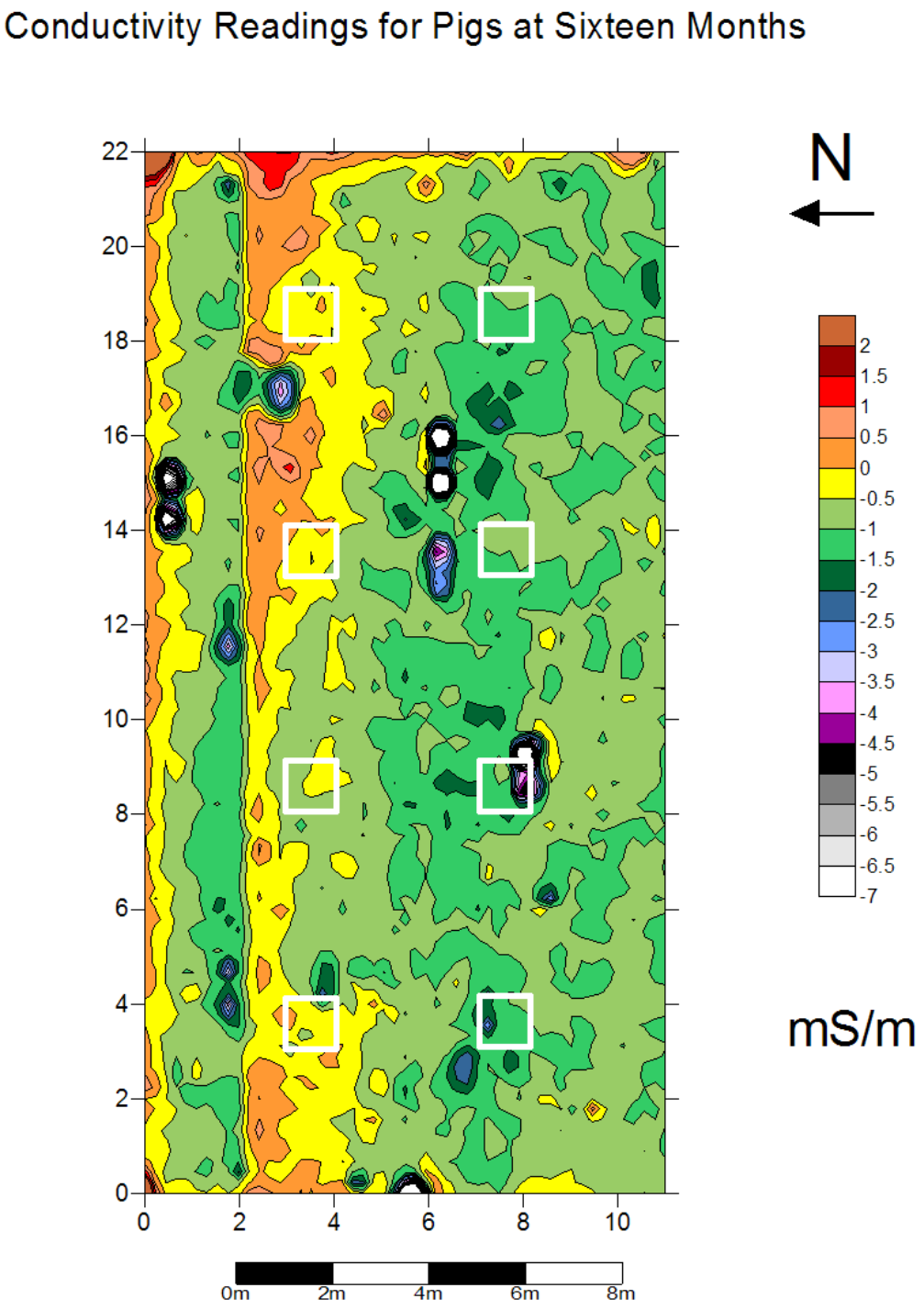

Figure A15: Conductivity map for pigs 16 months after interment

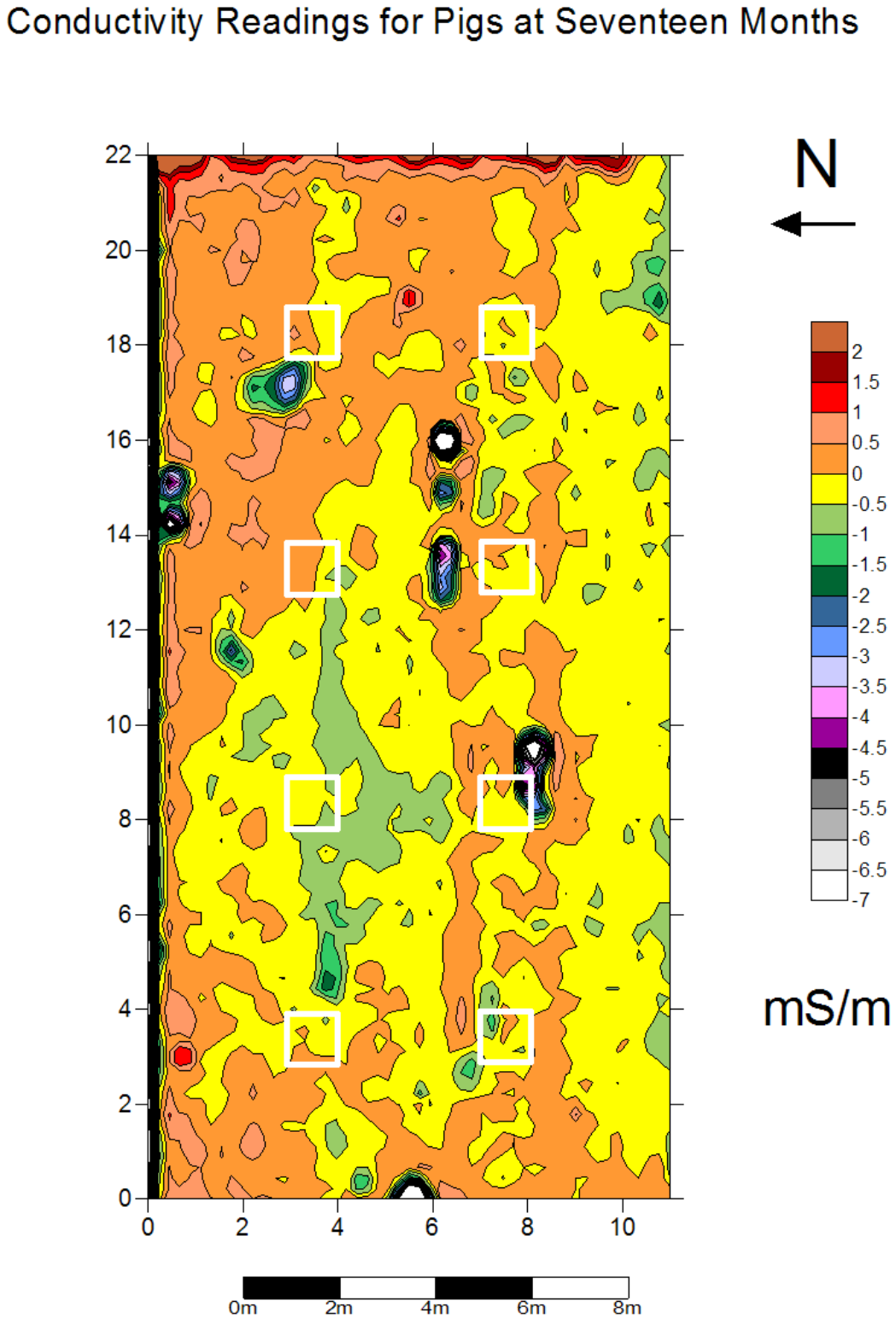

Figure A16: Conductivity map for pigs 17 months after interment

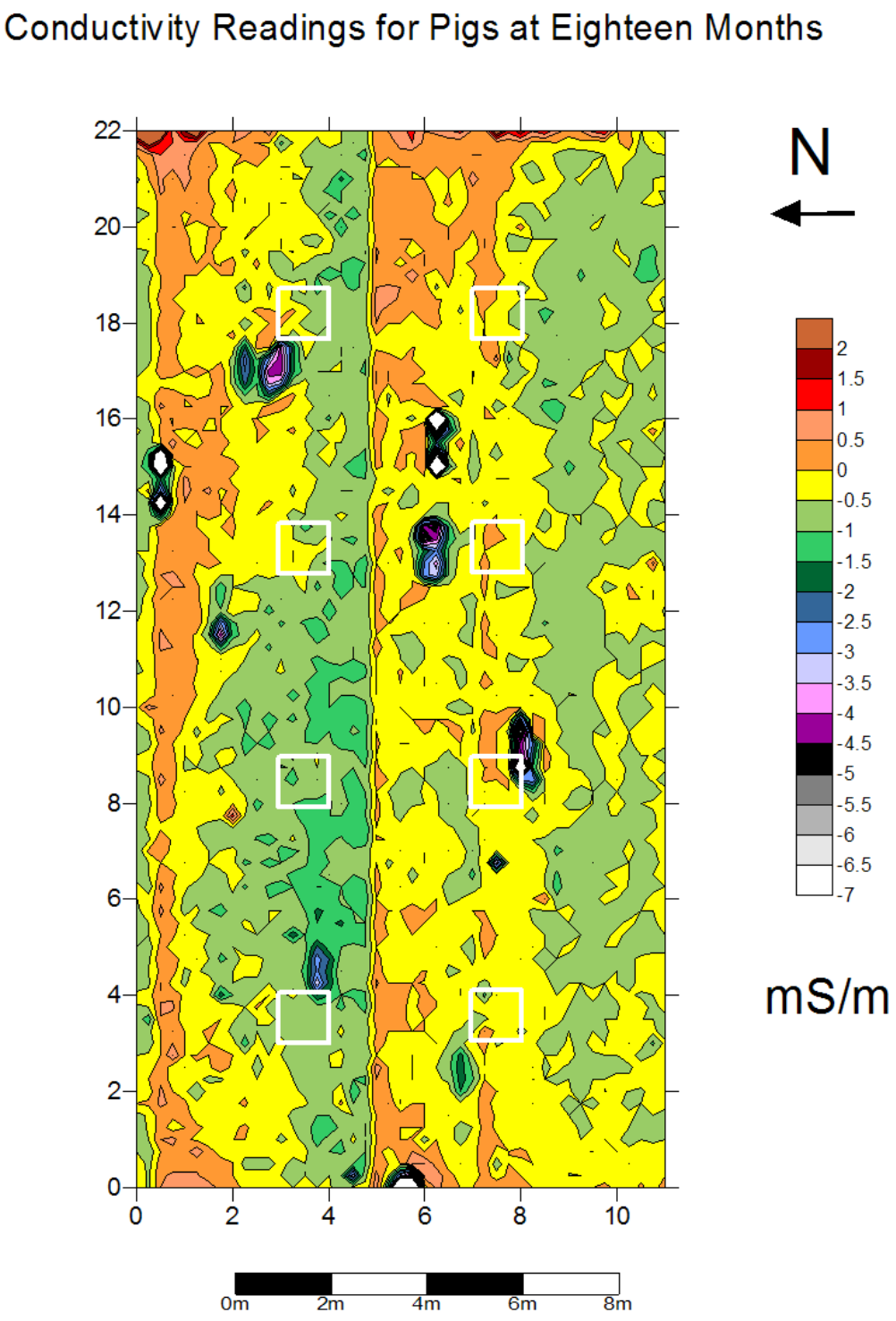

Figure 1: Conductivity map for pigs 18 months after interment

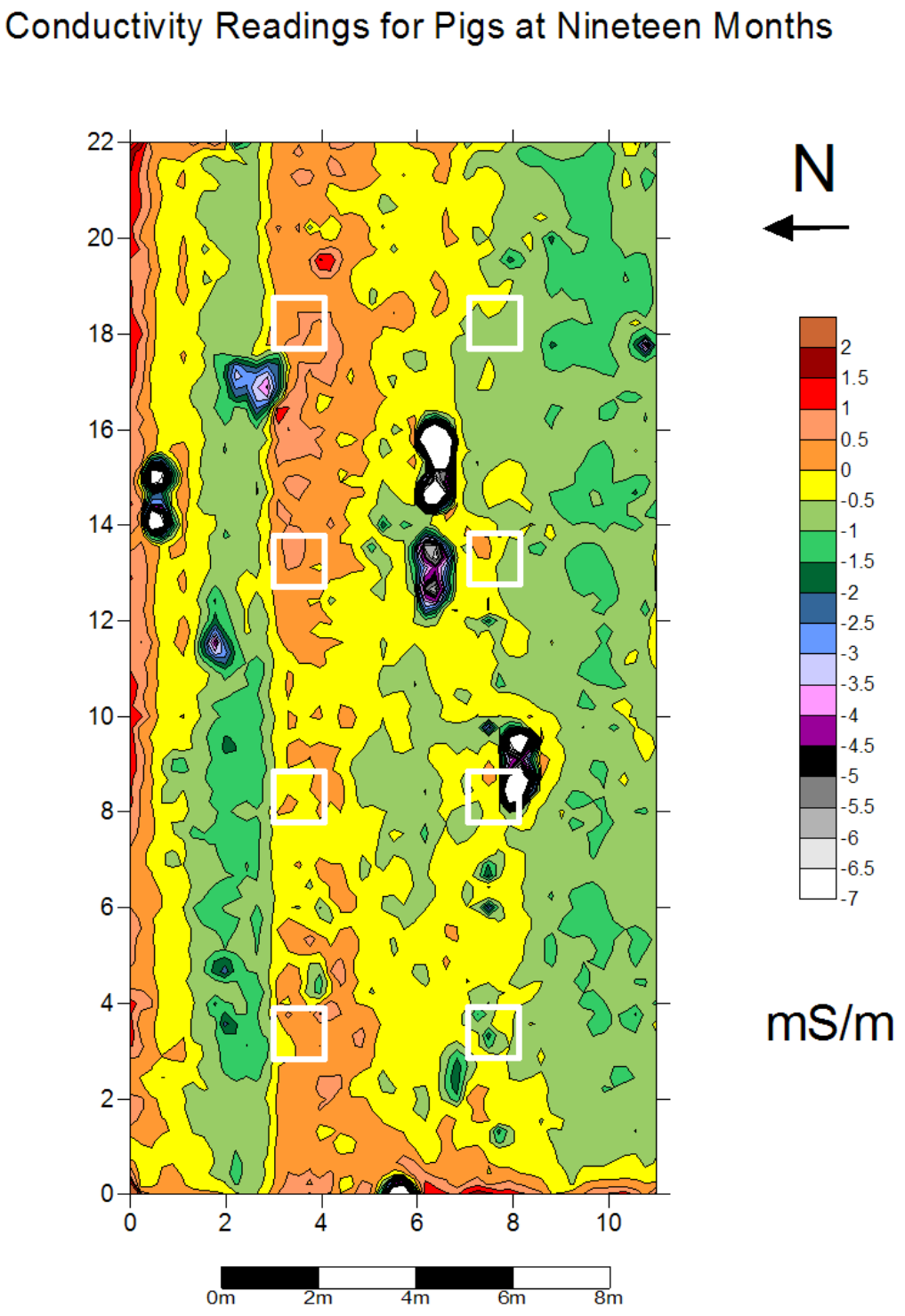

Figure A18: Conductivity map for pigs 19 months after interment

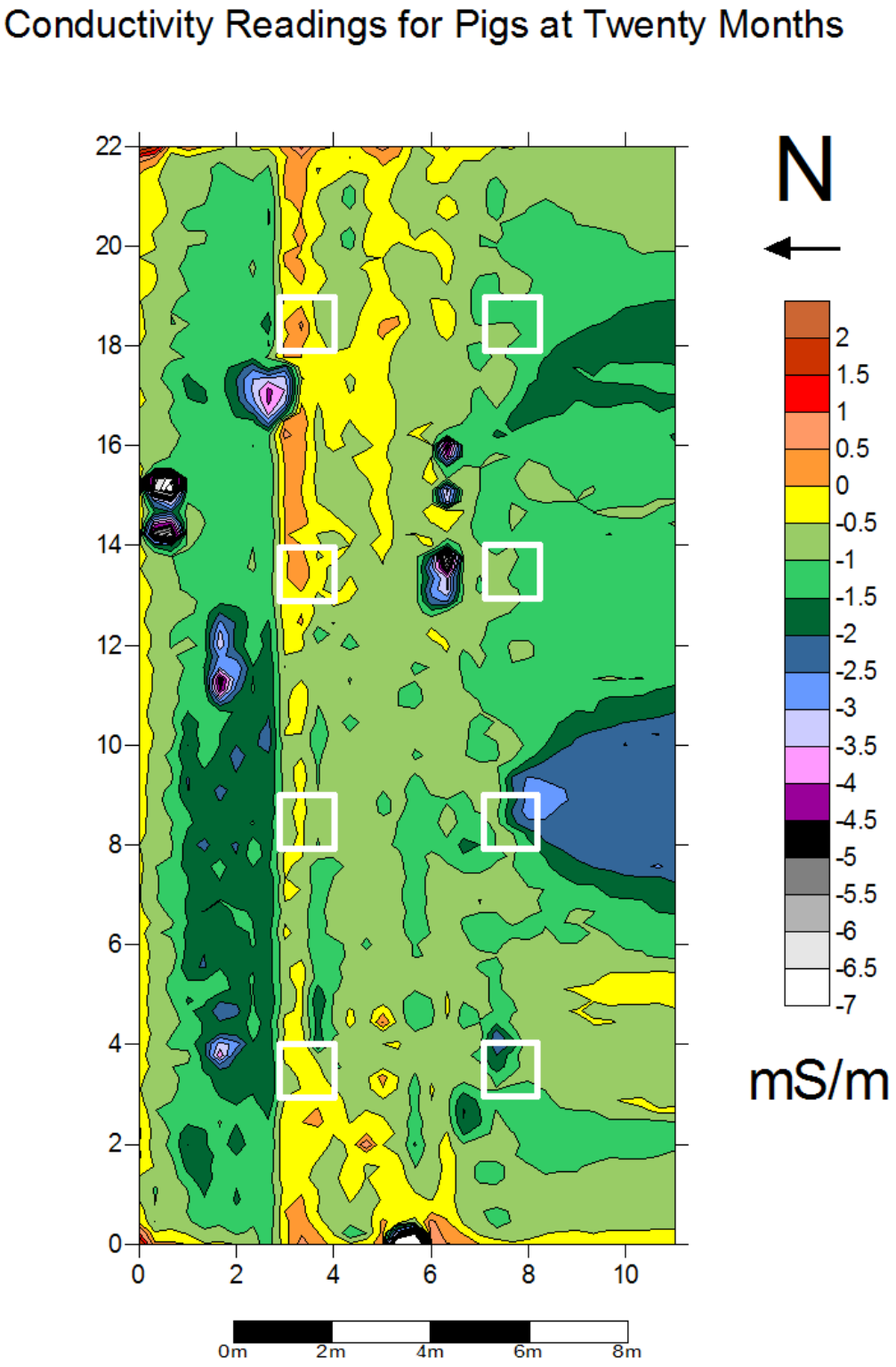

Figure A19: Conductivity map for pigs 20 months after interment

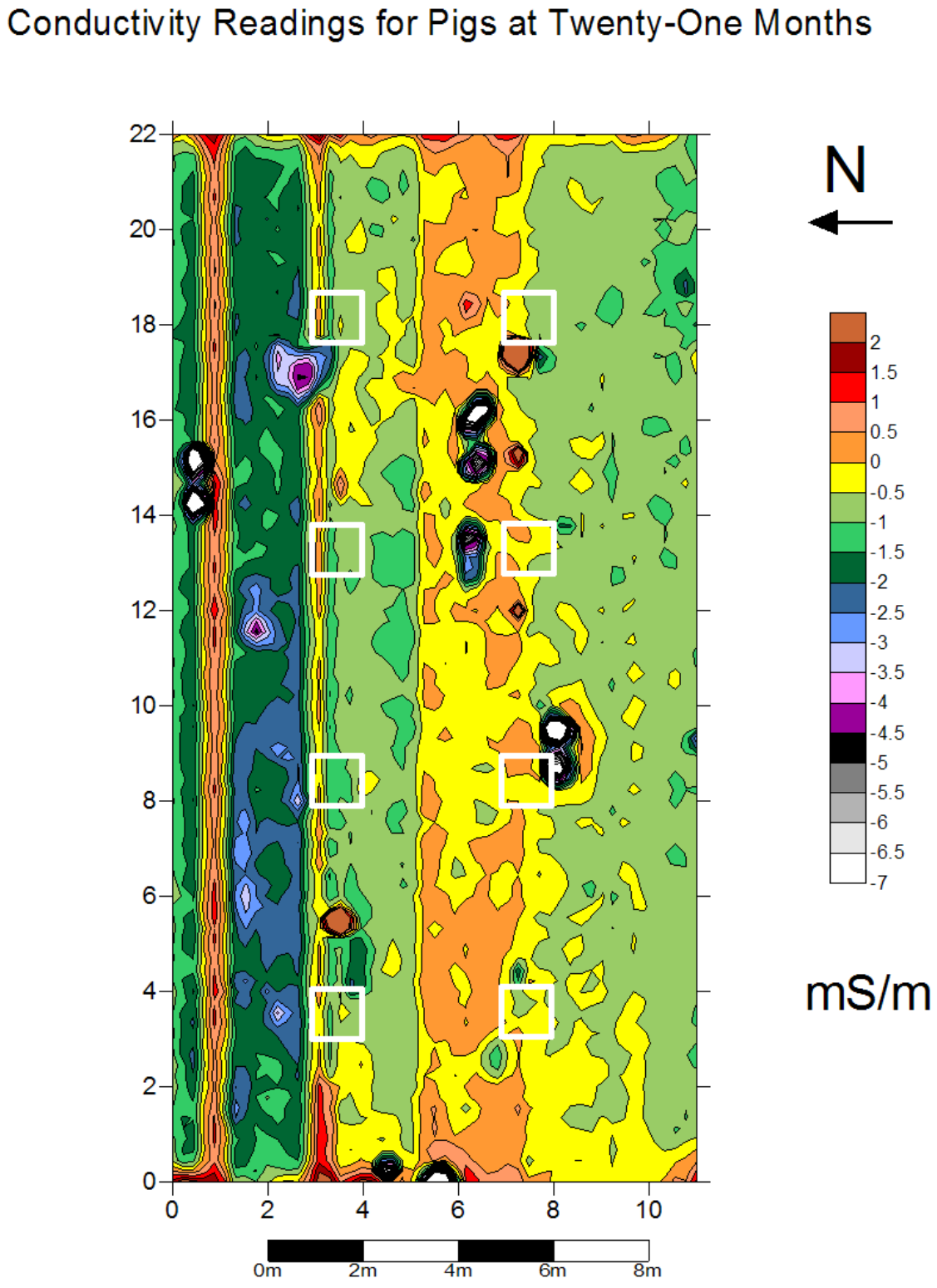

Figure A20: Conductivity map for pigs 21 months after interment

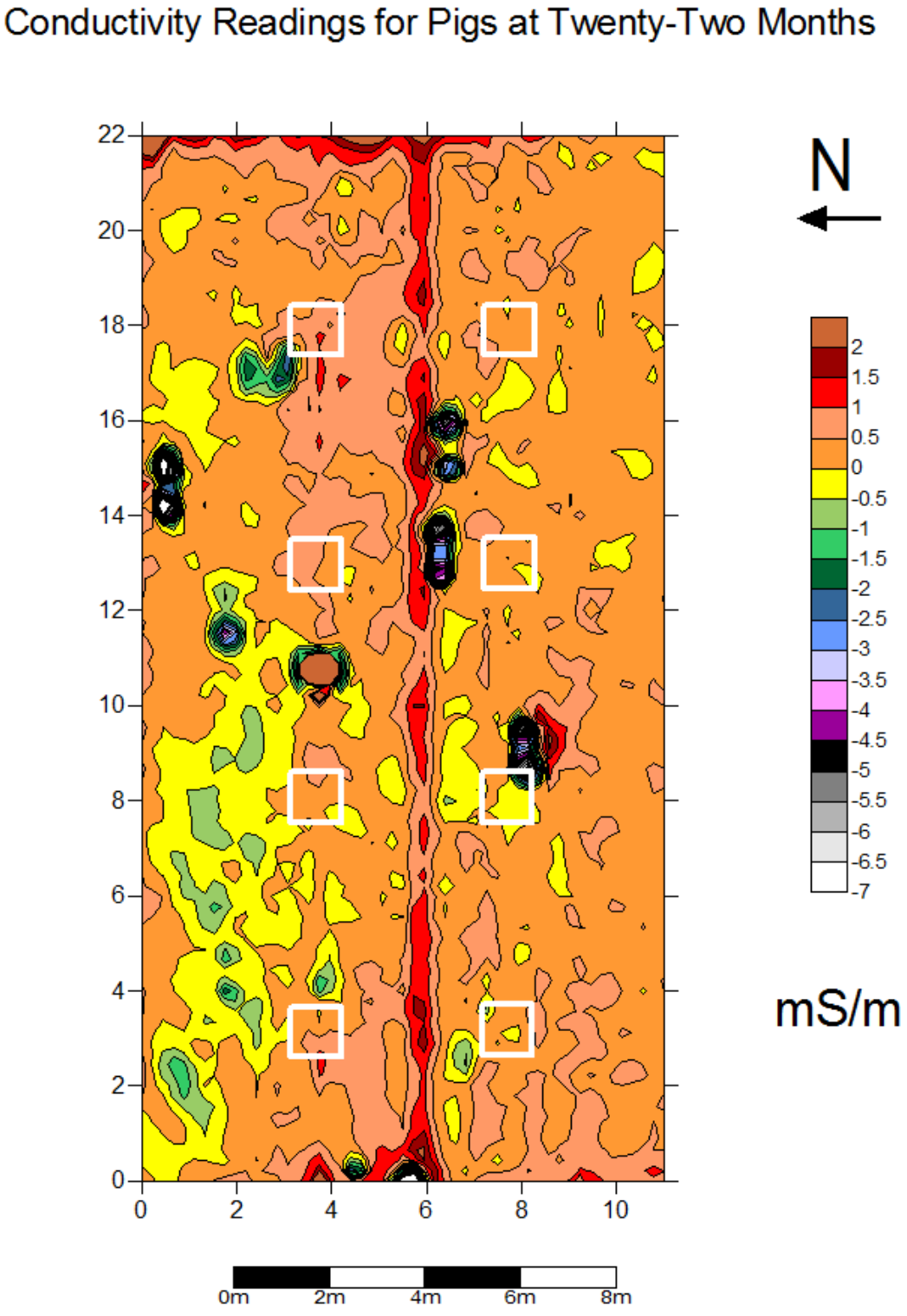

Figure A21: Conductivity map for pigs 22 months after interment

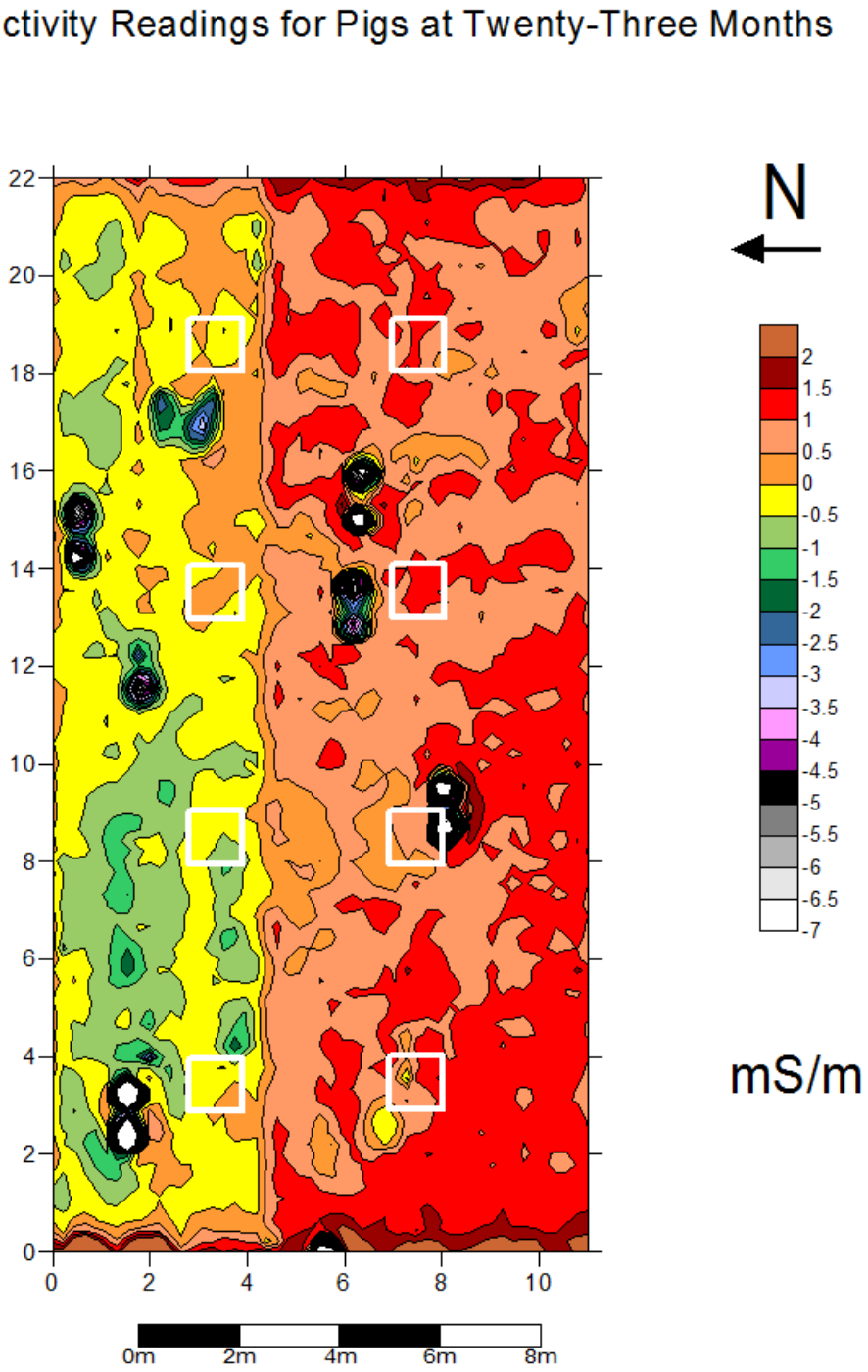

Figure A22: Conductivity map for pigs 23 months after interment

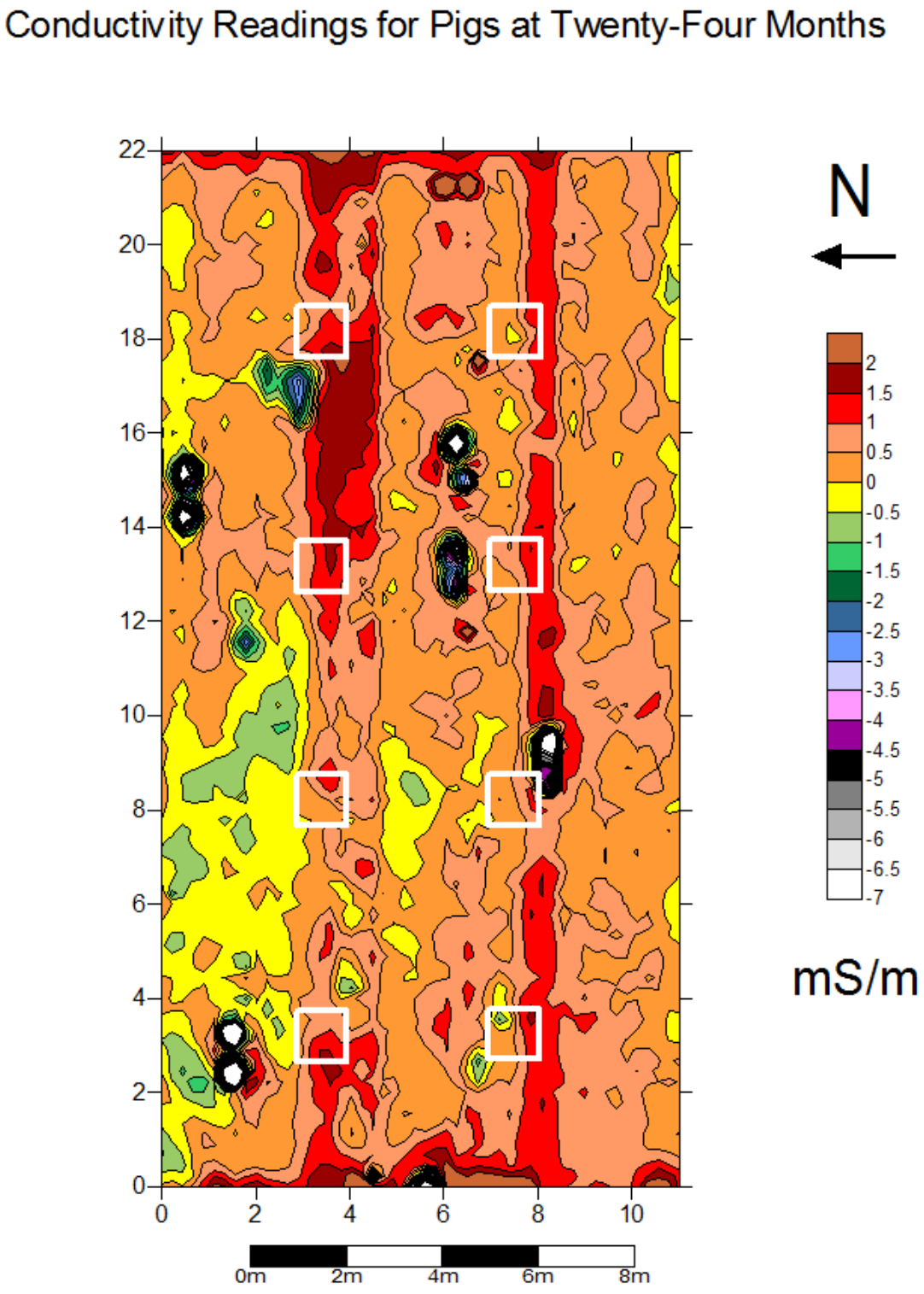

Figure A23: Conductivity map for pigs 24 months after interment

APPENDIX B: GROUND-PENETRATING RADAR 500-MHZ REFLECTION PROFILES

GPR 500 REFLECTION PROFILE AT MONTH 2

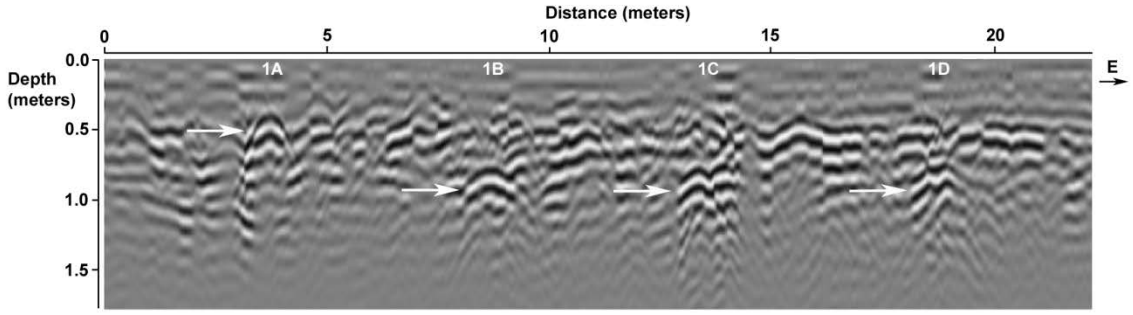

Figure B1: GPR reflection profile using the 500-MHz antenna of Row 1 at 2 months

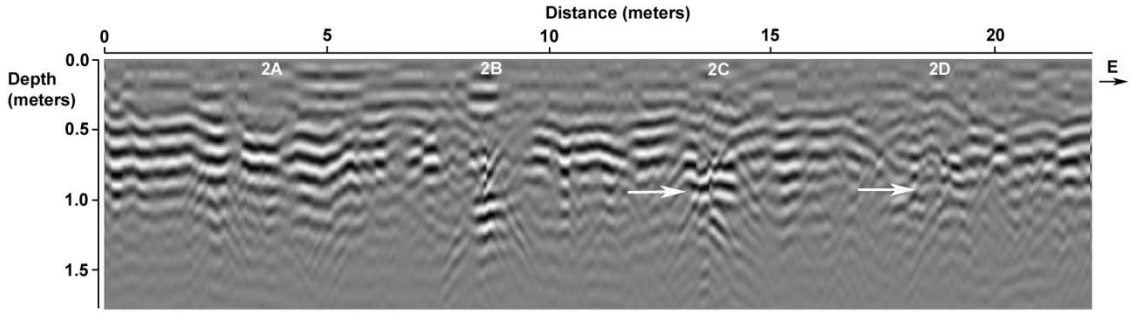

Figure B2: GPR reflection profile using the 500-MHz antenna of Row 2 at 2 months

GPR 500 REFLECTION PROFILE AT MONTH 3

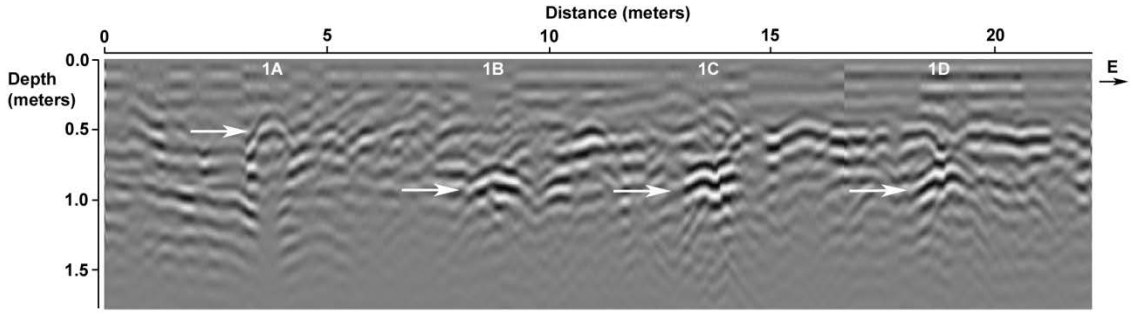

Figure B3: GPR reflection profile using the 500-MHz antenna of Row 1 at 3 months

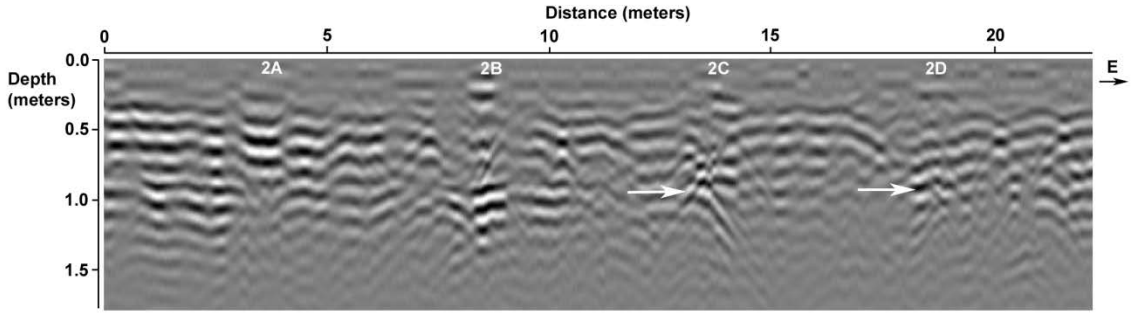

Figure B4: GPR reflection profile using the 500-MHz antenna of Row 2 at 3 months

GPR 500 REFLECTION PROFILE AT MONTH 4

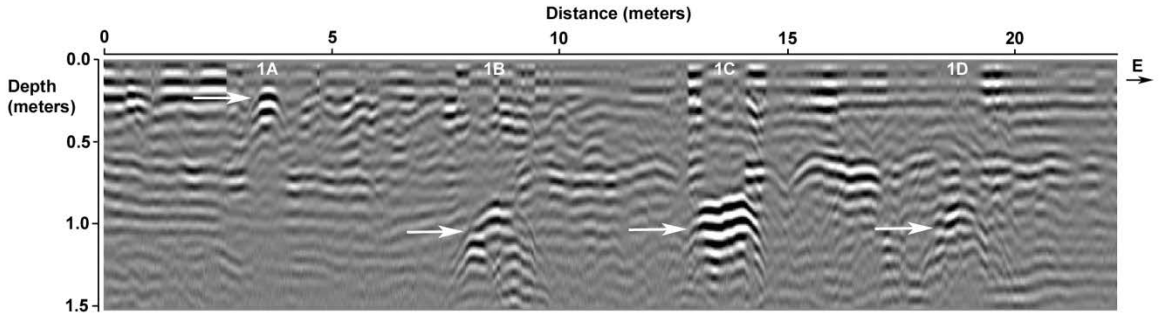

Figure B5: GPR reflection profile using the 500-MHz antenna of Row 1 at 4 months

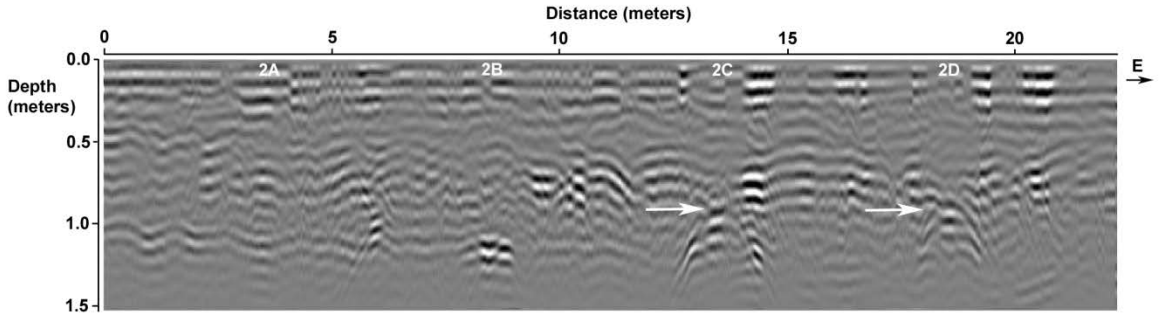

Figure B6: GPR reflection profile using the 500-MHz antenna of Row 2 at 4 months

GPR 500 REFLECTION PROFILE AT MONTH 5

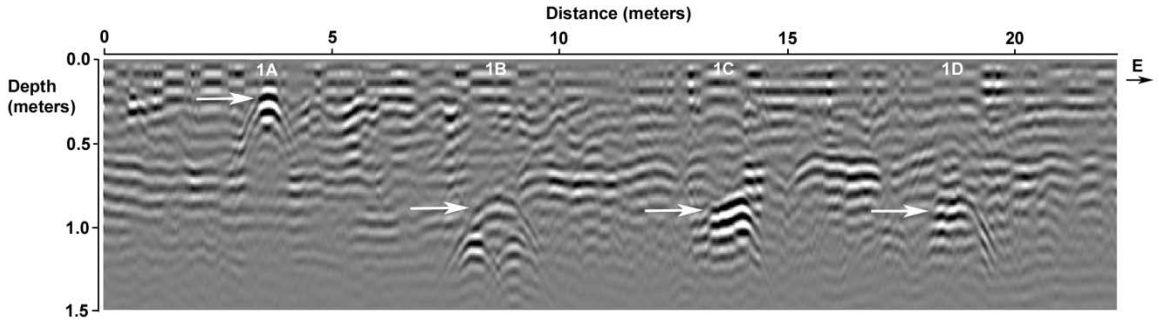

Figure B7: GPR reflection profile using the 500-MHz antenna of Row 1 at 5 months

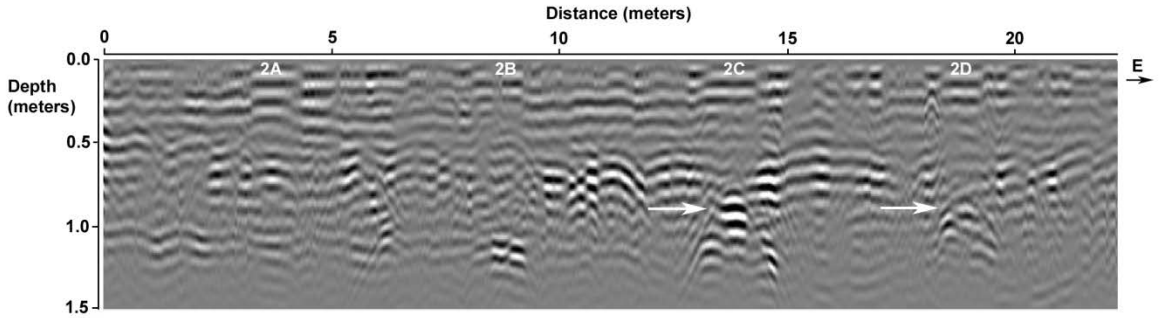

Figure B8: GPR reflection profile using the 500-MHz antenna of Row 2 at 5 months

GPR 500 REFLECTION PROFILE AT MONTH 6

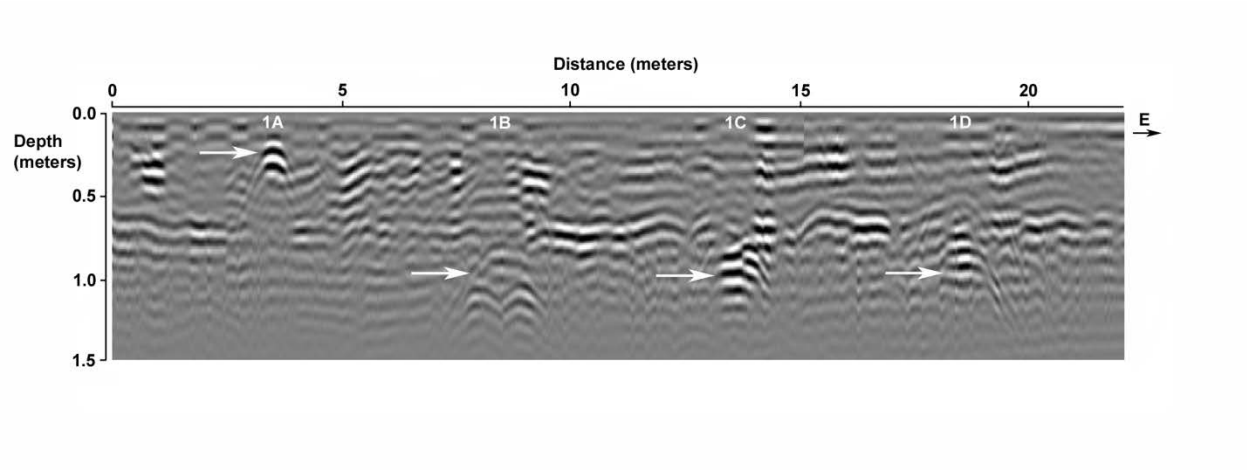

Figure B9: GPR reflection profile using the 500-MHz antenna of Row 1 at 6 months

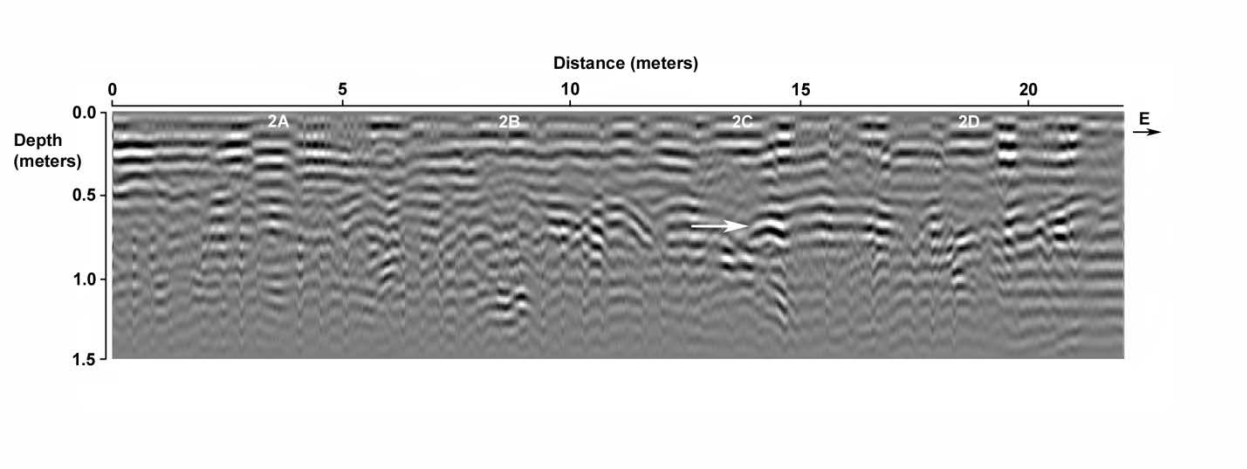

Figure B10: GPR reflection profile using the 500-MHz antenna of Row 2 at 6 months

GPR 500 REFLECTION PROFILE AT MONTH 7

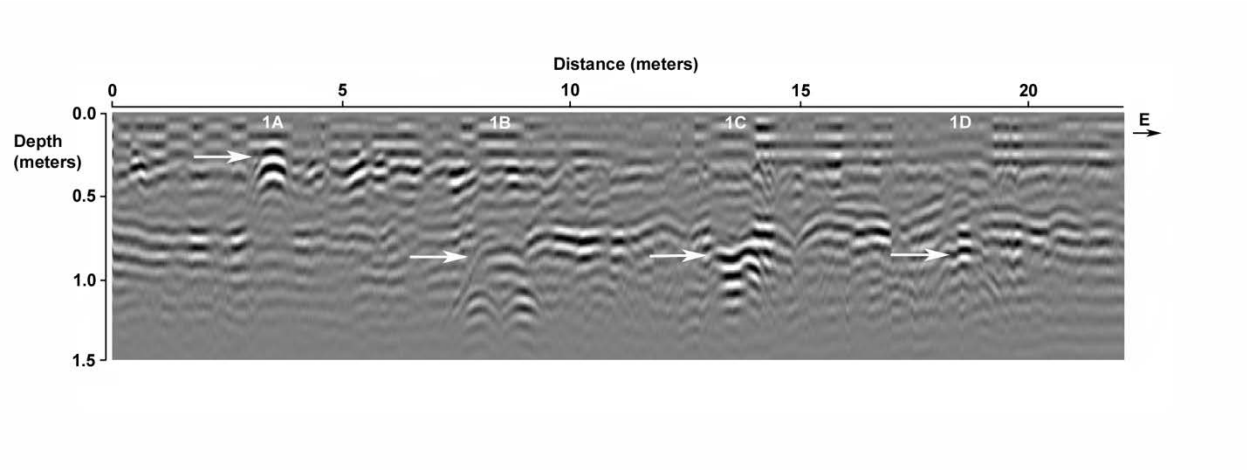

Figure B11: GPR reflection profile using the 500-MHz antenna of Row 1 at 7 months

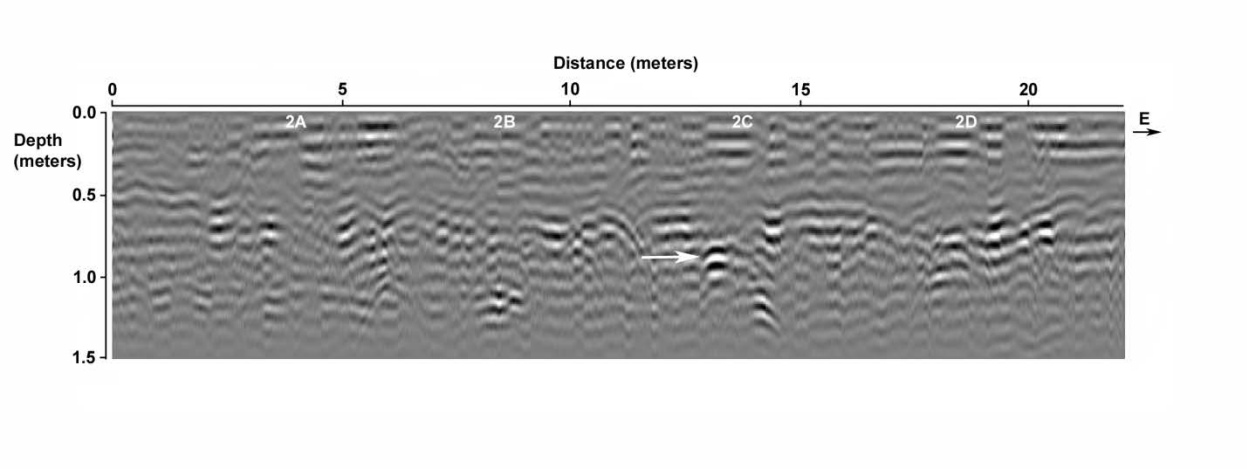

Figure B12: GPR reflection profile using the 500-MHz antenna of Row 2 at 7 months

GPR 500 REFLECTION PROFILE AT MONTH 8

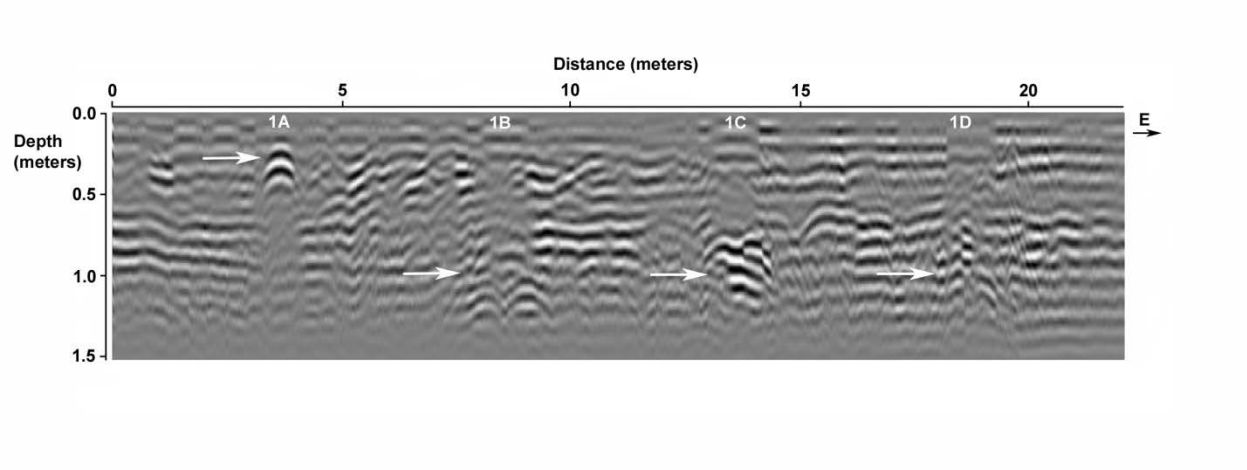

Figure B13: GPR reflection profile using the 500-MHz antenna of Row 1 at 8 months

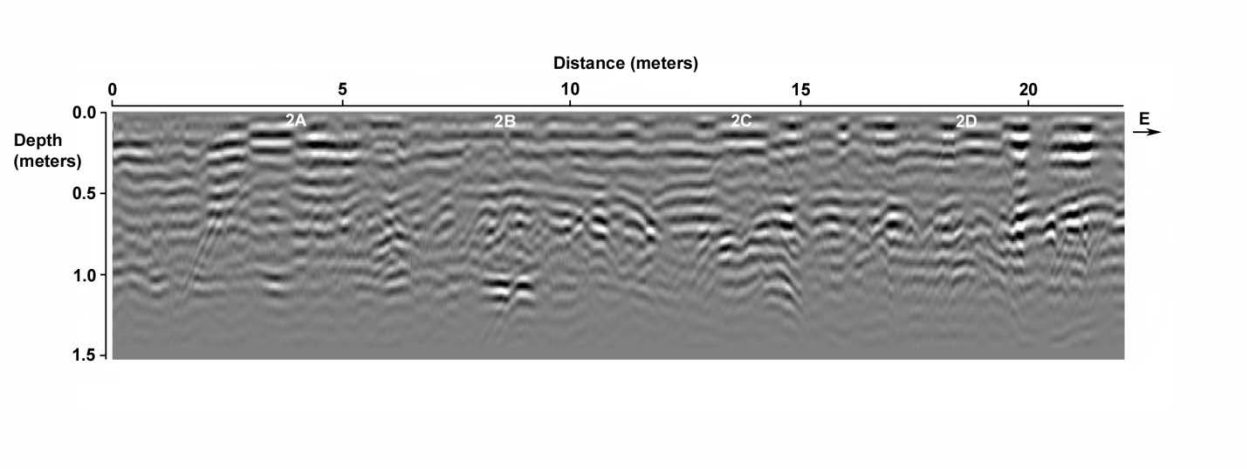

Figure B14: GPR reflection profile using the 500-MHz antenna of Row 2 at 8 months

GPR 500 REFLECTION PROFILE AT MONTH 9

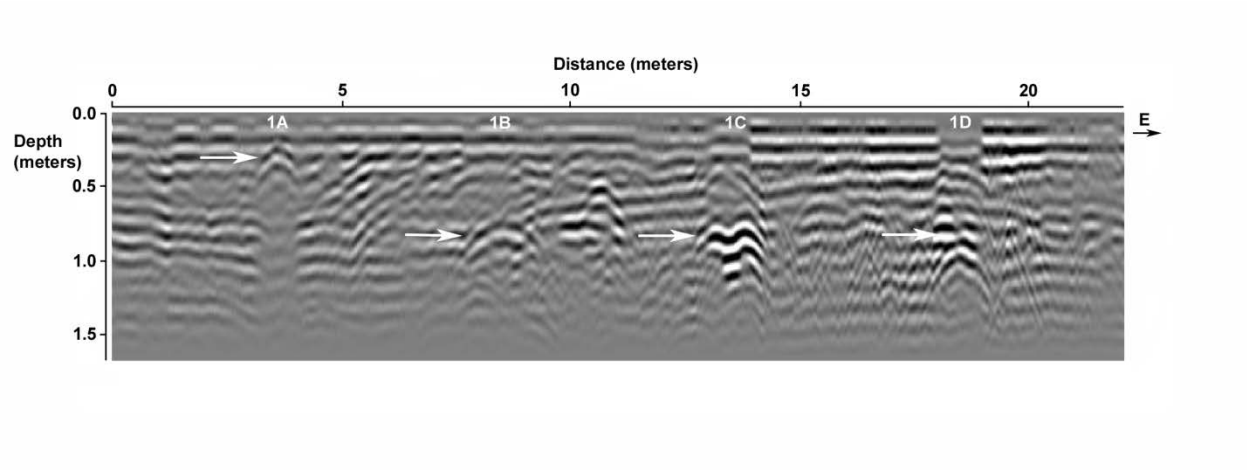

Figure B15: GPR reflection profile using the 500-MHz antenna of Row 1 at 9 months

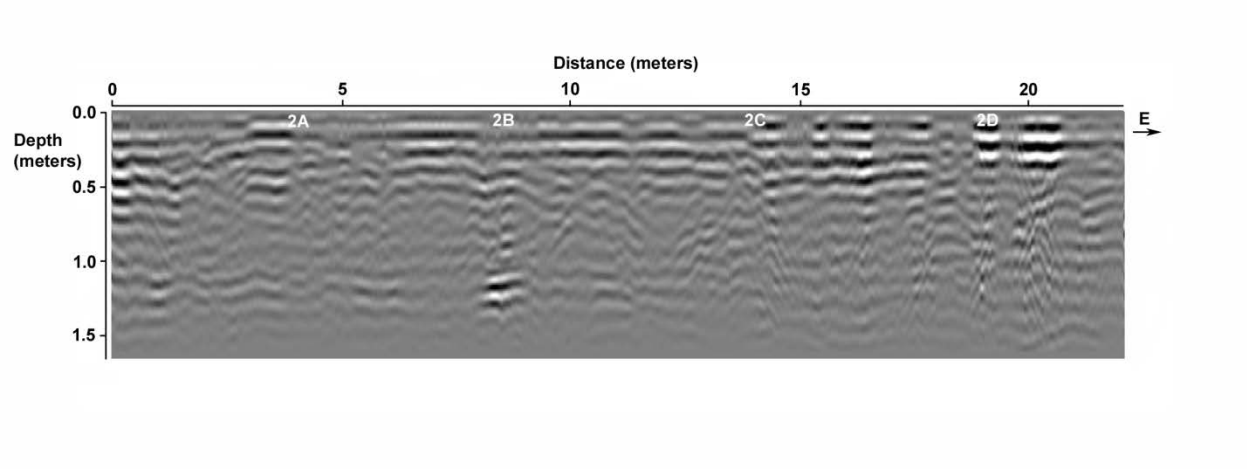

Figure B16: GPR reflection profile using the 500-MHz antenna of Row 2 at 9 months

GPR 500 REFLECTION PROFILE AT MONTH 10

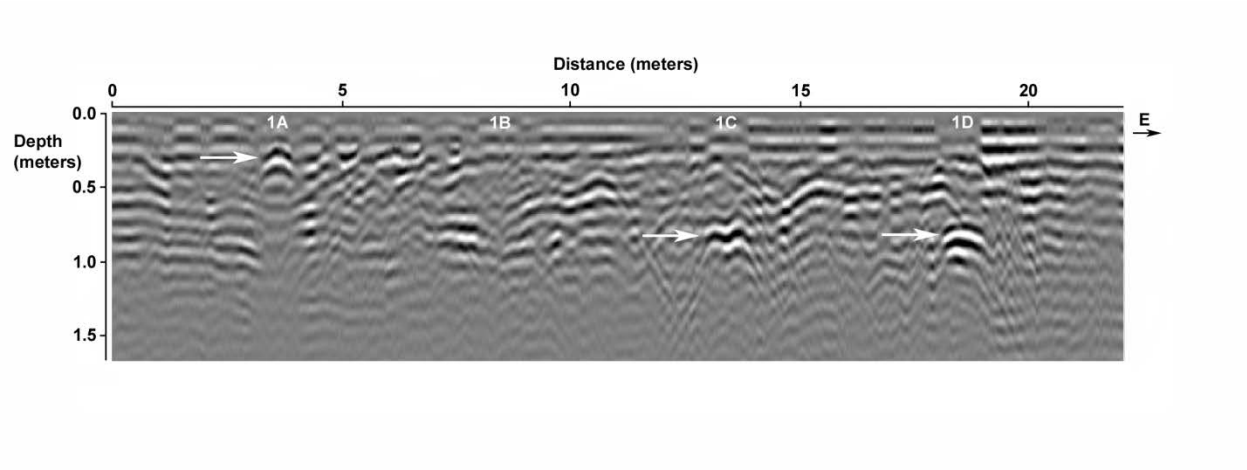

Figure B17: GPR reflection profile using the 500-MHz antenna of Row 1 at 10 months

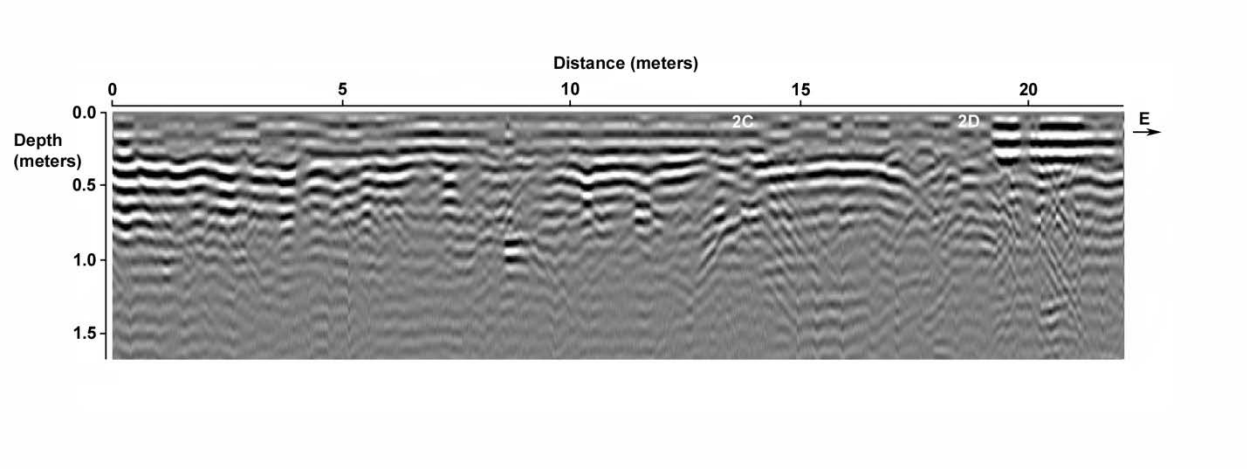

Figure B18: GPR reflection profile using the 500-MHz antenna of Row 2 at 10 months

GPR 500 REFLECTION PROFILE AT MONTH 11

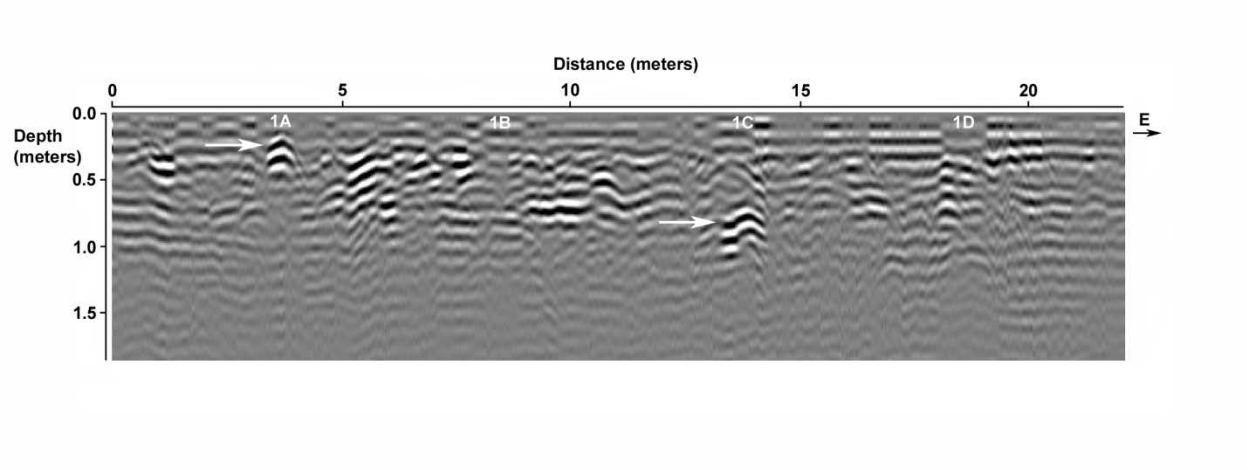

Figure B19: GPR reflection profile using the 500-MHz antenna of Row 1 at 11 months

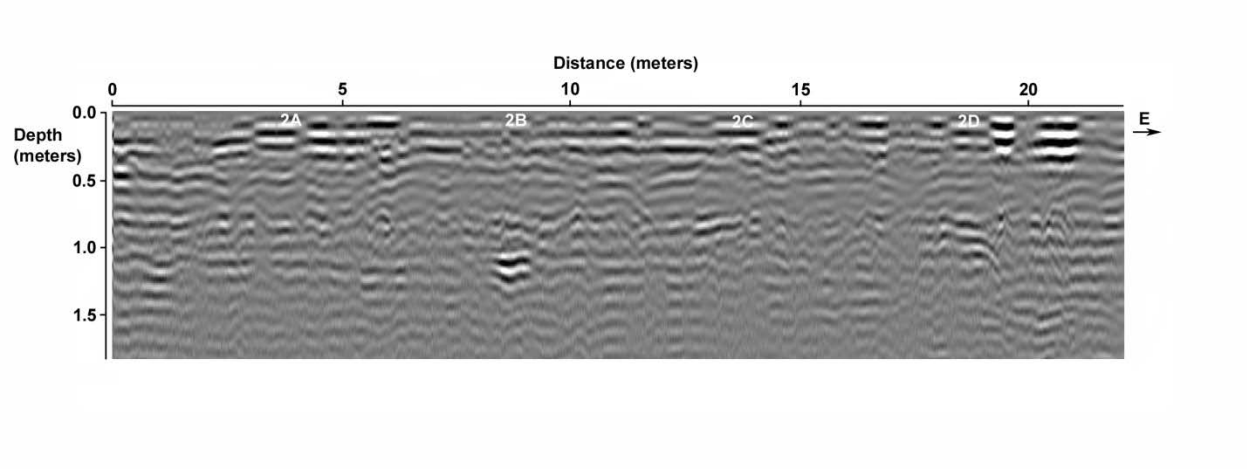

Figure B20: GPR reflection profile using the 500-MHz antenna of Row 2 at 11 months

GPR 500 REFLECTION PROFILE AT MONTH 12

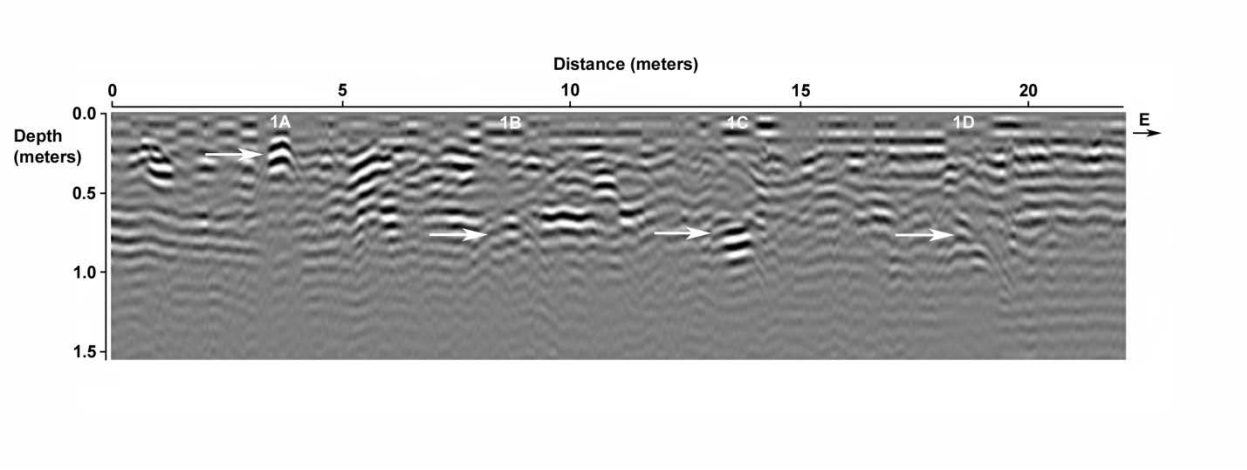

Figure B21: GPR reflection profile using the 500-MHz antenna of Row 1 at 12 months

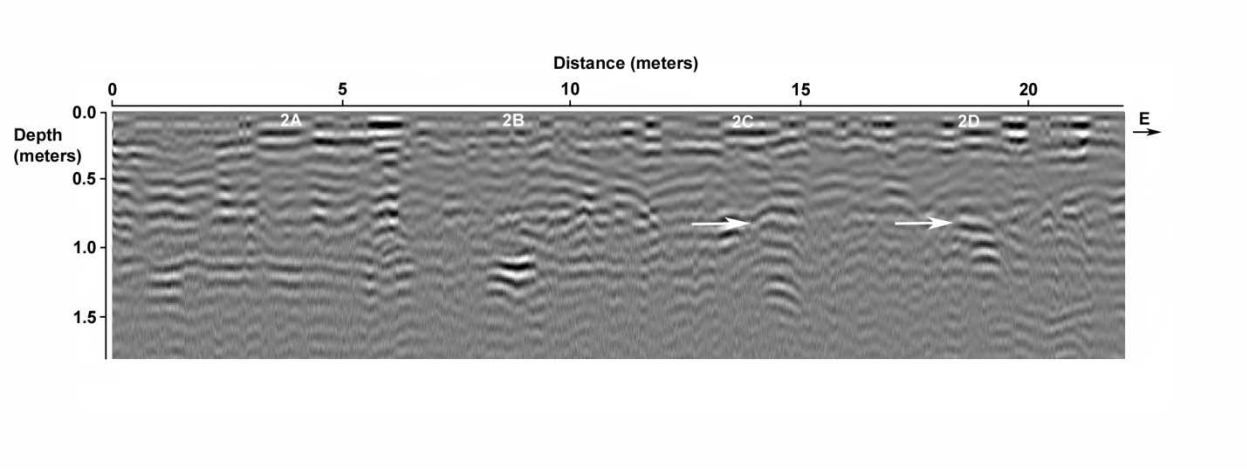

Figure B22: GPR reflection profile using the 500-MHz antenna of Row 2 at 12 months

GPR 500 REFLECTION PROFILE AT MONTH 13

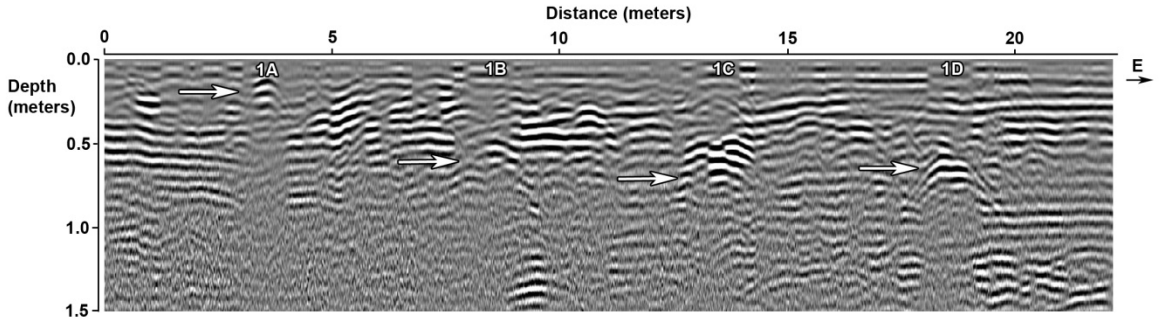

Figure B23: GPR reflection profile using the 500 MHz antenna of Row 1 at 13 months

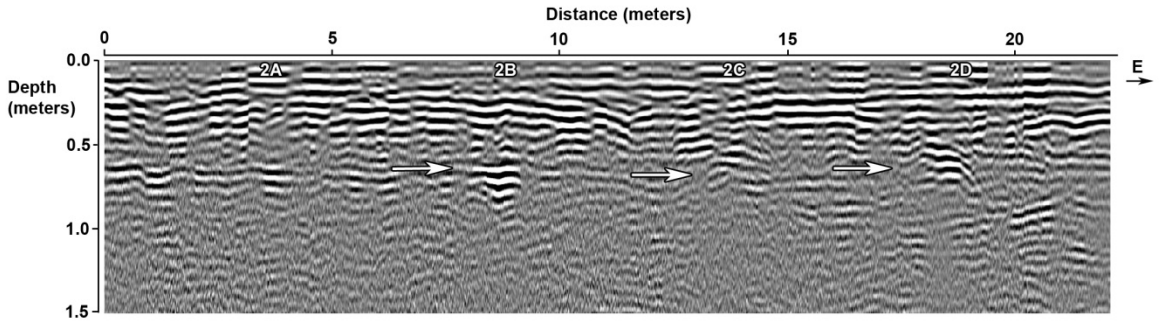

Figure B24: GPR reflection profile using the 500-MHz antenna of Row 2 at 13 months

GPR 500 REFLECTION PROFILE AT MONTH 14

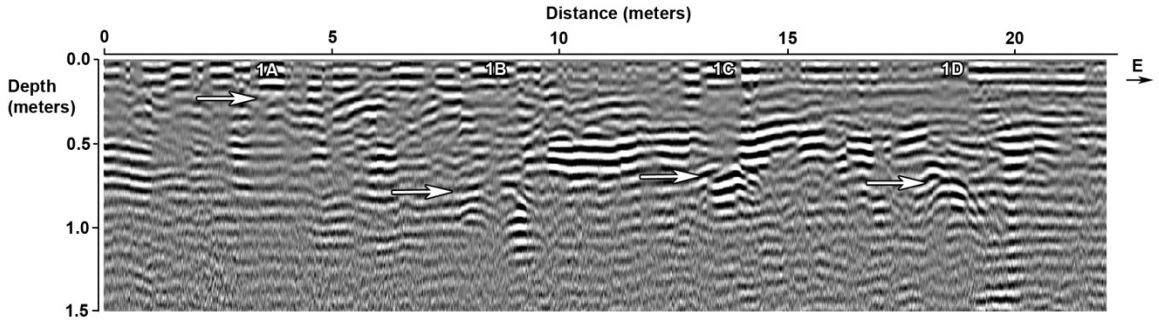

Figure B25: GPR reflection profile using the 500-MHz antenna of Row 1 at 14 months

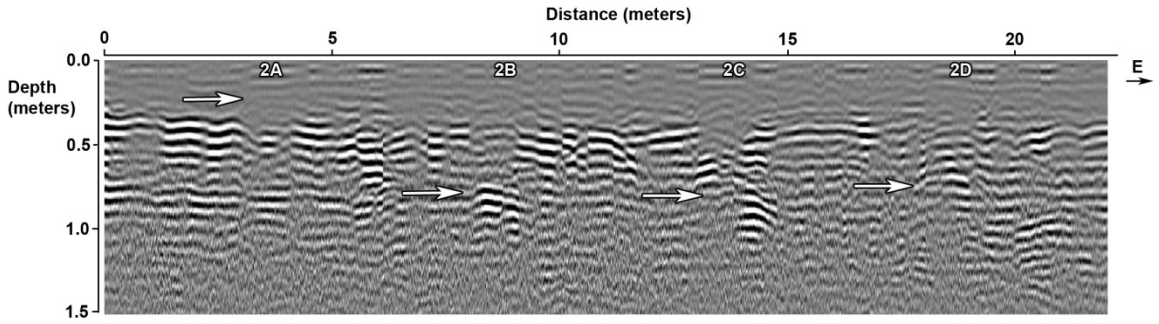

Figure B26: GPR reflection profile using the 500-MHz antenna of Row 2 at 14 months

GPR 500 REFLECTION PROFILE AT MONTH 15

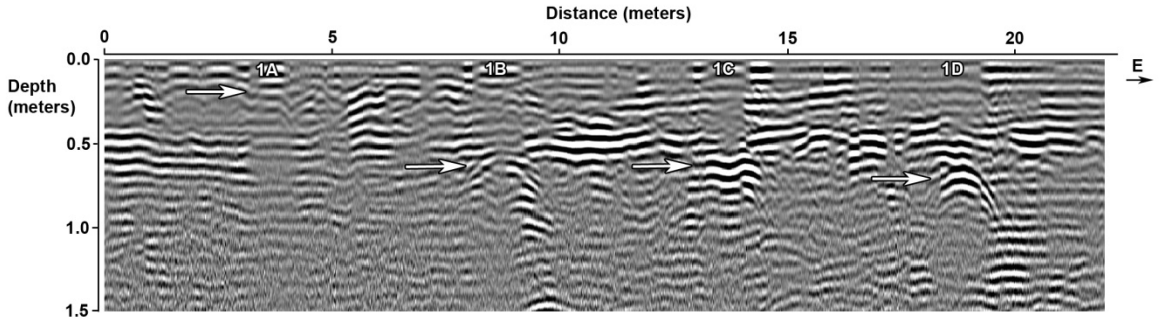

Figure B27: GPR reflection profile using the 500-MHz antenna of Row 1 at 15 months

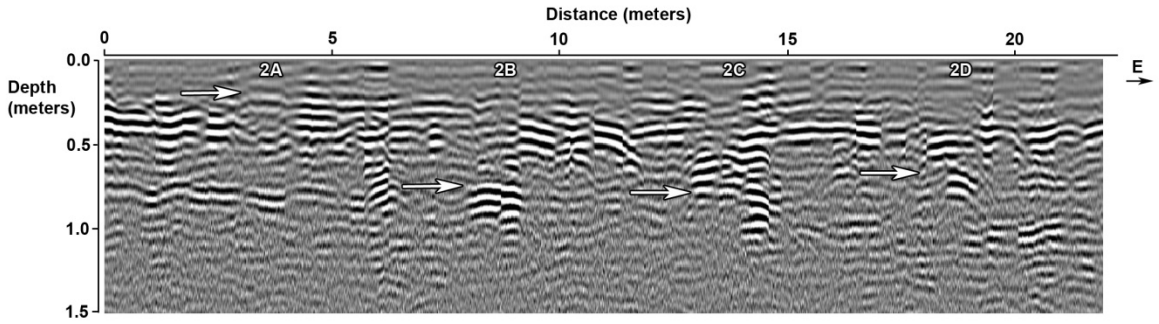

Figure B28: GPR reflection profile using the 500-MHz antenna of Row 2 at 15 months

GPR 500 REFLECTION PROFILE AT MONTH 16

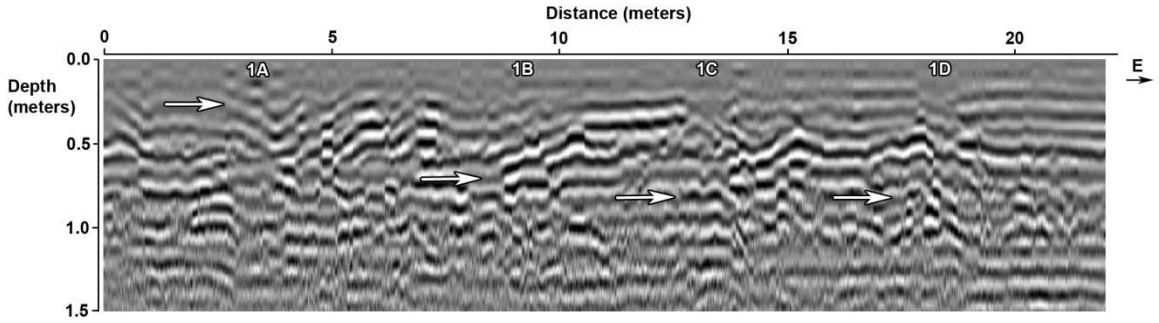

Figure B29: GPR reflection profile using the 500-MHz antenna of Row 1 at 16 months

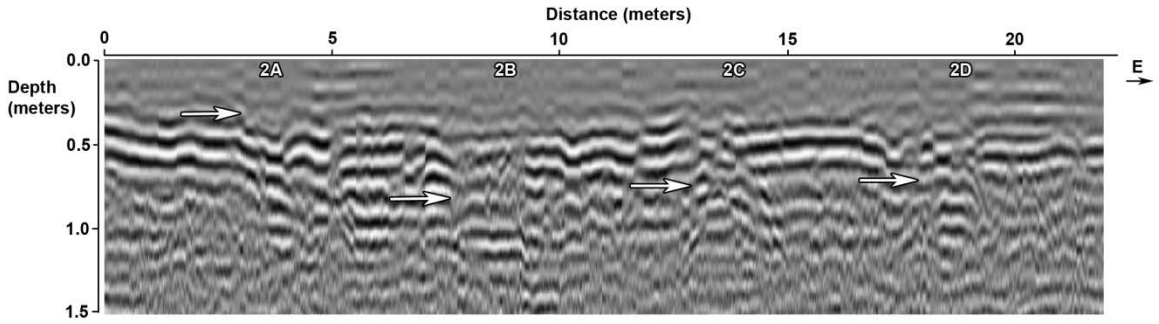

Figure B30: GPR reflection profile using the 500-MHz antenna of Row 2 at 16 months

GPR 500 REFLECTION PROFILE AT MONTH 17

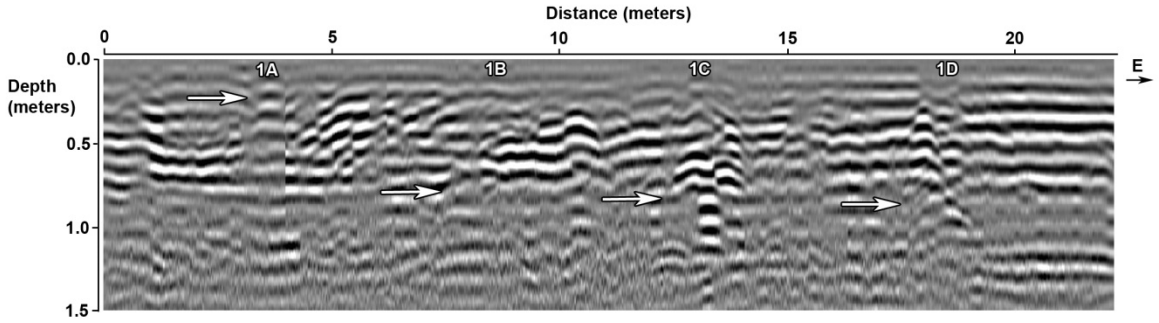

Figure B31: GPR reflection profile using the 500-MHz antenna of Row 1 at 17 months

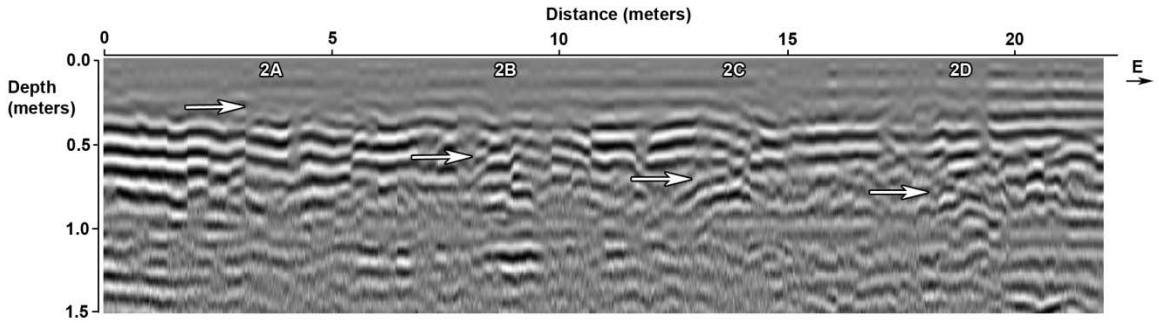

Figure B32: GPR reflection profile using the 500-MHz antenna of Row 2 at 17 months

GPR 500 REFLECTION PROFILE AT MONTH 18

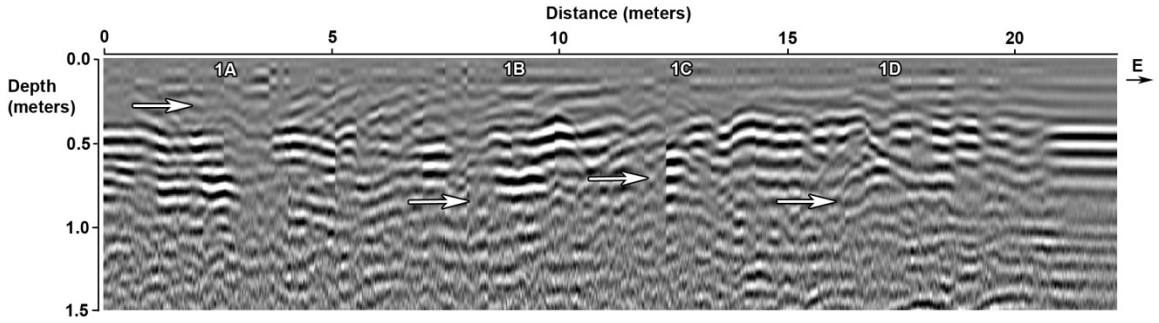

Figure B33: GPR reflection profile using the 500-MHz antenna of Row 1 at 18 months

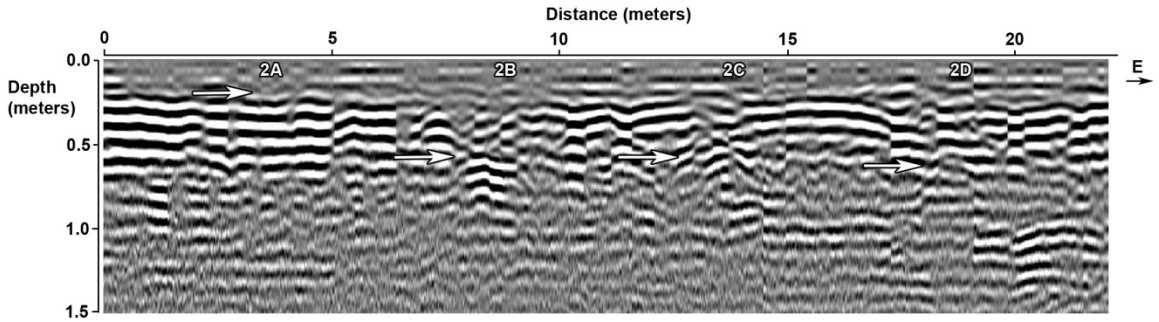

Figure B34: GPR reflection profile using the 500-MHz antenna of Row 2 at 18 months

GPR 500 REFLECTION PROFILE AT MONTH 19

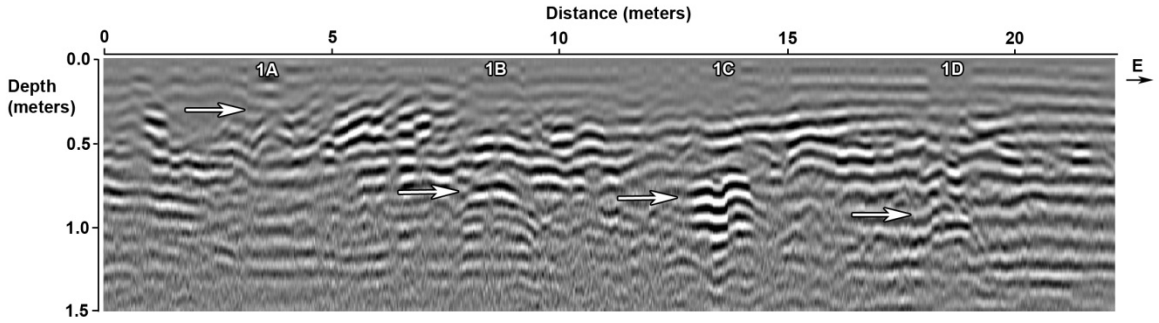

Figure B35: GPR reflection profile using the 500-MHz antenna of Row 1 at 19 months

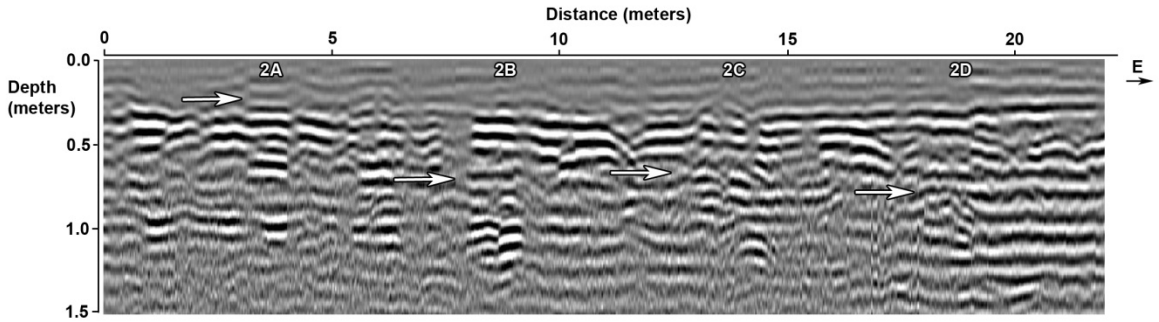

Figure B36: GPR reflection profile using the 500-MHz antenna of Row 2 at 19 months

GPR 500 REFLECTION PROFILE AT MONTH 20

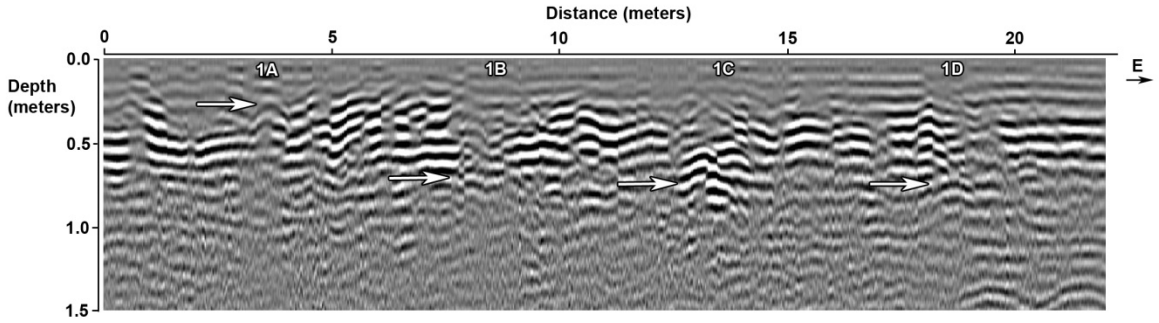

Figure B37: GPR reflection profile using the 500-MHz antenna of Row 1 at 20 months

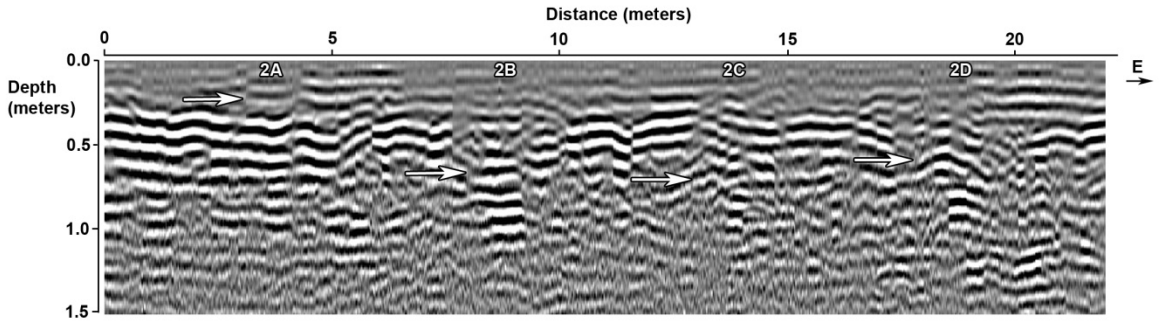

Figure B38: GPR reflection profile using the 500-MHz antenna of Row 2 at 20 months

GPR 500 REFLECTION PROFILE AT MONTH 21

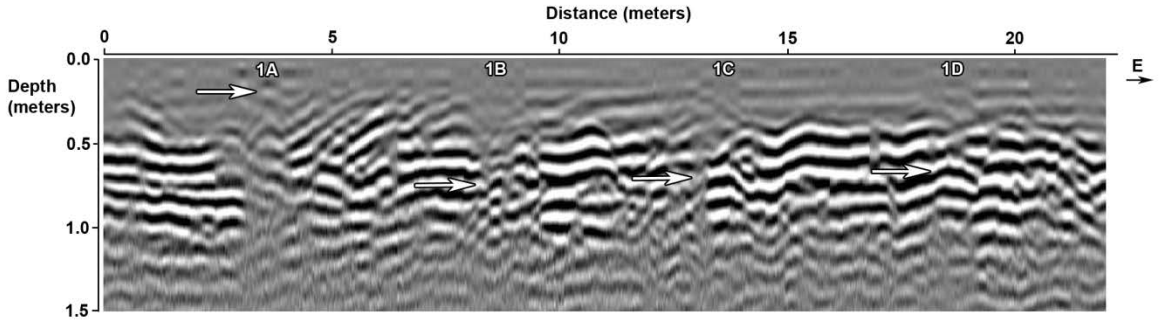

Figure B39: GPR reflection profile using the 500-MHz antenna of Row 1 at 21 months

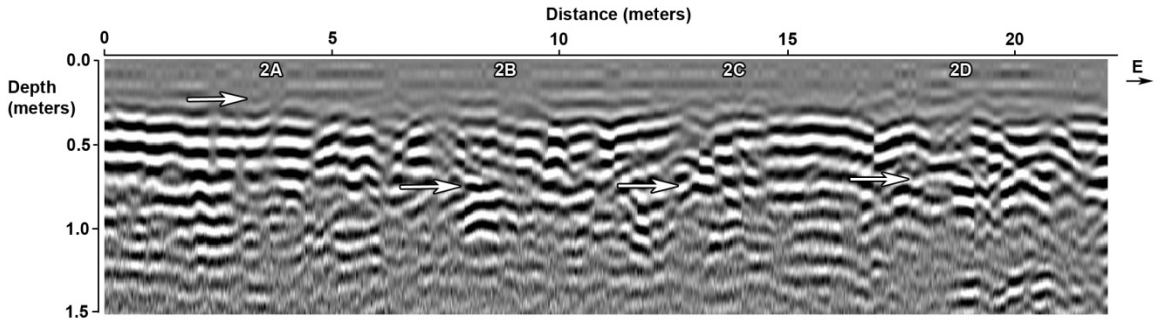

Figure B40: GPR reflection profile using the 500-MHz antenna of Row 2 at 21 months

GPR 500 REFLECTION PROFILE AT MONTH 22

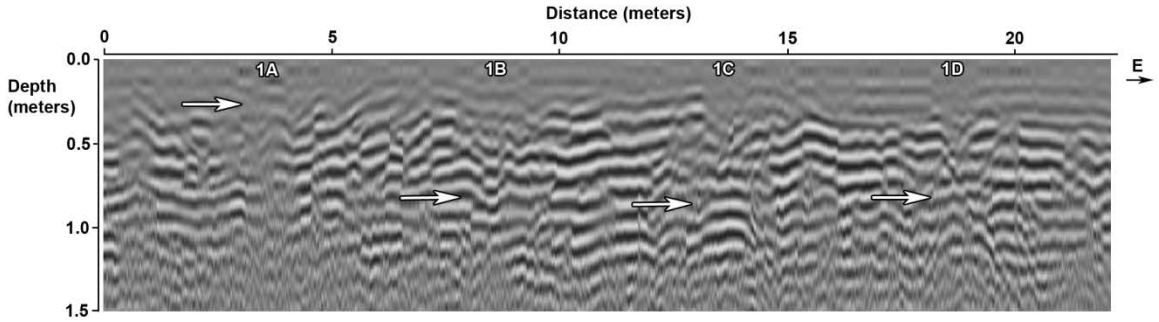

Figure B41: GPR reflection profile using the 500-MHz antenna of Row 1 at 22 montsh

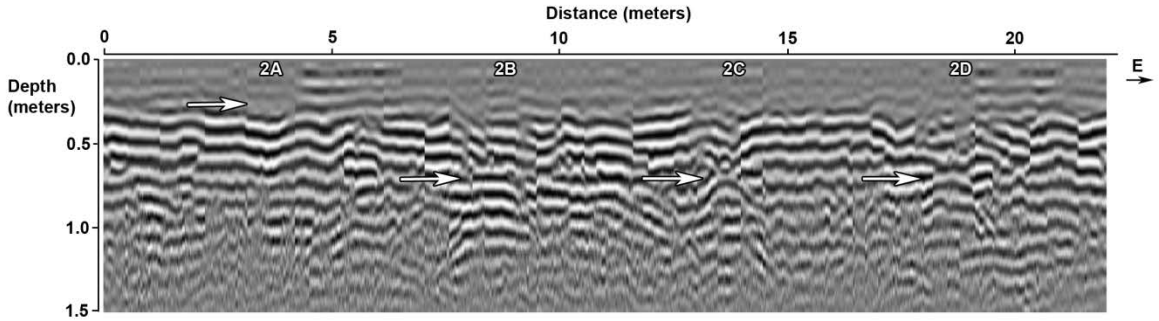

Figure B42: GPR reflection profile using the 500-MHz antenna of Row 2 at 22 months

GPR 500 REFLECTION PROFILE AT MONTH 23

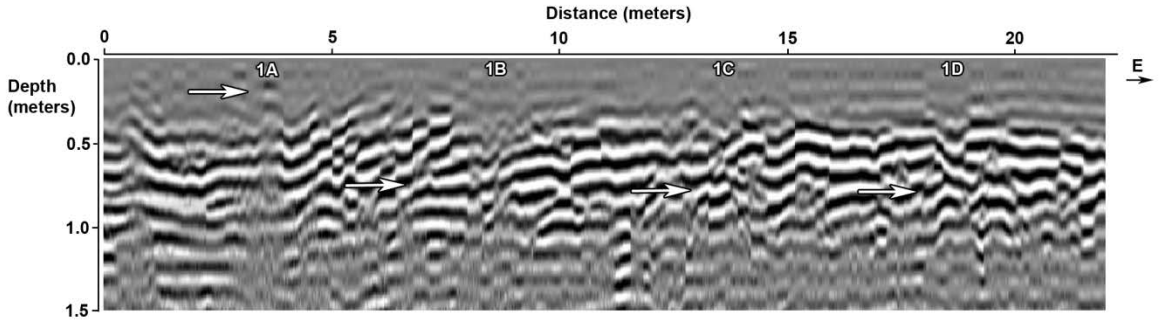

Figure B43: GPR reflection profile using the 500-MHz antenna of Row 1 at 23 months

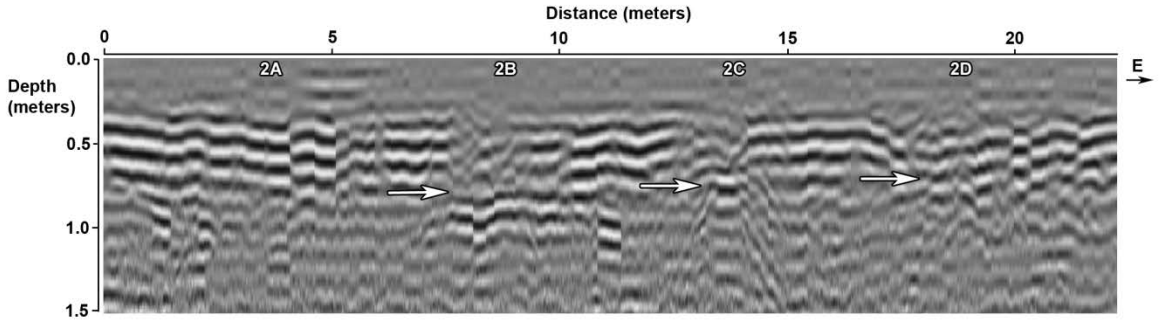

Figure B44: GPR reflection profile using the 500-MHz antenna of Row 2 at 23 months

GPR 500 REFLECTION PROFILE AT MONTH 24

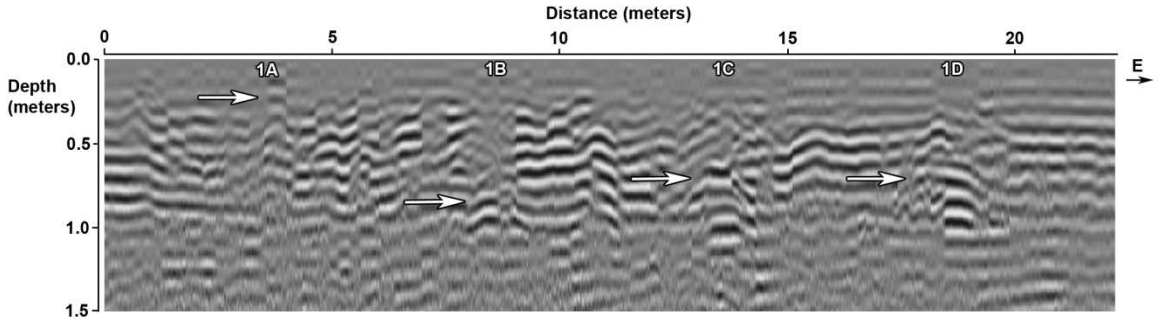

Figure B45: GPR reflection profile using the 500-MHz antenna of Row 1 at 24 months

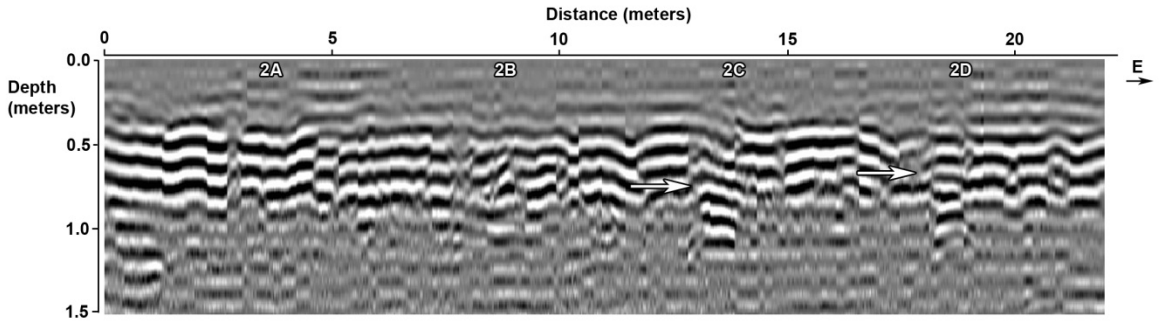

Figure B46: GPR reflection profile using the 500-MHz antenna of Row 2 at 24 months

GPR 500 REFLECTION PROFILE AT MONTH 25

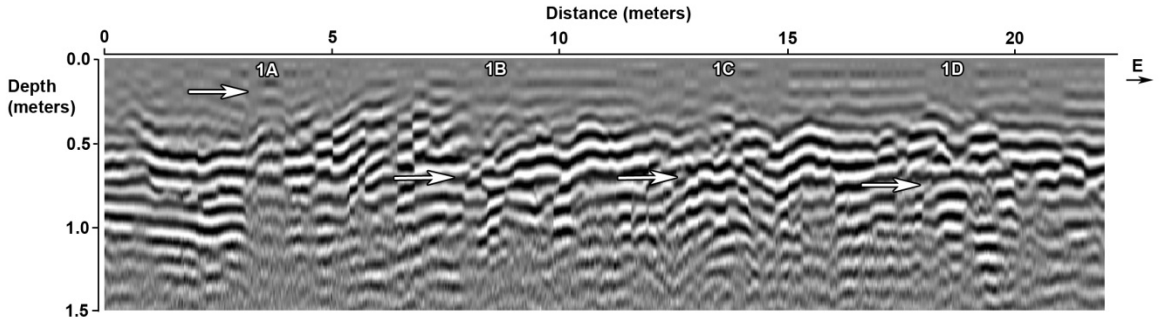

Figure B47: GPR reflection profile using the 500-MHz antenna of Row 1 at 25 months

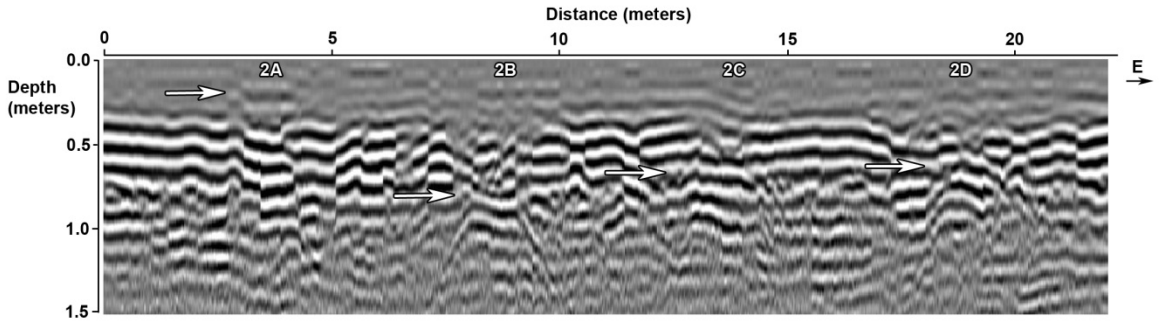

Figure B48: GPR reflection profile using the 500-MHz antenna of Row 2 at 25 months

GPR 500 REFLECTION PROFILE AT MONTH 26

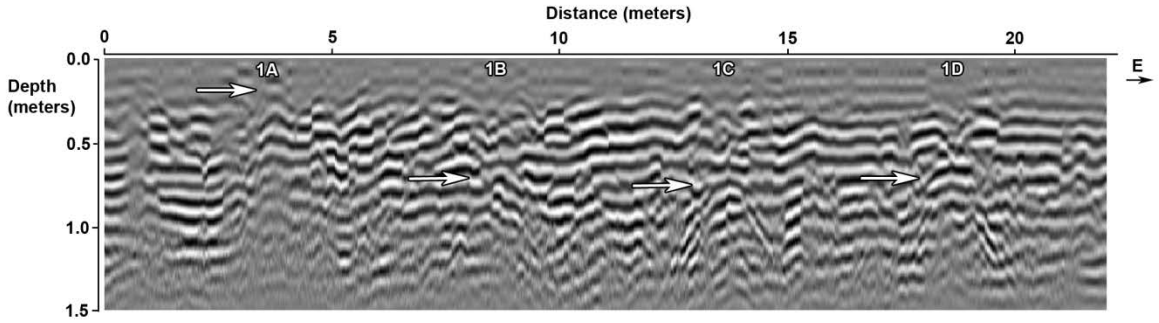

Figure B49: GPR reflection profile using the 500-MHz antenna of Row 1 at 26 months

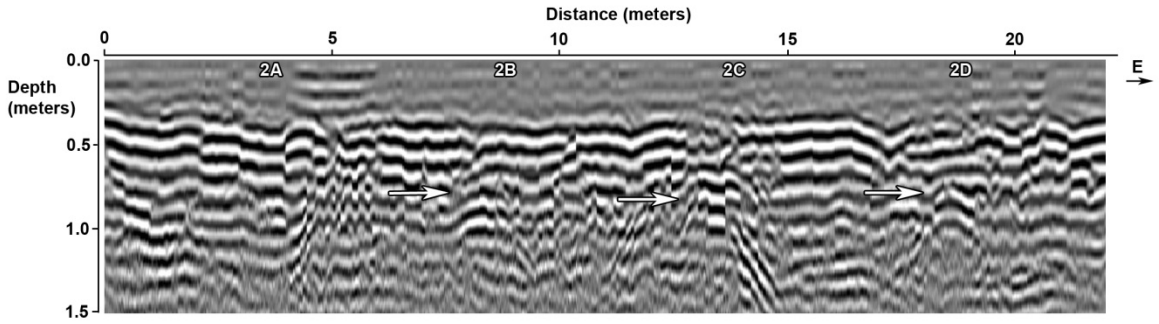

Figure B50: GPR reflection profile using the 500-MHz antenna of Row 2 at 26 months

GPR 500 REFLECTION PROFILE AT MONTH 27

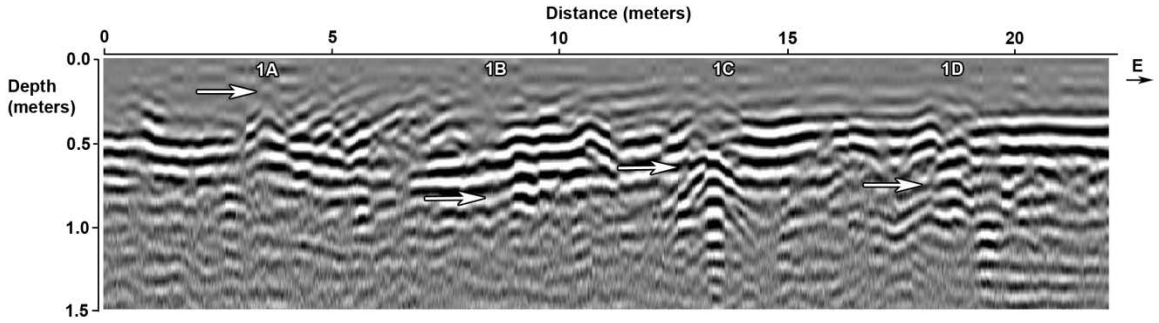

Figure B49: GPR reflection profile using the 500-MHz antenna of Row 1 at 27 months

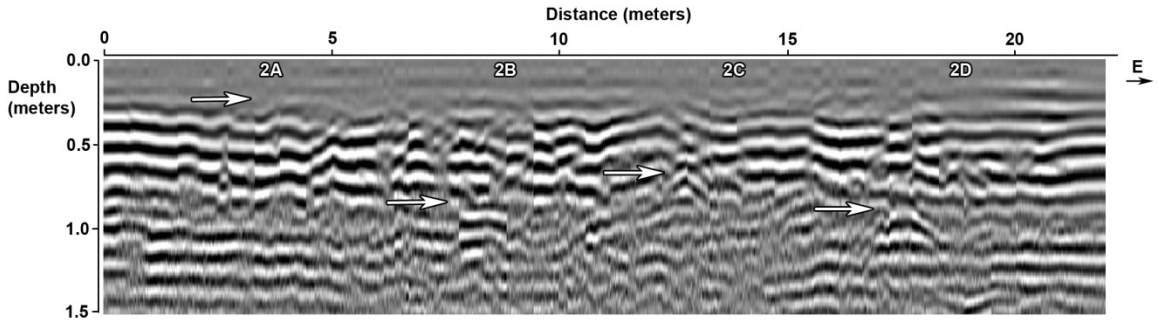

Figure B50: GPR reflection profile using the 500-MHz antenna of Row 2 at 27 months

GPR 500 REFLECTION PROFILE AT MONTH 28

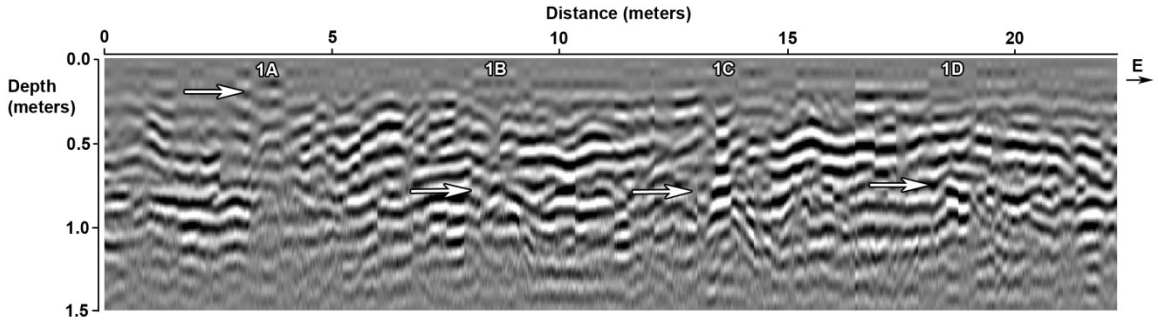

Figure B49: GPR reflection profile using the 500-MHz antenna of Row 1 at 28 months

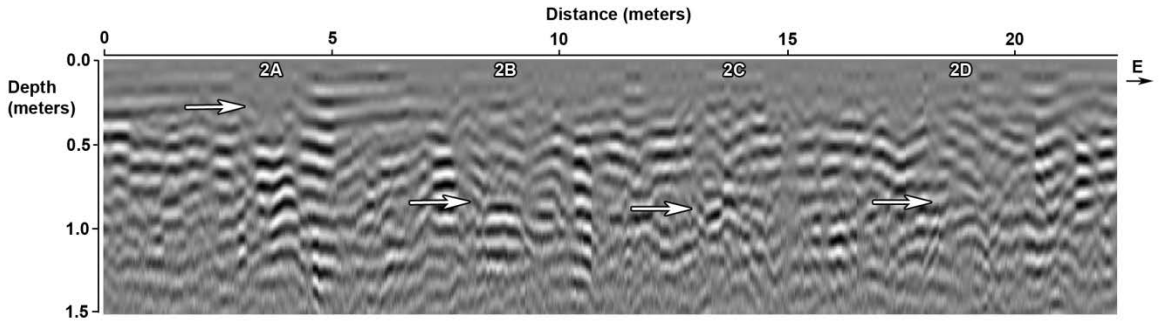

Figure B50: GPR reflection profile using the 500-MHz antenna of Row 2 at 28 months

GPR 500 REFLECTION PROFILE AT MONTH 29

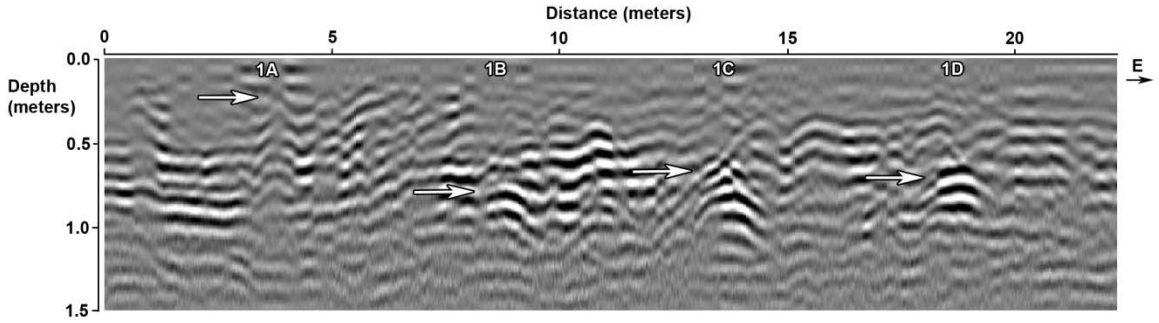

Figure B49: GPR reflection profile using the 500-MHz antenna of Row 1 at 29 months

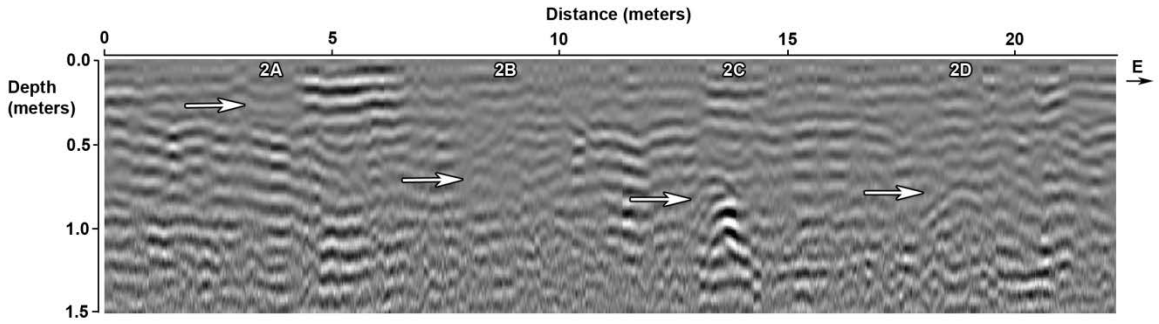

Figure B50: GPR reflection profile using the 500-MHz antenna of Row 2 at 29 months

GPR 500 REFLECTION PROFILE AT MONTH 30

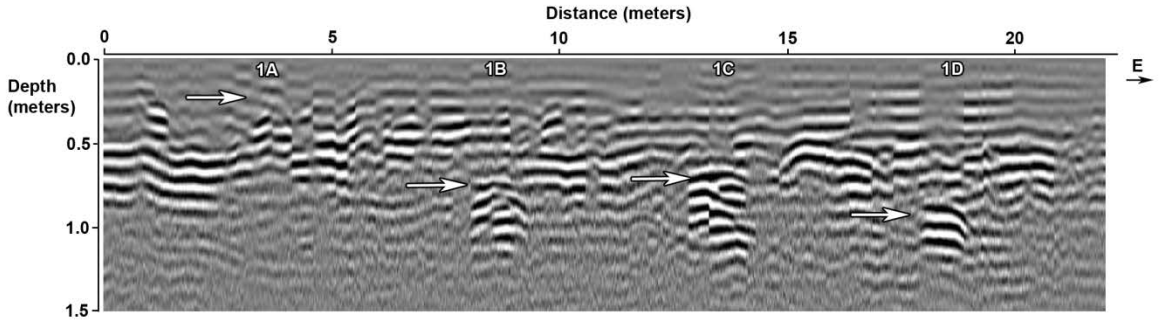

Figure B49: GPR reflection profile using the 500-MHz antenna of Row 1 at 30 months

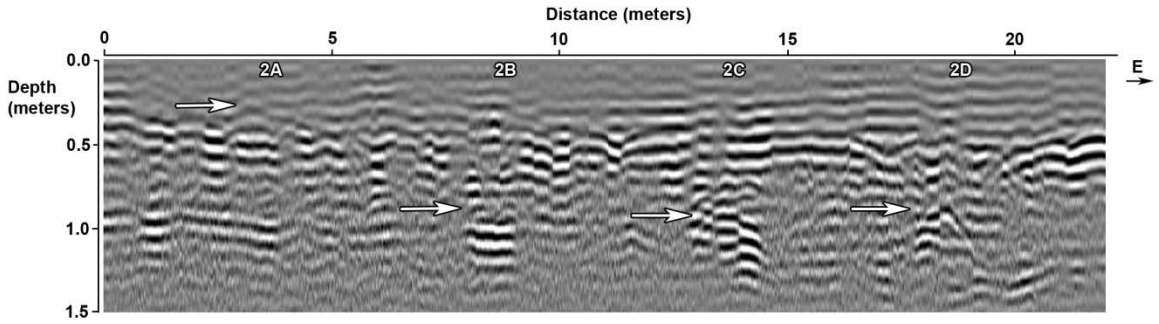

Figure B50: GPR reflection profile using the 500-MHz antenna of Row 2 at 30 months

APPENDIX C: GROUND-PENETRATING RADAR 500-MHZ HORIZONTAL TIME SLICES

GPR 500 TIME SLICE AT MONTH 1
(shallow)

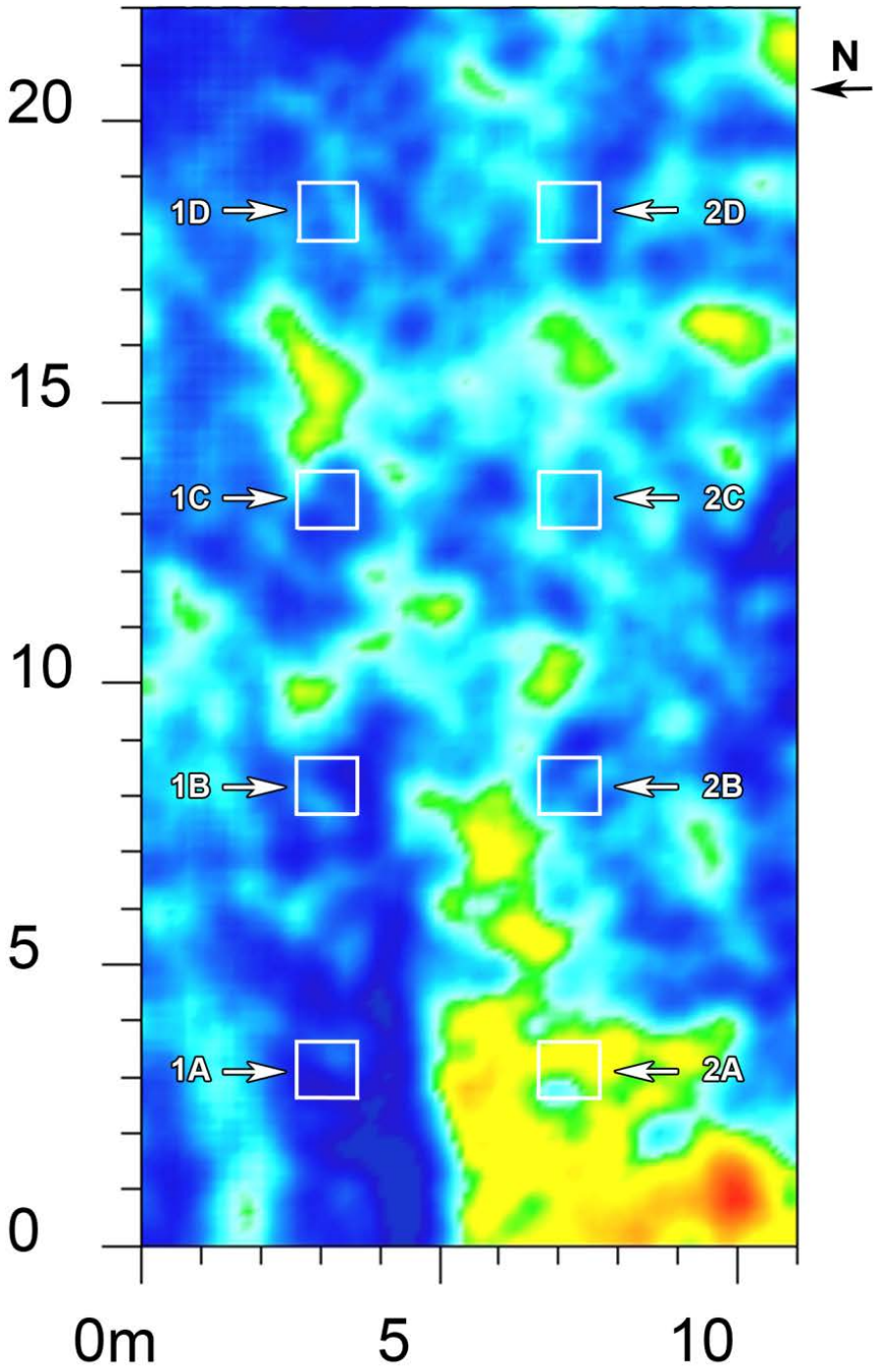

Figure C1: GPR horizontal slice using the 500-MHz antenna at 1 month. The horizontal slice is approximately 0.45 m in depth.

GPR 500 TIME SLICE AT MONTH 1
(deep)

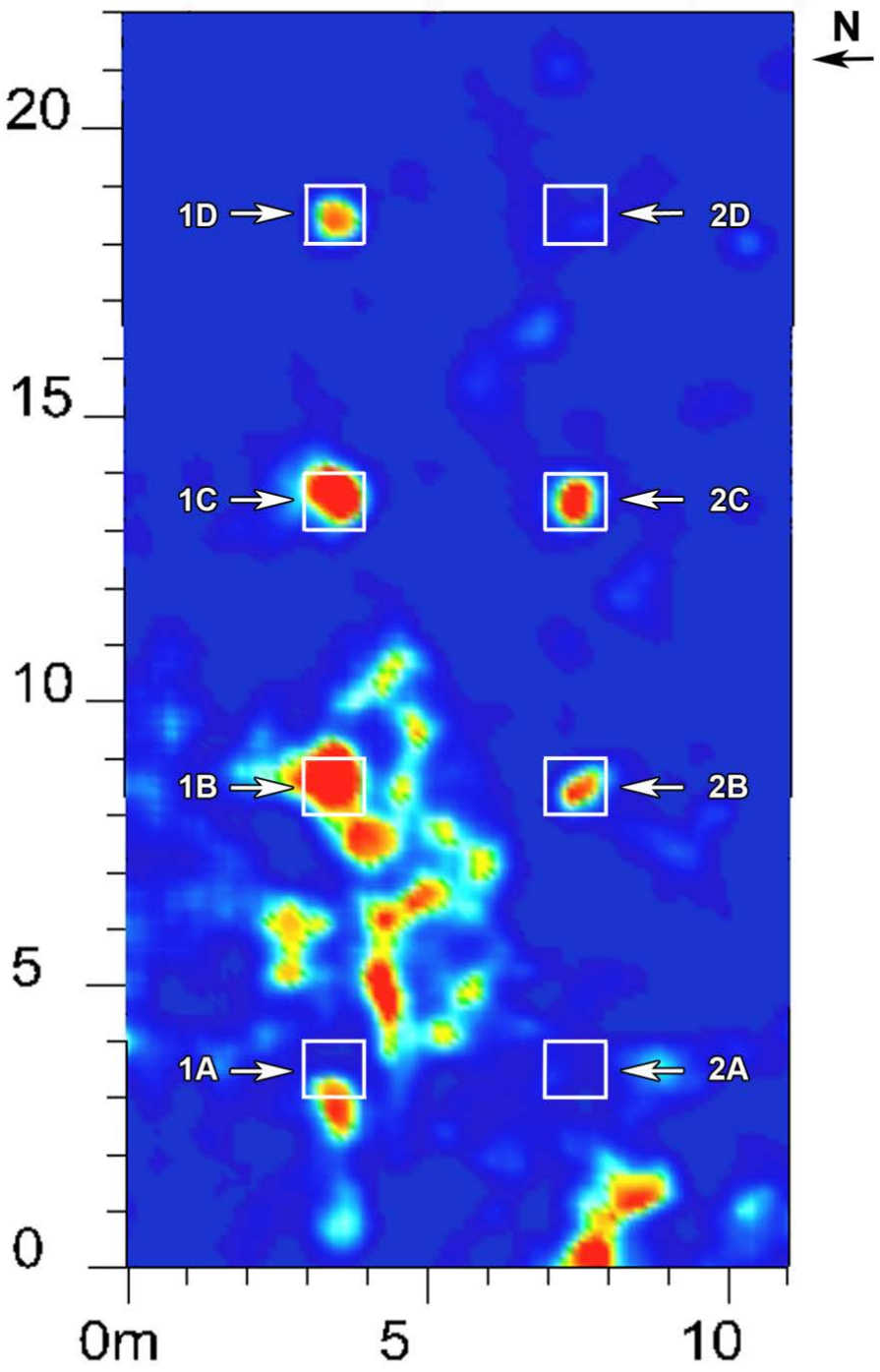

Figure C2: GPR horizontal slice using the 500-MHz antenna at 1 month. The horizontal slice is between 0.85 and 1.0 m in depth.

GPR 500 TIME SLICE AT MONTH 2
(shallow)

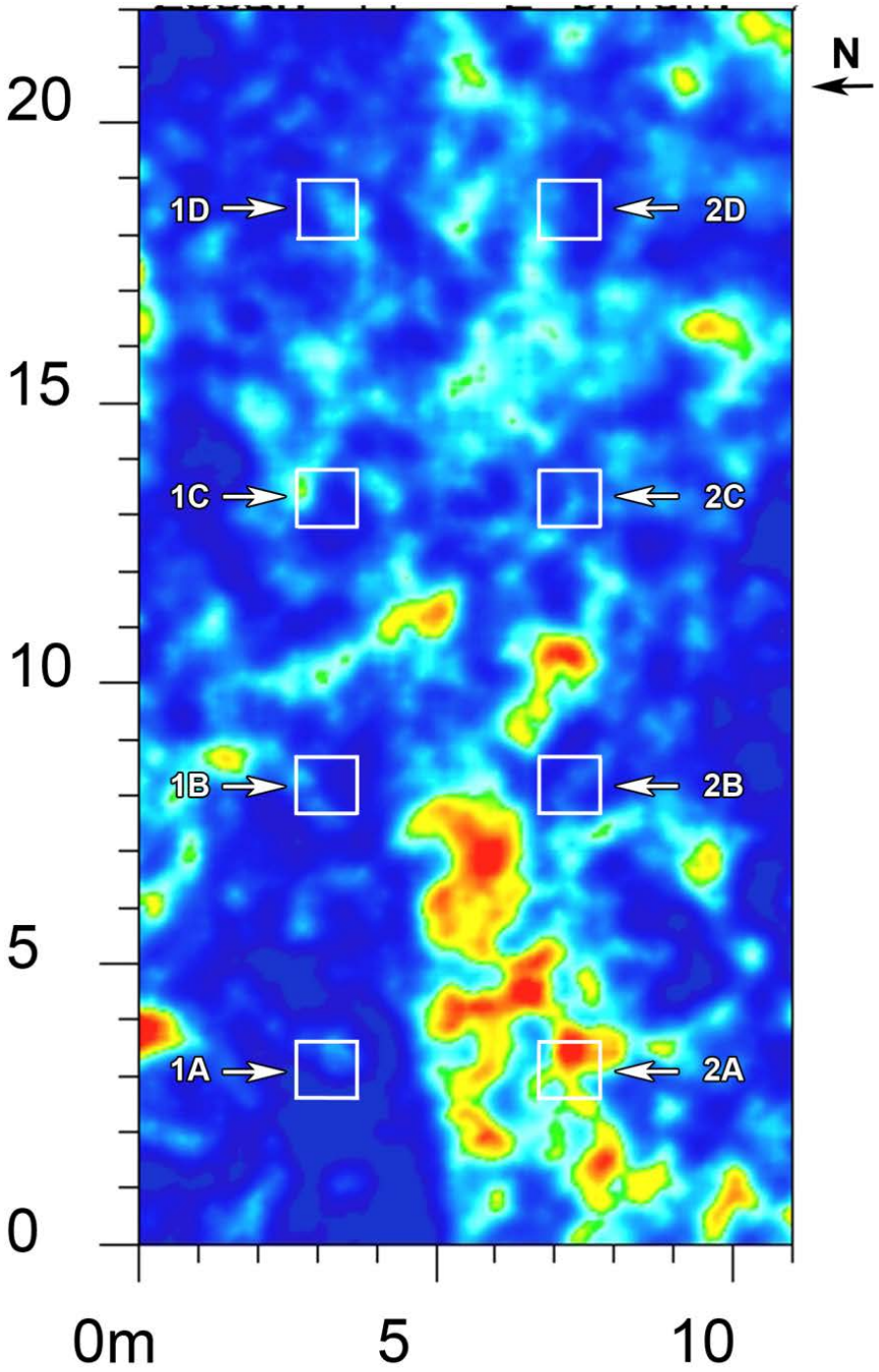

Figure C3: GPR horizontal slice using the 500-MHz antenna at 2 months. The horizontal slice is approximately 0.45 m in depth.

GPR 500 TIME SLICE AT MONTH 2
(deep)

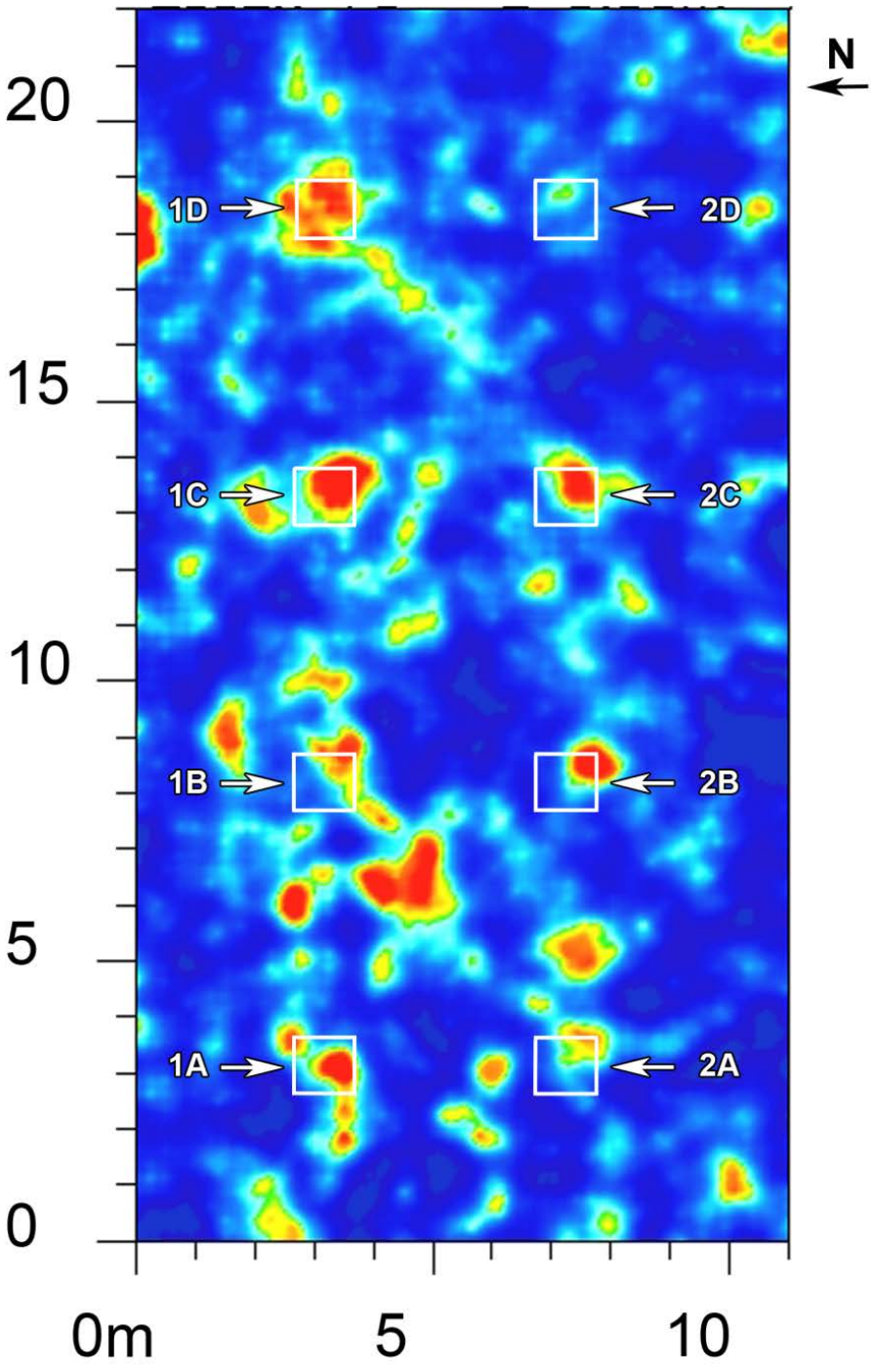

Figure C4: GPR horizontal slice using the 500-MHz antenna at 2 months. The horizontal slice is between 0.85 and 1.0 m in depth.

GPR 500 TIME SLICE AT MONTH 3
(shallow)

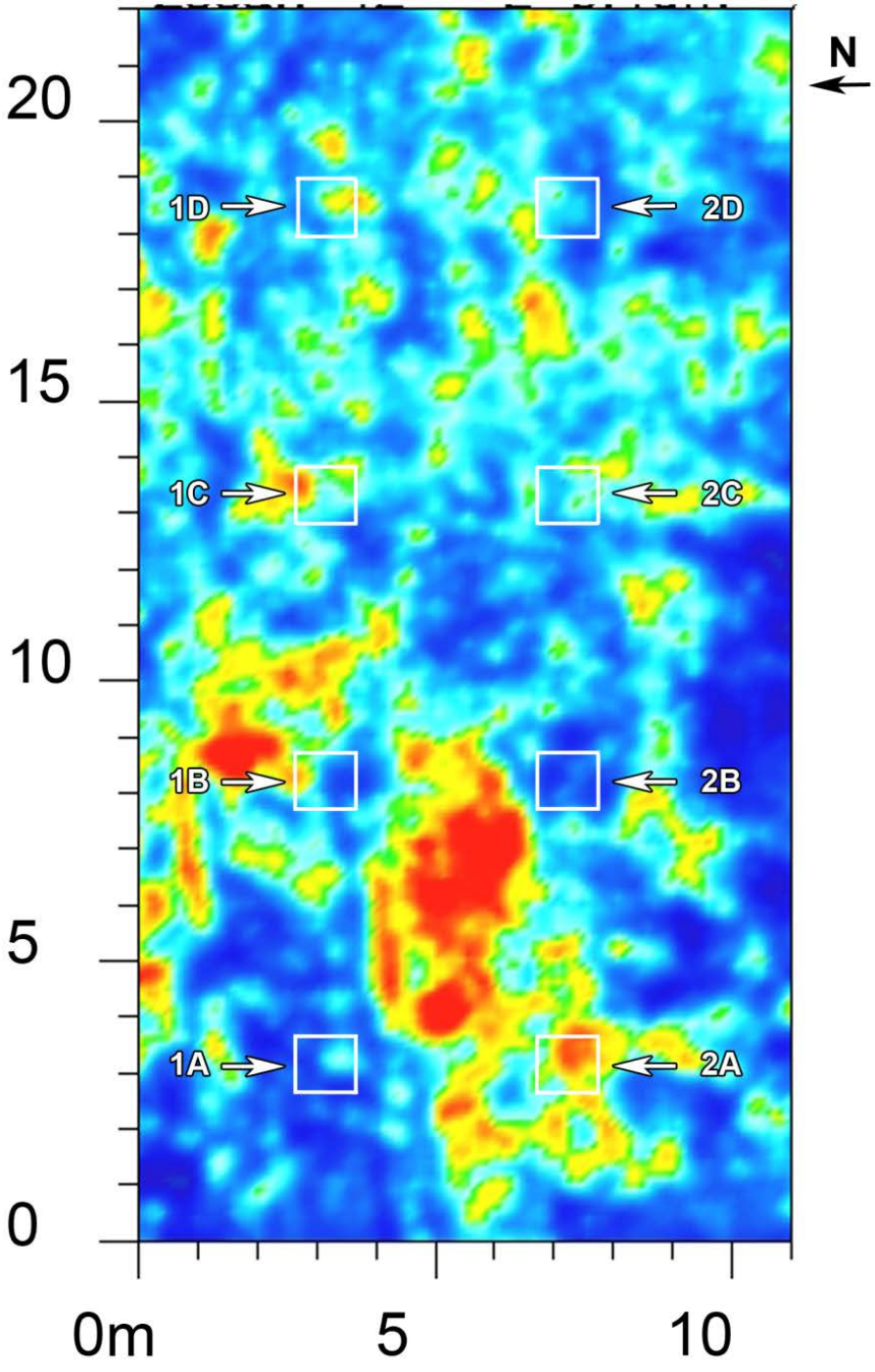

Figure C5: GPR horizontal slice using the 500-MHz antenna at 3 months. The horizontal slice is approximately 0.45 m in depth.

GPR 500 TIME SLICE AT MONTH 3
(deep)

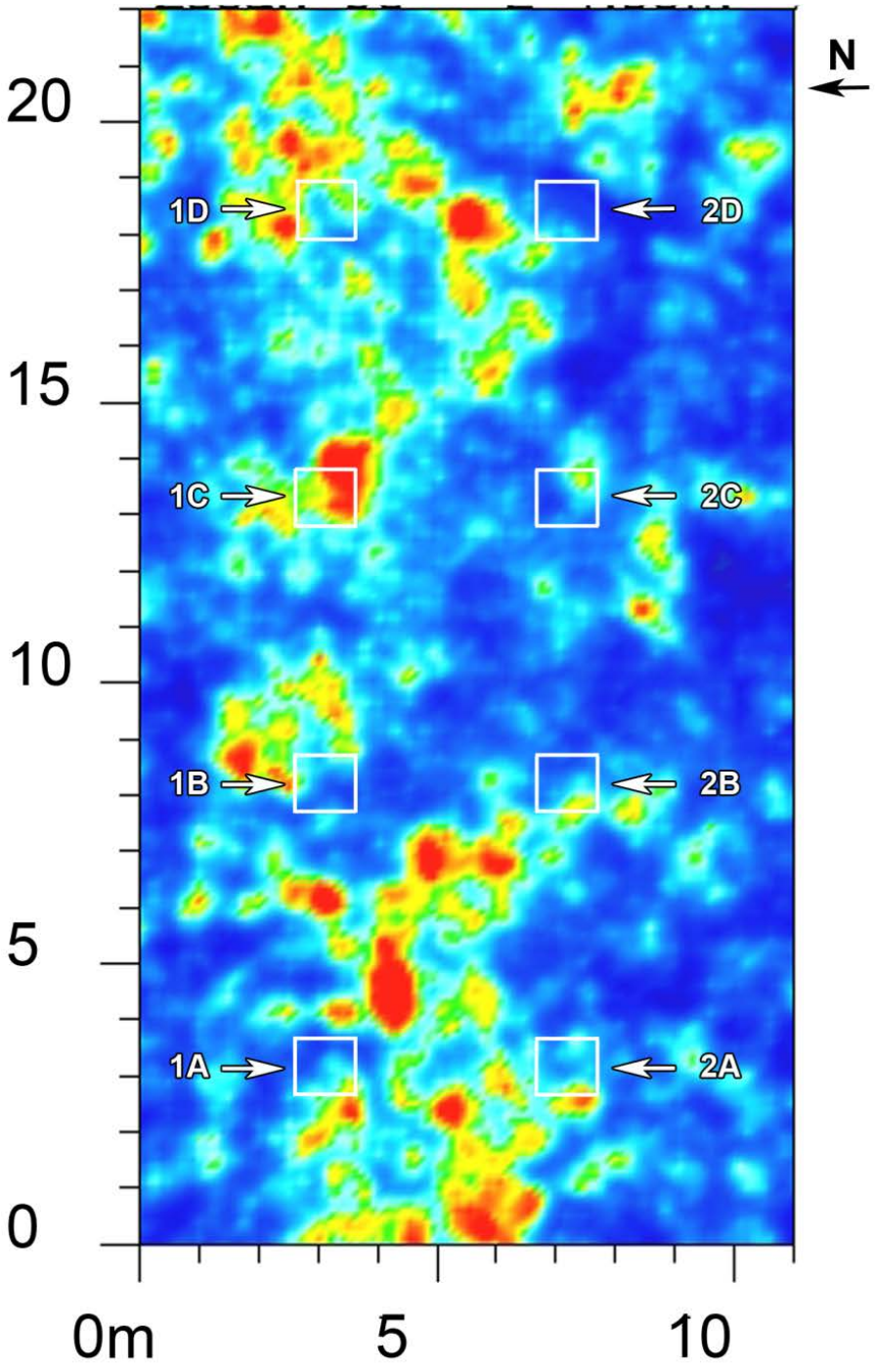

Figure C6: GPR horizontal slice using the 500-MHz antenna at 3 months. The horizontal slice is between 0.85 and 1.0 m in depth.

GPR 500 TIME SLICE AT MONTH 4

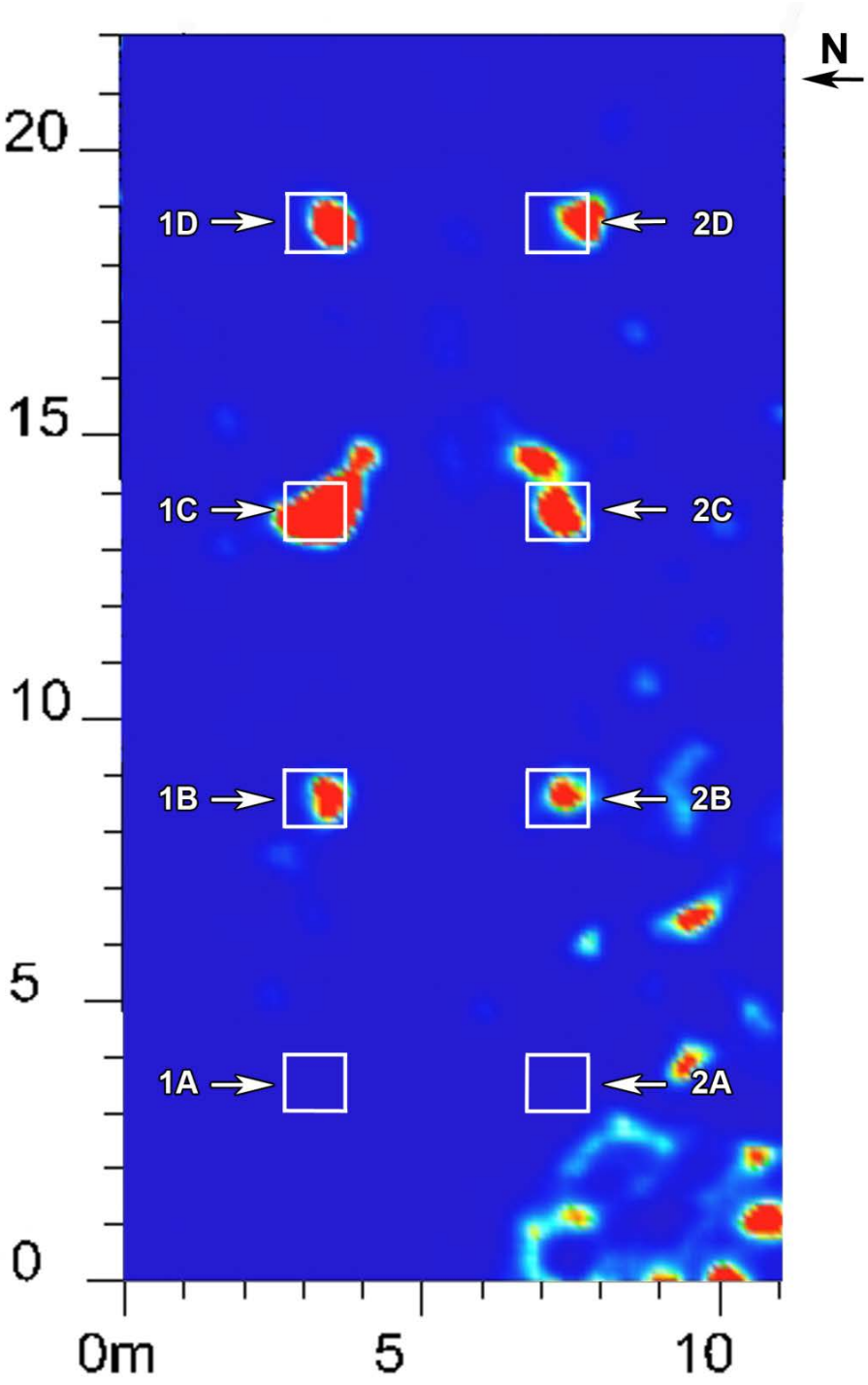

Figure C7: GPR horizontal slice using the 500-MHz antenna at 4 months. The horizontal slice is between 0.85 and 1.0 m in depth.

GPR 500 TIME SLICE AT MONTH 5

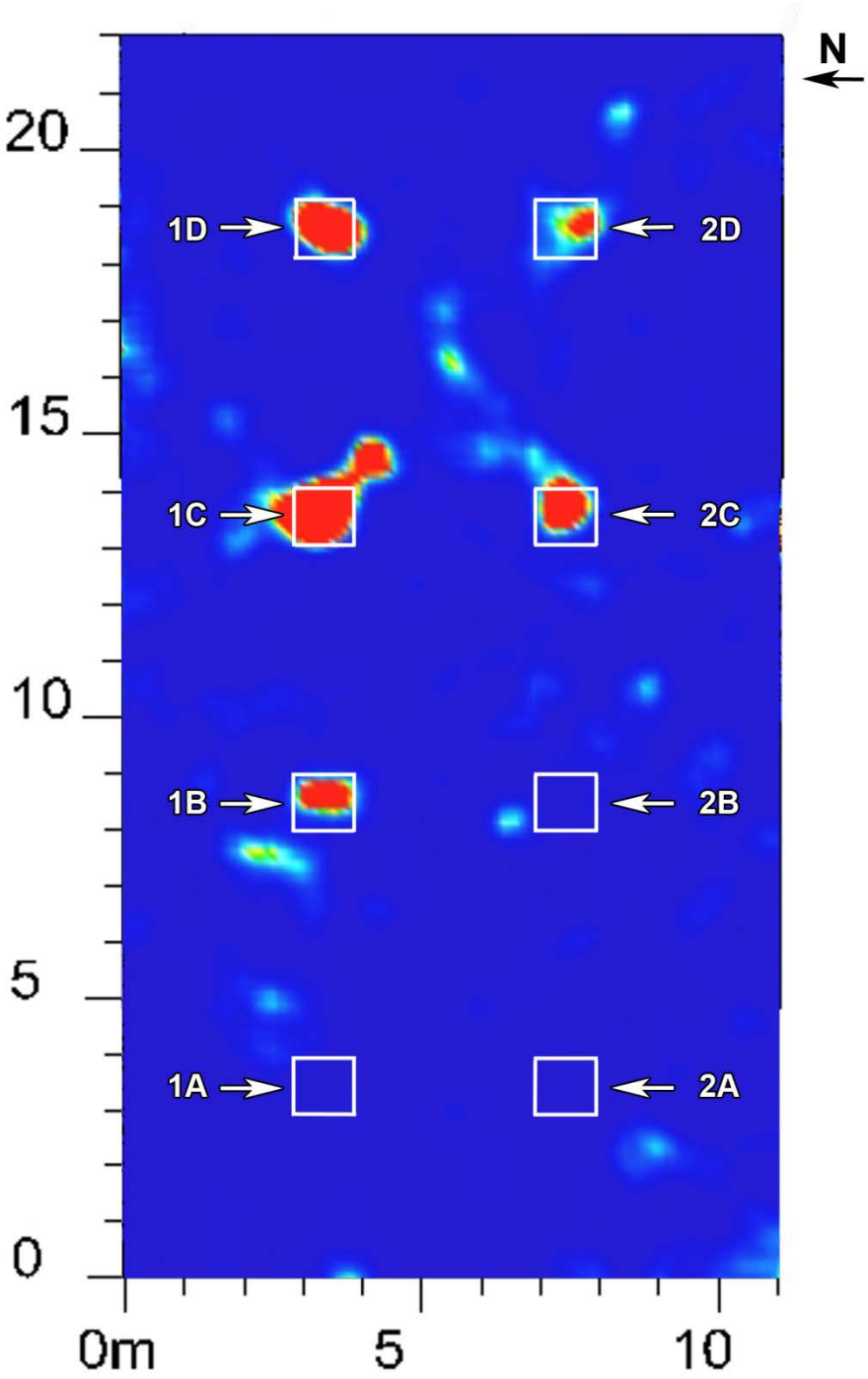

Figure C8: GPR horizontal slice using the 500-MHz antenna at 5 months. The horizontal slice is between 0.85 and 1.0 m in depth.

GPR 500 TIME SLICE AT MONTH 6

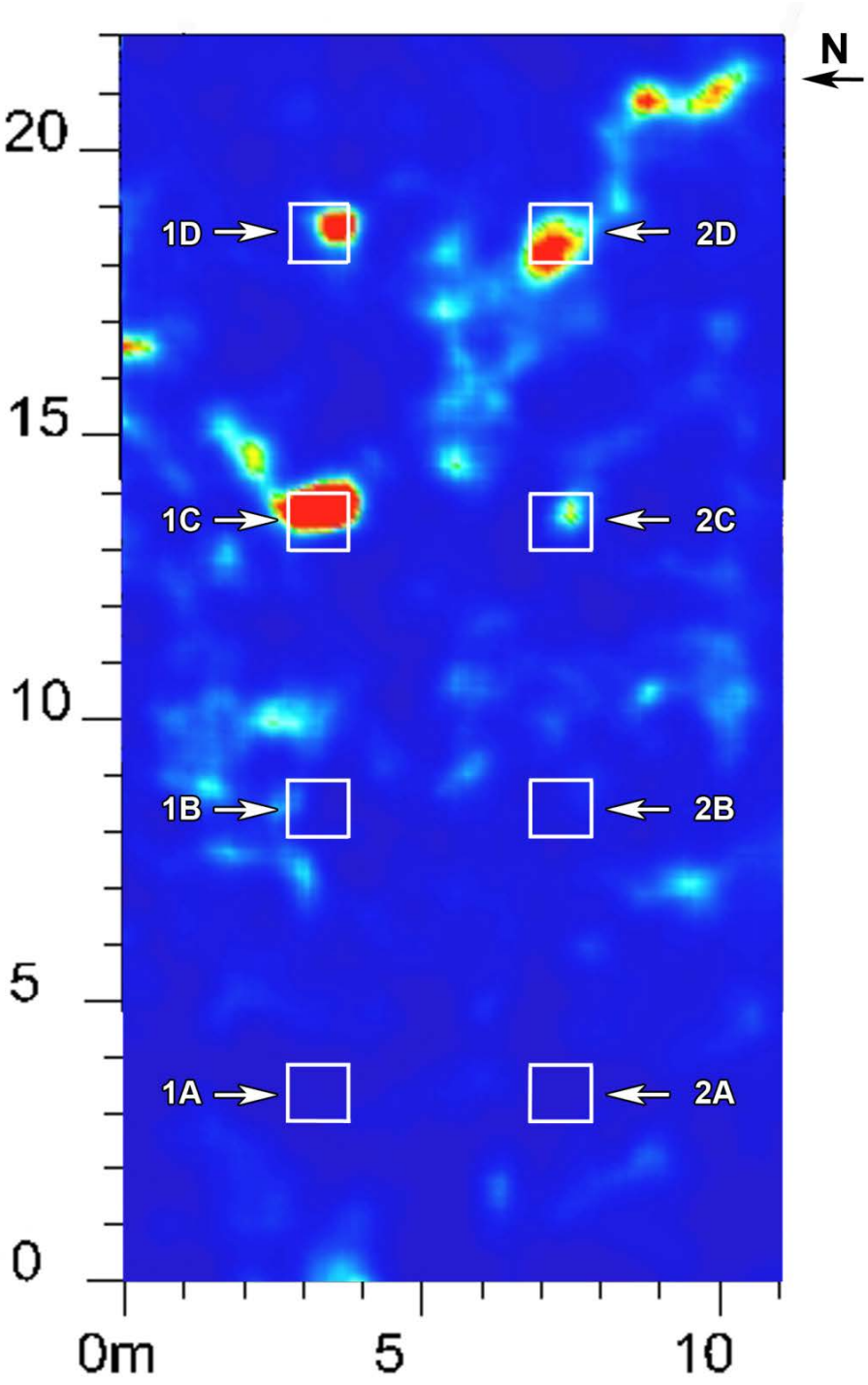

Figure C9: GPR horizontal slice using the 500-MHz antenna at 6 months. The horizontal slice is between 0.85 and 1.0 m in depth.

GPR 500 TIME SLICE AT MONTH 7

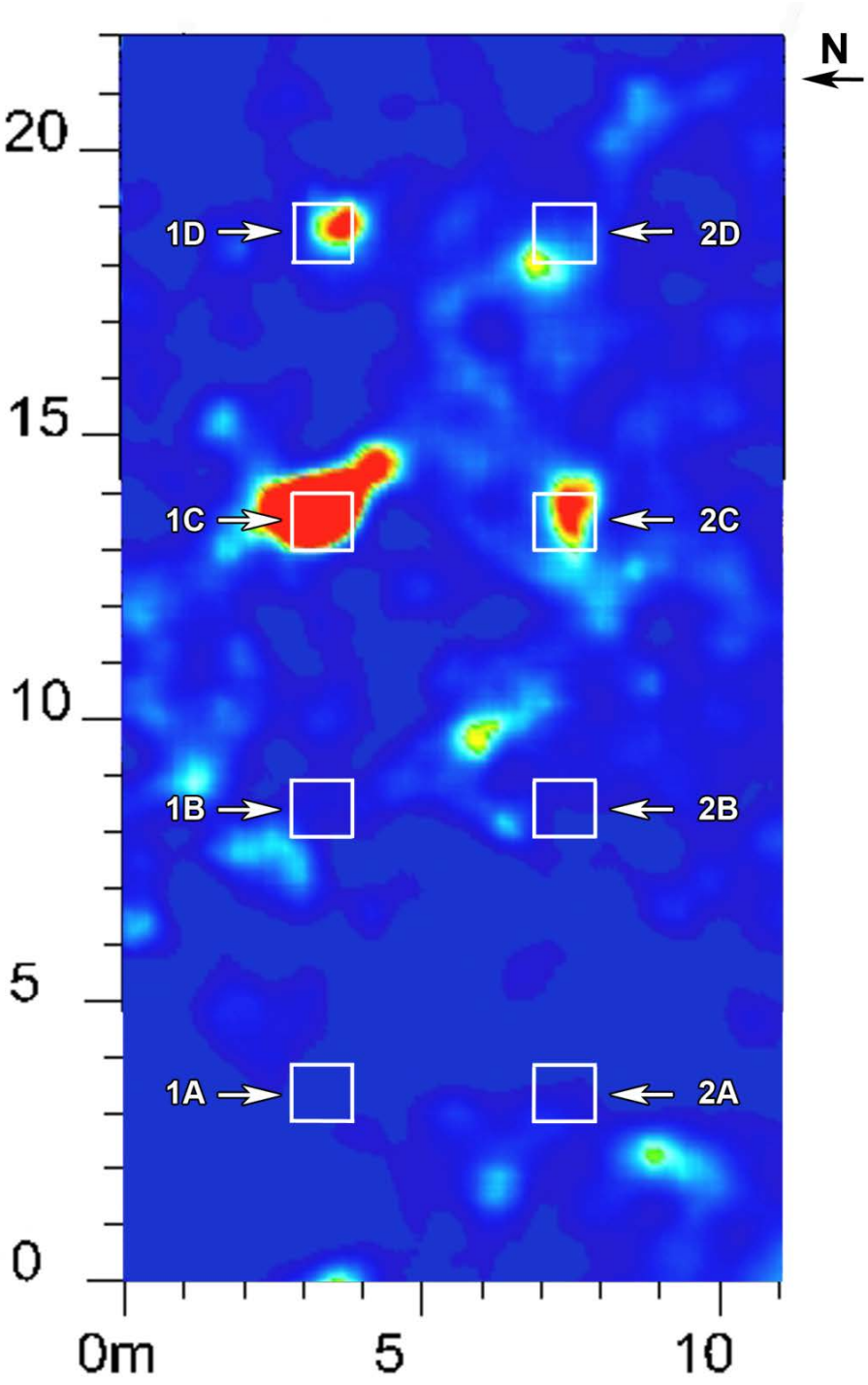

Figure C10: GPR horizontal slice using the 500-MHz antenna at 7 months. The horizontal slice is between 0.85 and 1.0 m in depth.

GPR 500 TIME SLICE AT MONTH 8

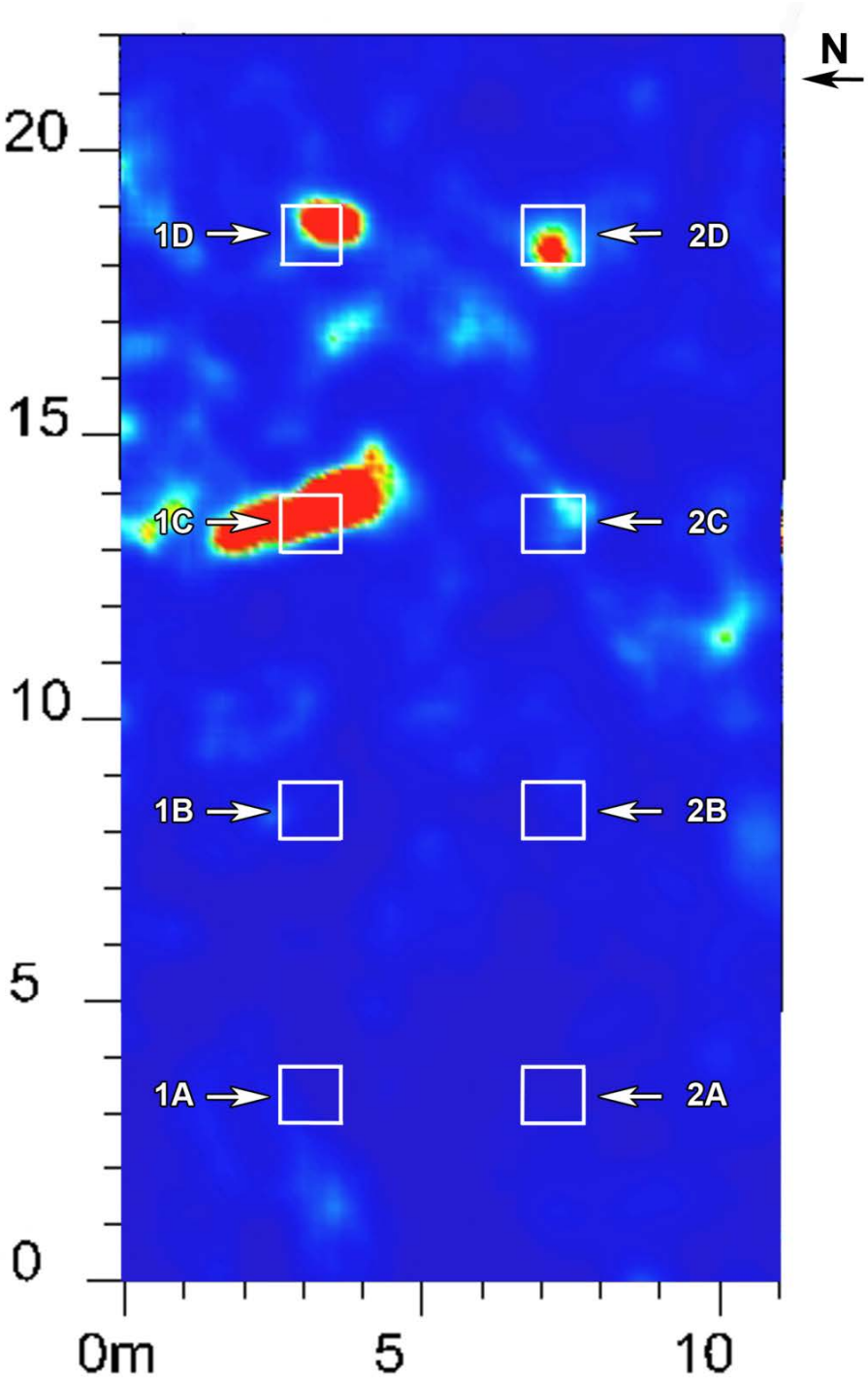

Figure C11: GPR horizontal slice using the 500-MHz antenna at 8 months. The horizontal slice is between 0.85 and 1.0 m in depth.

GPR 500 TIME SLICE AT MONTH 9

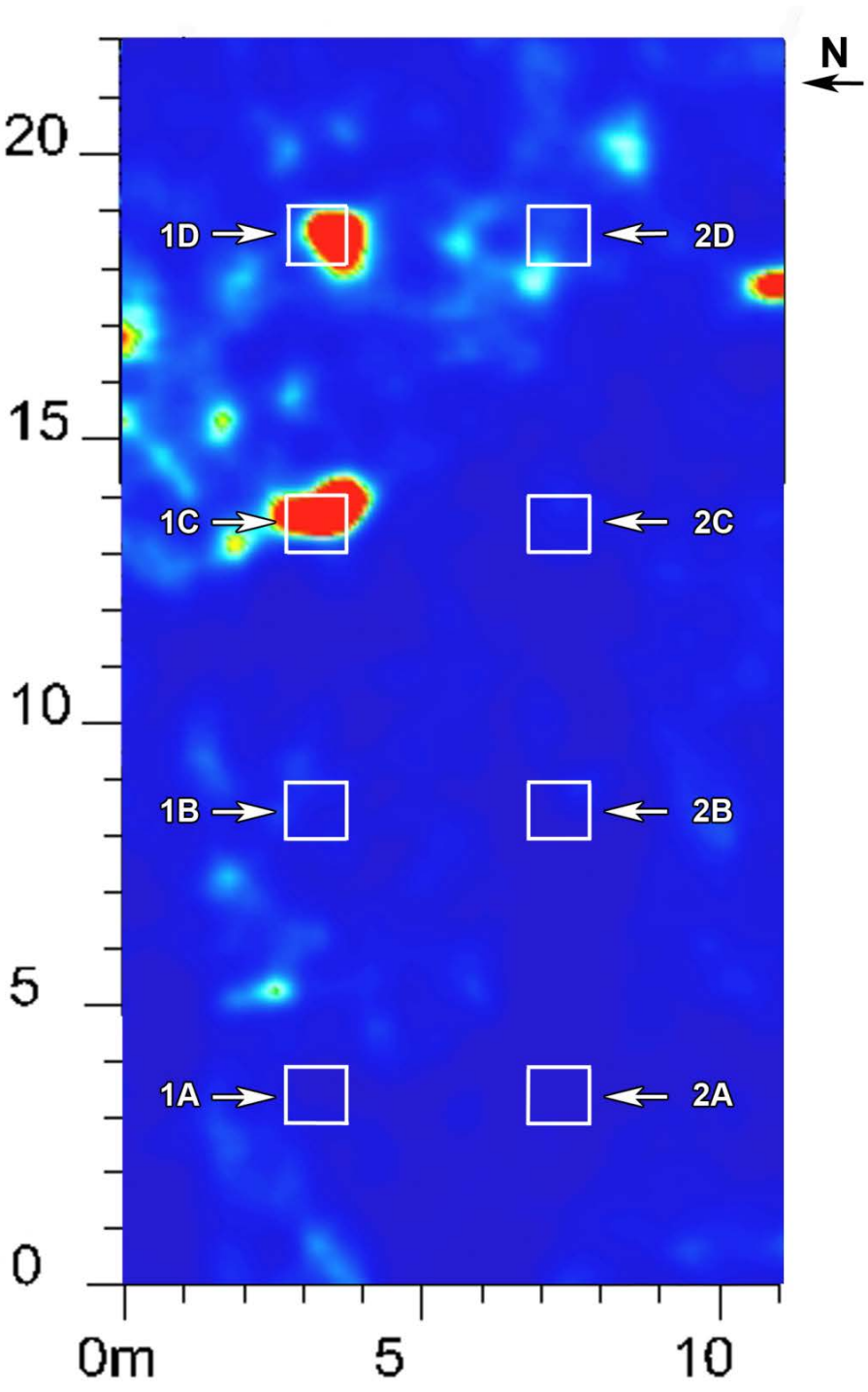

Figure C12: GPR horizontal slice using the 500-MHz antenna at 9 months. The horizontal slice is between 0.85 and 1.0 m in depth.

GPR 500 TIME SLICE AT MONTH 10

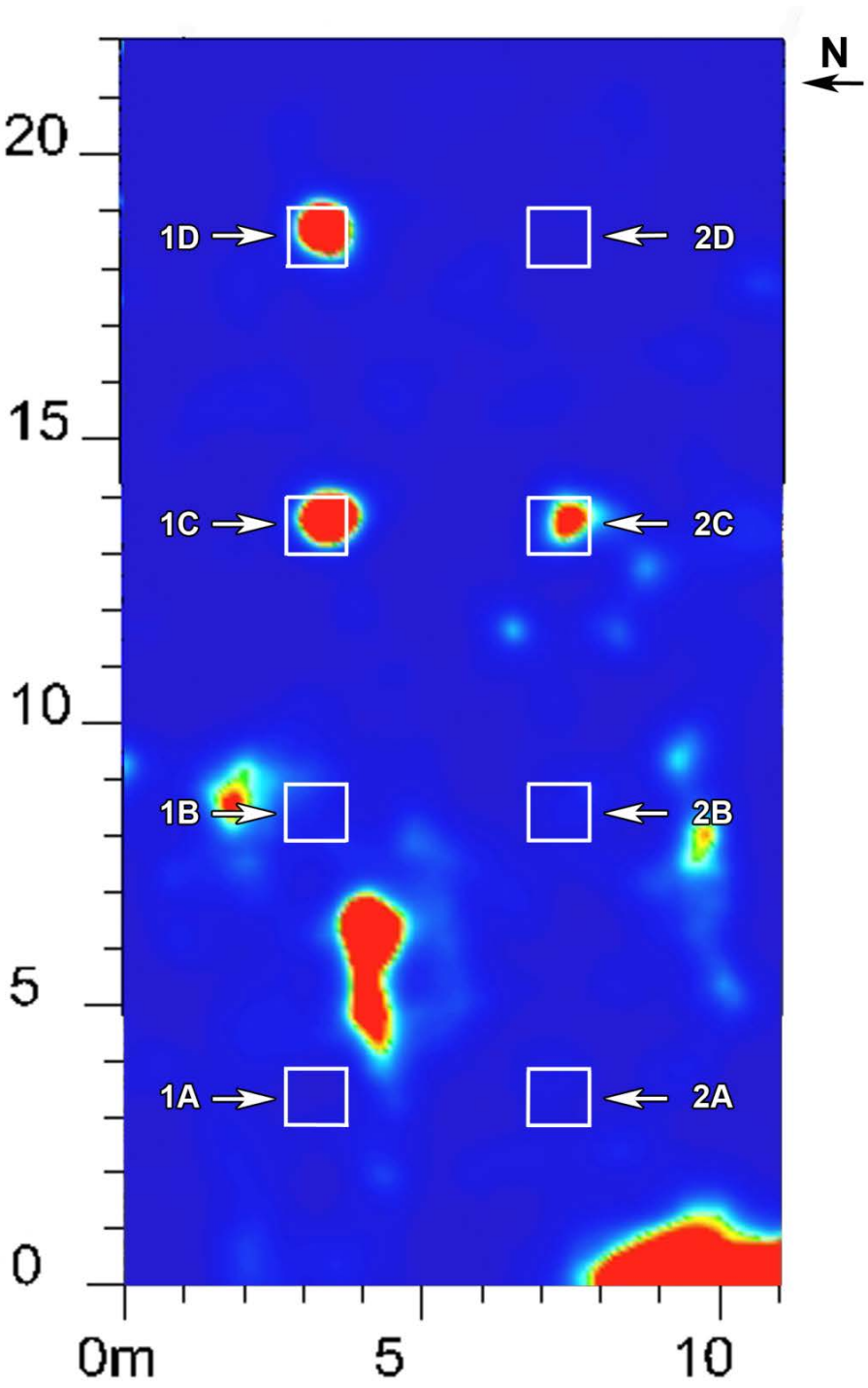

Figure C13: GPR horizontal slice using the 500-MHz antenna at 10 months. The horizontal slice is between 0.85 and 1.0 m in depth.

GPR 500 TIME SLICE AT MONTH 11

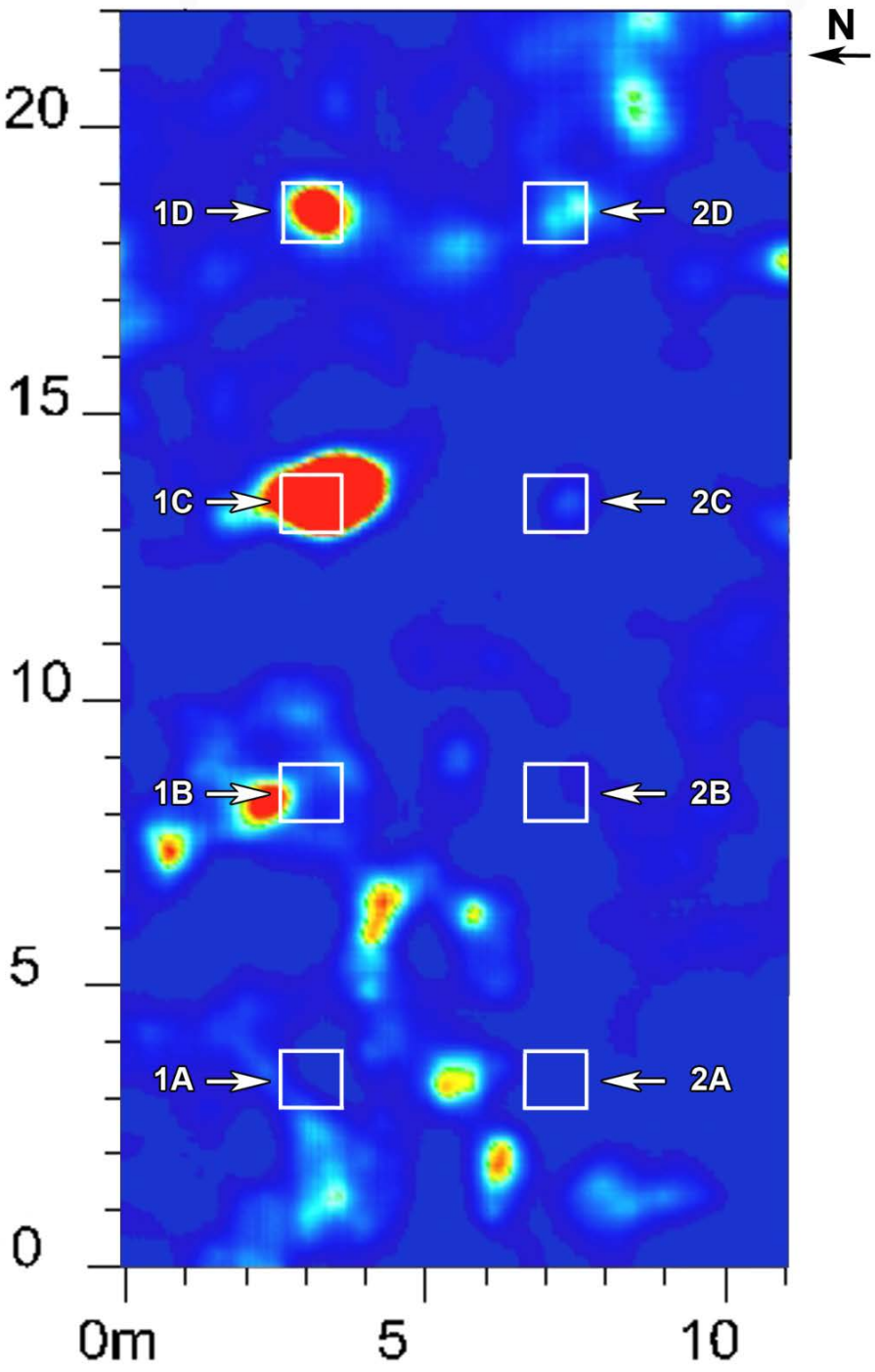

Figure C14: GPR horizontal slice using the 500-MHz antenna at 11 months. The horizontal slice is between 0.85 and 1.0 m in depth.

GPR 500 TIME SLICE AT MONTH 12

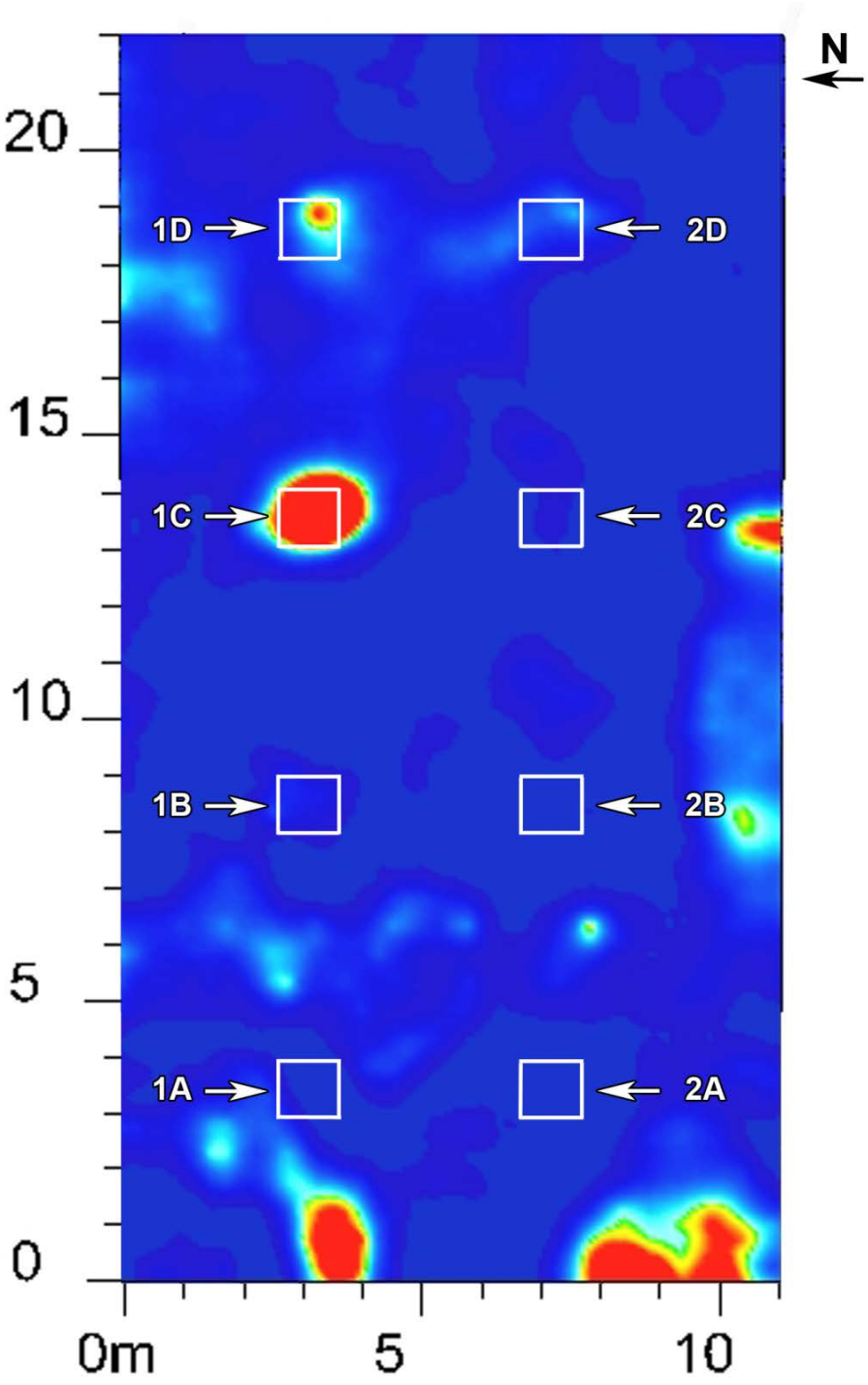

Figure C15: GPR horizontal slice using the 500-MHz antenna at 12 months. The horizontal slice is between 0.85 and 1.0 m in depth.

GPR 500 TIME SLICE AT MONTH 13

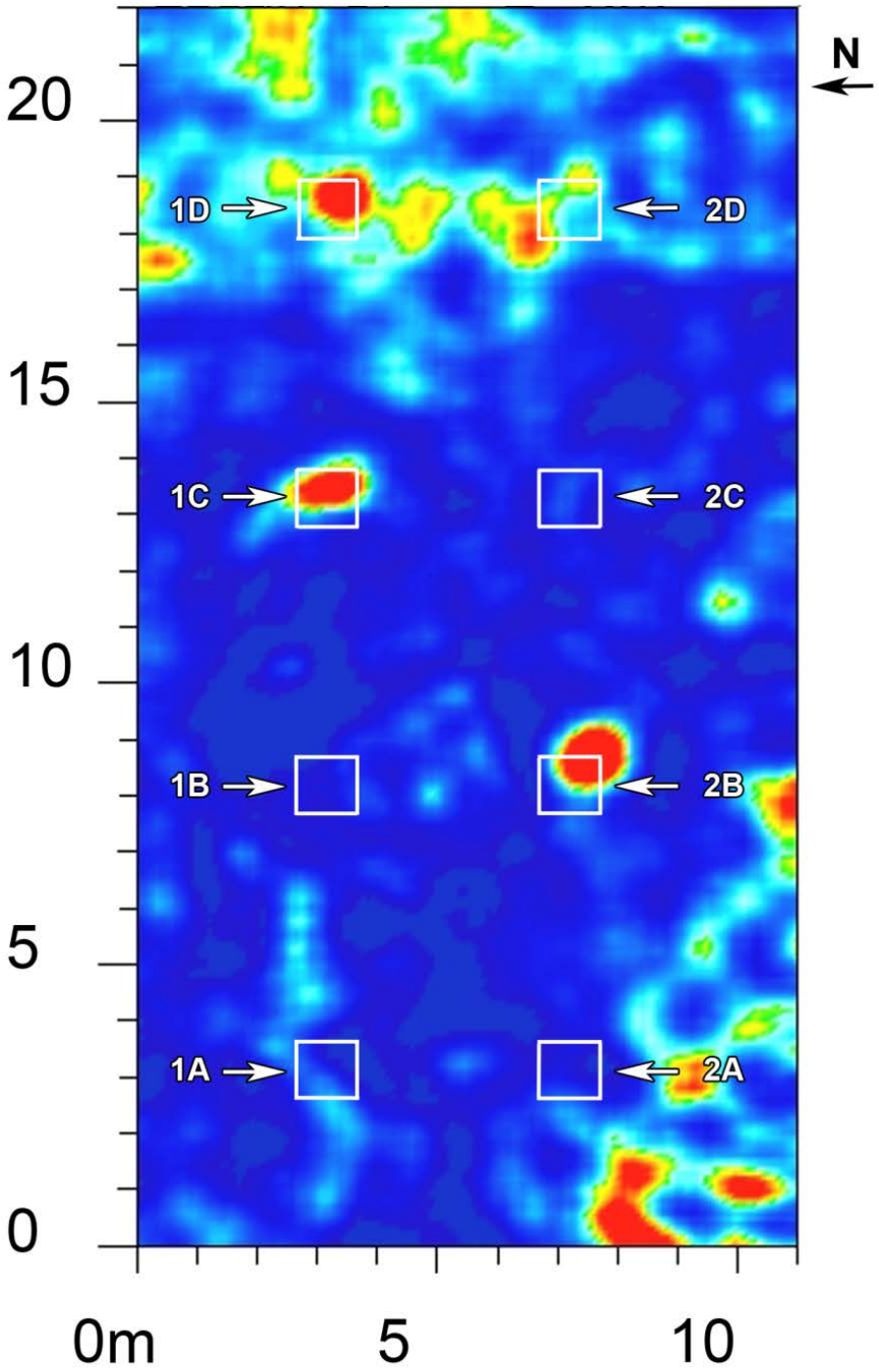

Figure C16: GPR horizontal slice using the 500-MHz antenna at 13 months. The horizontal slice is between 0.85 and 1.0 m in depth.

GPR 500 TIME SLICE AT MONTH 14

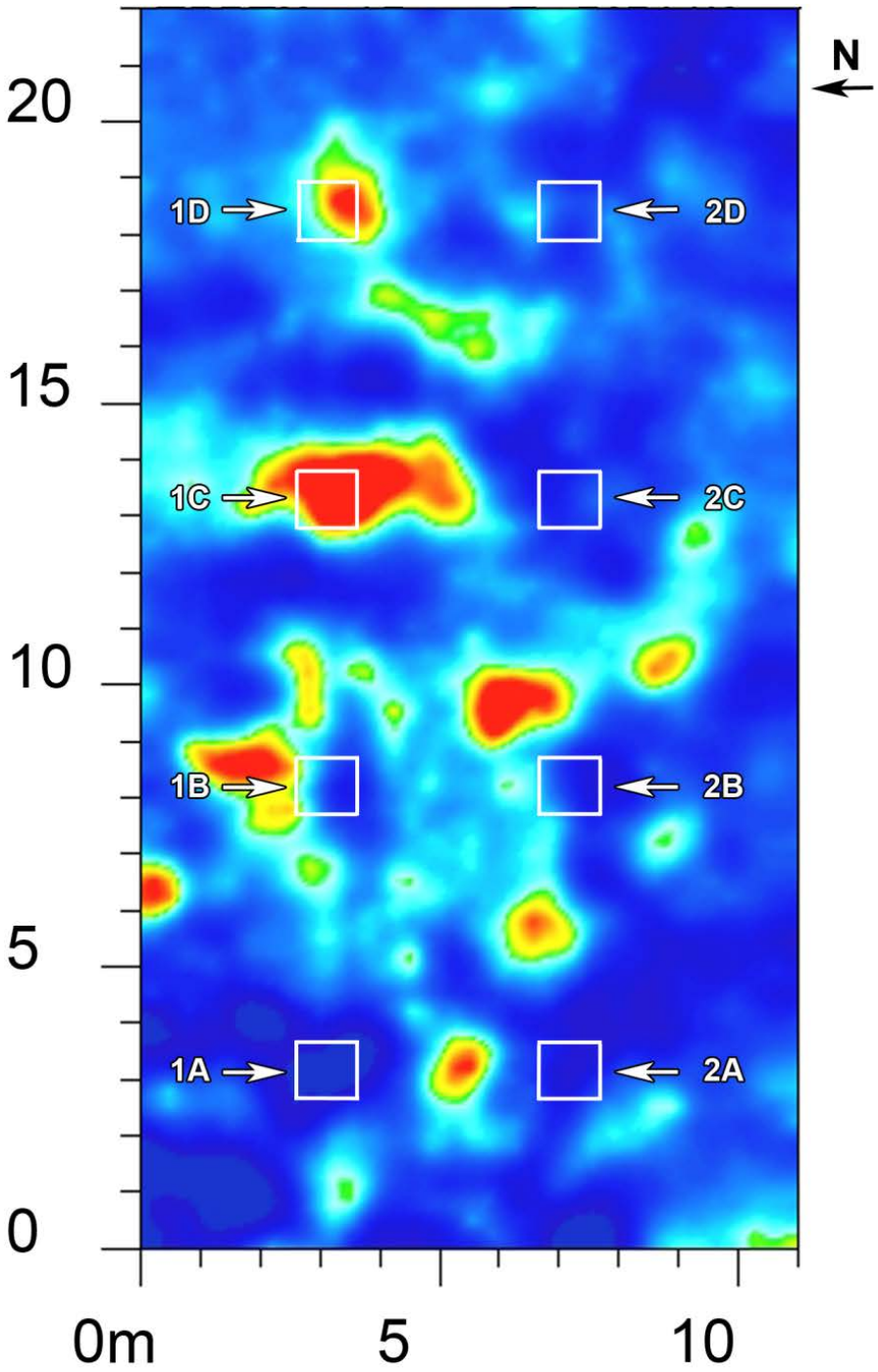

Figure C17: GPR horizontal slice using the 500-MHz antenna at 14 months. The horizontal slice is between 0.85 and 1.0 m in depth.

GPR 500 TIME SLICE AT MONTH 15

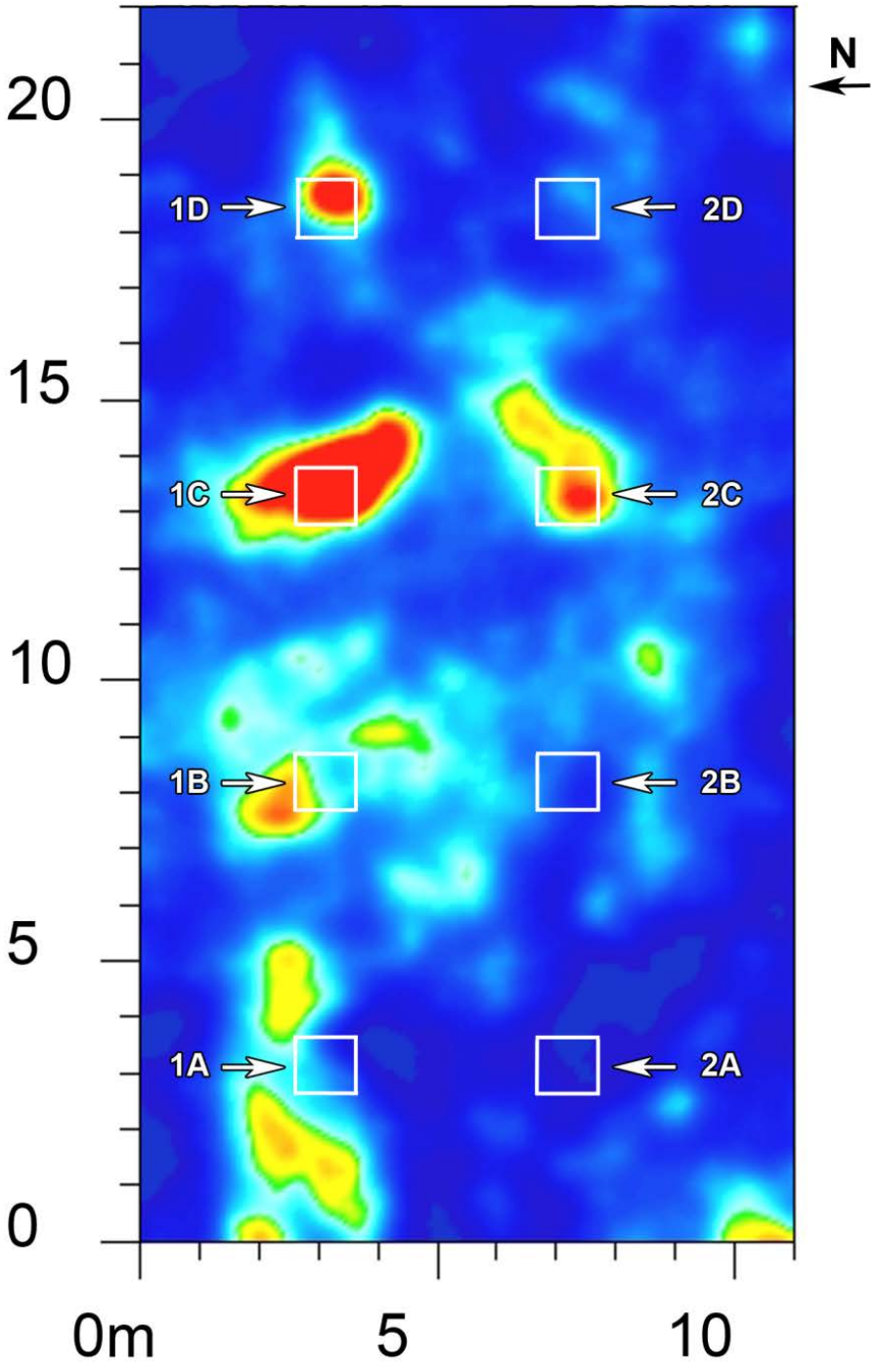

Figure C18: GPR horizontal slice using the 500-MHz antenna at 15 months. The horizontal slice is between 0.85 and 1.0 m in depth.

GPR 500 TIME SLICE AT MONTH 16

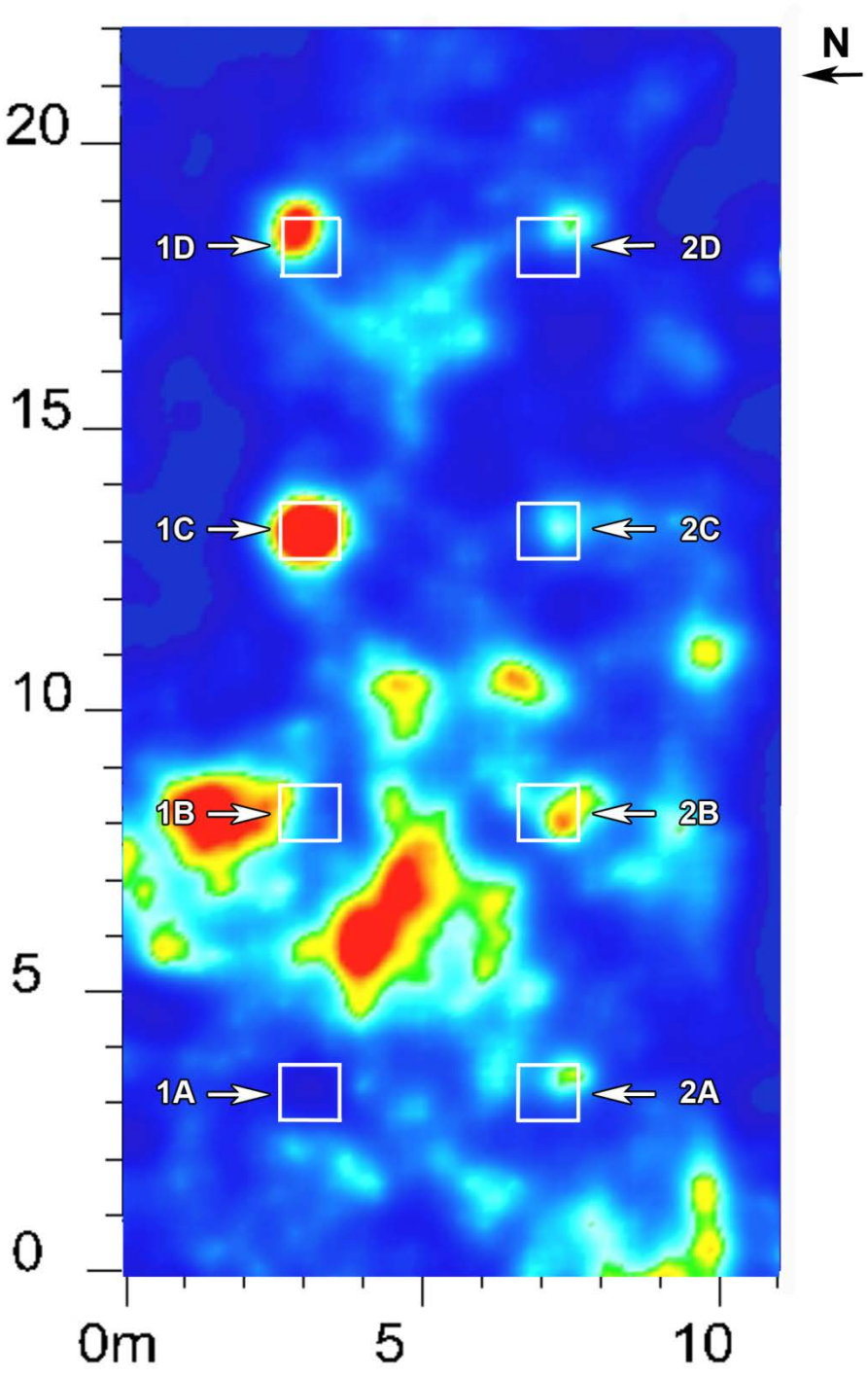

Figure C19: GPR horizontal slice using the 500-MHz antenna at 16 months. The horizontal slice is between 0.85 and 1.0 m in depth.

GPR 500 TIME SLICE AT MONTH 17

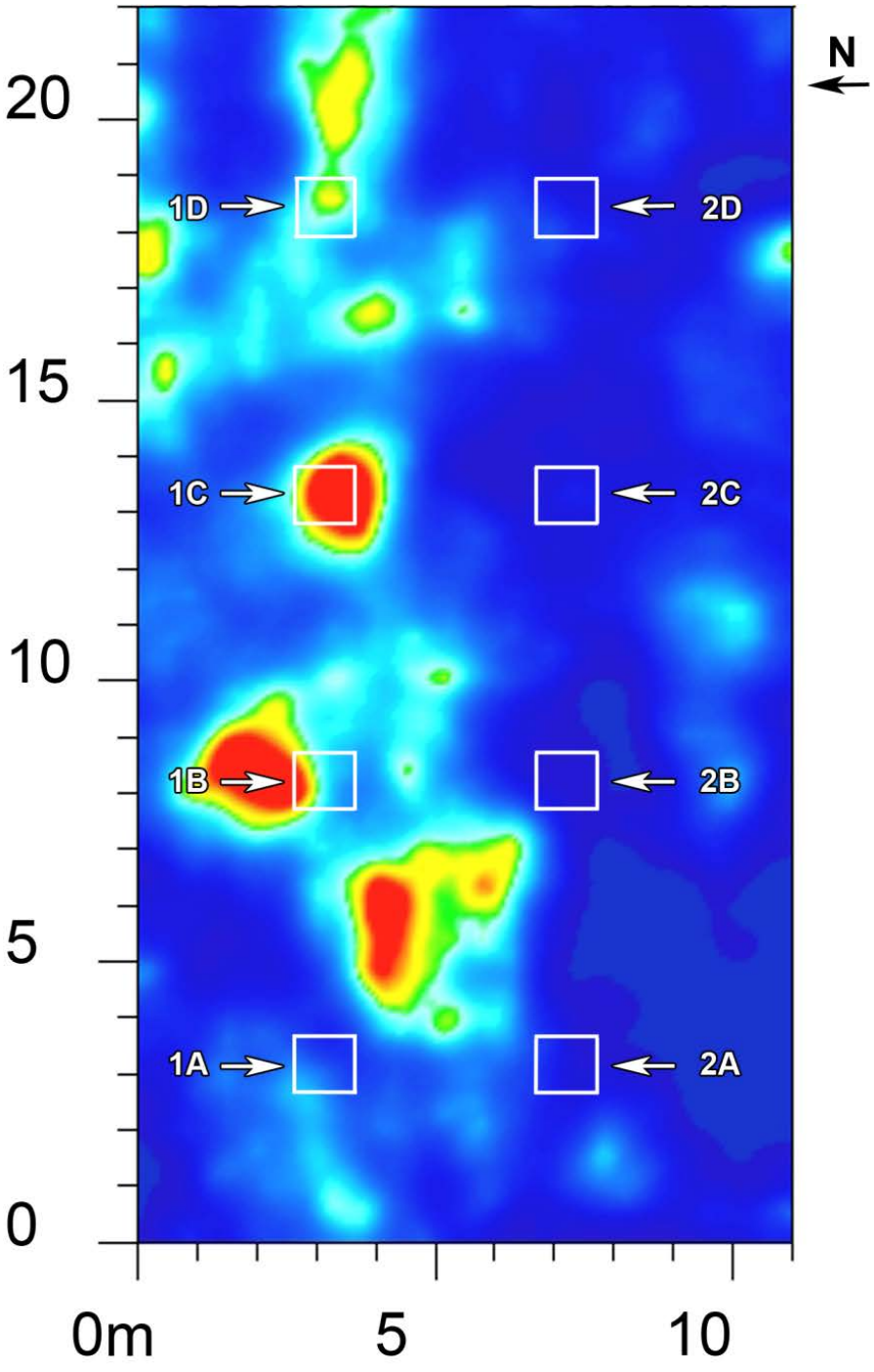

Figure C20: GPR horizontal slice using the 500-MHz antenna at 17 months. The horizontal slice is between 0.85 and 1.0 m in depth.

GPR 500 TIME SLICE AT MONTH 18

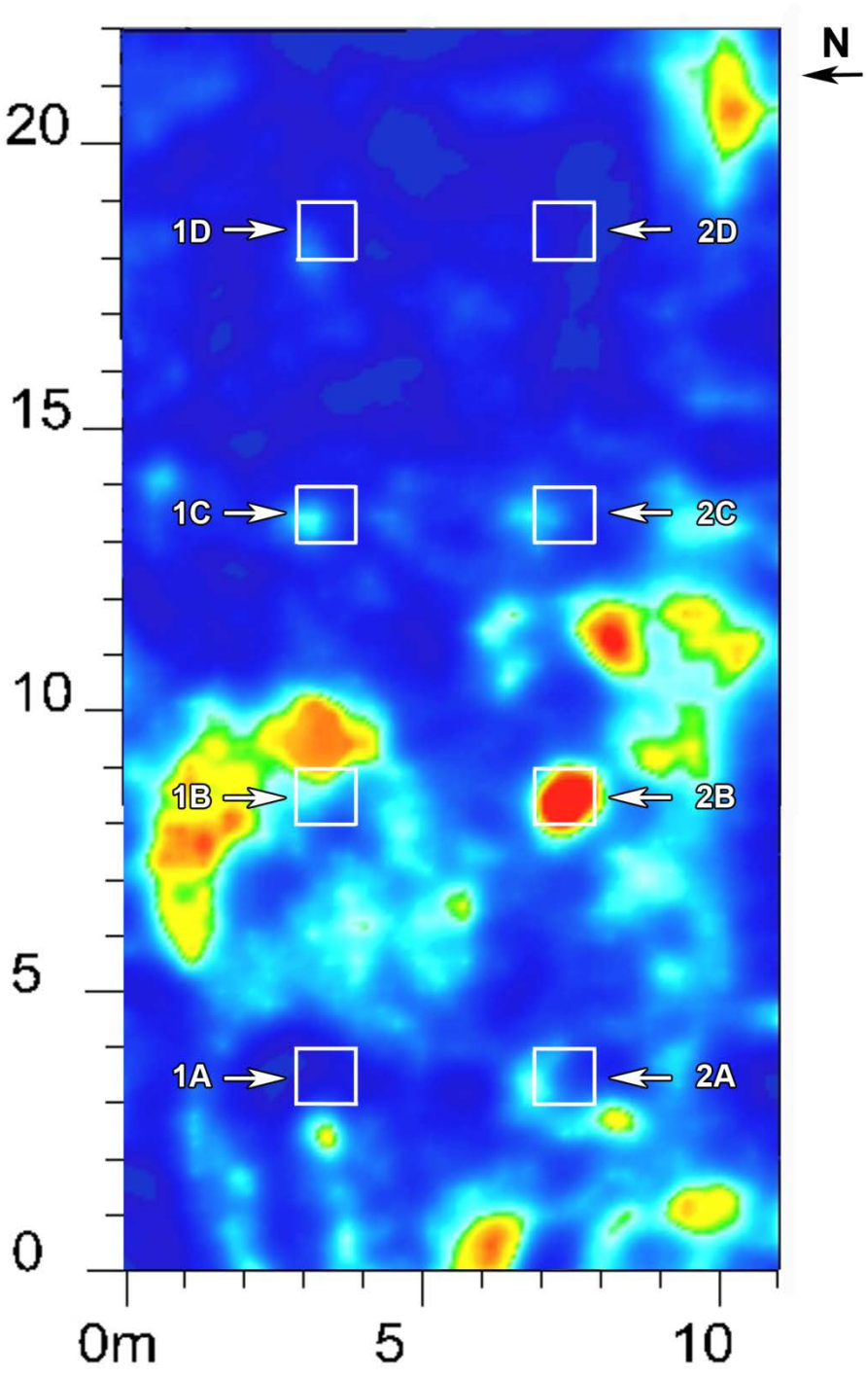

Figure C21: GPR horizontal slice using the 500-MHz antenna at 18 months. The horizontal slice is between 0.85 and 1.0 m in depth.

GPR 500 TIME SLICE AT MONTH 19

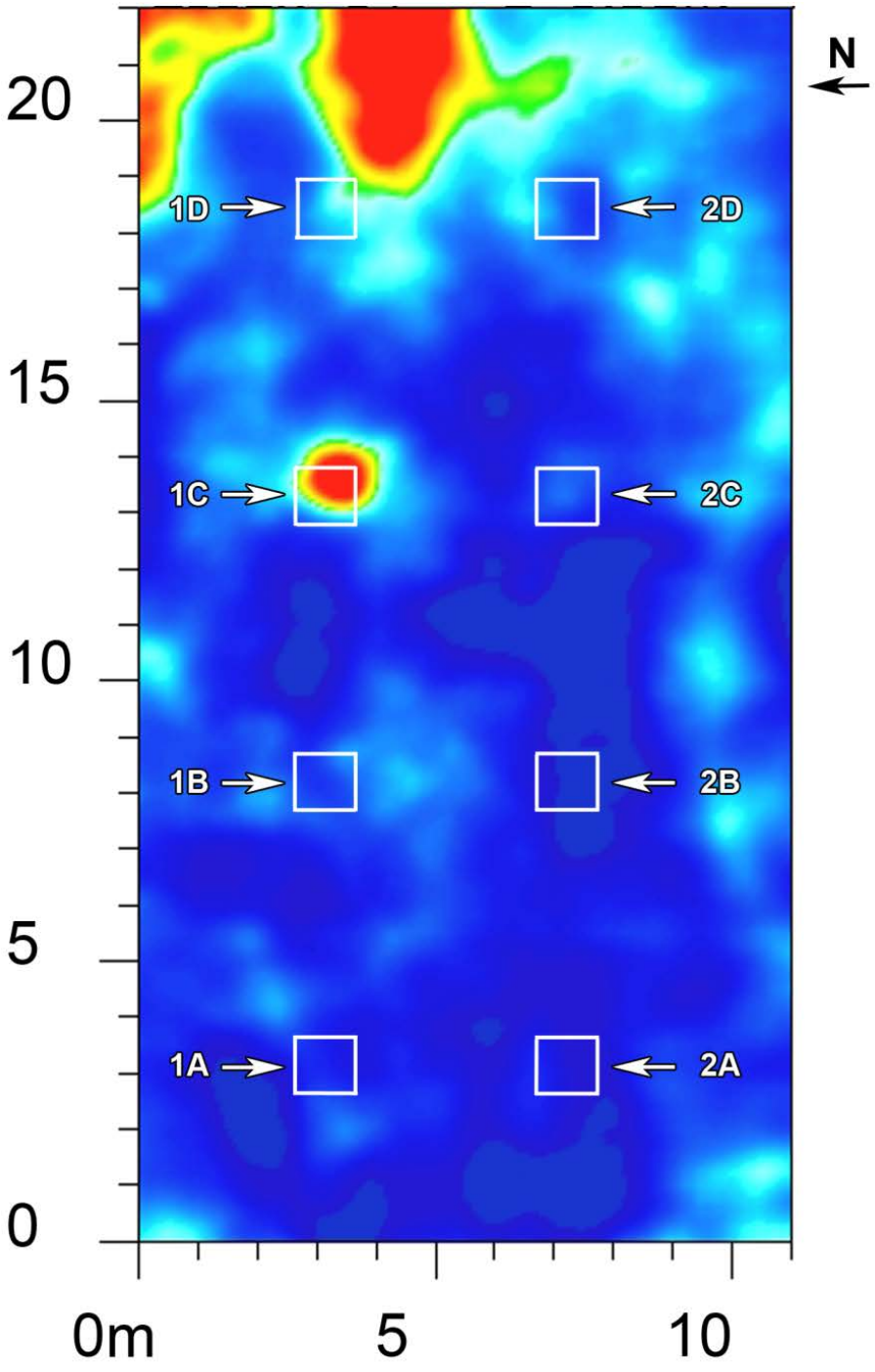

Figure C22: GPR horizontal slice using the 500-MHz antenna at 19 months. The horizontal slice is between 0.85 and 1.0 m in depth.

GPR 500 TIME SLICE AT MONTH 20

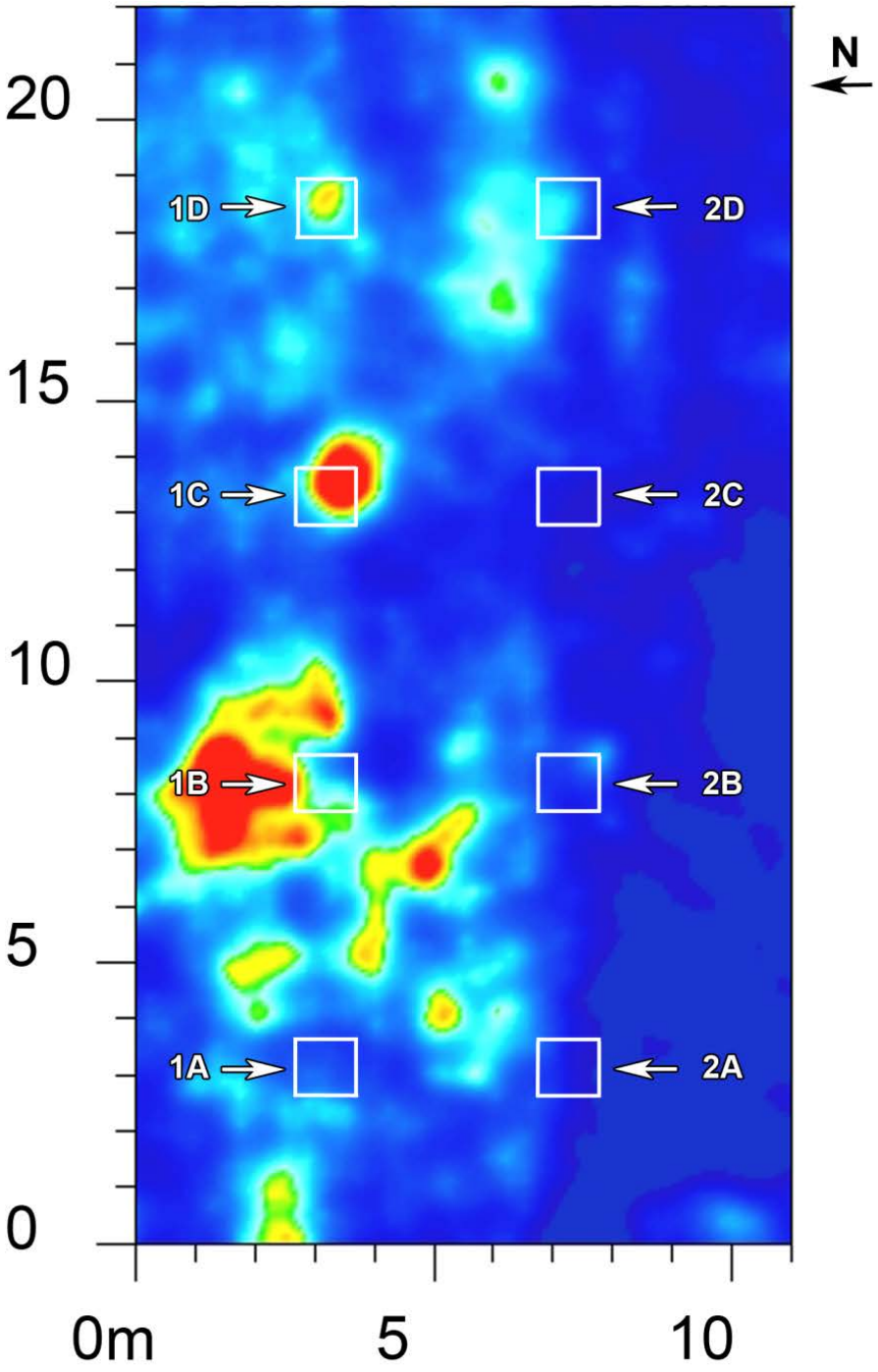

Figure C23: GPR horizontal slice using the 500-MHz antenna at 20 months. The horizontal slice is between 0.85 and 1.0 m in depth.

GPR 500 TIME SLICE AT MONTH 21

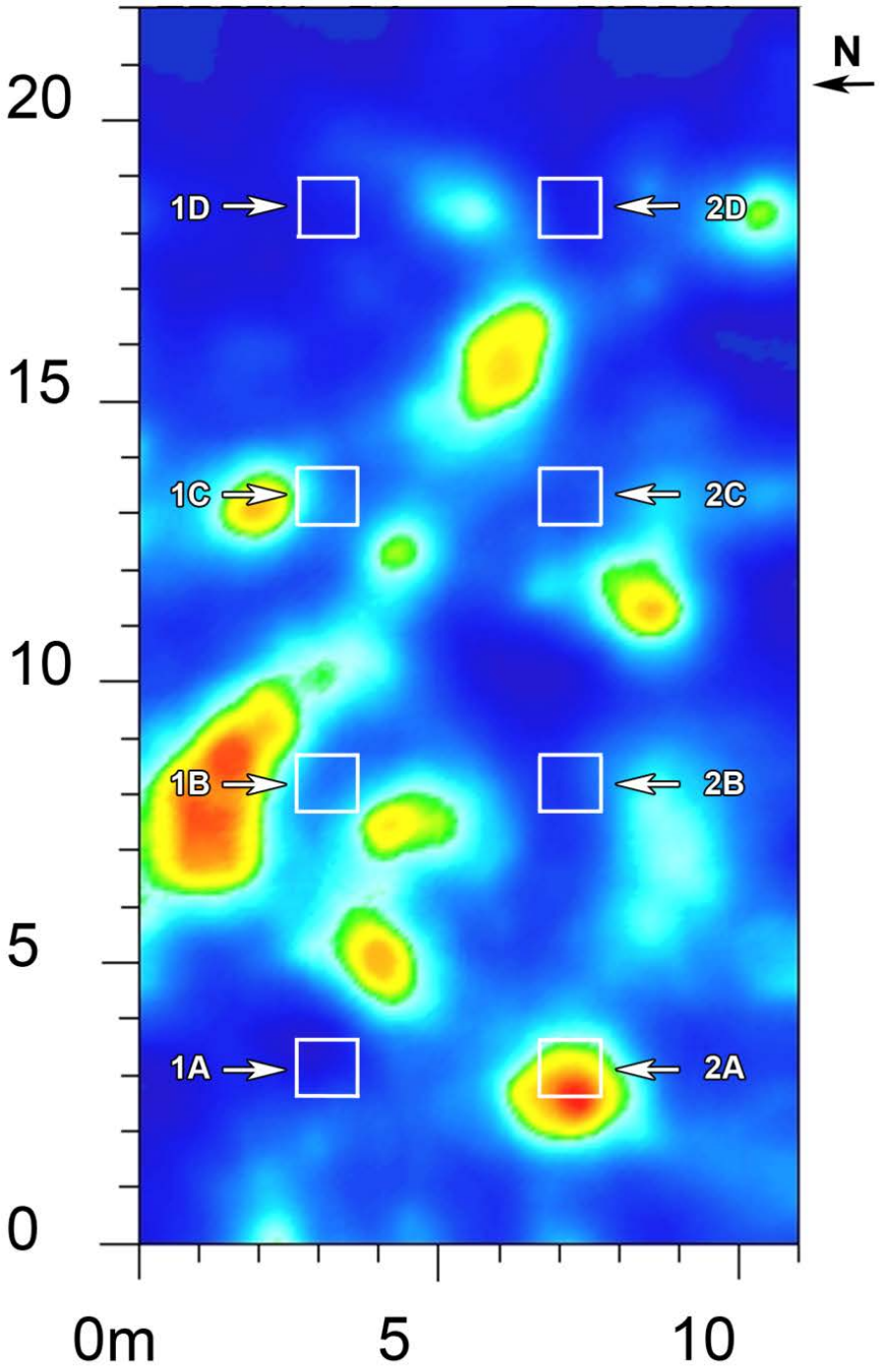

Figure C24: GPR horizontal slice using the 500-MHz antenna at 21 months. The horizontal slice is between 0.85 and 1.0 m in depth.

GPR 500 TIME SLICE AT MONTH 22

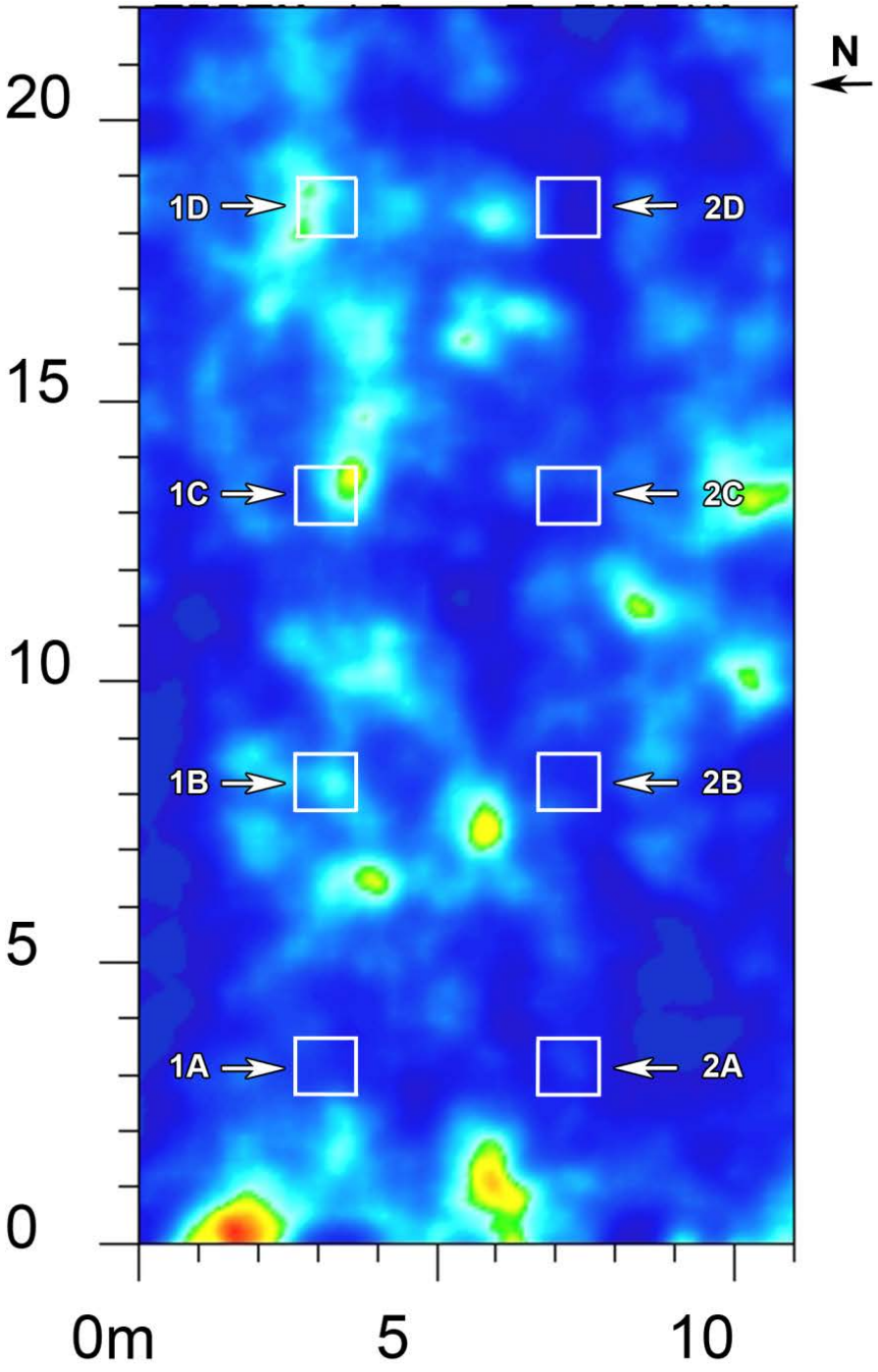

Figure C25: GPR horizontal slice using the 500-MHz antenna at 22 months. The horizontal slice is between 0.85 and 1.0 m in depth.

GPR 500 TIME SLICE AT MONTH 23

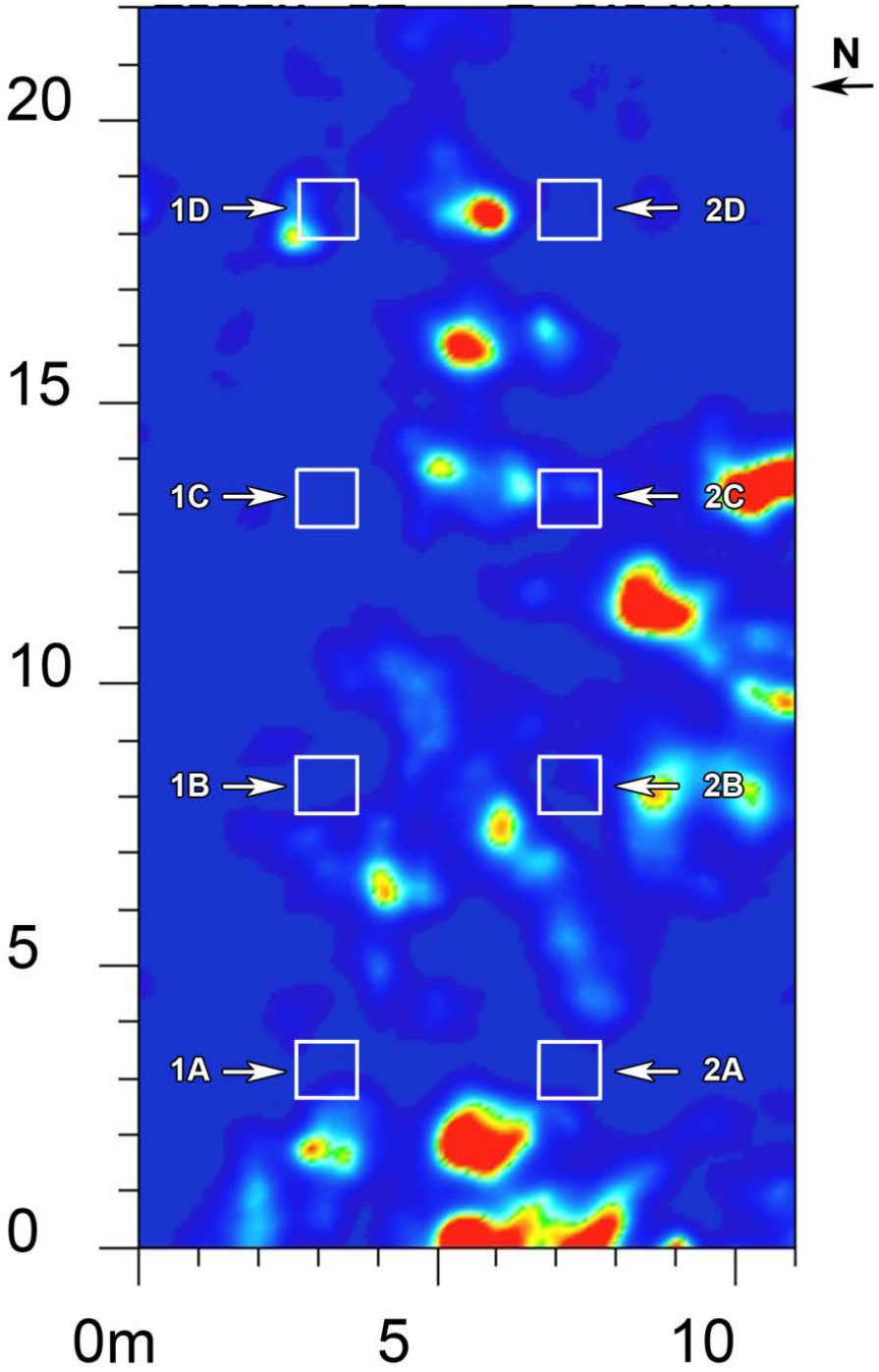

Figure C26: GPR horizontal slice using the 500-MHz antenna at 23 months. The horizontal slice is between 0.85 and 1.0 m in depth.

GPR 500 TIME SLICE AT MONTH 24

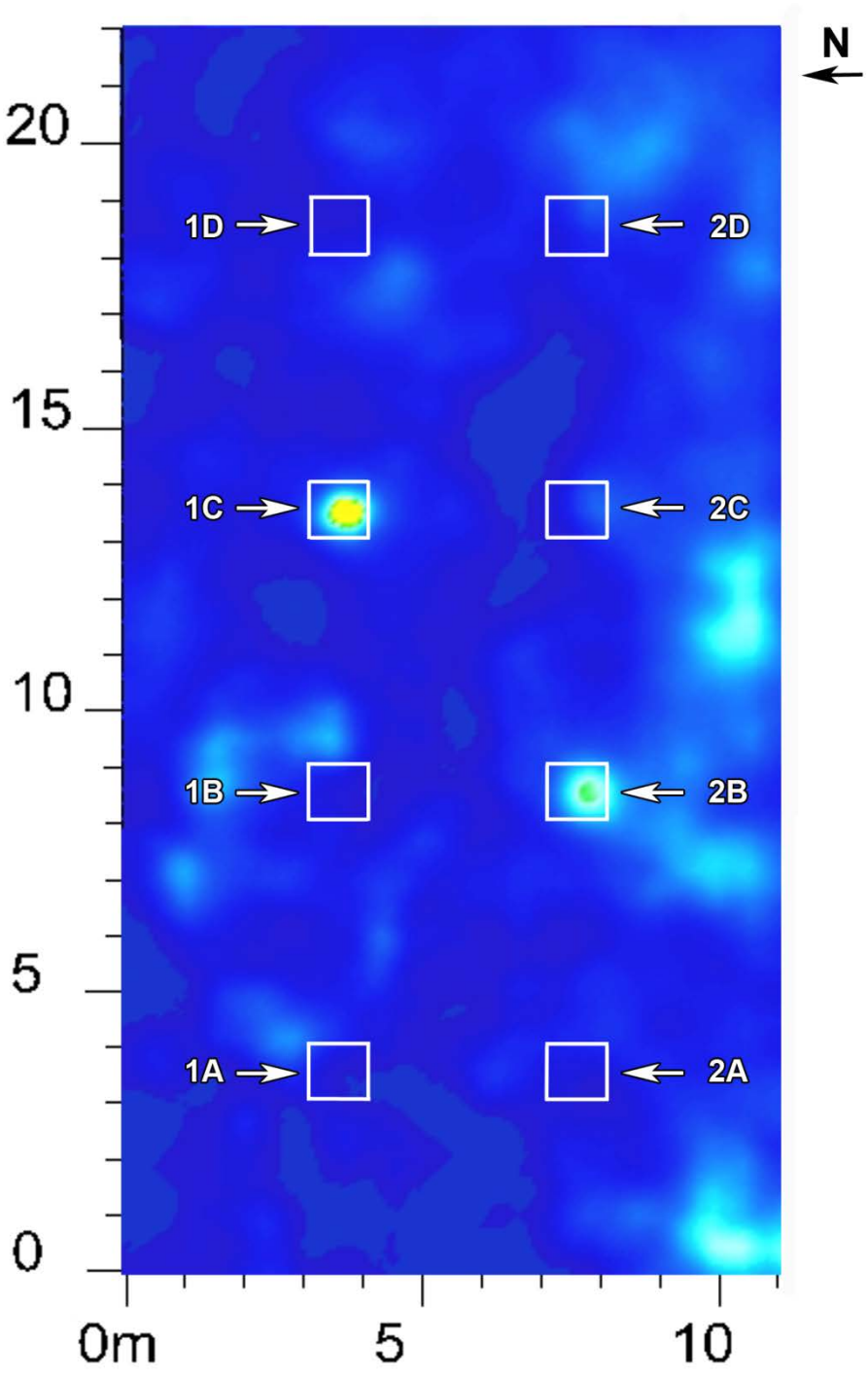

Figure C27: GPR horizontal slice using the 500-MHz antenna at 24 months. The horizontal slice is between 0.85 and 1.0 m in depth.

GPR 500 TIME SLICE AT MONTH 25

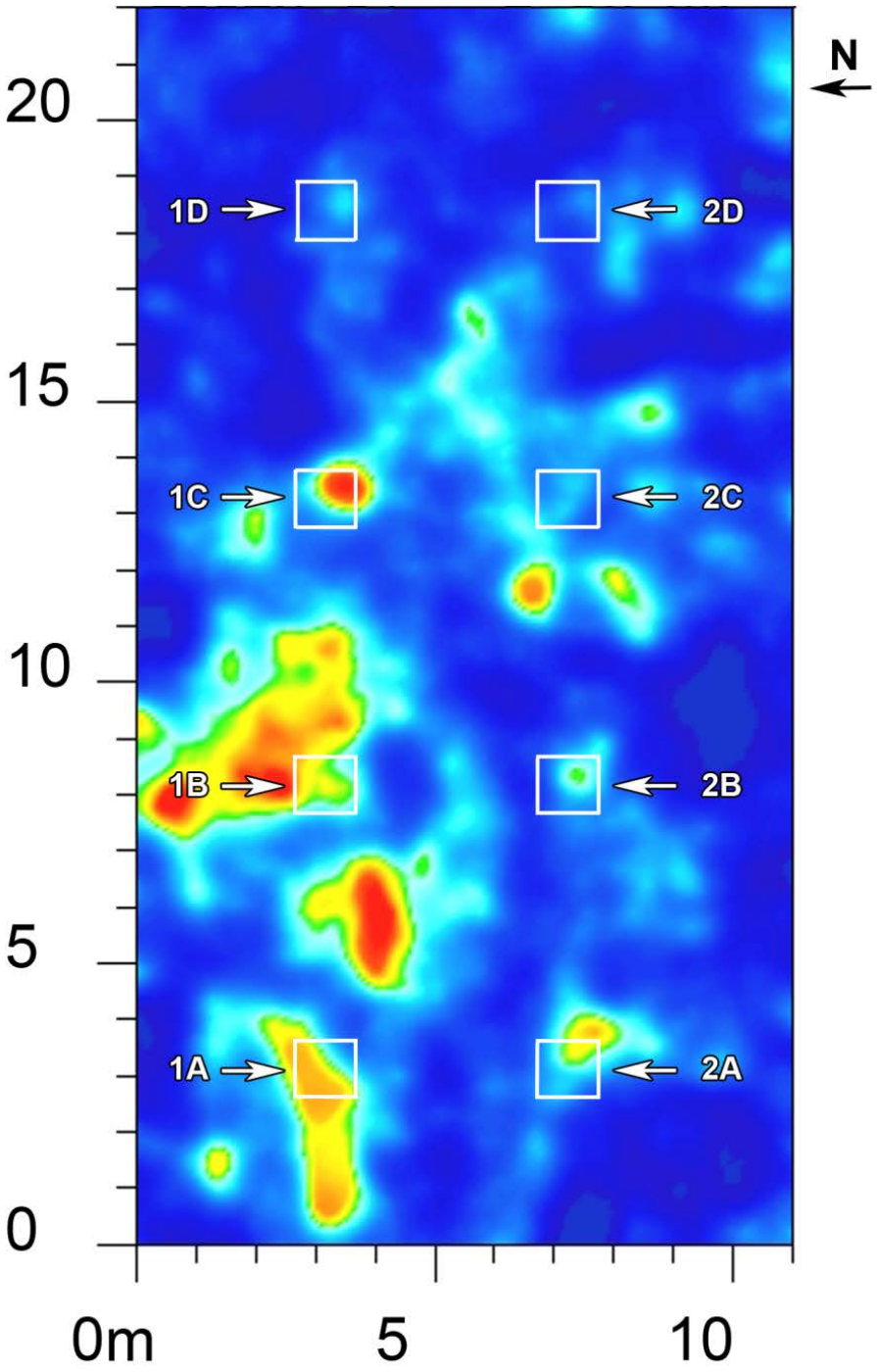

Figure C28: GPR horizontal slice using the 500-MHz antenna at 25 months. The horizontal slice is between 0.85 and 1.0 m in depth.

GPR 500 TIME SLICE AT MONTH 26

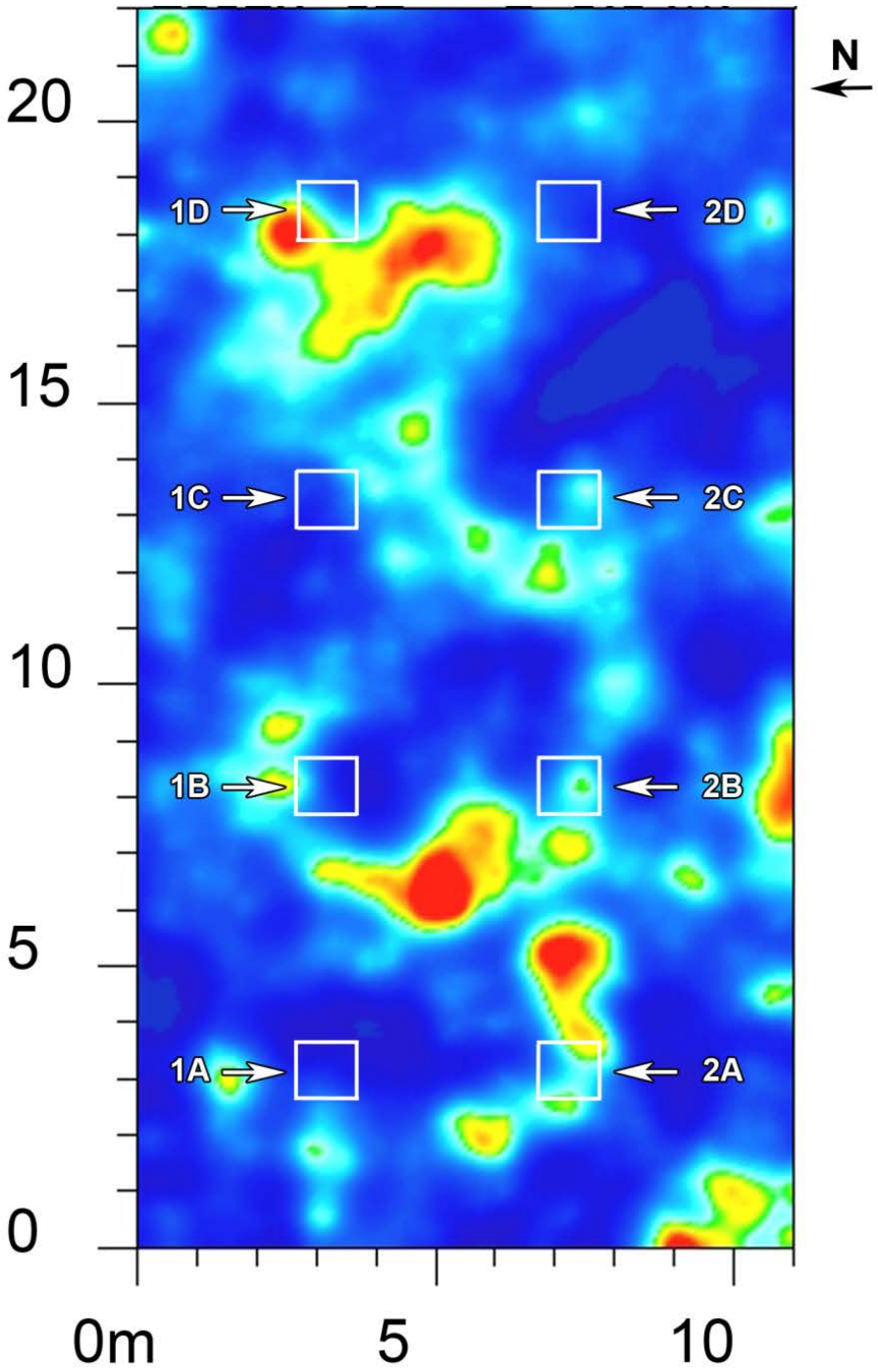

Figure C29: GPR horizontal slice using the 500-MHz antenna at 26 months. The horizontal slice is between 0.85 and 1.0 m in depth.

GPR 500 TIME SLICE AT MONTH 27

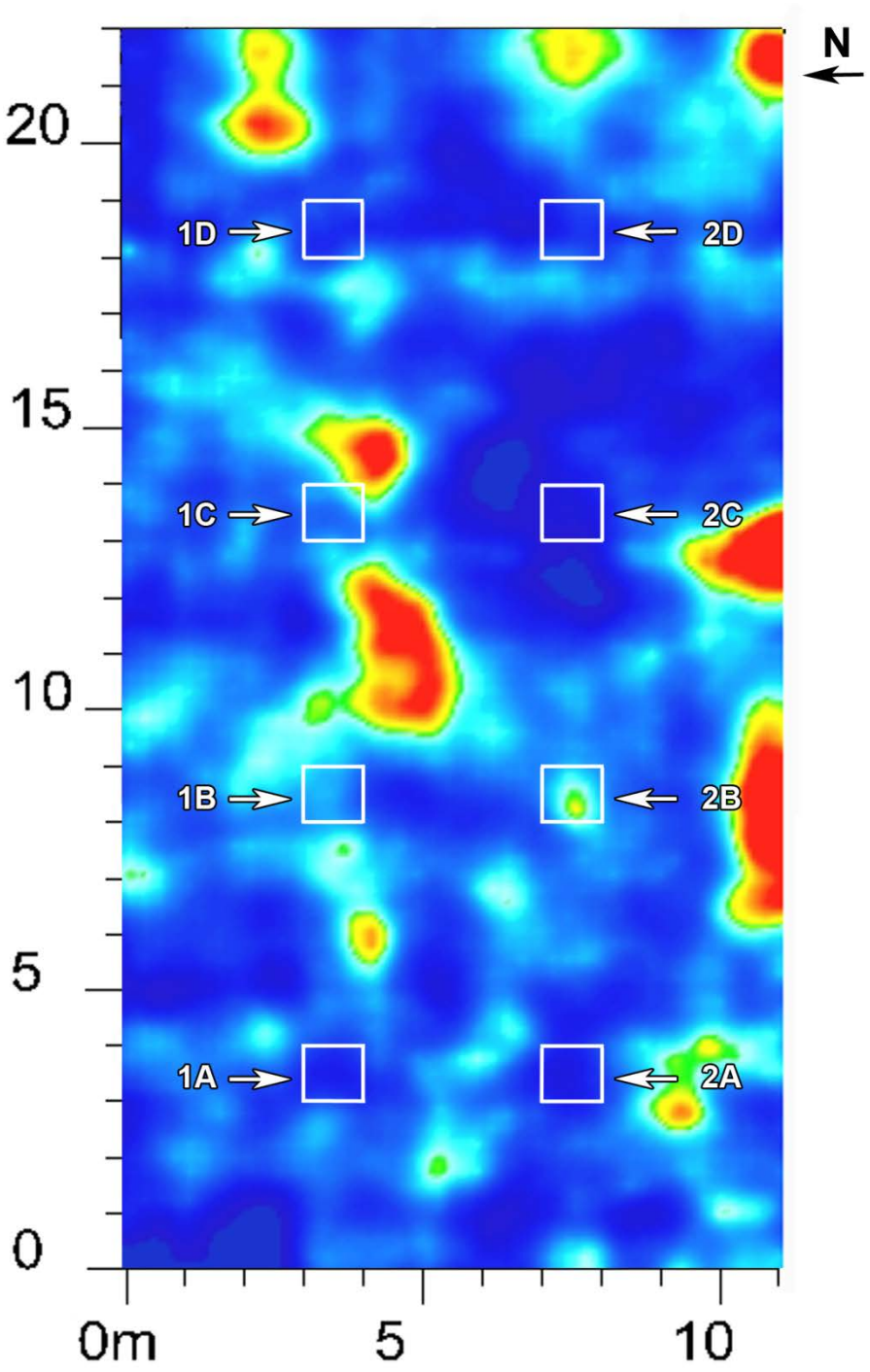

Figure C30: GPR horizontal slice using the 500-MHz antenna at 27 months. The horizontal slice is between 0.85 and 1.0 m in depth.

GPR 500 TIME SLICE AT MONTH 28

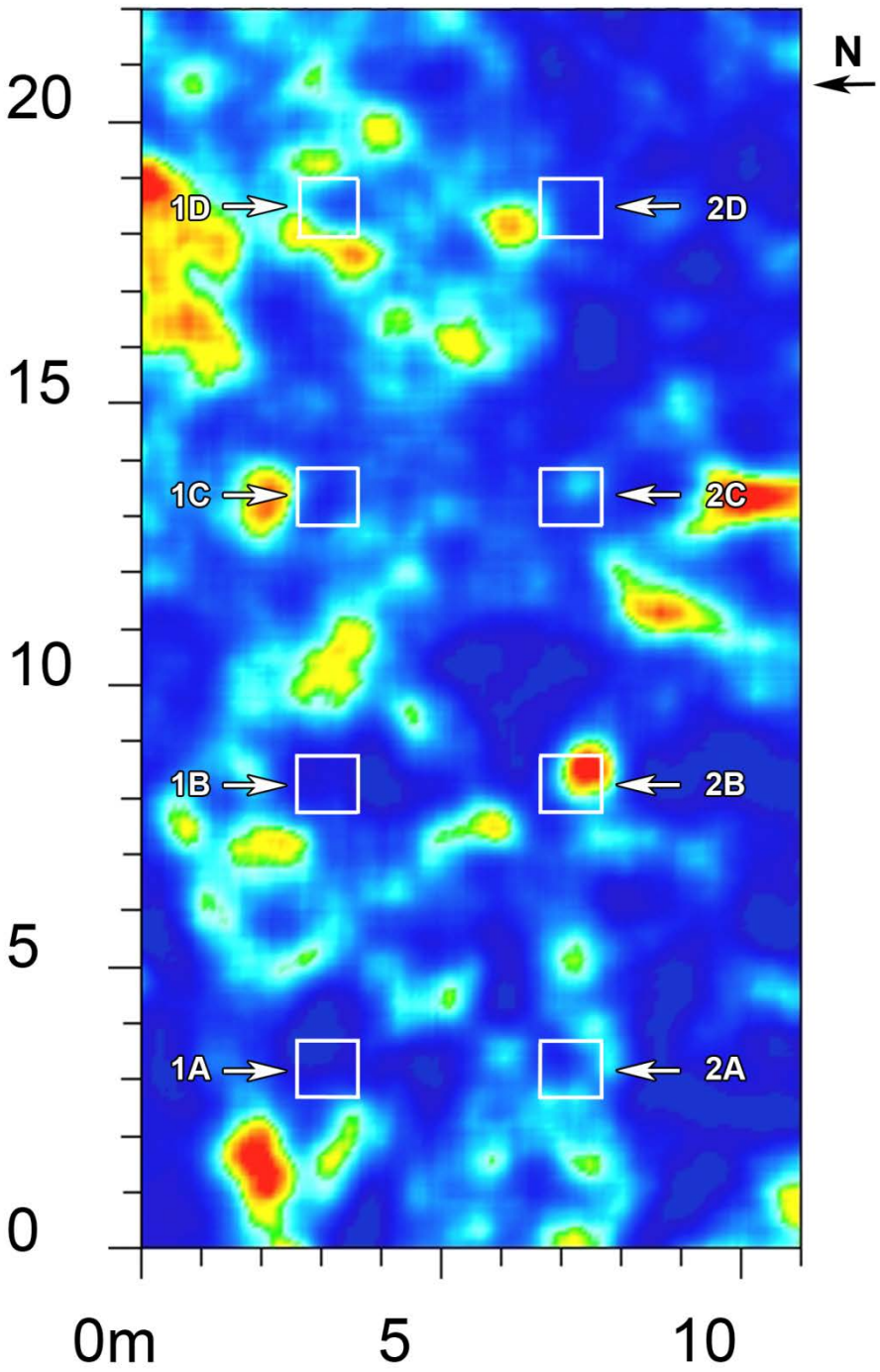

Figure C31: GPR horizontal slice using the 500-MHz antenna at 28 months. The horizontal slice is between 0.85 and 1.0 m in depth.

GPR 500 TIME SLICE AT MONTH 29

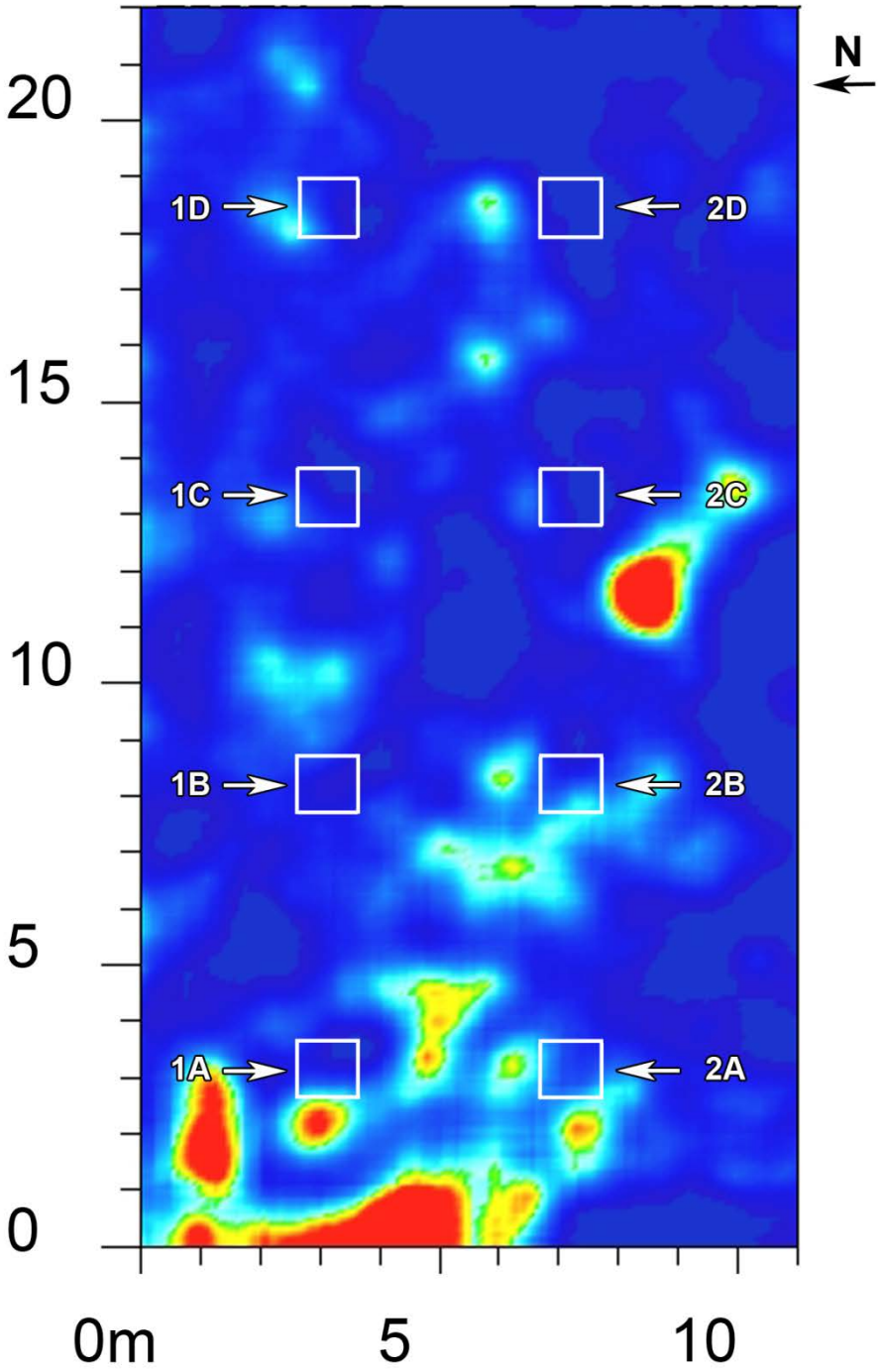

Figure C32: GPR horizontal slice using the 500-MHz antenna at 28.5 months. The horizontal slice is between 0.85 and 1.0 m in depth.

GPR 500 TIME SLICE AT MONTH 30

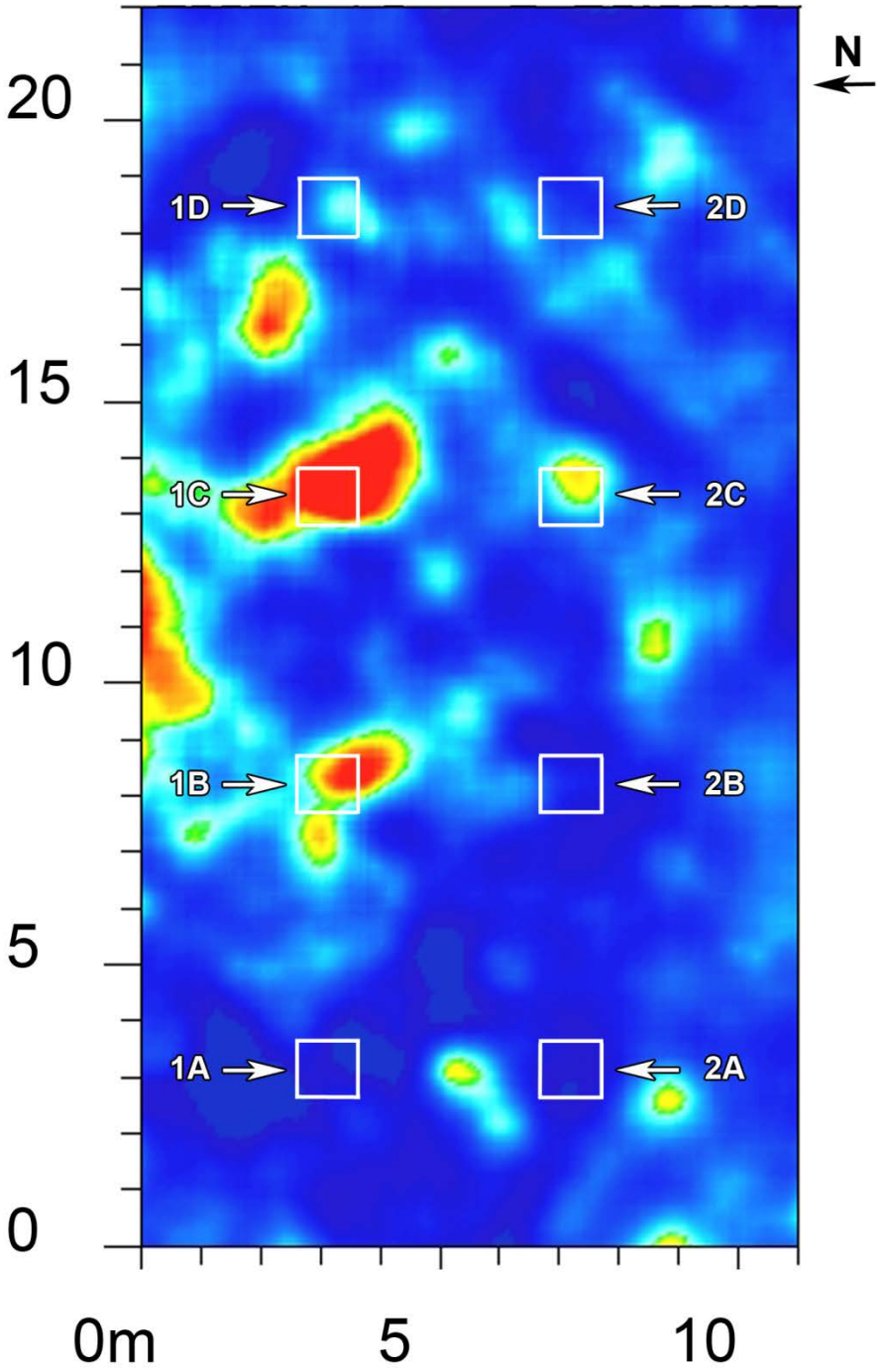

Figure C33: GPR horizontal slice using the 500-MHz antenna at 30 months. The horizontal slice is between 0.85 and 1.0 m in depth.

APPENDIX D: GROUND-PENETRATING RADAR 250-MHZ REFLECTION PROFILES

GPR 250 REFLECTION PROFILE AT MONTH 2

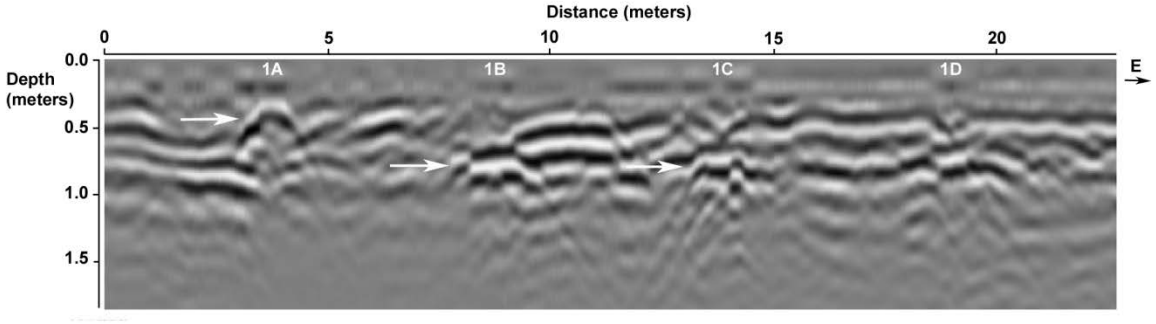

Figure D1: GPR reflection profile using the 250-MHz antenna of Row 1 at 2 months

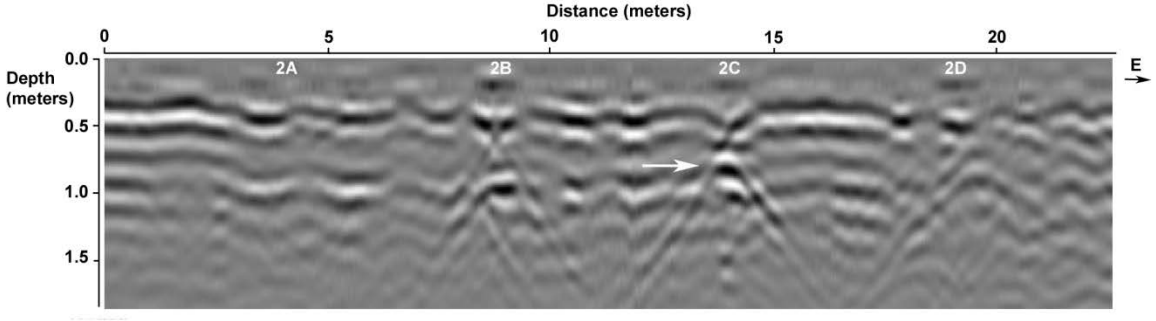

Figure D2: GPR reflection profile using the 250-MHz antenna of Row 2 at 2 months

GPR 250 REFLECTION PROFILE AT MONTH 3

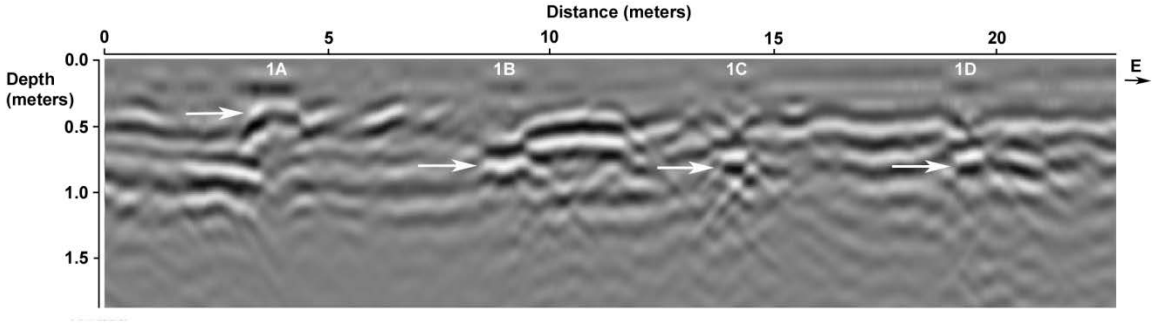

Figure D3: GPR reflection profile using the 250-MHz antenna of Row 1 at 3 months

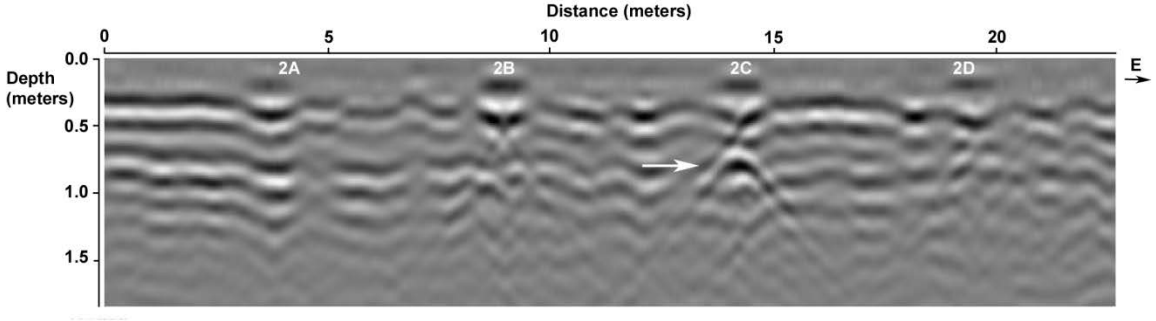

Figure D4: GPR reflection profile using the 250-MHz antenna of Row 2 at 3 months

GPR 250 REFLECTION PROFILE AT MONTH 4

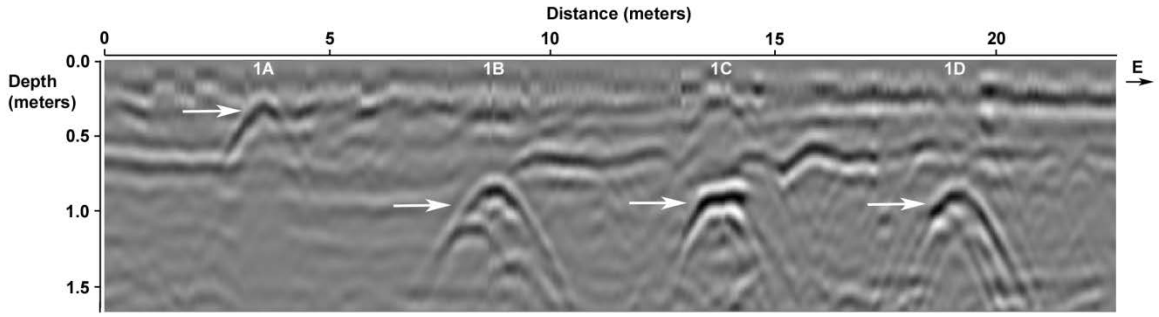

Figure D5: GPR reflection profile using the 250-MHz antenna of Row 1 at 4 months

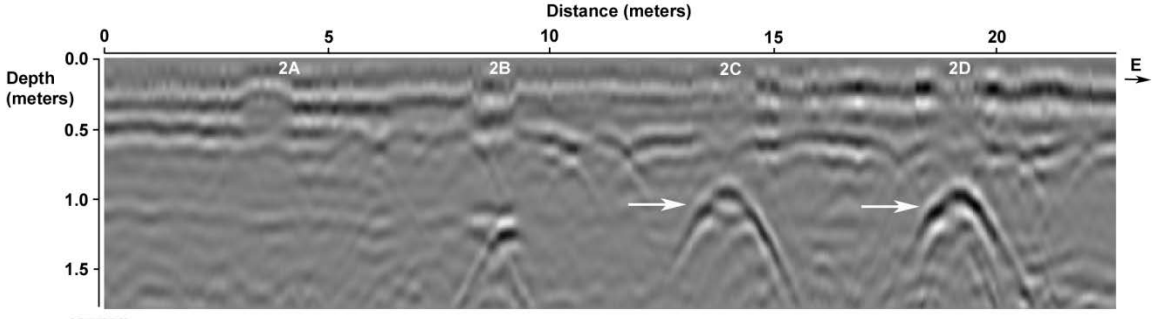

Figure D6: GPR reflection profile using the 250-MHz antenna of Row 2 at 4 months

GPR 250 REFLECTION PROFILE AT MONTH 5

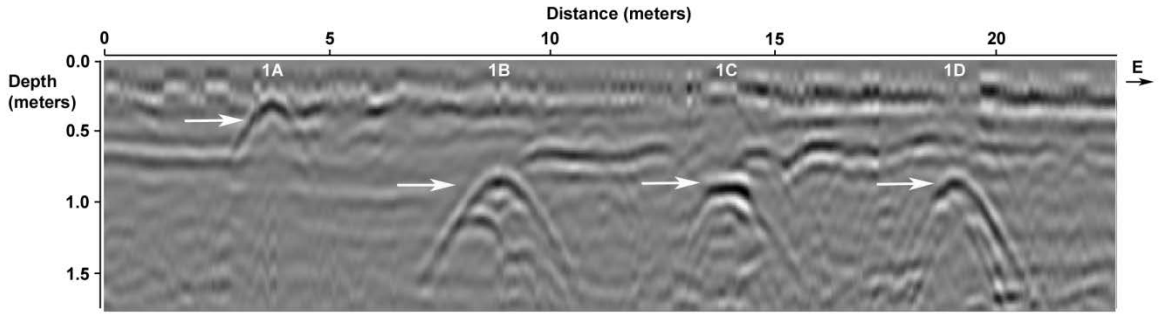

Figure D7: GPR reflection profile using the 250-MHz antenna of Row 1 at 5 months

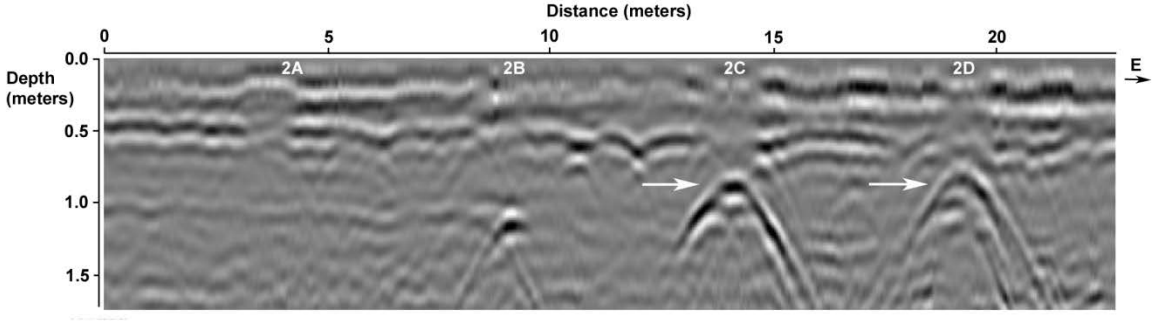

Figure D8: GPR reflection profile using the 250-MHz antenna of Row 2 at 5 months

GPR 250 REFLECTION PROFILE AT MONTH 6

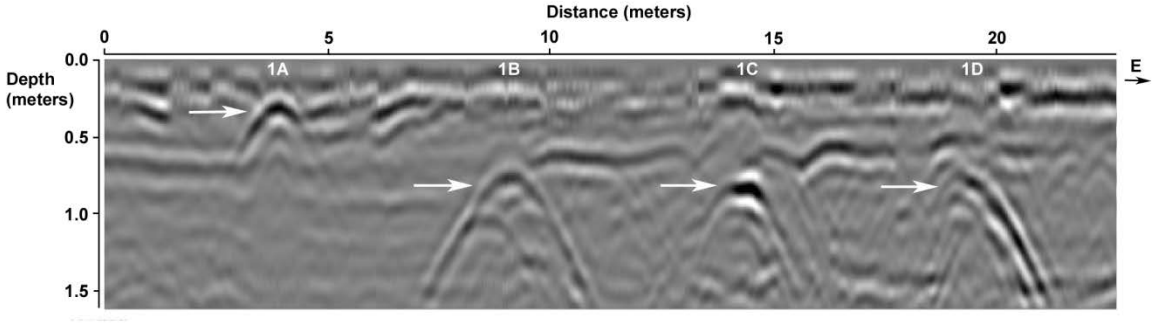

Figure D9: GPR reflection profile using the 250-MHz antenna of Row 1 at 6 months

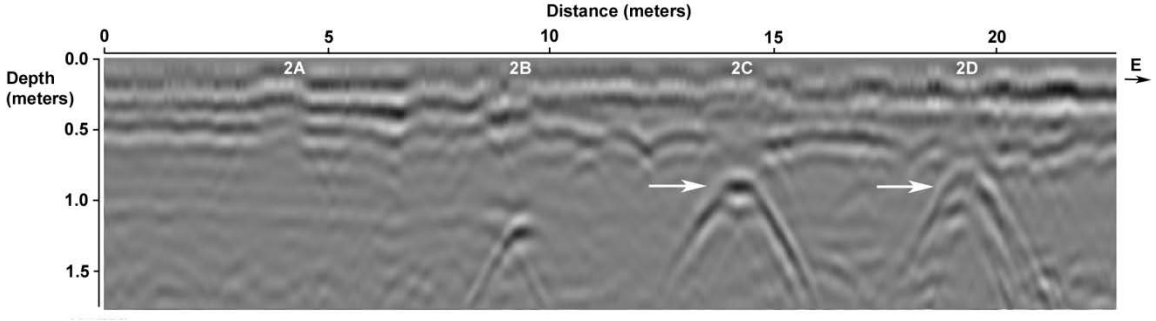

Figure D10: GPR reflection profile using the 250-MHz antenna of Row 2 at 6 months

GPR 250 REFLECTION PROFILE AT MONTH 7

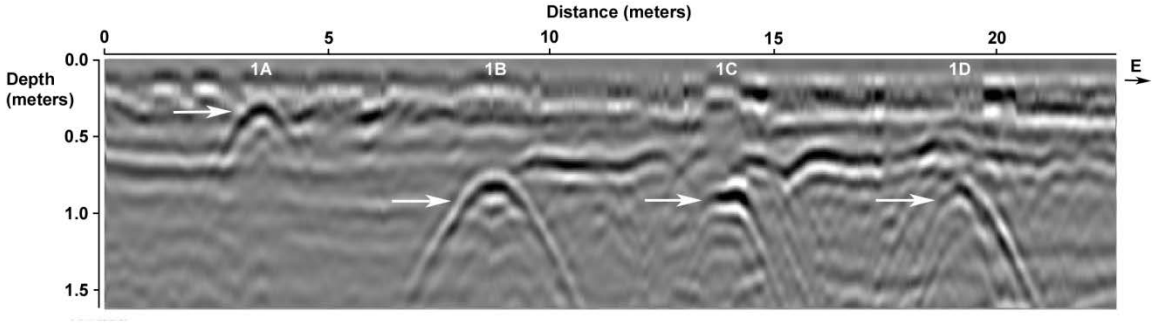

Figure D11: GPR reflection profile using the 250-MHz antenna of Row 1 at 7 months

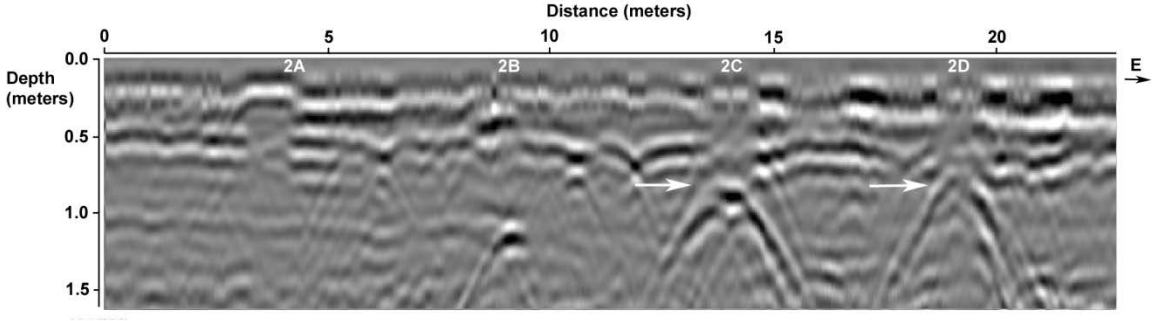

Figure D12: GPR reflection profile using the 250-MHz antenna of Row 2 at 7 months

GPR 250 REFLECTION PROFILE AT MONTH 8

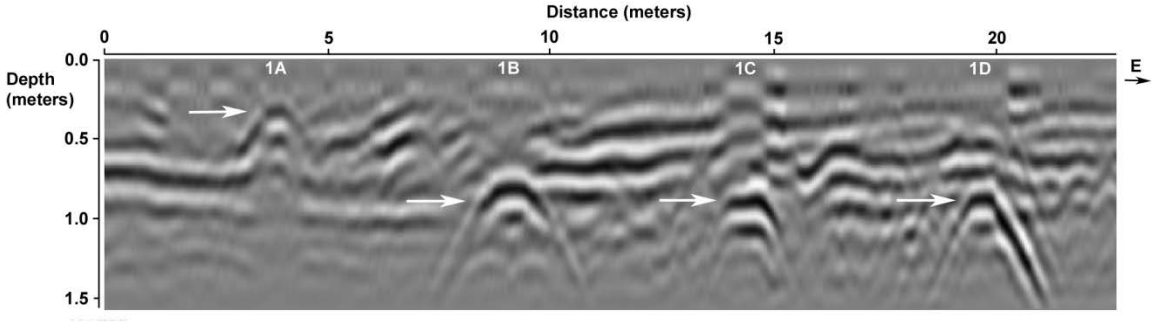

Figure D13: GPR reflection profile using the 250-MHz antenna of Row 1 at 8 months

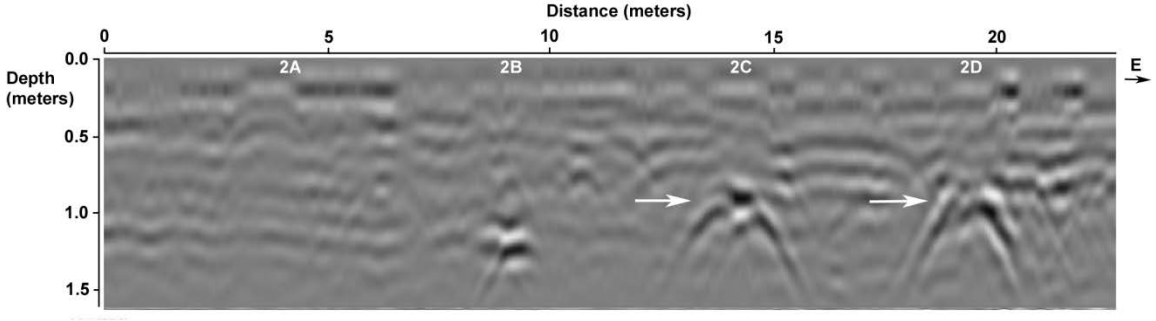

Figure D14: GPR reflection profile using the 250-MHz antenna of Row 2 at 8 months

GPR 250 REFLECTION PROFILE AT MONTH 9

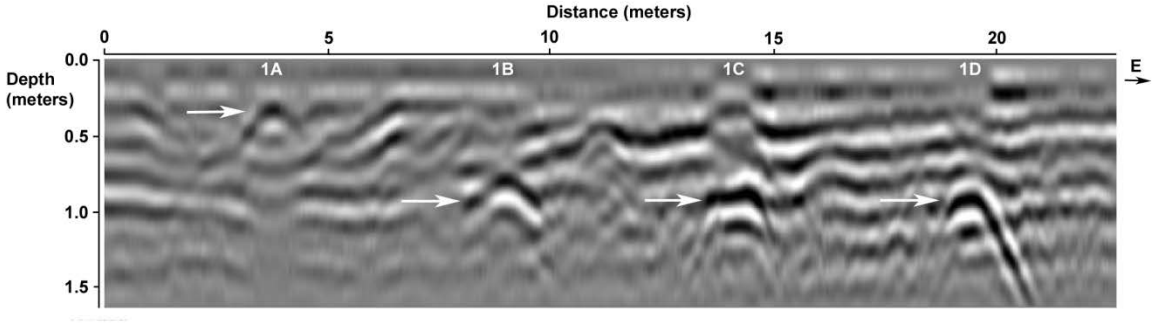

Figure D15: GPR reflection profile using the 250-MHz antenna of Row 1 at 9 months

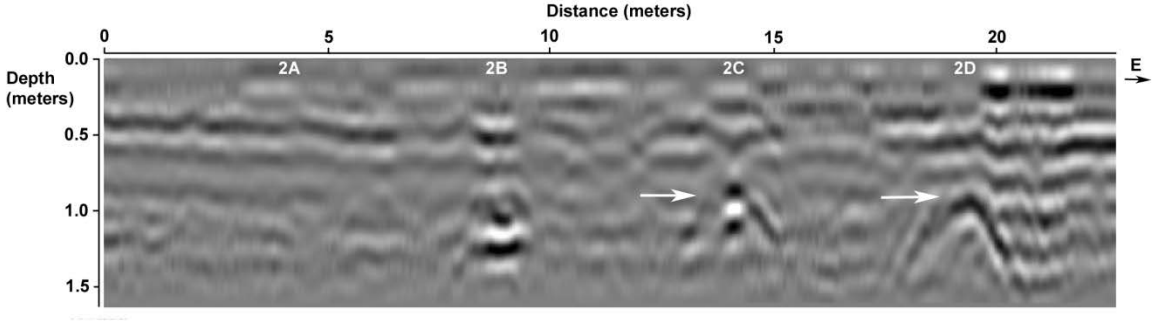

Figure D16: GPR reflection profile using the 250-MHz antenna of Row 2 at 9 months

GPR 250 REFLECTION PROFILE AT MONTH 10

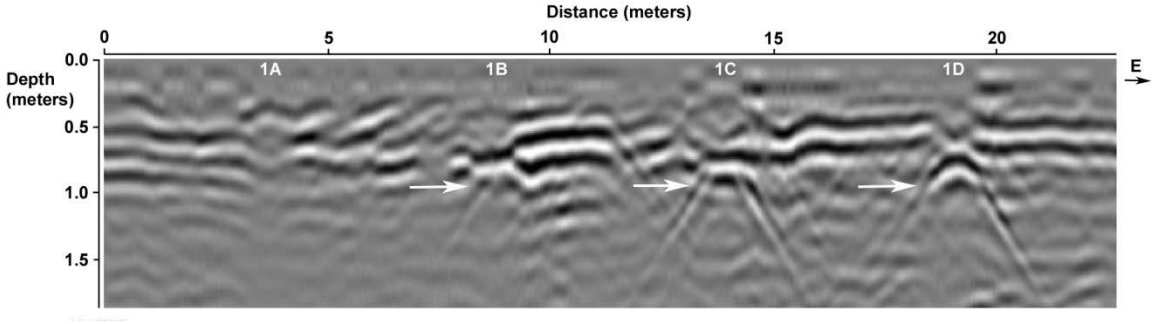

Figure D17: GPR reflection profile using the 250-MHz antenna of Row 1 at 10 months

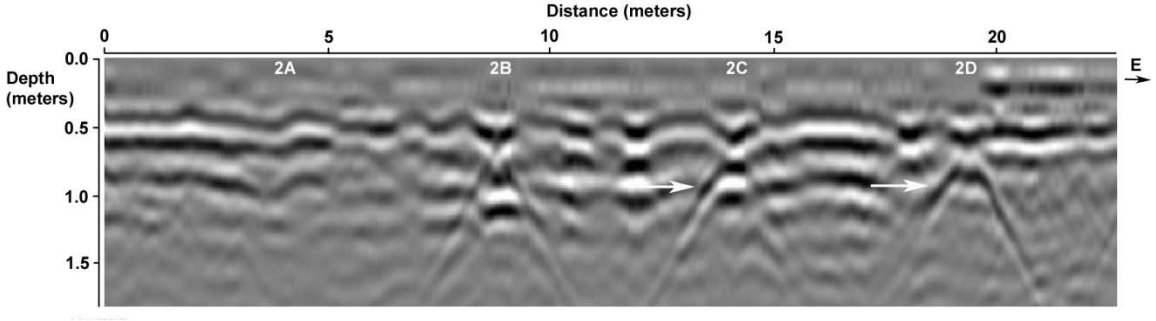

Figure D18: GPR reflection profile using the 250-MHz antenna of Row 2 at 10 months

GPR 250 REFLECTION PROFILE AT MONTH 11

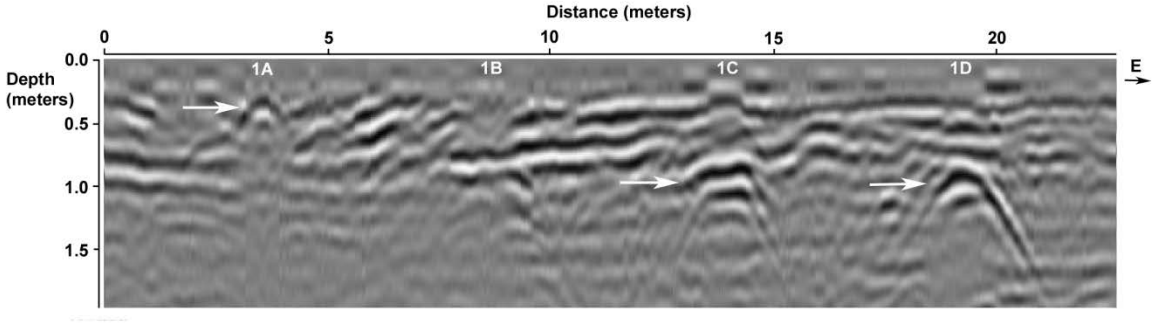

Figure D19: GPR reflection profile using the 250-MHz antenna of Row 1 at 11 months

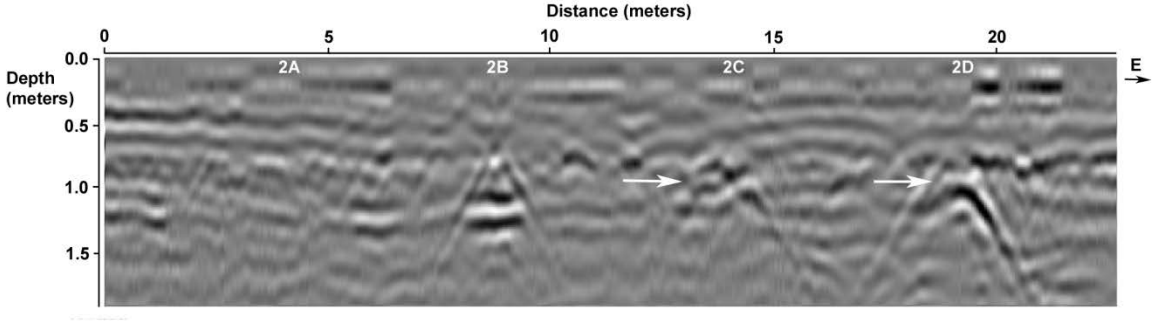

Figure D20: GPR reflection profile using the 250-MHz antenna of Row 2 at 11 months

GPR 250 REFLECTION PROFILE AT MONTH 12

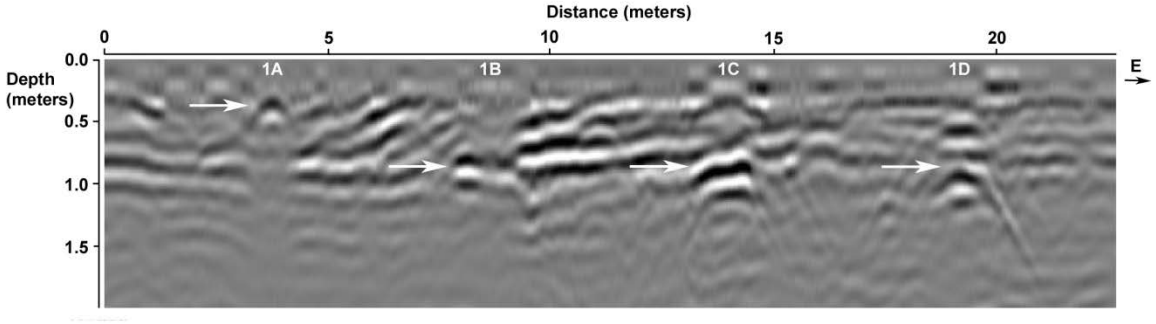

Figure D21: GPR reflection profile using the 250-MHz antenna of Row 1 at 12 months

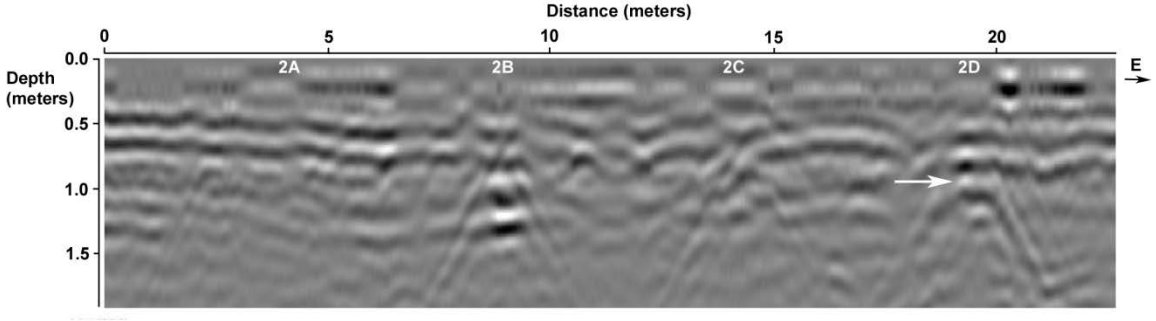

Figure D22: GPR reflection profile using the 250-MHz antenna of Row 2 at 12 months

GPR 250 REFLECTION PROFILE AT MONTH 13

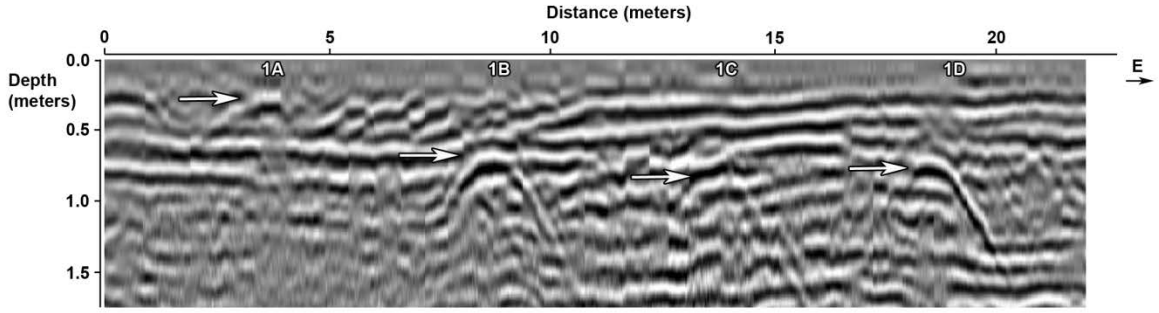

Figure D23: GPR reflection profile using the 250-MHz antenna of Row 1 at 13 months

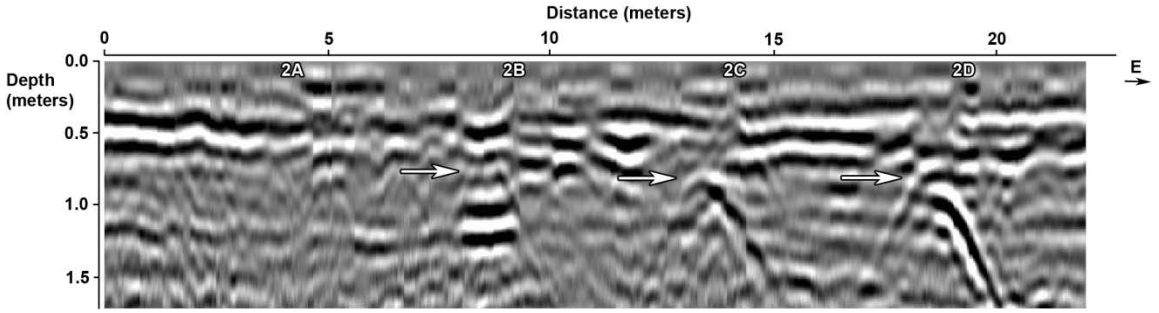

Figure D24: GPR reflection profile using the 250-MHz antenna of Row 2 at 13 months

GPR 250 REFLECTION PROFILE AT MONTH 14

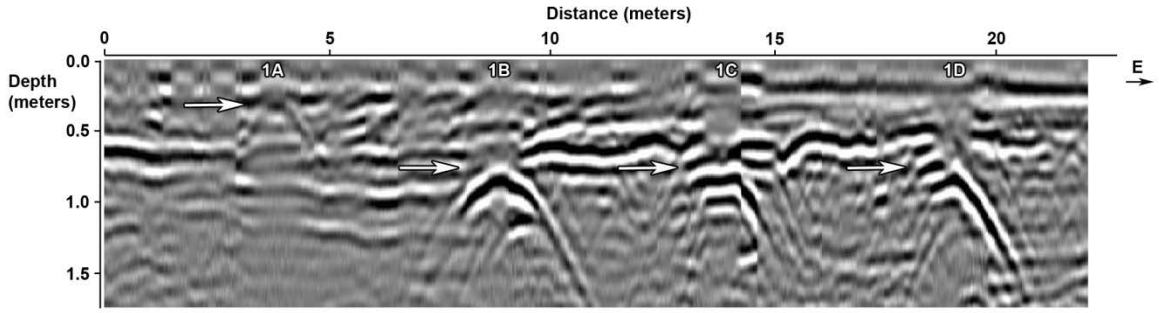

Figure D25: GPR reflection profile using the 250-MHz antenna of Row 1 at 14 months

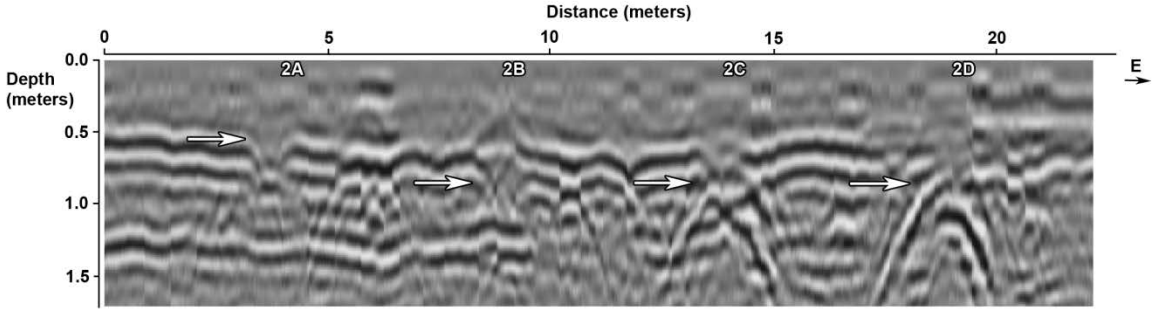

Figure D26: GPR reflection profile using the 250-MHz antenna of Row 2 at 14 months

GPR 250 REFLECTION PROFILE AT MONTH 15

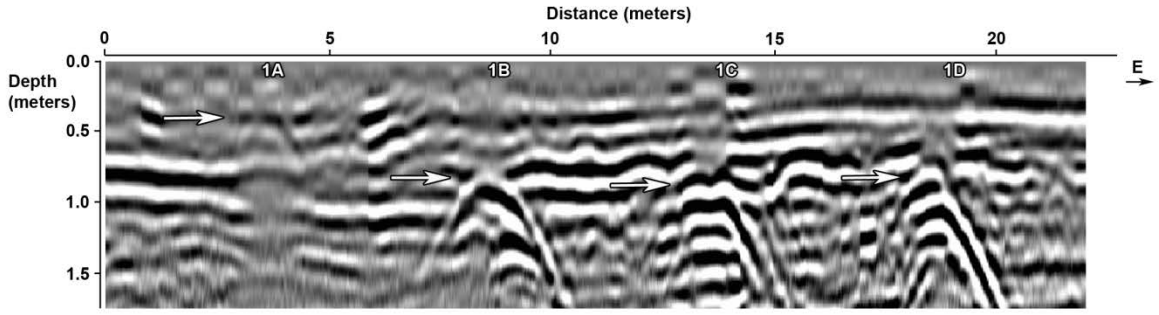

Figure D27: GPR reflection profile using the 250-MHz antenna of Row 1 at 15 months

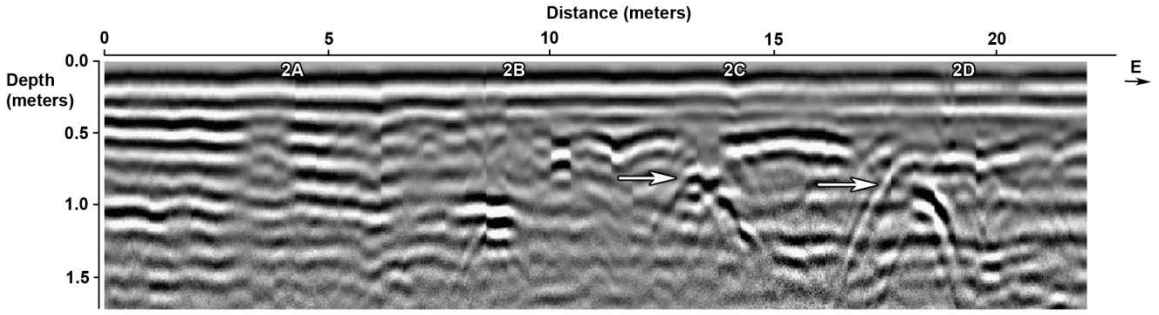

Figure D28: GPR reflection profile using the 250-MHz antenna of Row 2 at 15 months

GPR 250 REFLECTION PROFILE AT MONTH 16

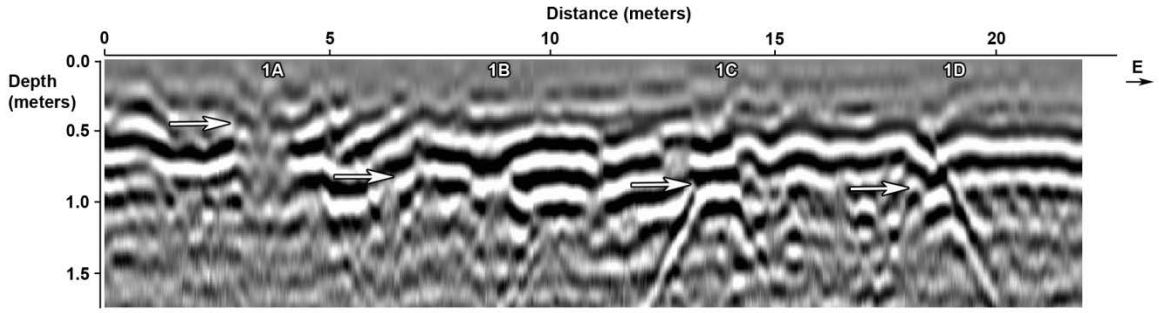

Figure D29: GPR reflection profile using the 250-MHz antenna of Row 1 at 16 months

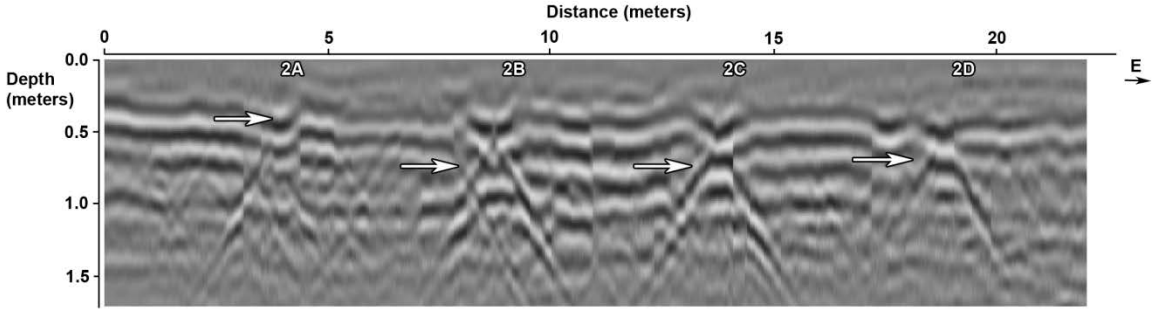

Figure D30: GPR reflection profile using the 250-MHz antenna of Row 2 at 16 months

GPR 250 REFLECTION PROFILE AT MONTH 17

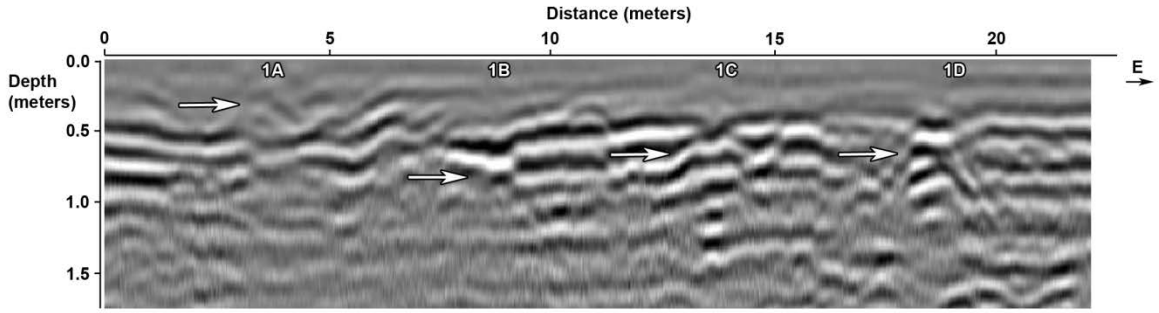

Figure D31: GPR reflection profile using the 250-MHz antenna of Row 1 at 17 months

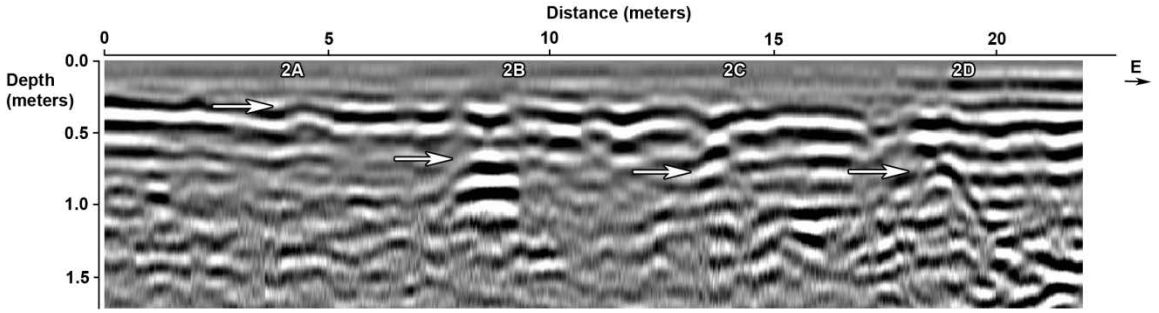

Figure D32: GPR reflection profile using the 250-MHz antenna of Row 2 at 17 months

GPR 250 REFLECTION PROFILE AT MONTH 18

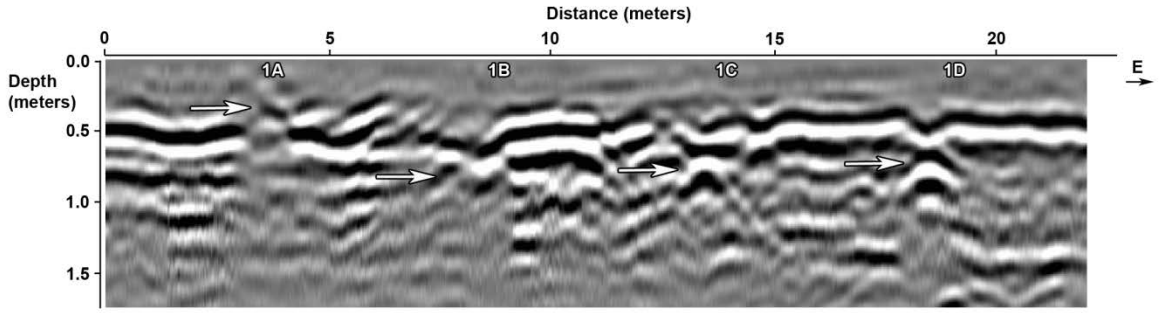

Figure D33: GPR reflection profile using the 250-MHz antenna of Row 1 at 18 months

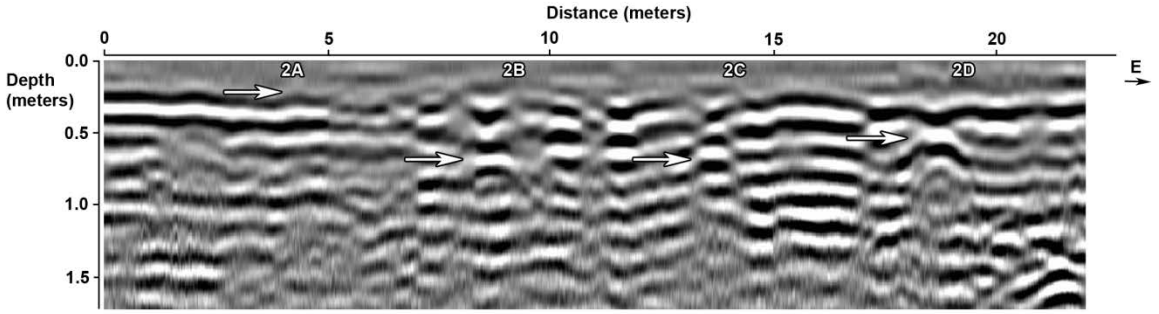

Figure D34: GPR reflection profile using the 250-MHz antenna of Row 2 at 18 months

GPR 250 REFLECTION PROFILE AT MONTH 19

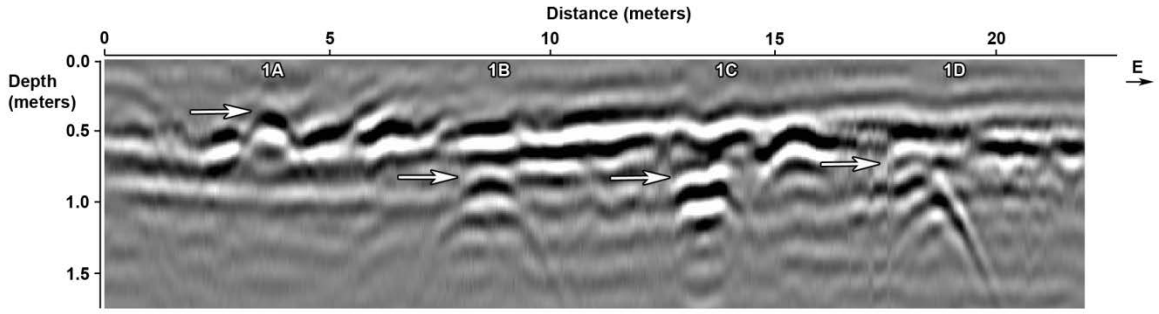

Figure D35: GPR reflection profile using the 250-MHz antenna of Row 1 at 19 months

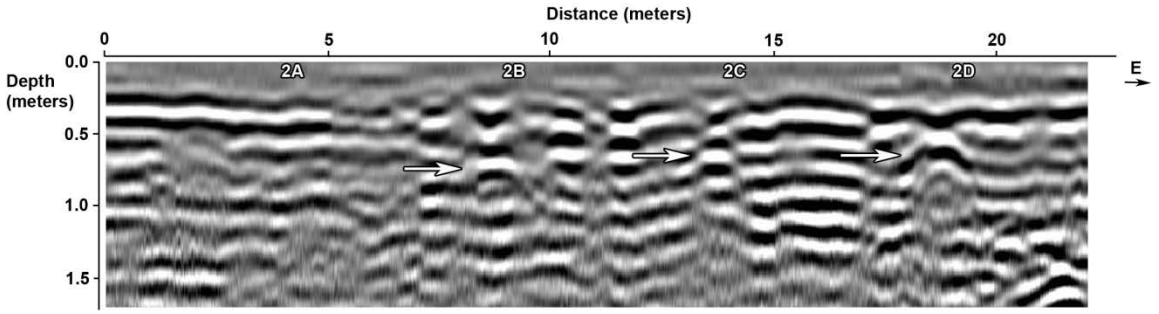

Figure D36: GPR reflection profile using the 250-MHz antenna of Row 2 at 19 months

GPR 250 REFLECTION PROFILE AT MONTH 20

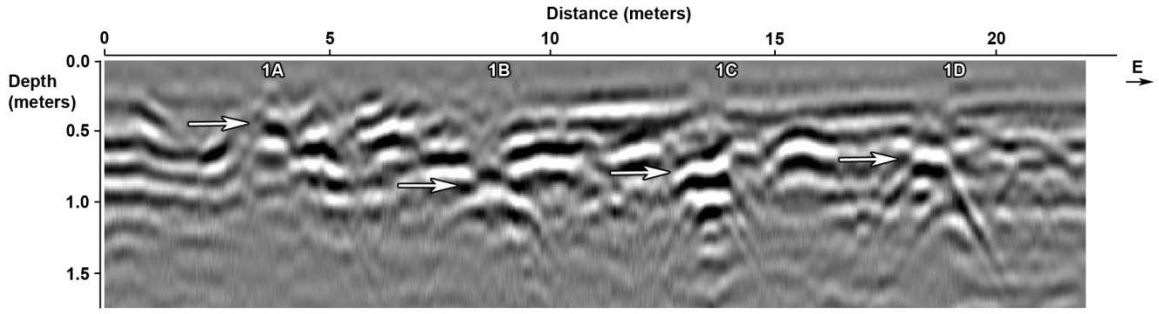

Figure D37: GPR reflection profile using the 250-MHz antenna of Row 1 at 20 months

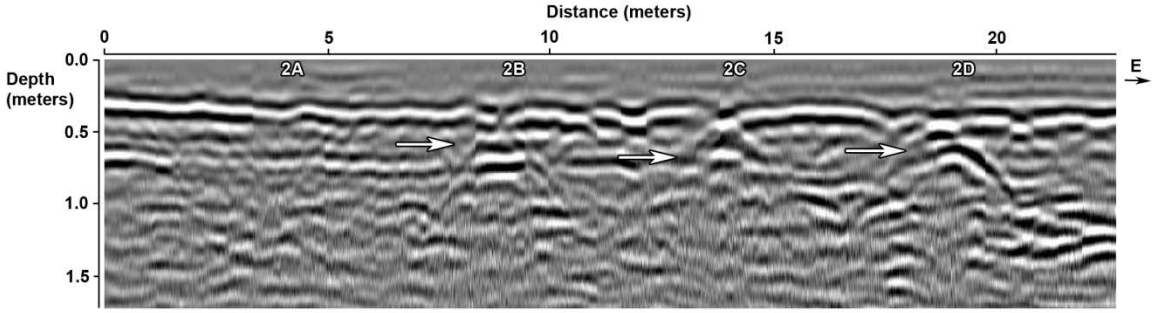

Figure D38: GPR reflection profile using the 250-MHz antenna of Row 2 at 20 months

GPR 250 REFLECTION PROFILE AT MONTH 21

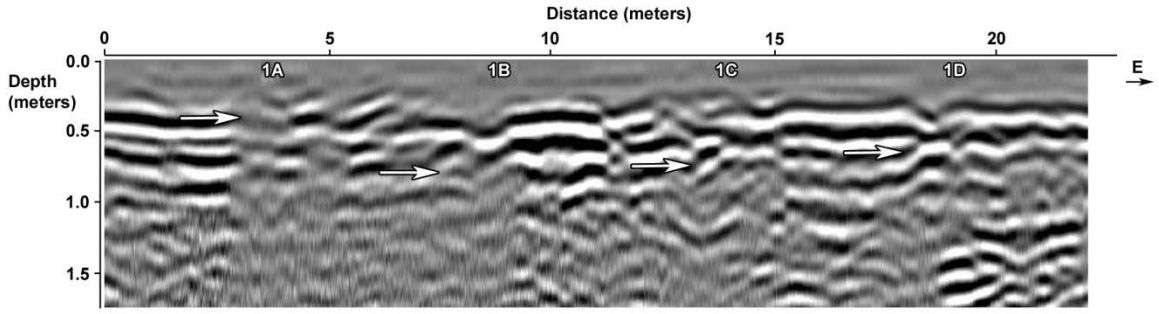

Figure D39: GPR reflection profile using the 250-MHz antenna of Row 1 at 21 months

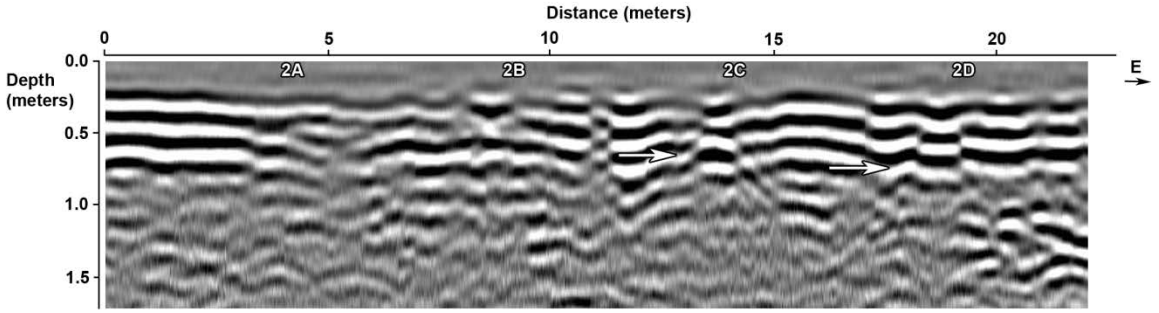

Figure D40: GPR reflection profile using the 250-MHz antenna of Row 2 at 21 months

GPR 250 REFLECTION PROFILE AT MONTH 22

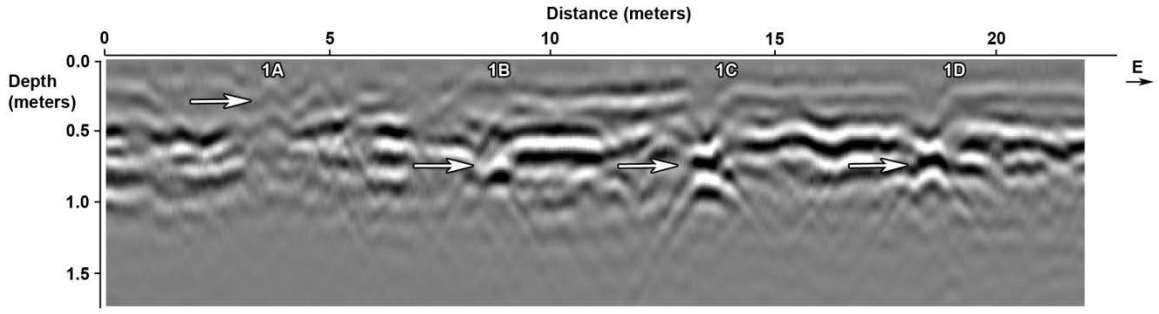

Figure D41: GPR reflection profile using the 250-MHz antenna of Row 1 at 22 months

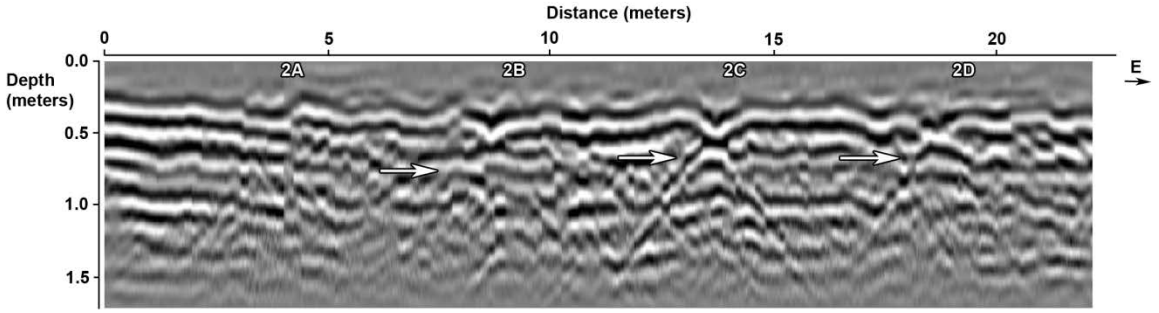

Figure D42: GPR reflection profile using the 250-MHz antenna of Row 2 at 22 months

GPR 250 REFLECTION PROFILE AT MONTH 23

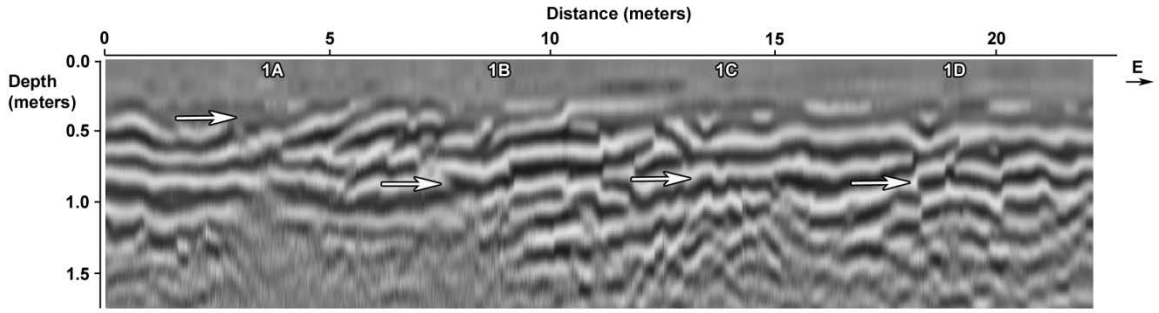

Figure D43: GPR reflection profile using the 250-MHz antenna of Row 1 at 23 months

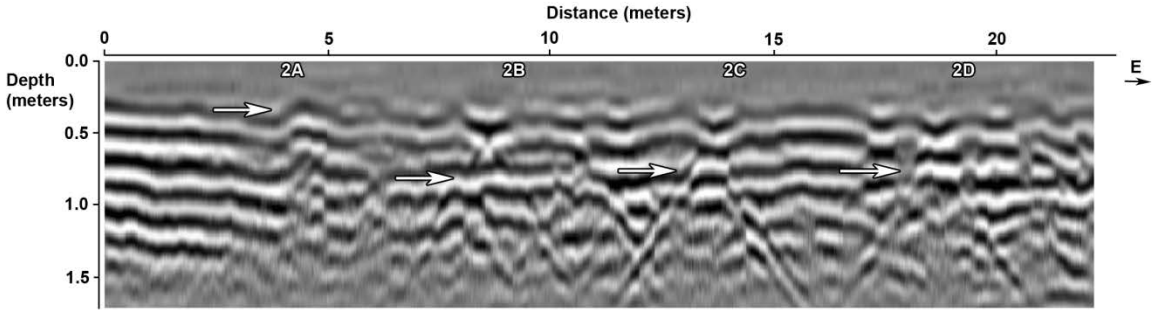

Figure D44: GPR reflection profile using the 250-MHz antenna of Row 2 at 23 months

GPR 250 REFLECTION PROFILE AT MONTH 24

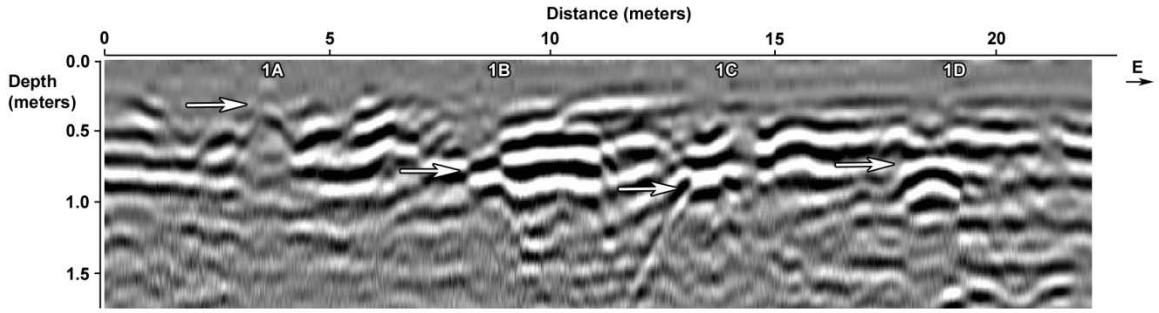

Figure D45: GPR reflection profile using the 250-MHz antenna of Row 1 at 24 months

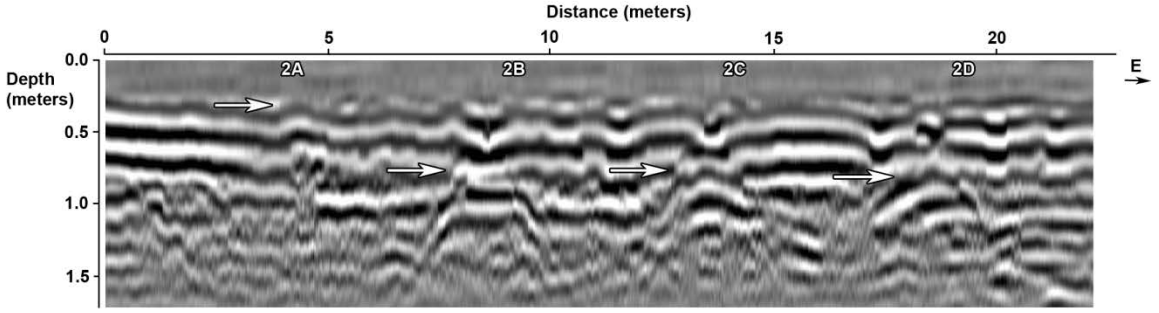

Figure D46: GPR reflection profile using the 250-MHz antenna of Row 2 at 24 months

GPR 250 REFLECTION PROFILE AT MONTH 25

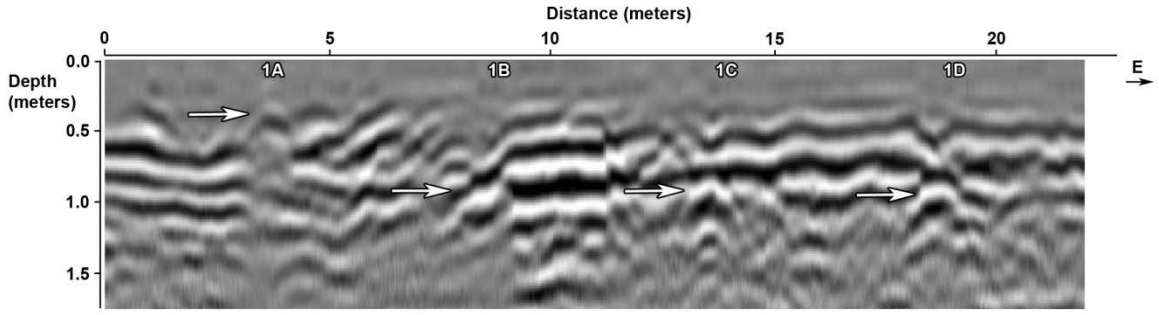

Figure D47: GPR reflection profile using the 250-MHz antenna of Row 1 at 25 months

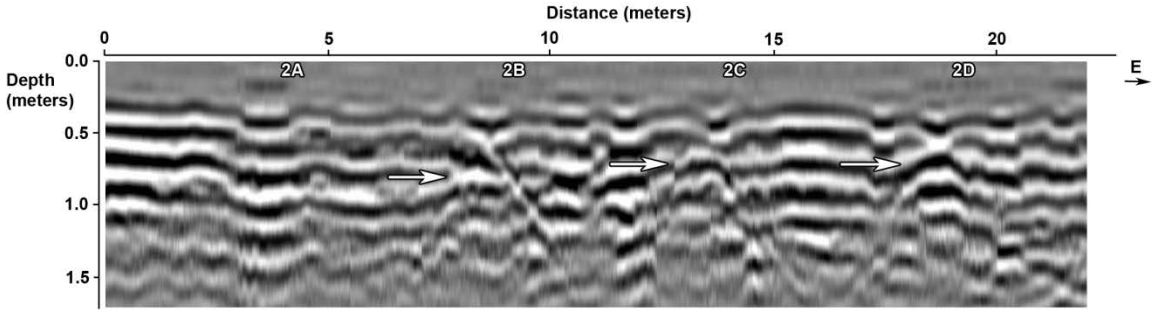

Figure D48: GPR reflection profile using the 250-MHz antenna of Row 2 at 25 months

GPR 250 REFLECTION PROFILE AT MONTH 26

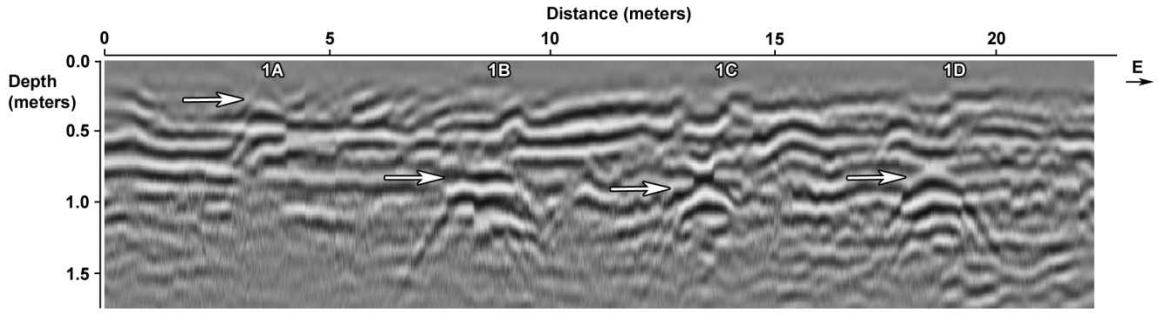

Figure D49: GPR reflection profile using the 250-MHz antenna of Row 1 at 26 months

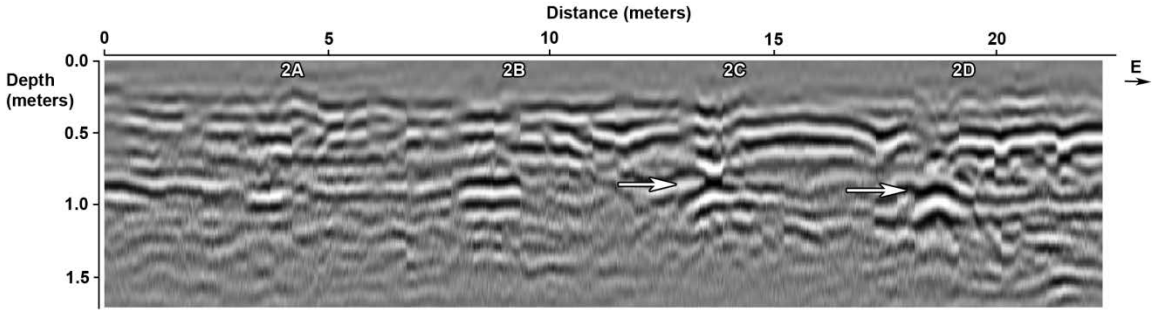

Figure D50: GPR reflection profile using the 250-MHz antenna of Row 2 at 26 months

GPR 250 REFLECTION PROFILE AT MONTH 27

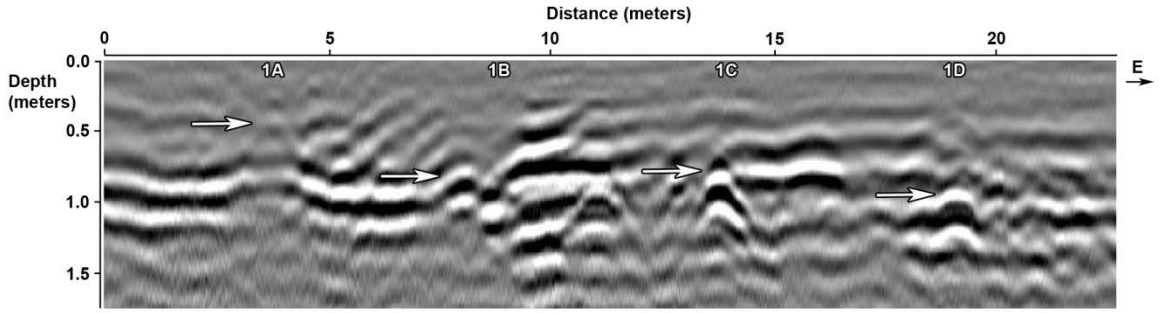

Figure D49: GPR reflection profile using the 250-MHz antenna of Row 1 at 27 months

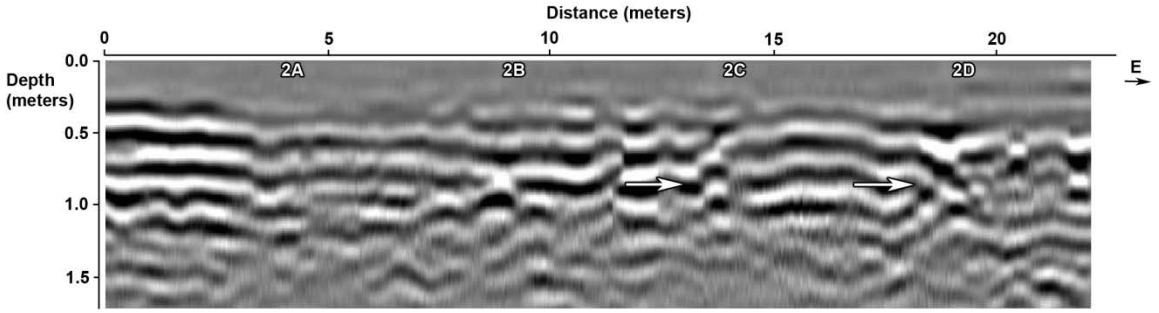

Figure D50: GPR reflection profile using the 250-MHz antenna of Row 2 at 27 months

GPR 250 REFLECTION PROFILE AT MONTH 28

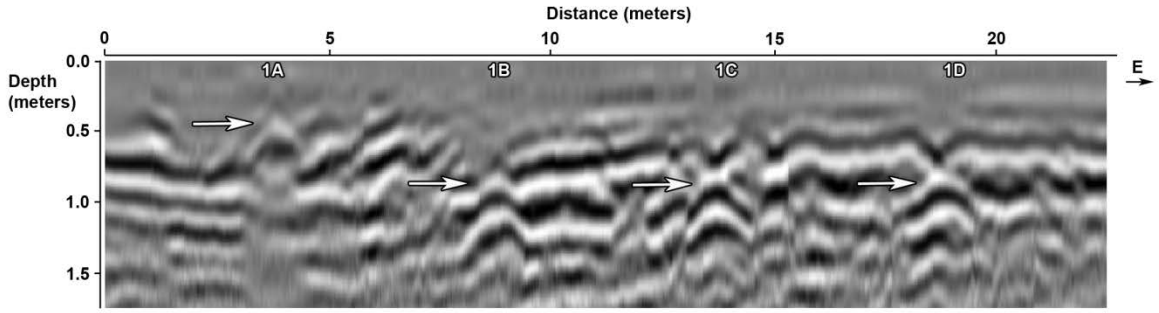

Figure D49: GPR reflection profile using the 250-MHz antenna of Row 1 at 28 months

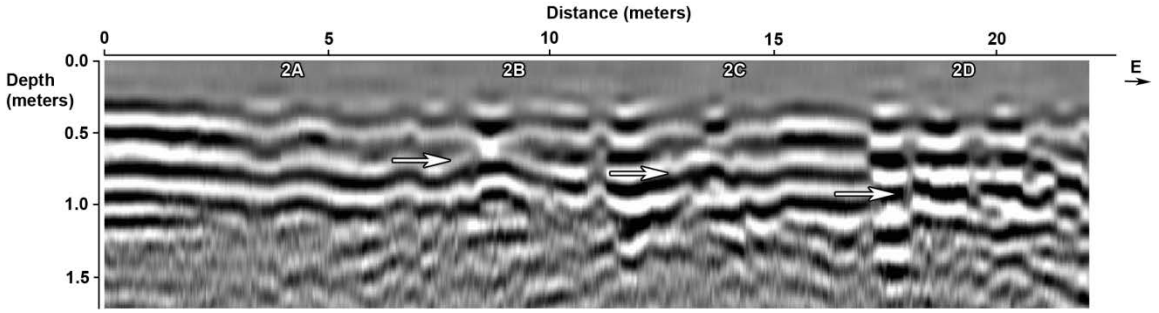

Figure D50: GPR reflection profile using the 250-MHz antenna of Row 2 at 28 months

GPR 250 REFLECTION PROFILE AT MONTH 29

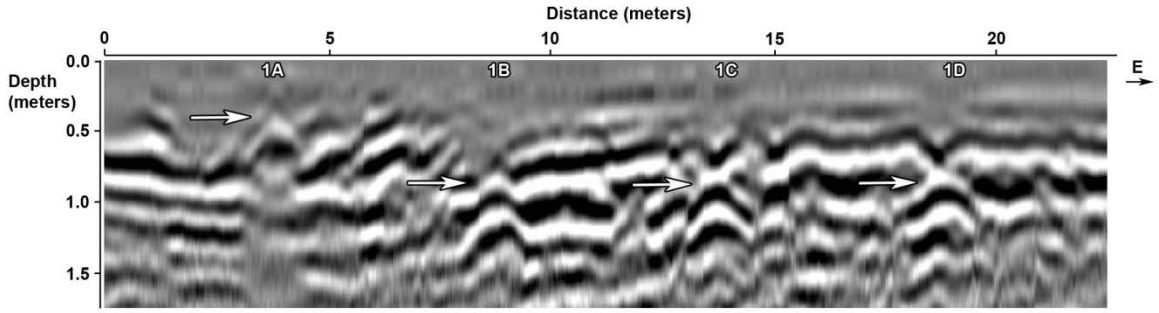

Figure D49: GPR reflection profile using the 250-MHz antenna of Row 1 at 29 months

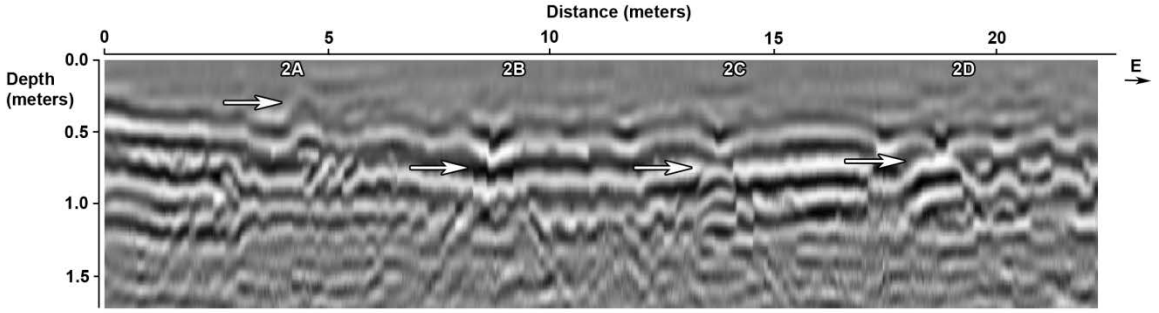

Figure D50: GPR reflection profile using the 250-MHz antenna of Row 2 at 29 months

GPR 250 REFLECTION PROFILE AT MONTH 30

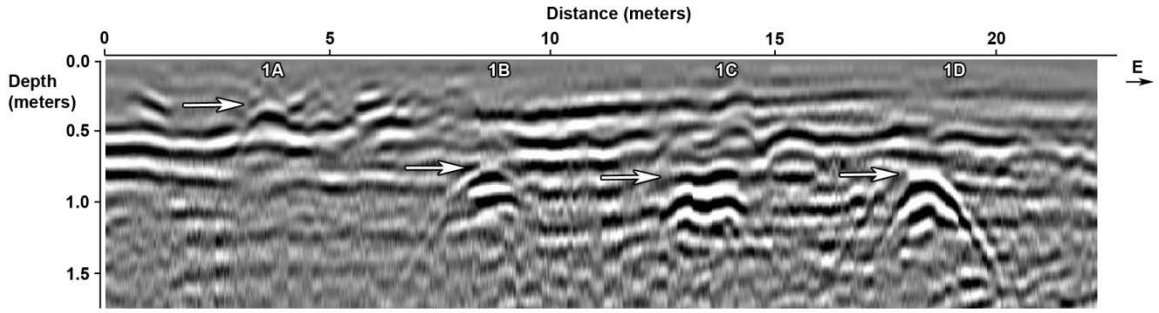

Figure D49: GPR reflection profile using the 250-MHz antenna of Row 1 at 30 months

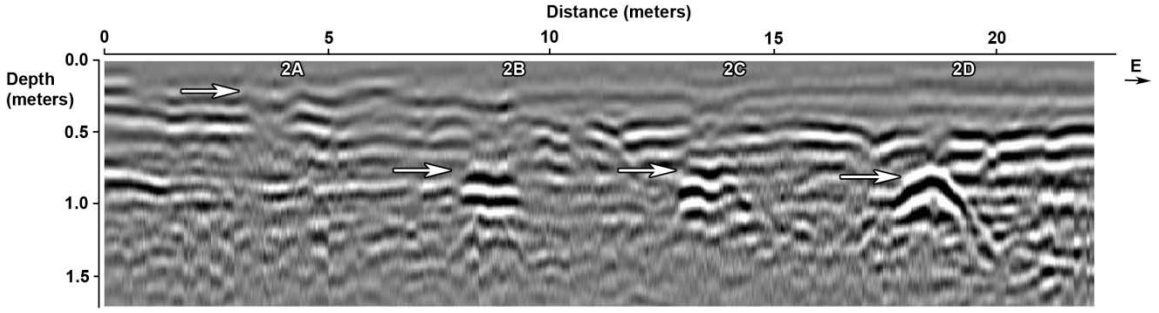

Figure D50: GPR reflection profile using the 250-MHz antenna of Row 2 at 30 months

APPENDIX E: GROUND-PENETRATING RADAR 250-MHZ HORIZONTAL TIME SLICES

GPR 250 TIME SLICE AT MONTH 1
(shallow)

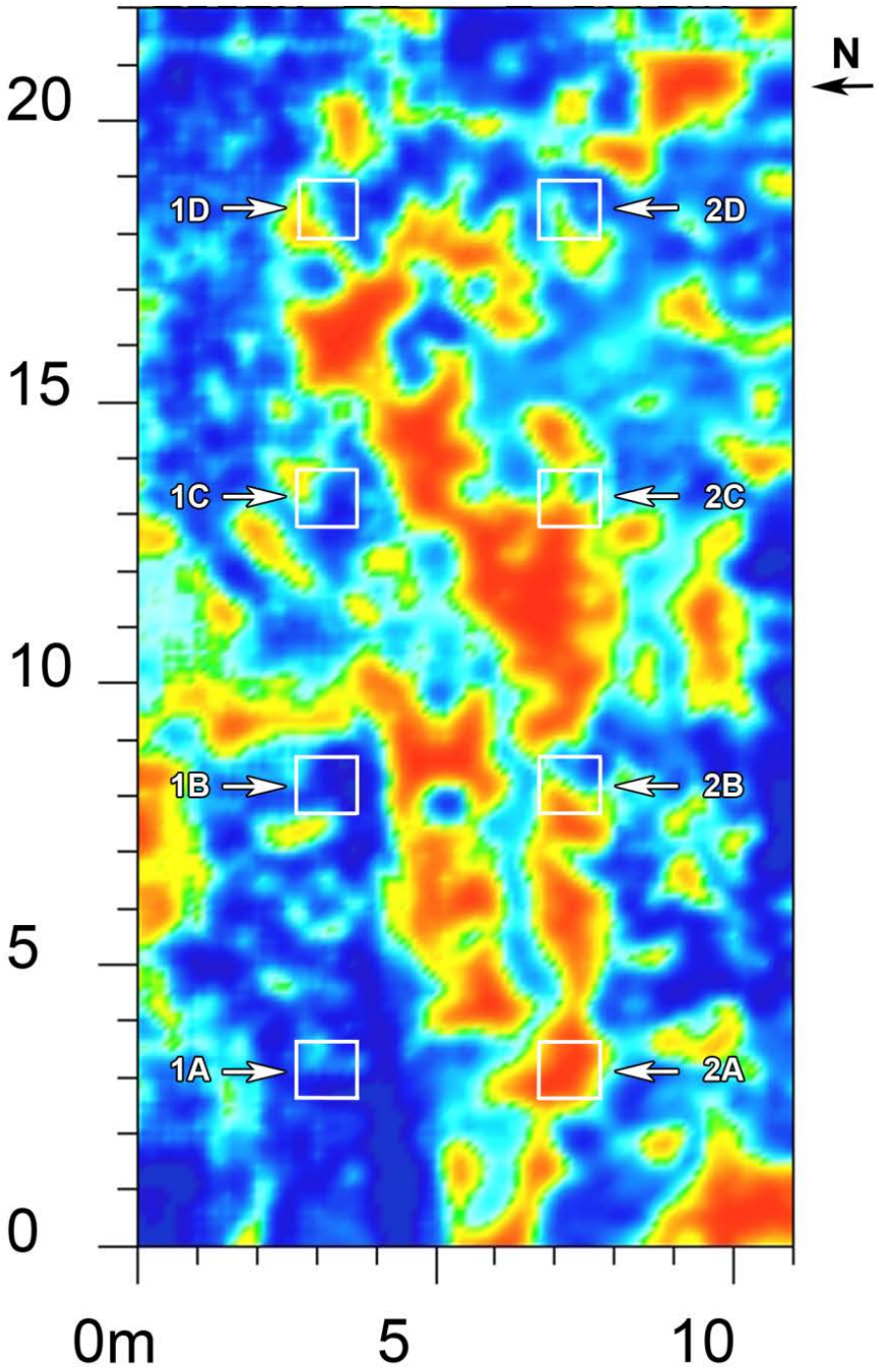

Figure E1: GPR horizontal slice using the 250-MHz antenna at 1 month. The horizontal slice is approximately 0.45 m in depth.

GPR 250 TIME SLICE AT MONTH 1
(deep)

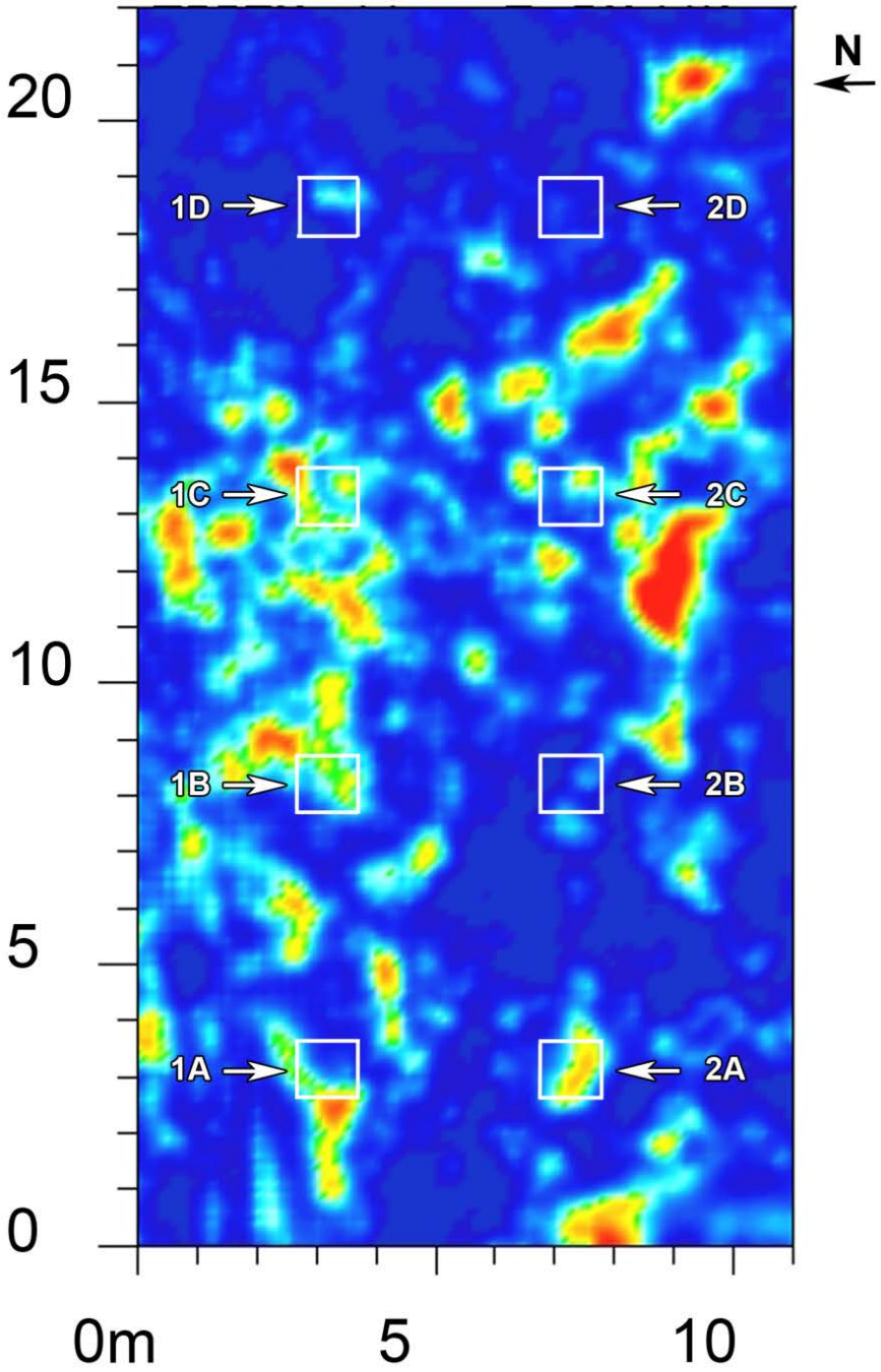

Figure E2: GPR horizontal slice using the 250-MHz antenna at 2 months. The horizontal slice is between 0.85 and 1.0 m in depth.

GPR 250 TIME SLICE AT MONTH 2
(shallow)

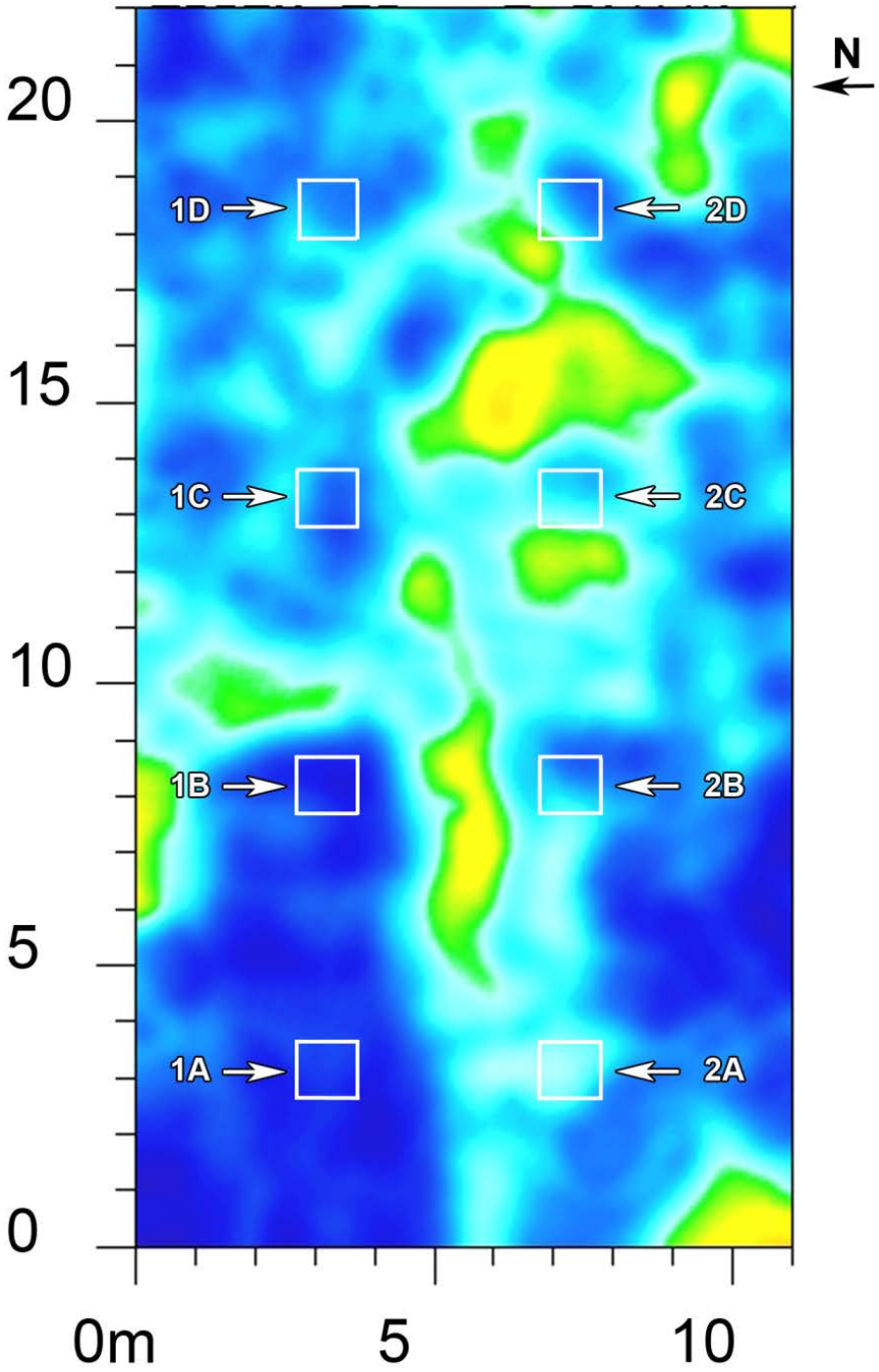

Figure E3: GPR horizontal slice using the 250-MHz antenna at 2 months. The horizontal slice is approximately 0.46 m in depth.

GPR 250 TIME SLICE AT MONTH 2
(deep)

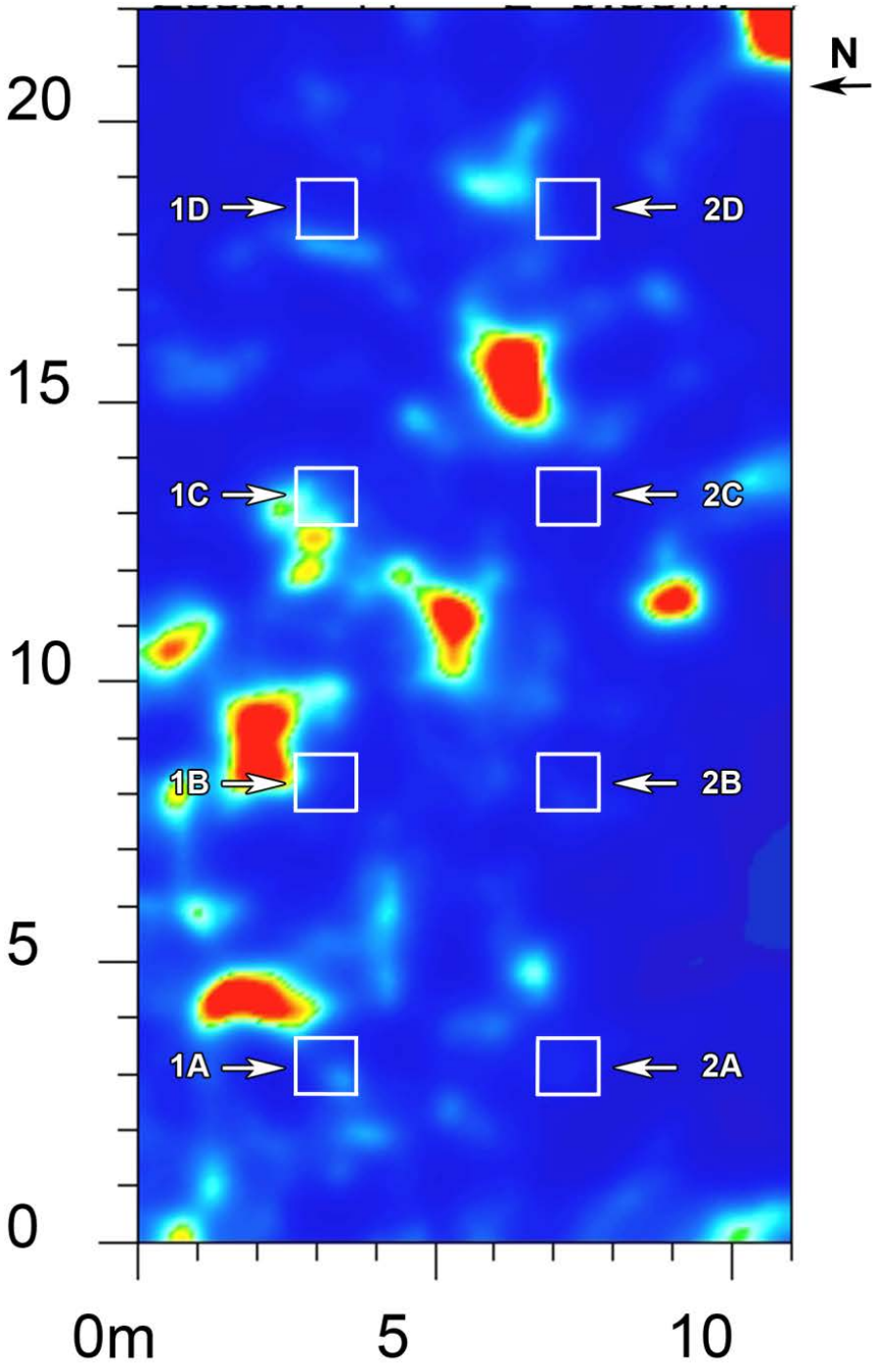

Figure E4: GPR horizontal slice using the 250-MHz antenna at 2 months. The horizontal slice is between 0.85 and 1.0 m in depth.

GPR 250 TIME SLICE AT MONTH 3
(shallow)

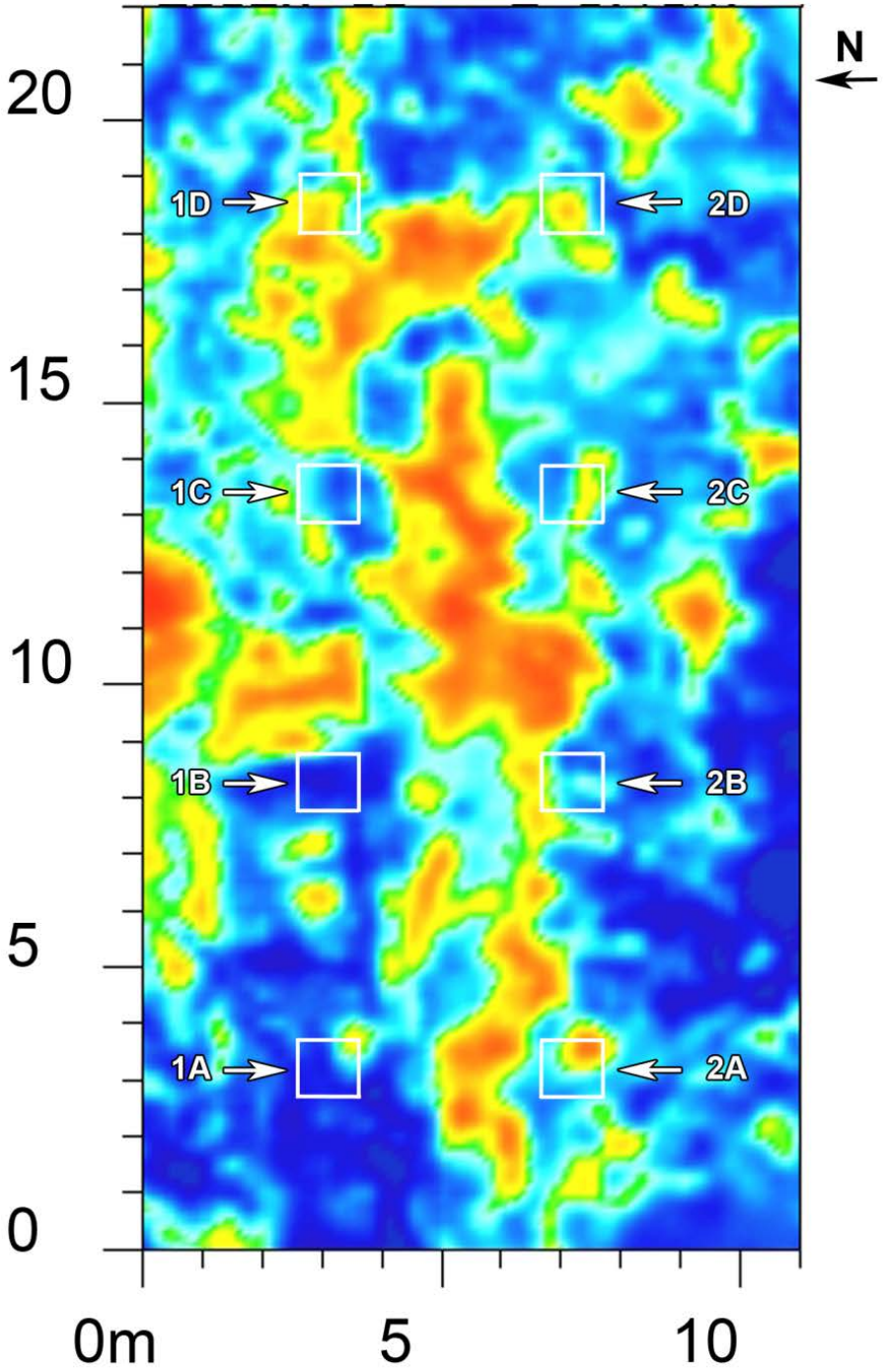

Figure E5: GPR horizontal slice using the 250-MHz antenna at 3 months. The horizontal slice is approximately 0.46 m in depth.

GPR 250 TIME SLICE AT MONTH 3
(deep)

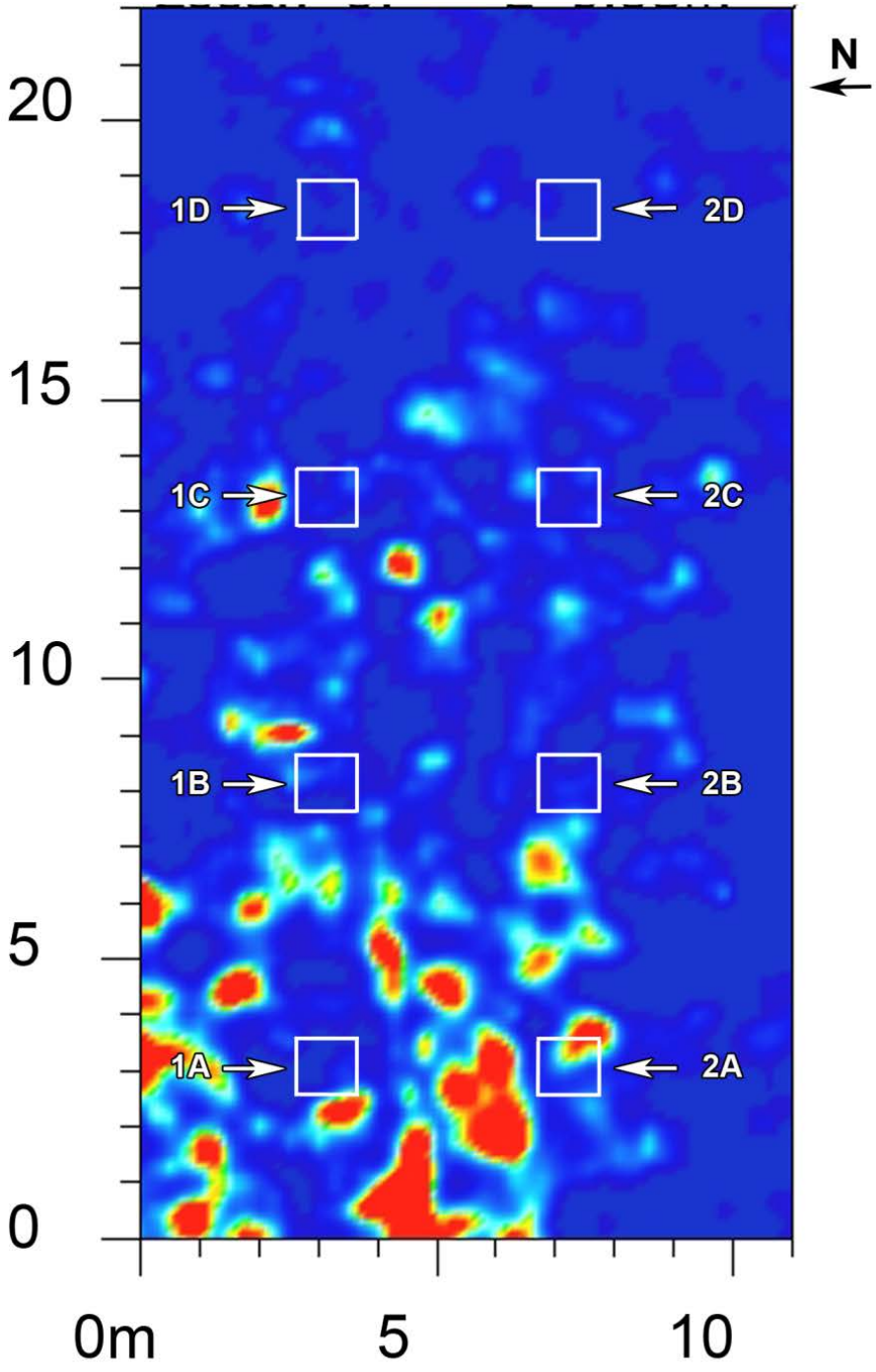

Figure E6: GPR horizontal slice using the 250-MHz antenna at 3 months. The horizontal slice is between 0.85 and 1.0 m in depth.

GPR 250 TIME SLICE AT MONTH 4

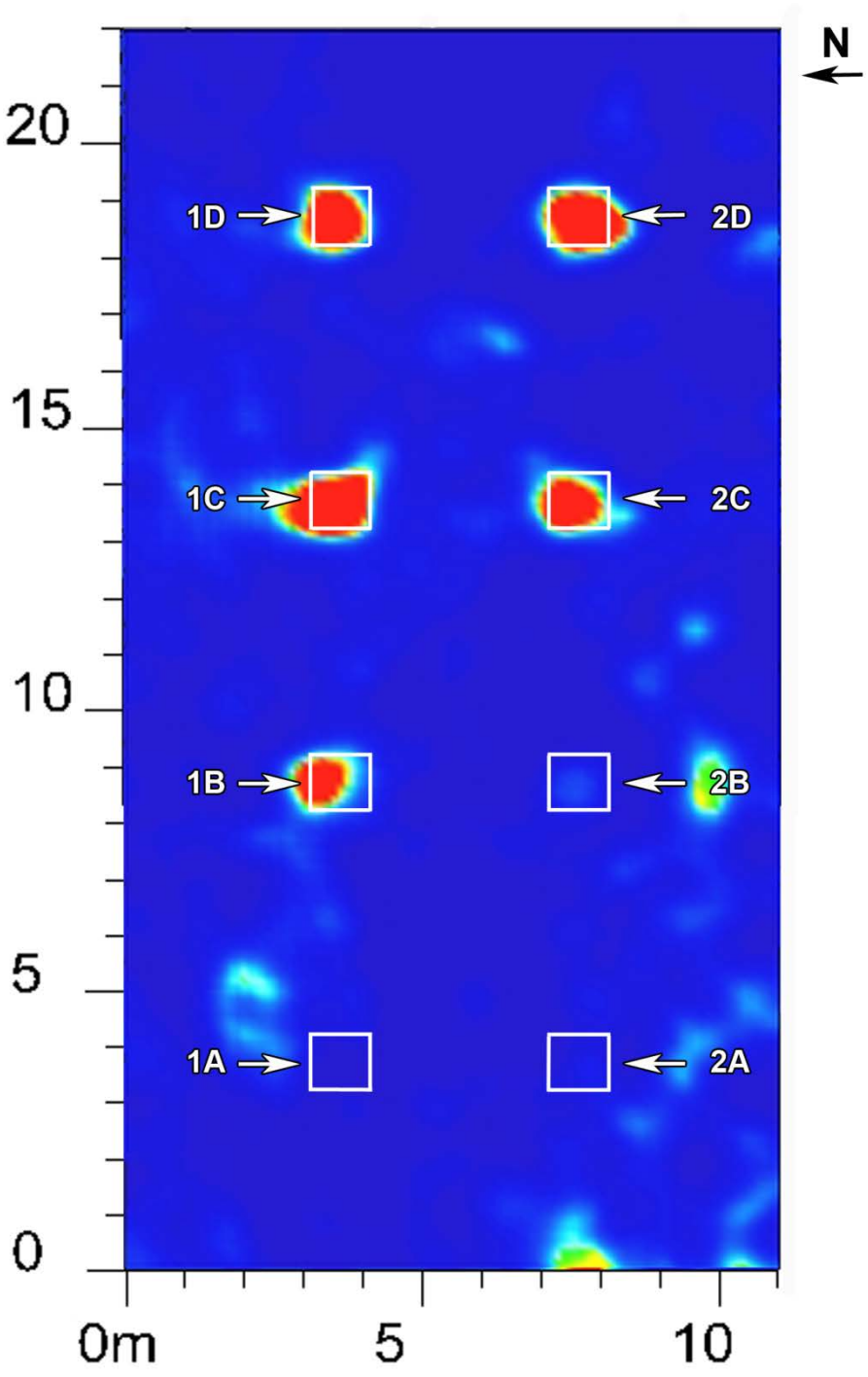

Figure E7: GPR horizontal slice using the 250-MHz antenna at 4 months. The horizontal slice is between 0.85 and 1.0 m in depth.

GPR 250 TIME SLICE AT MONTH 5

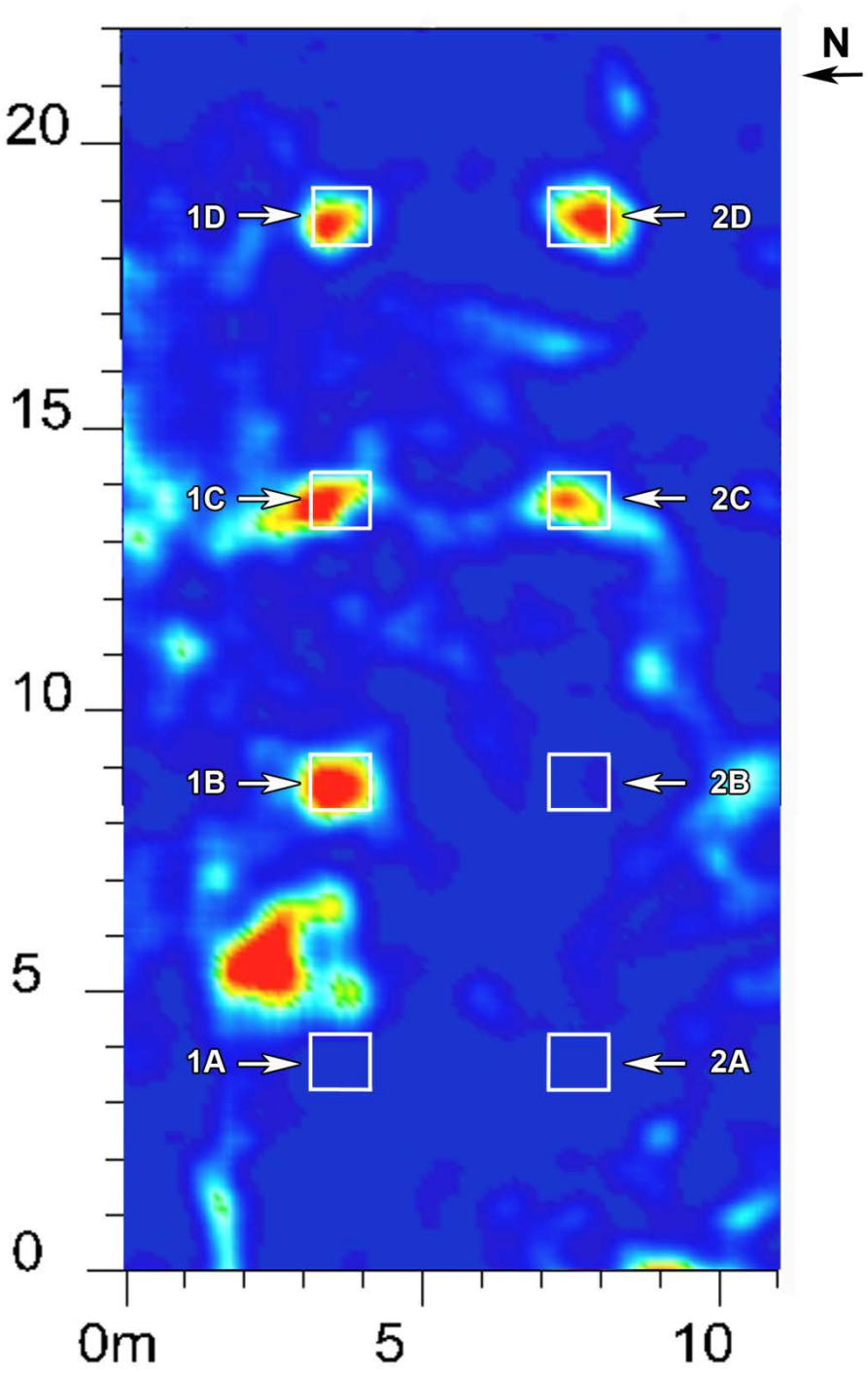

Figure E8: GPR horizontal slice using the 250-MHz antenna at 5 months. The horizontal slice is between 0.85 and 1.0 m in depth.

GPR 250 TIME SLICE AT MONTH 6

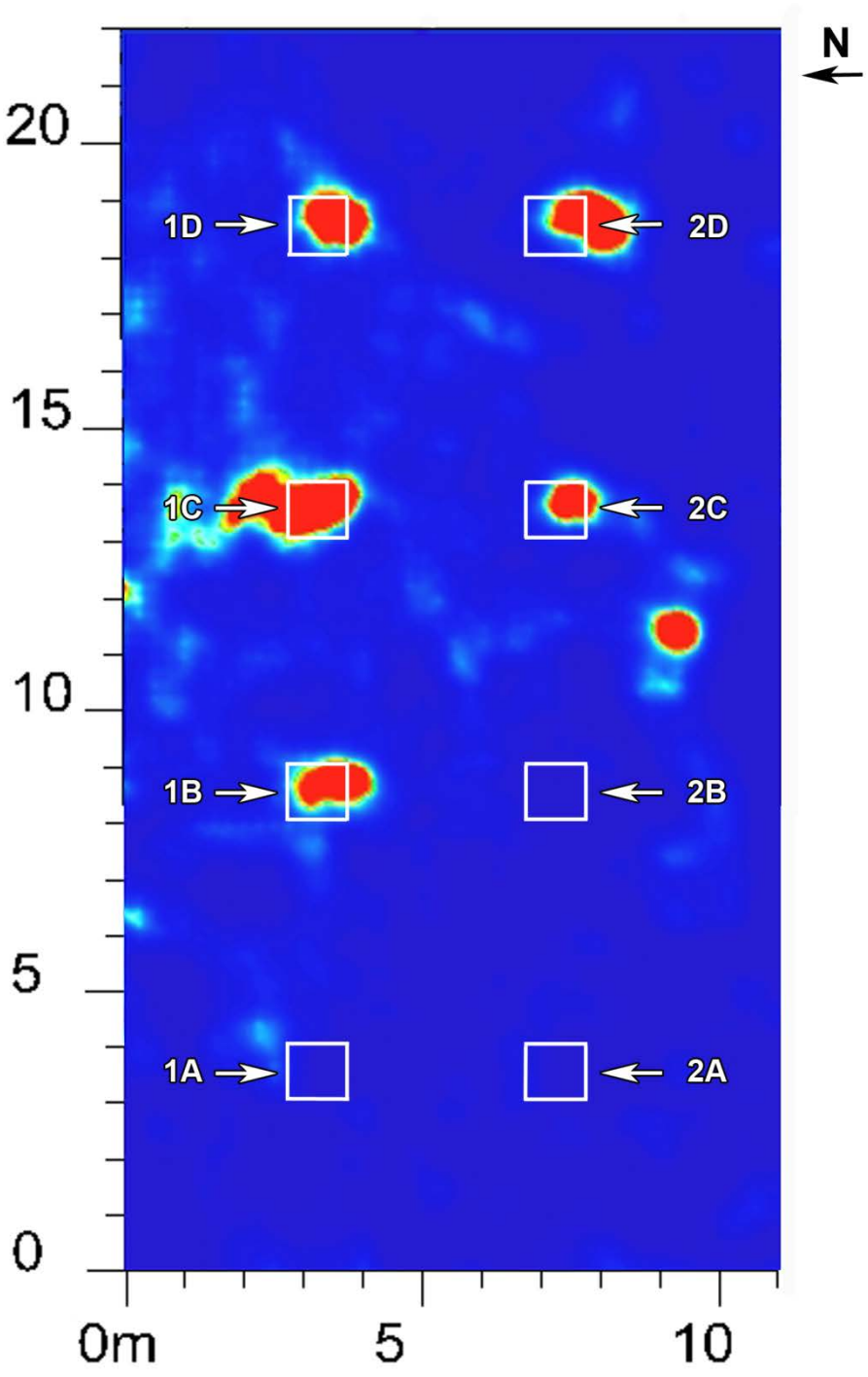

Figure E9: GPR horizontal slice using the 250-MHz antenna at 6 months. The horizontal slice is between 0.85 and 1.0 m in depth.

GPR 250 TIME SLICE AT MONTH 7

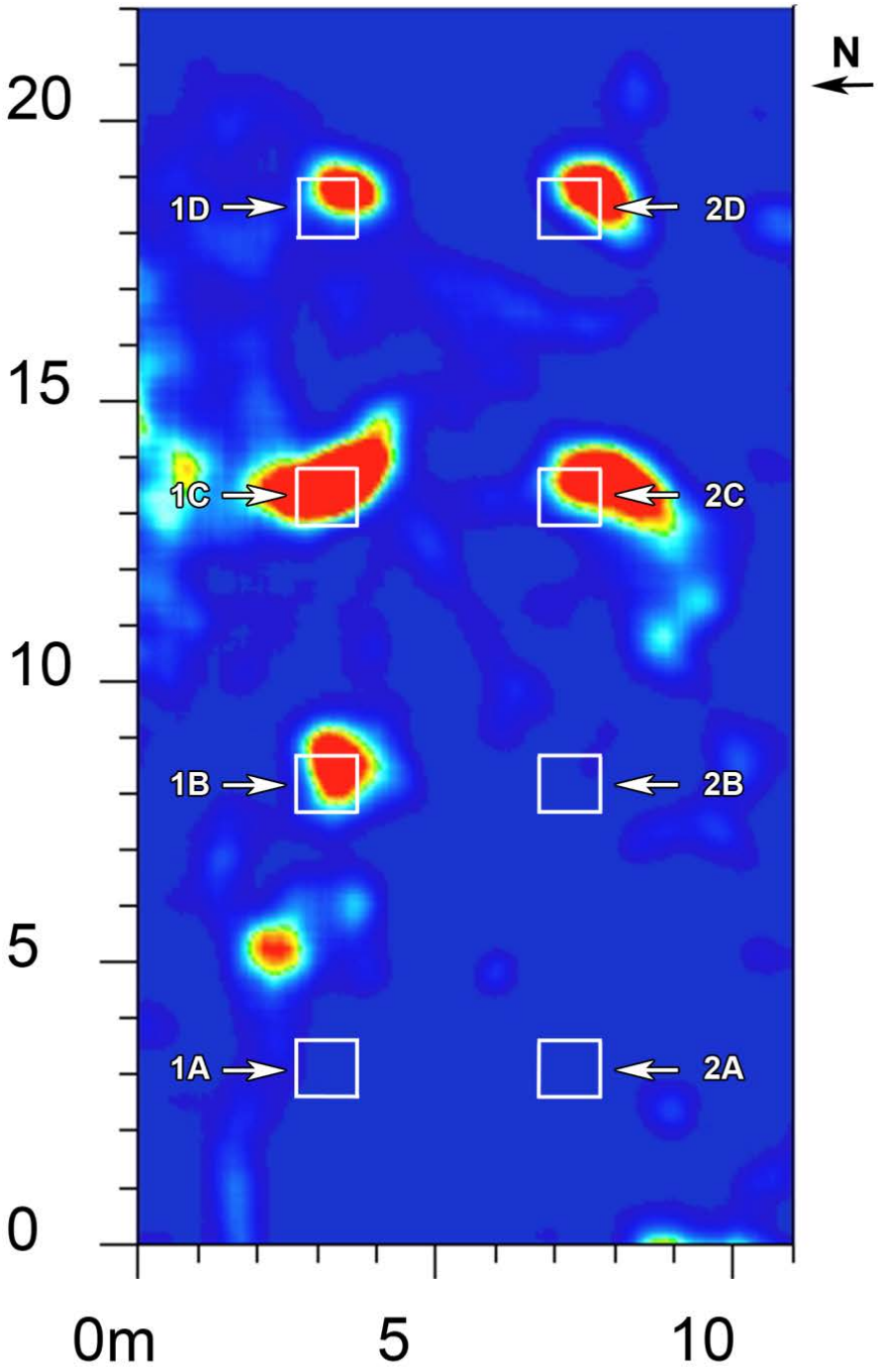

Figure E10: GPR horizontal slice using the 250-MHz antenna at 7 months. The horizontal slice is between 0.85 and 1.0 m in depth.

GPR 250 TIME SLICE AT MONTH 8

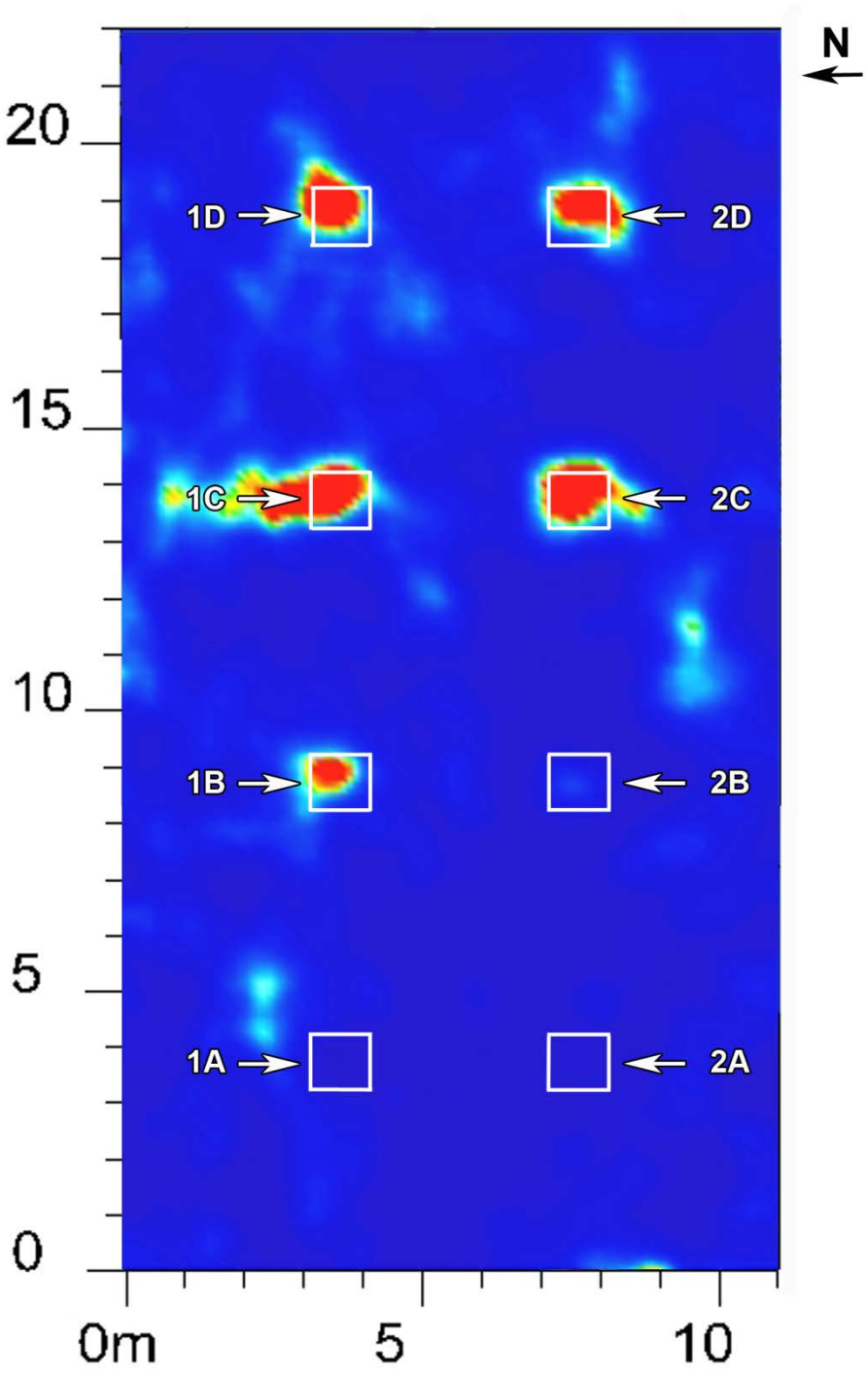

Figure E11: GPR horizontal slice using the 250-MHz antenna at 8 months. The horizontal slice is between 0.85 and 1.0 m in depth.

GPR 250 TIME SLICE AT MONTH 9

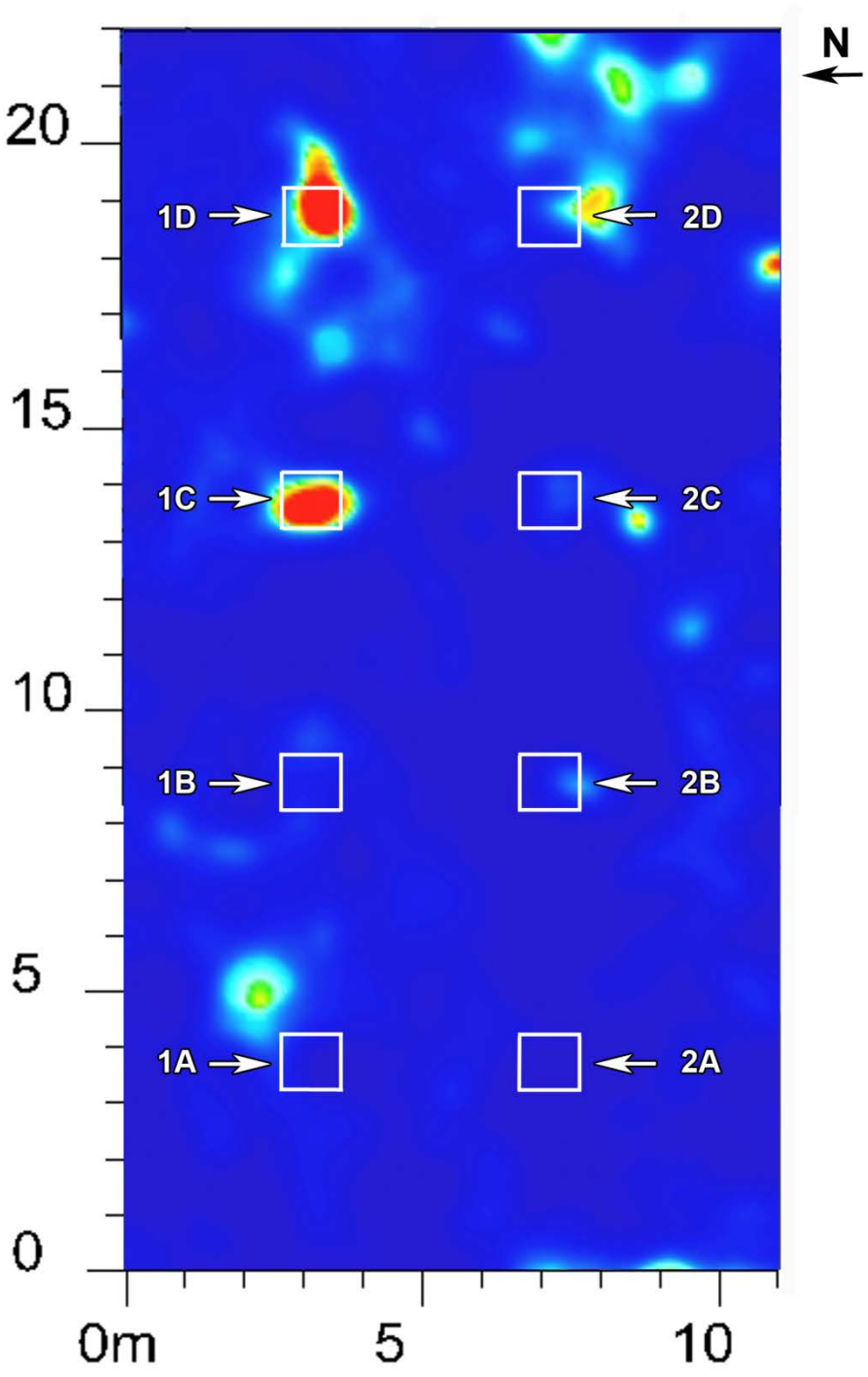

Figure E12: GPR horizontal slice using the 250-MHz antenna at 9 months. The horizontal slice is between 0.85 and 1.0 m in depth.

GPR 250 TIME SLICE AT MONTH 10

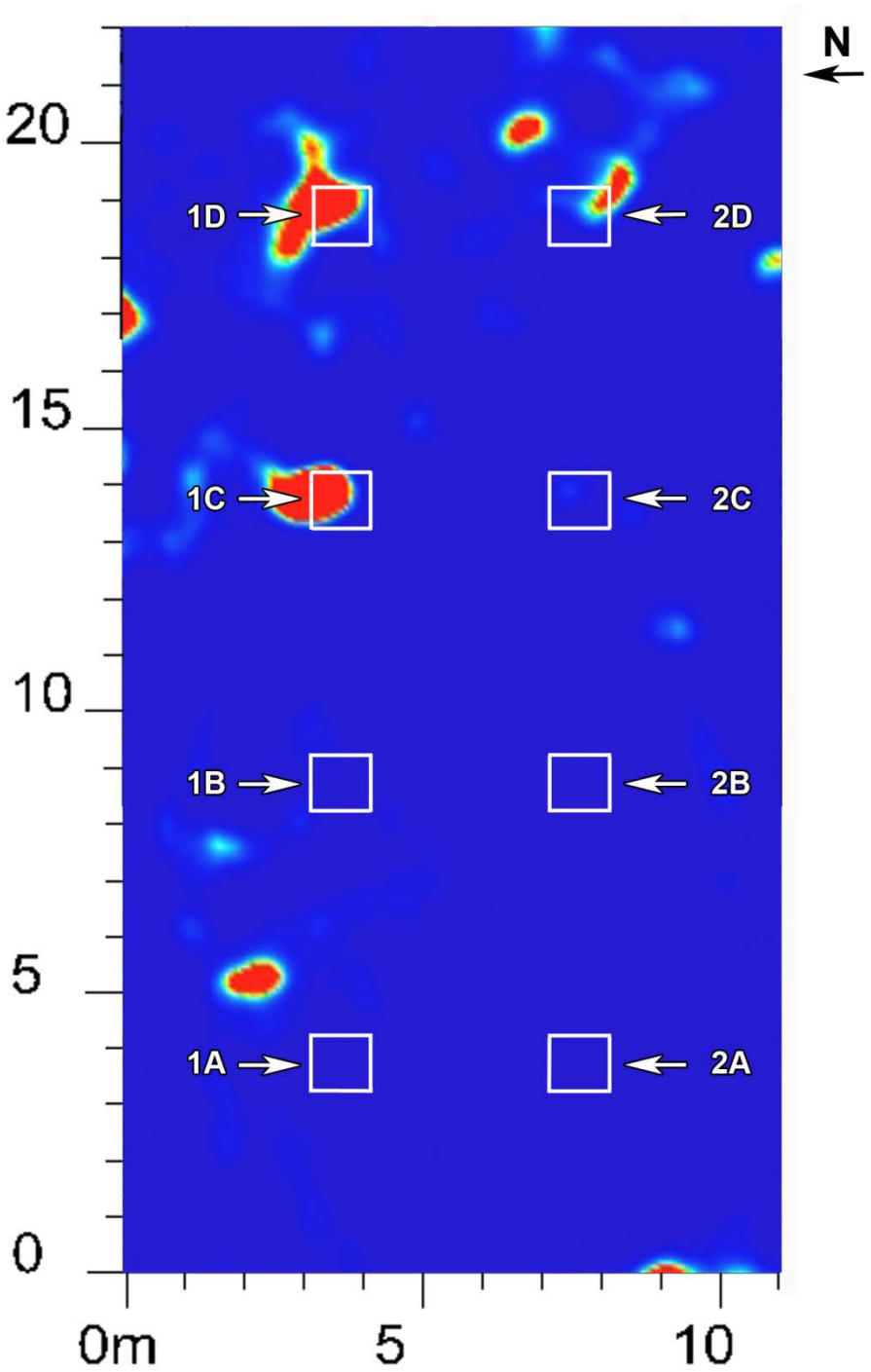

Figure E13: GPR horizontal slice using the 250-MHz antenna at 10 months. The horizontal slice is between 0.85 and 1.0 m in depth.

GPR 250 TIME SLICE AT MONTH 11

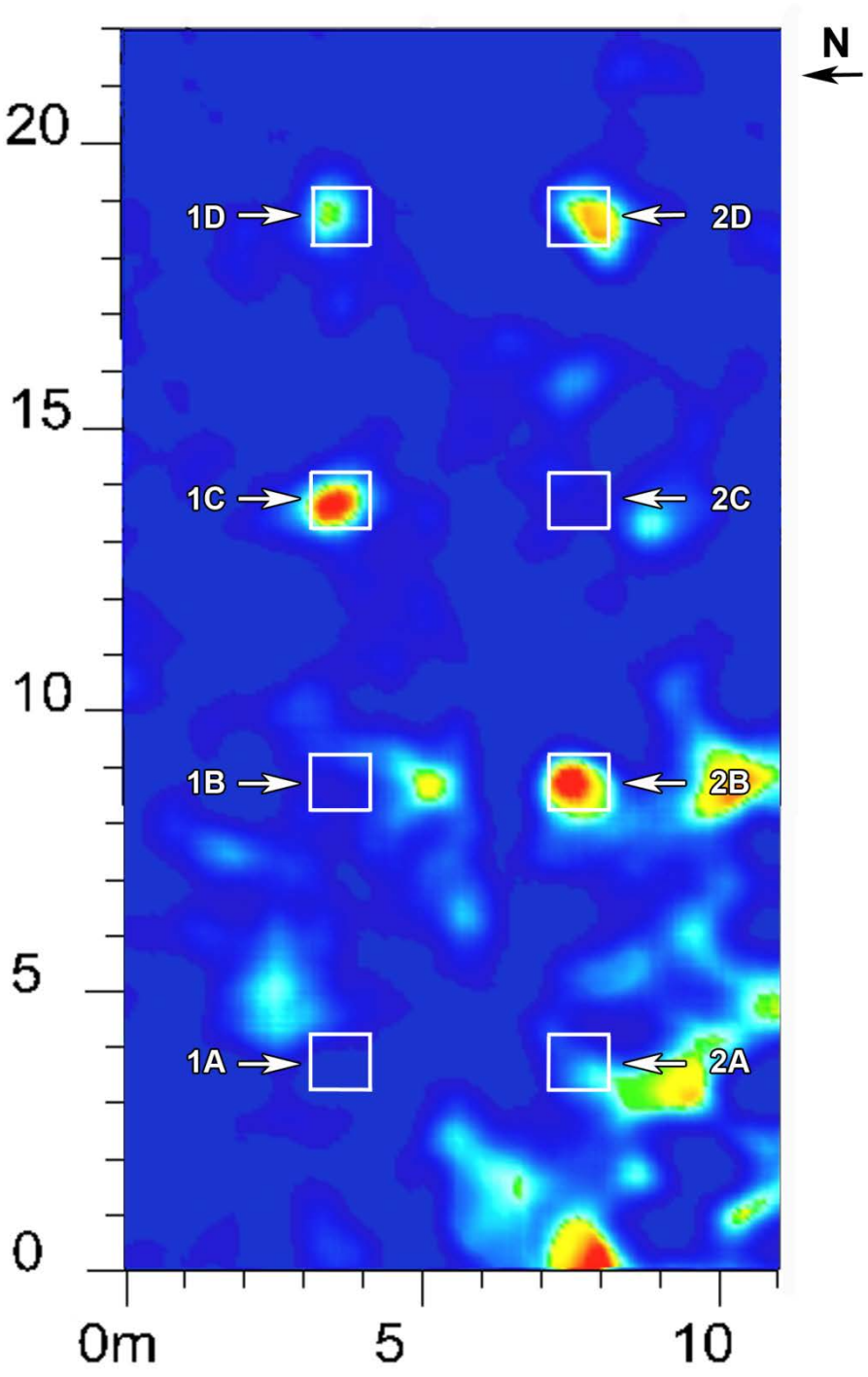

Figure E14: GPR horizontal slice using the 250-MHz antenna at 11 months. The horizontal slice is between 0.85 and 1.0 m in depth.

GPR 250 TIME SLICE AT MONTH 12

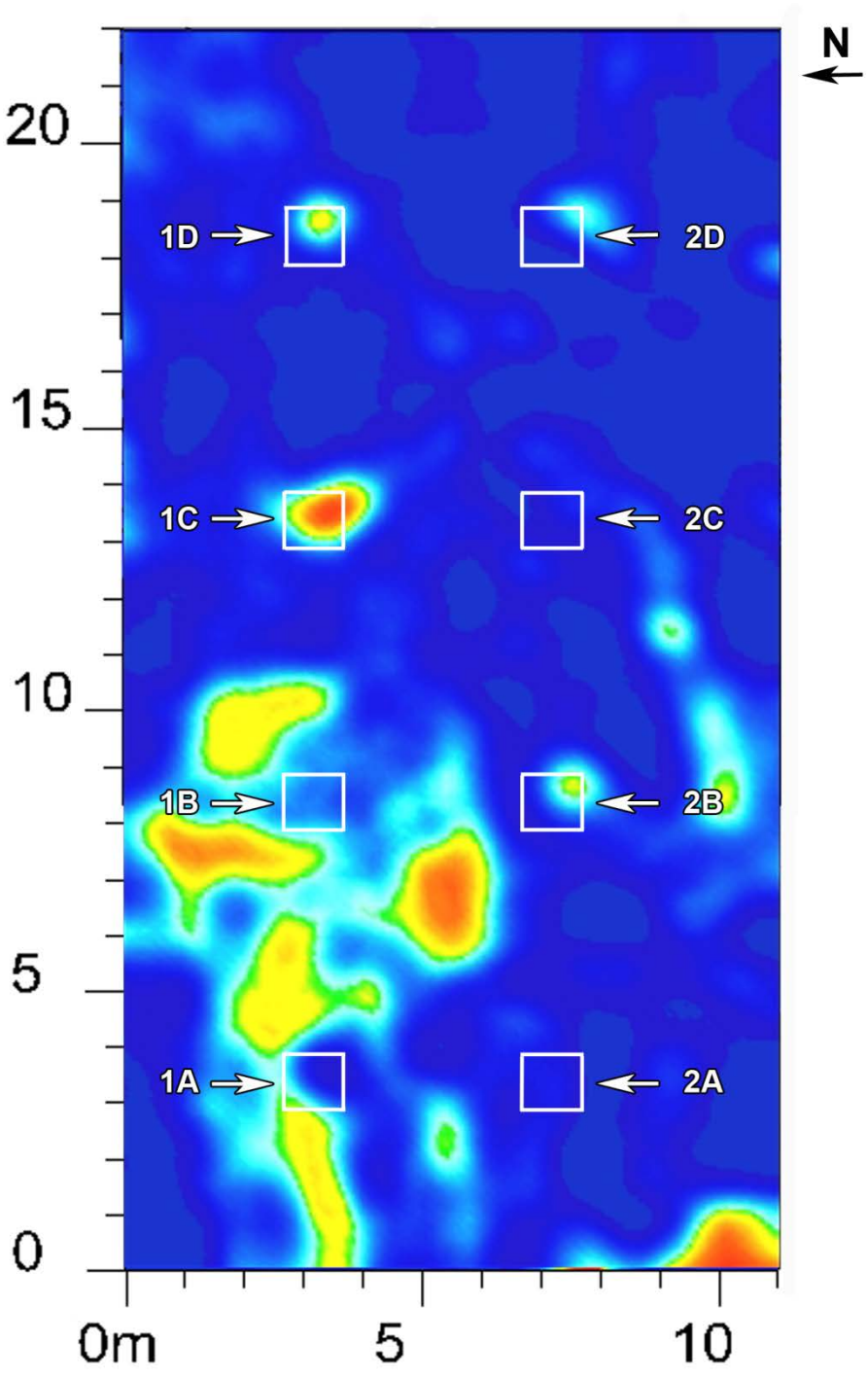

Figure E15: GPR horizontal slice using the 250-MHz antenna at 12 months. The horizontal slice is between 0.85 and 1.0 m in depth.

GPR 250 TIME SLICE AT MONTH 13

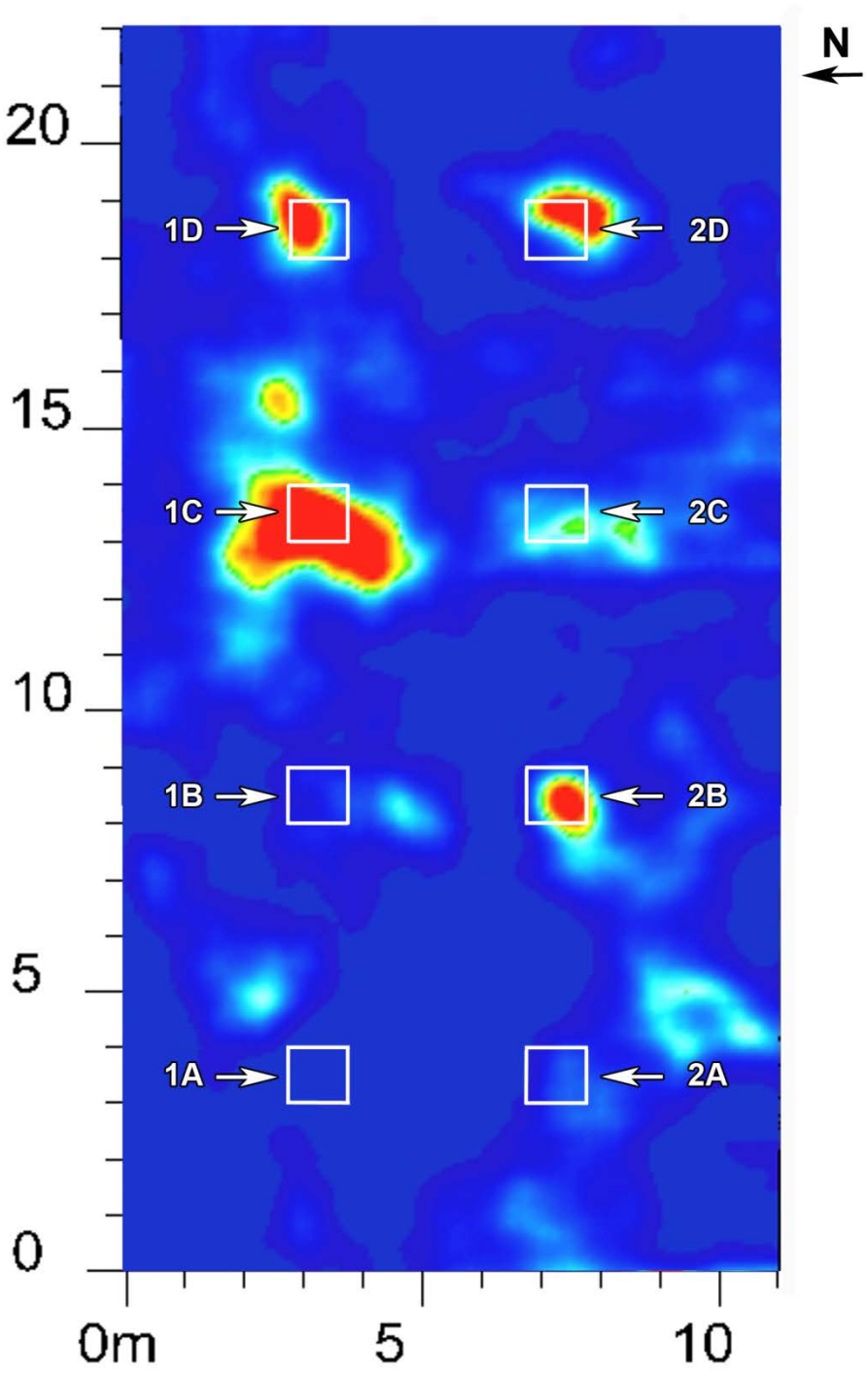

Figure E16: GPR horizontal slice using the 250-MHz antenna at 13 months. The horizontal slice is between 0.85 and 1.0 m in depth.

GPR 250 TIME SLICE AT MONTH 14

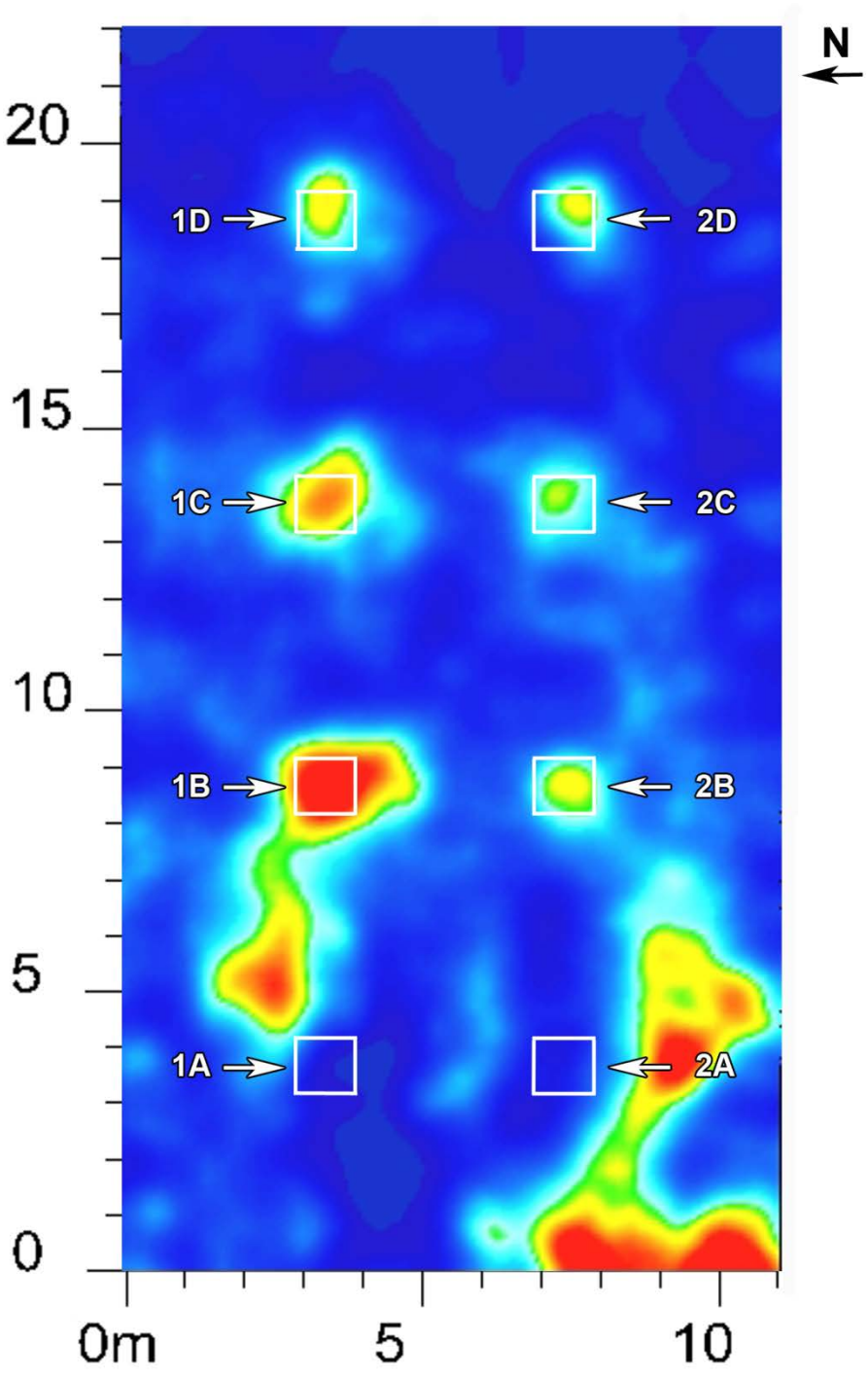

Figure E17: GPR horizontal slice using the 250-MHz antenna at 14 months. The horizontal slice is between 0.85 and 1.0 m in depth.

GPR 250 TIME SLICE AT MONTH 15

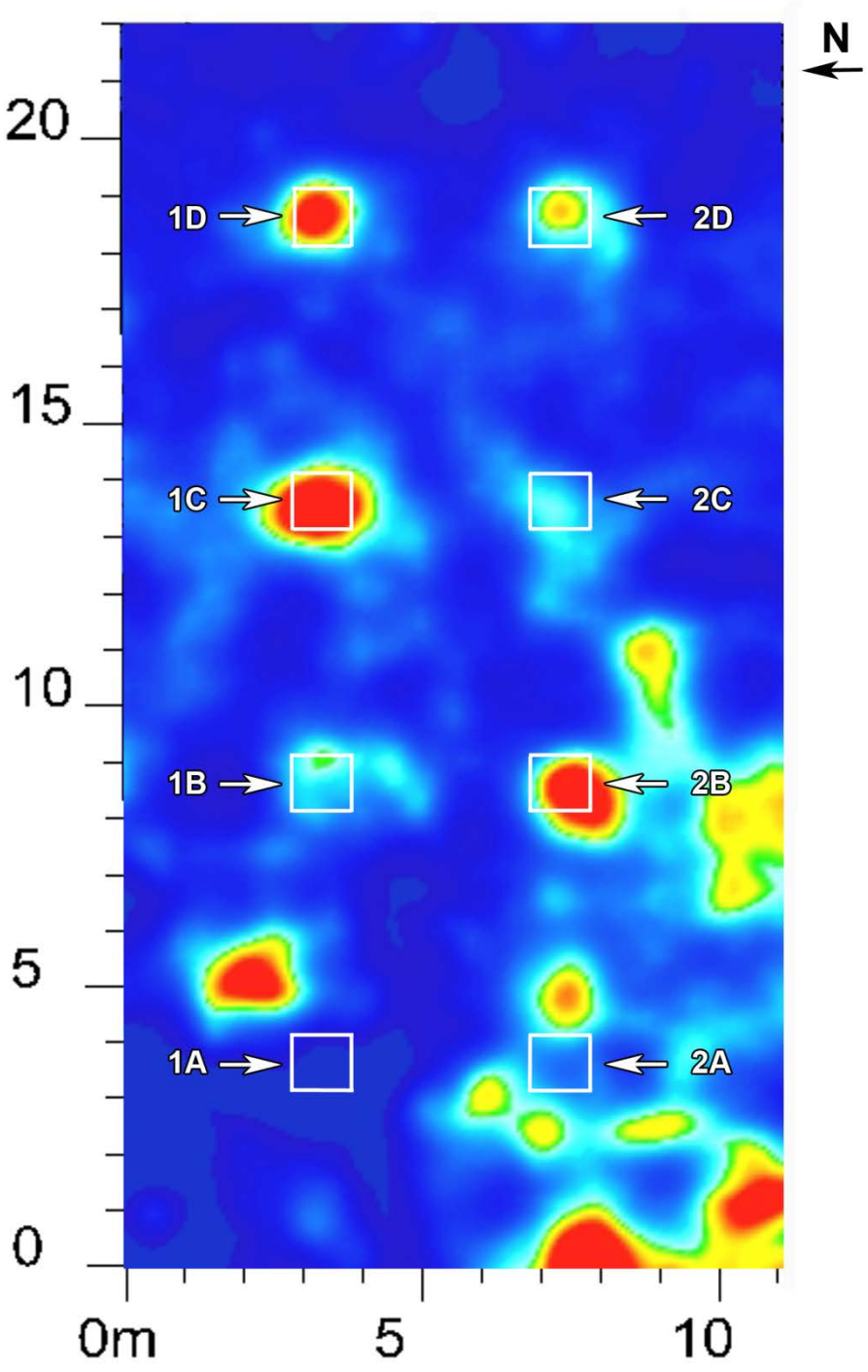

Figure E18: GPR horizontal slice using the 250-MHz antenna at 15 months. The horizontal slice is between 0.85 and 1.0 m in depth.

GPR 250 TIME SLICE AT MONTH 16

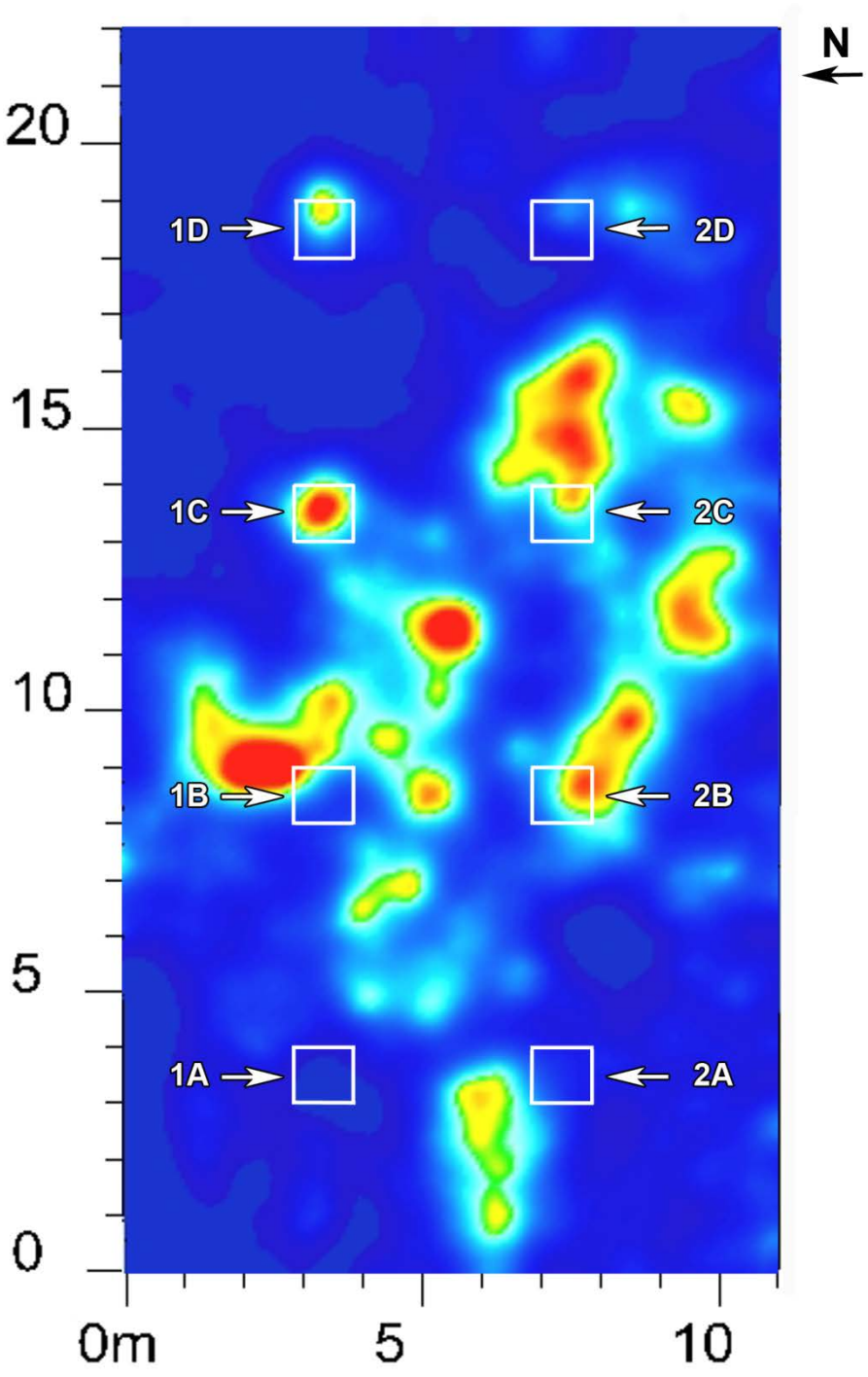

Figure E19: GPR horizontal slice using the 250-MHz antenna at 16 months. The horizontal slice is between 0.85 and 1.0 m in depth.

GPR 250 TIME SLICE AT MONTH 17

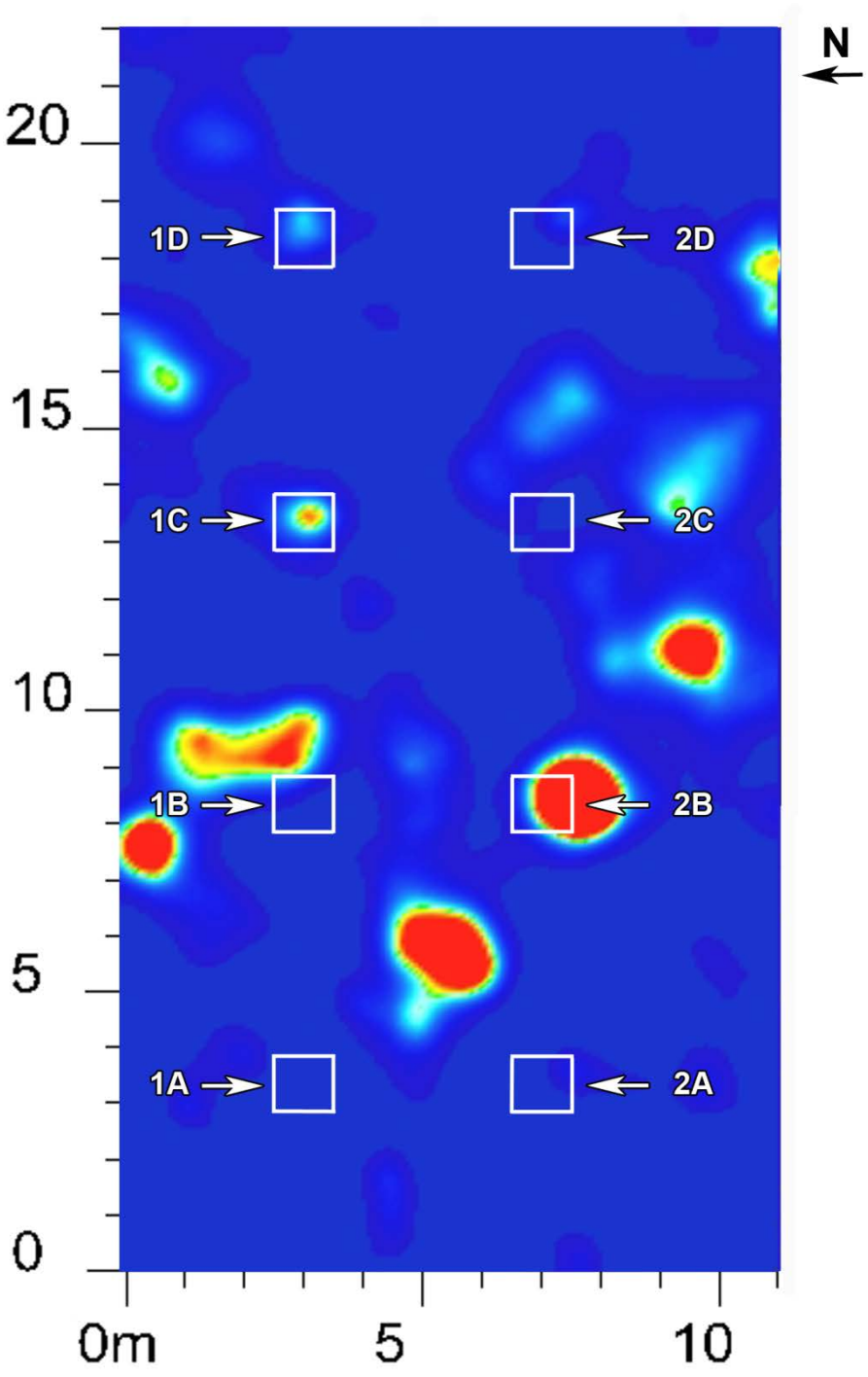

Figure E20: GPR horizontal slice using the 250-MHz antenna at 17 months. The horizontal slice is between 0.85 and 1.0 m in depth.

GPR 250 TIME SLICE AT MONTH 18

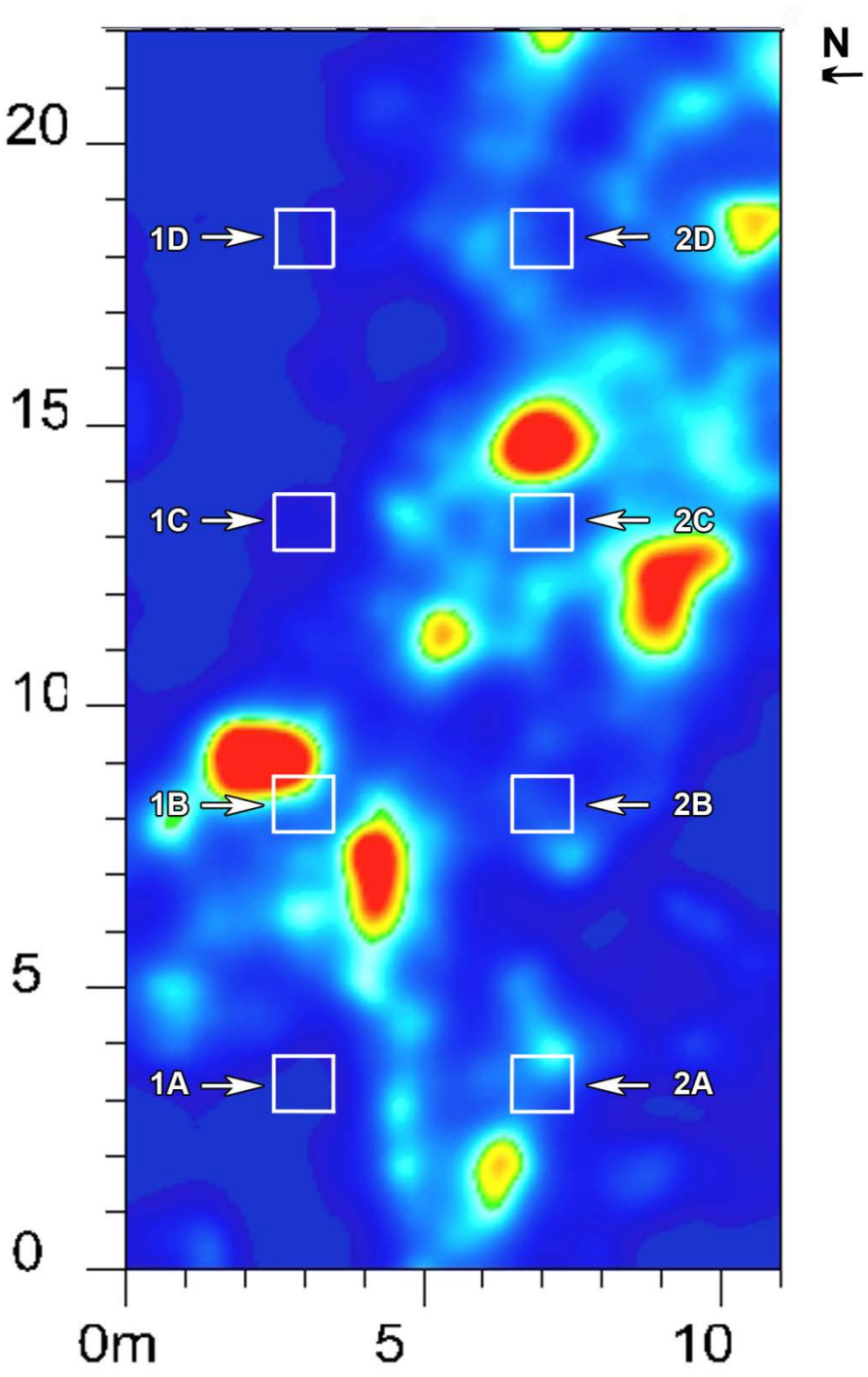

Figure E21: GPR horizontal slice using the 250-MHz antenna at 18 months. The horizontal slice is between 0.85 and 1.0 m in depth.

GPR 250 TIME SLICE AT MONTH 19

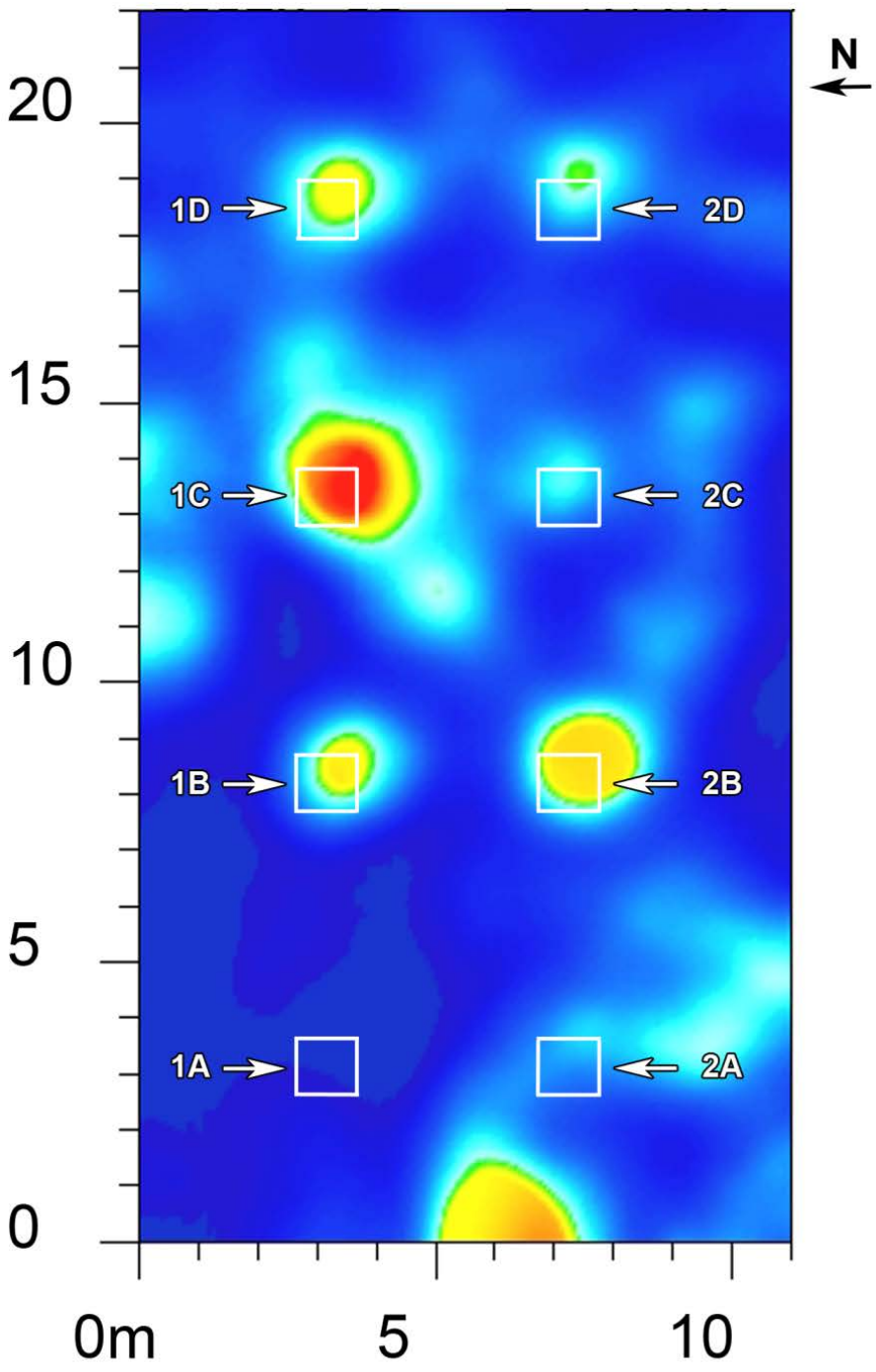

Figure E22: GPR horizontal slice using the 250-MHz antenna at 19 months. The horizontal slice is between 0.85 and 1.0 m in depth.

GPR 250 TIME SLICE AT MONTH 20

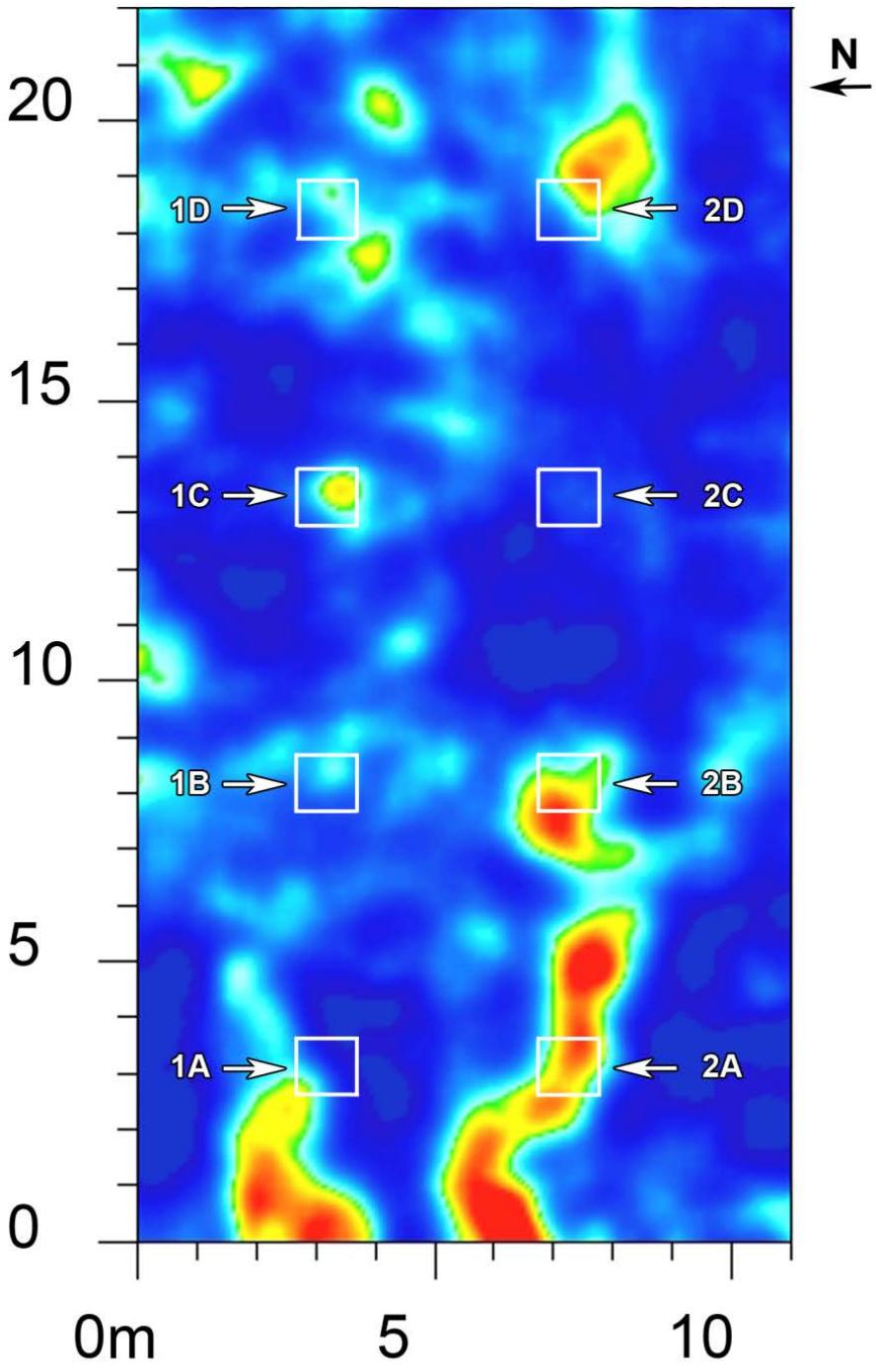

Figure E23: GPR horizontal slice using the 250-MHz antenna at 20 months. The horizontal slice is between 0.85 and 1.0 m in depth.

GPR 250 TIME SLICE AT MONTH 21

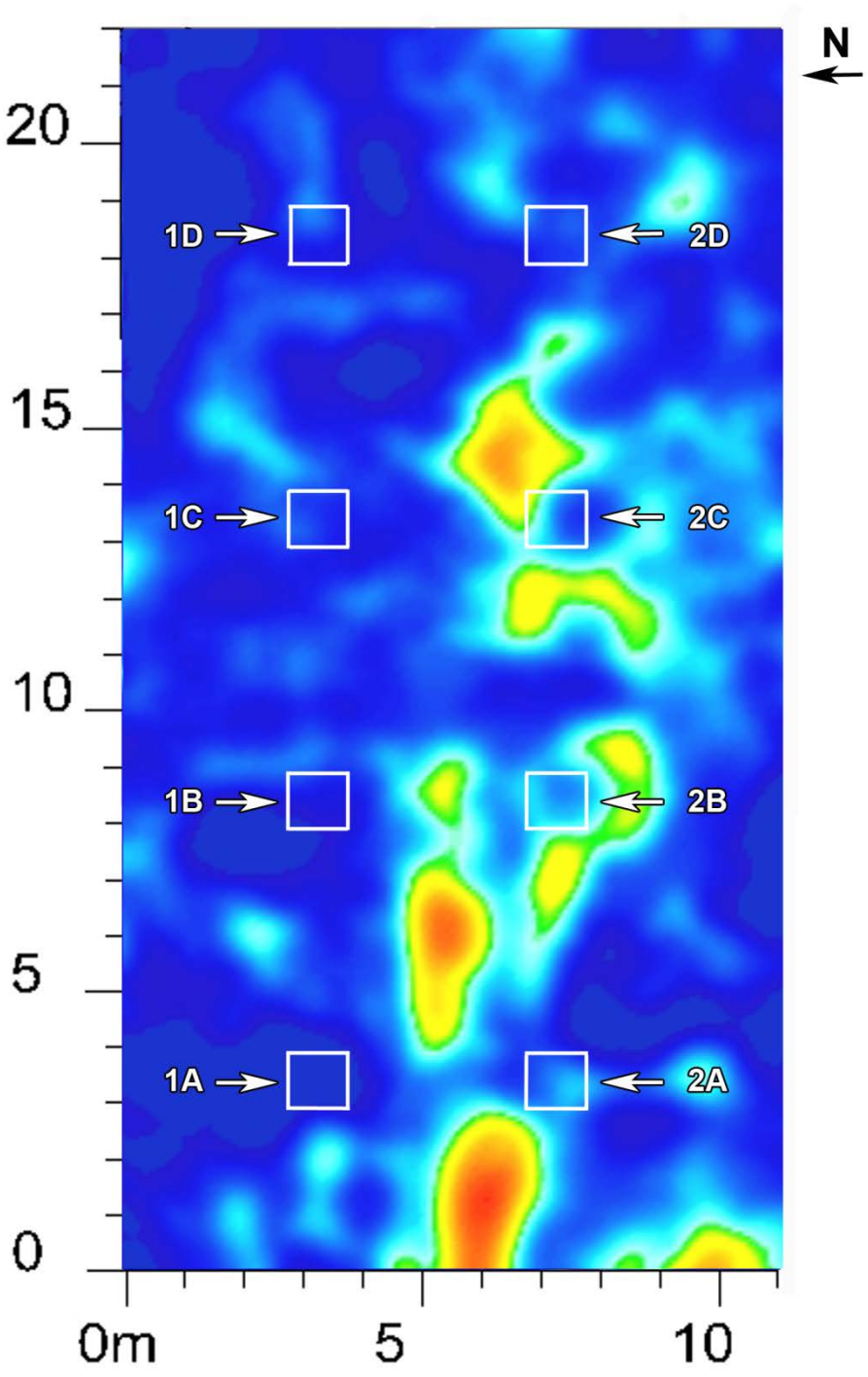

Figure E24: GPR horizontal slice using the 250-MHz antenna at 21 months. The horizontal slice is between 0.85 and 1.0 m in depth.

GPR 250 TIME SLICE AT MONTH 22

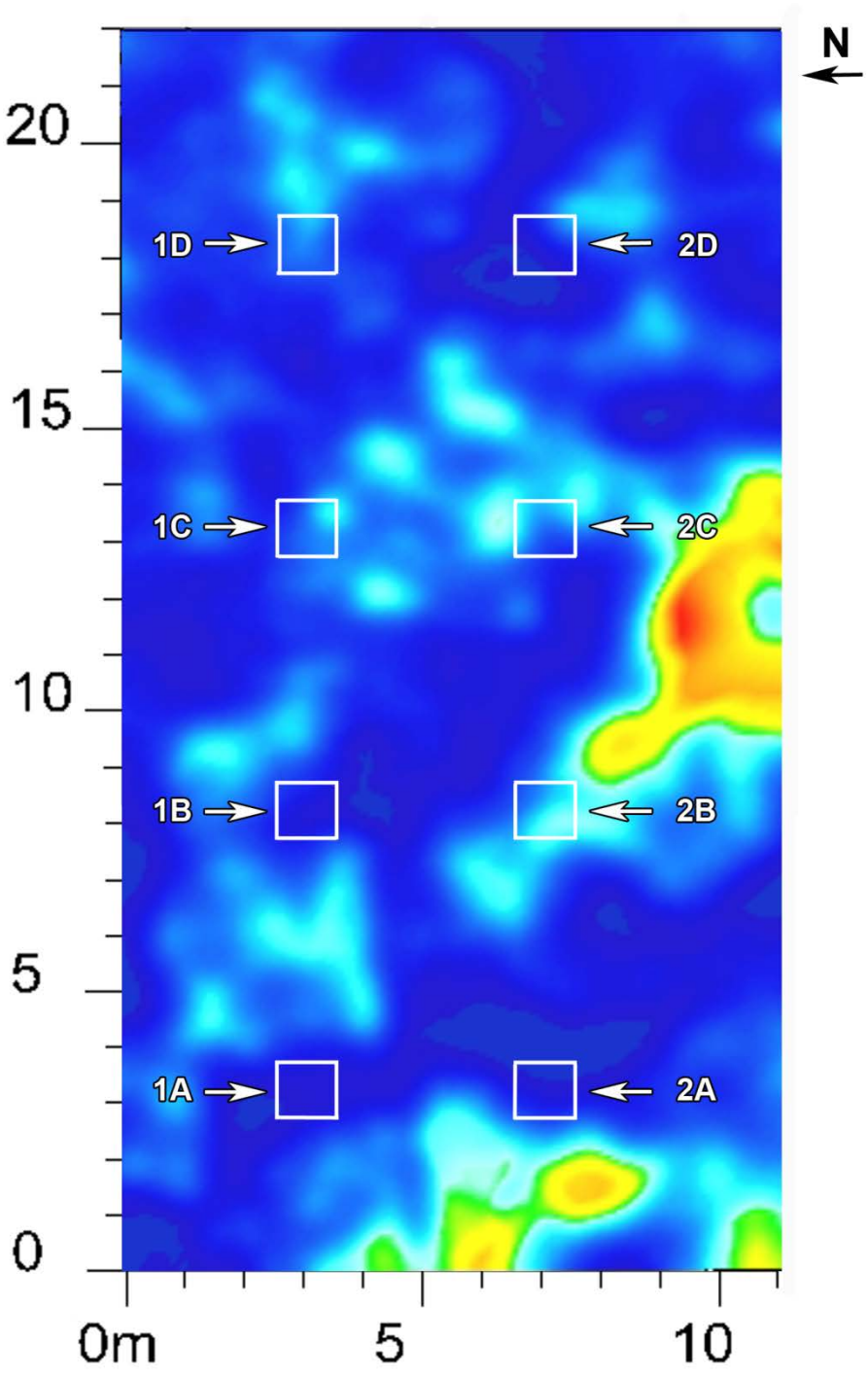

Figure E25: GPR horizontal slice using the 250-MHz antenna at 22 months. The horizontal slice is between 0.85 and 1.0 m in depth.

GPR 250 TIME SLICE AT MONTH 23

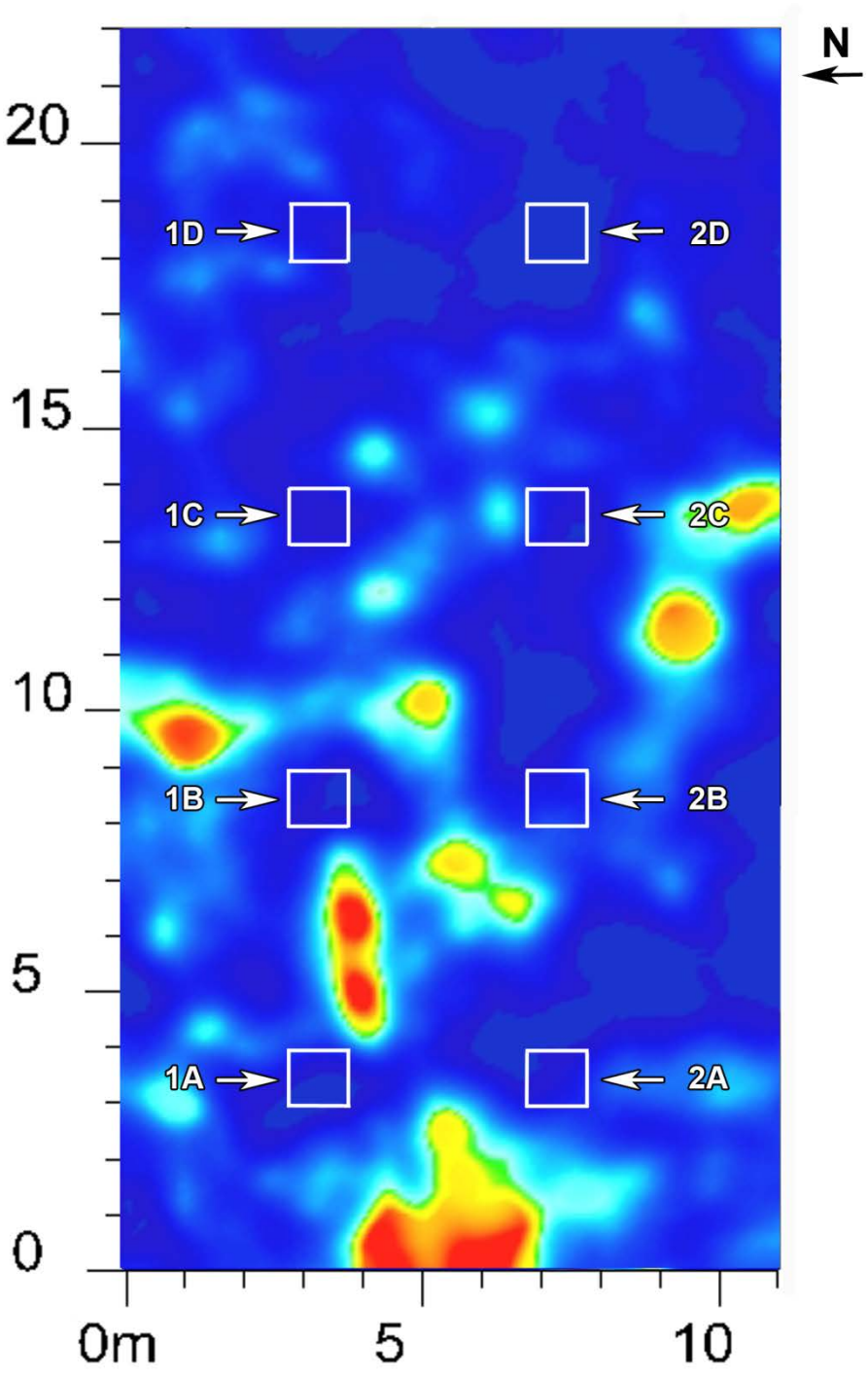

Figure E26: GPR horizontal slice using the 250-MHz antenna at 23 months. The horizontal slice is between 0.85 and 1.0 m in depth.

GPR 250 TIME SLICE AT MONTH 24

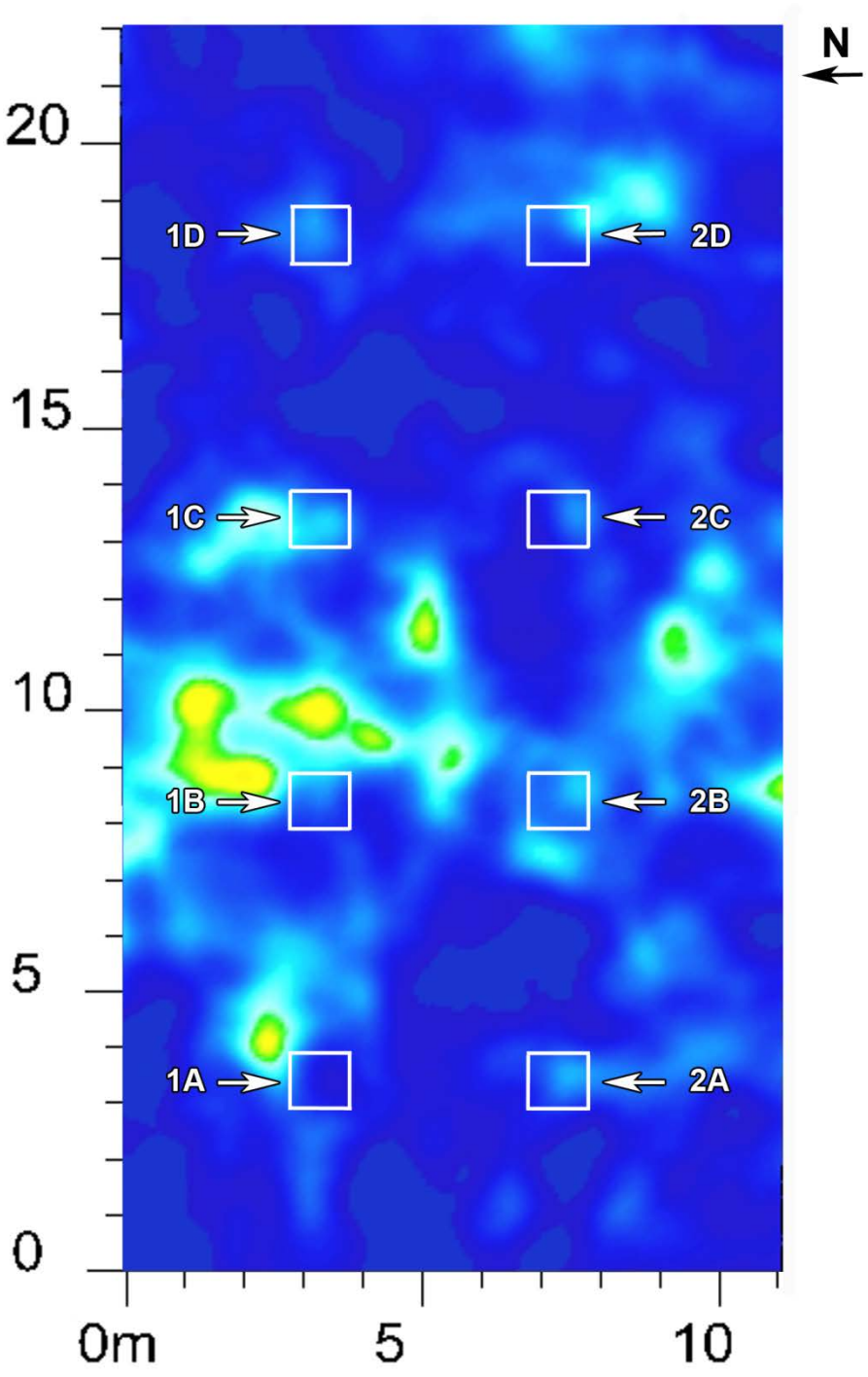

Figure E27: GPR horizontal slice using the 250-MHz antenna at 24 months. The horizontal slice is between 0.85 and 1.0 m in depth.

GPR 250 TIME SLICE AT MONTH 25

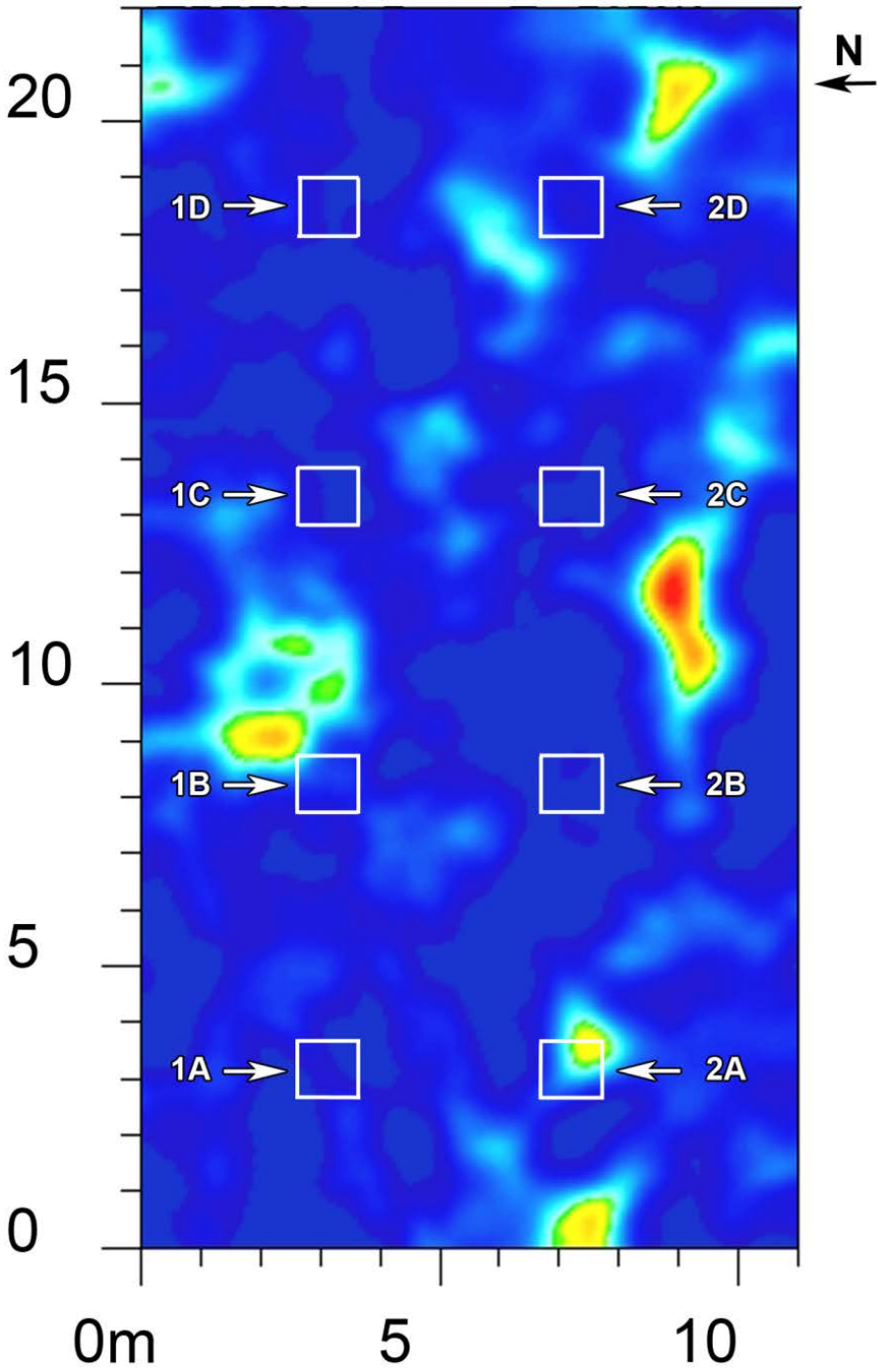

Figure E28: GPR horizontal slice using the 250-MHz antenna at 25 months. The horizontal slice is between 0.85 and 1.0 m in depth.

GPR 250 TIME SLICE AT MONTH 26

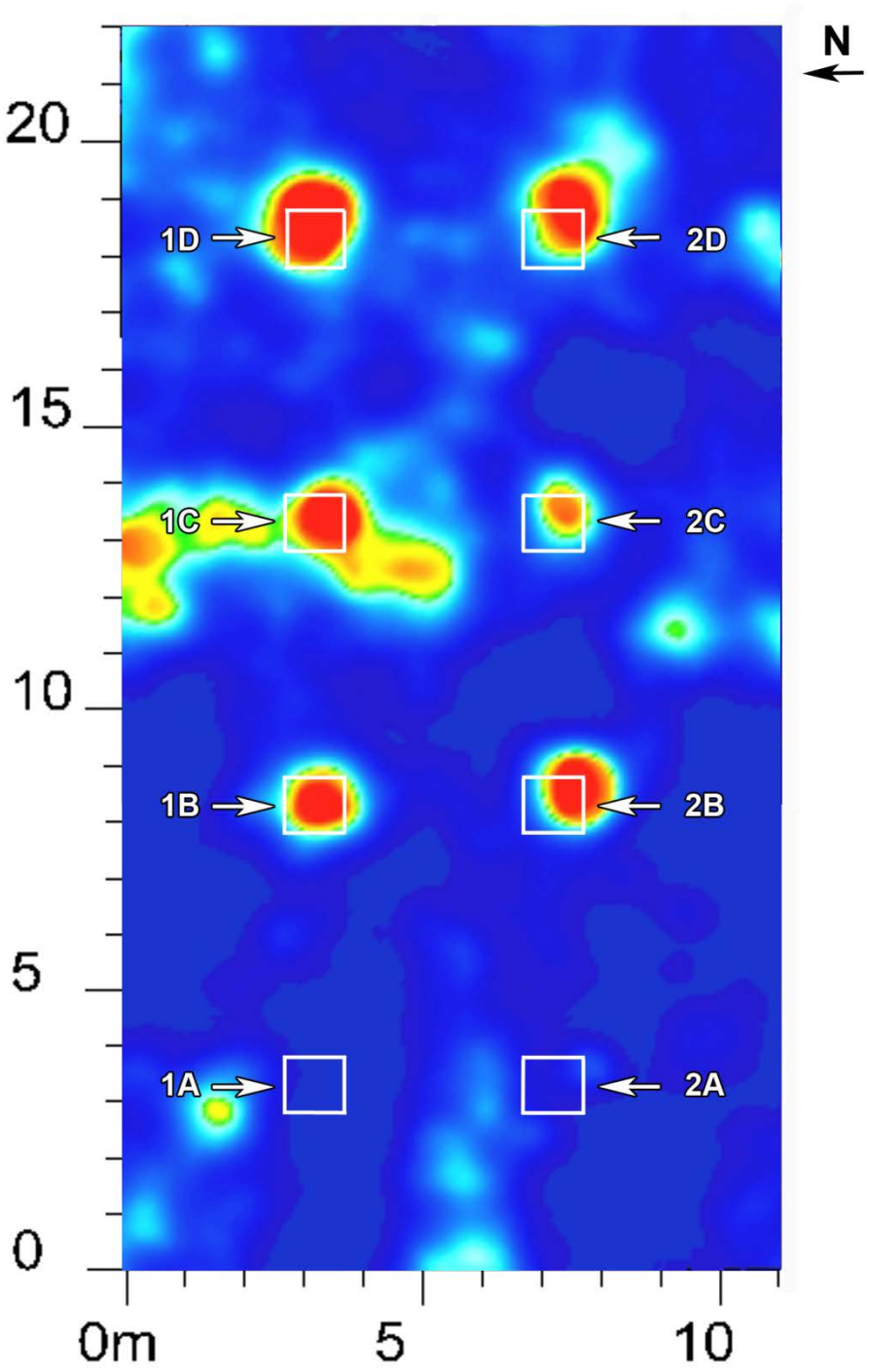

Figure E29: GPR horizontal slice using the 250-MHz antenna at 26 months. The horizontal slice is between 0.85 and 1.0 m in depth.

GPR 250 TIME SLICE AT MONTH 27

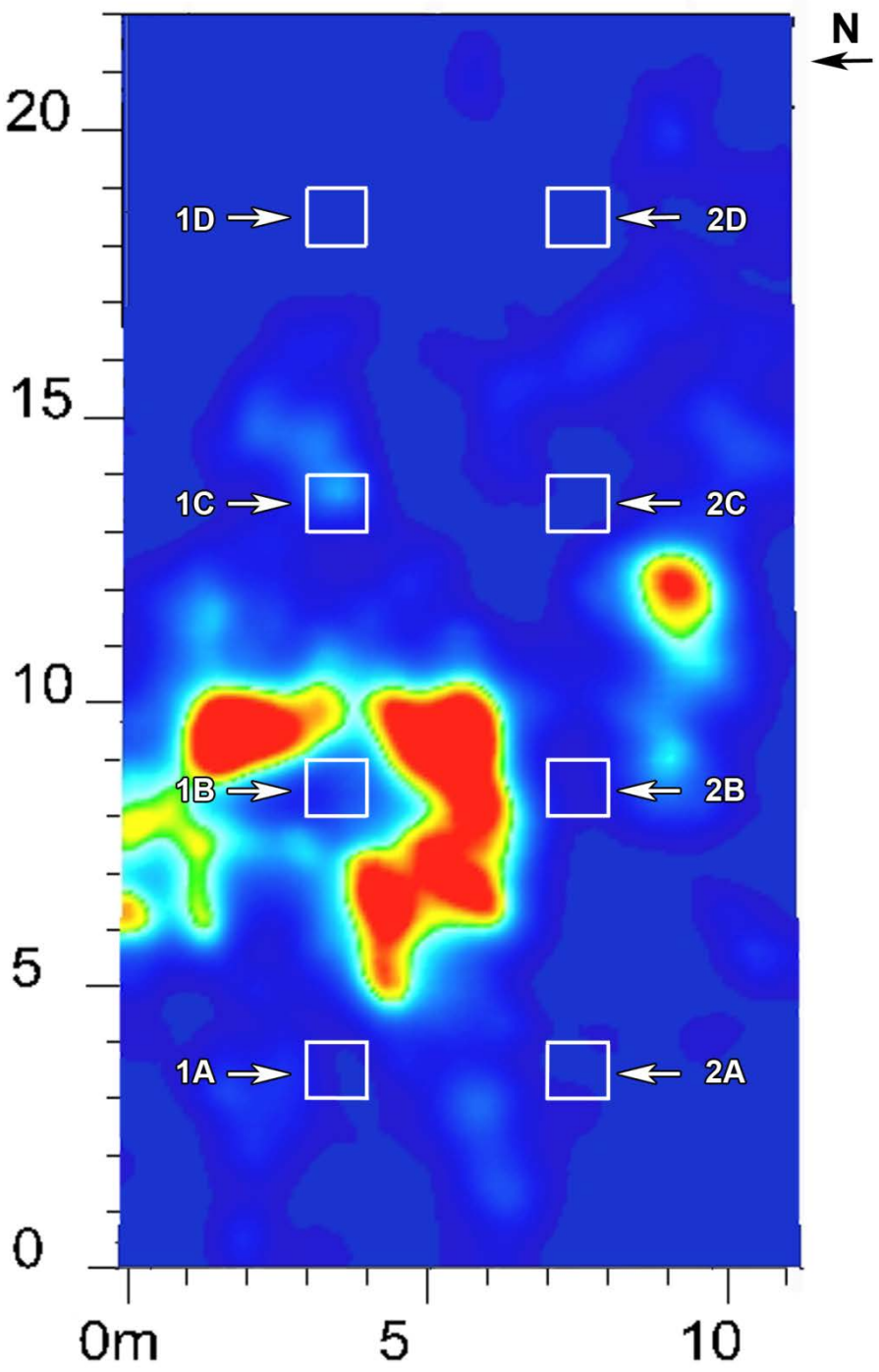

Figure E30: GPR horizontal slice using the 250-MHz antenna at 27 months. The horizontal slice is between 0.85 and 1.0 m in depth.

GPR 250 TIME SLICE AT MONTH 28

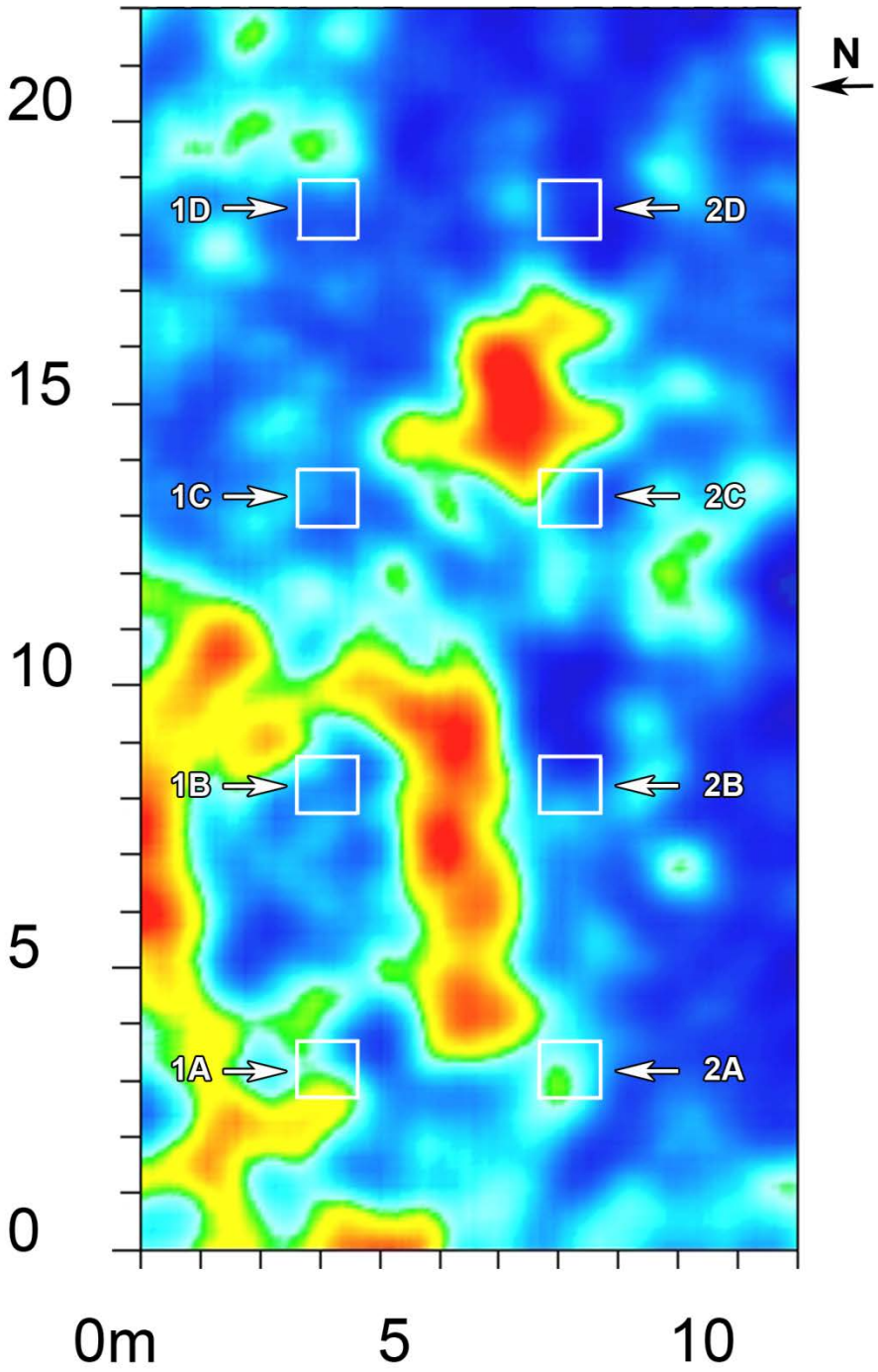

Figure E31: GPR horizontal slice using the 250-MHz antenna at 28 months. The horizontal slice is between 0.85 and 1.0 m in depth.

GPR 250 TIME SLICE AT MONTH 29

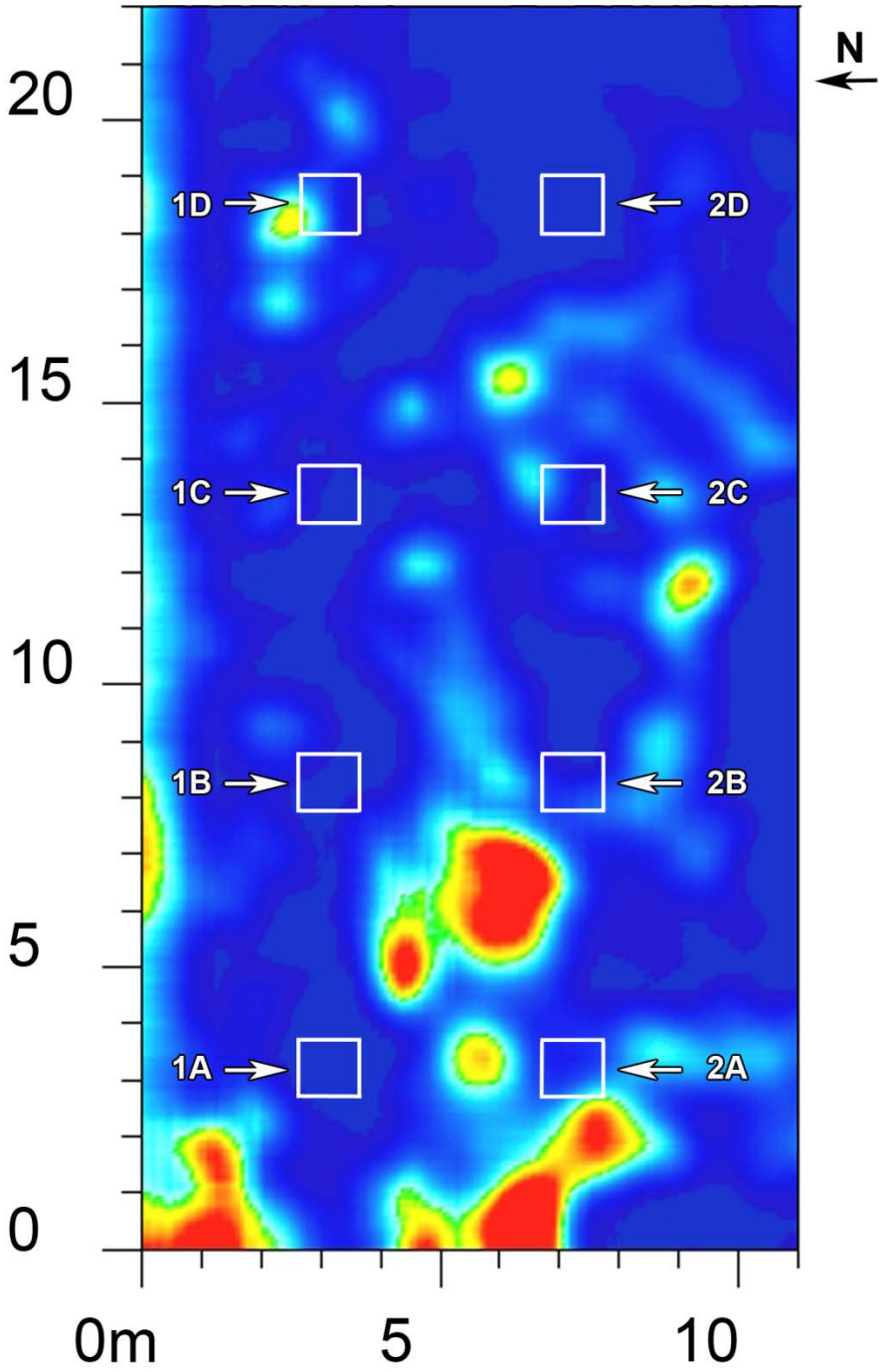

Figure E32: GPR horizontal slice using the 250-MHz antenna at 28.5 months. The horizontal slice is between 0.85 and 1.0 m in depth.

GPR 250 TIME SLICE AT MONTH 30

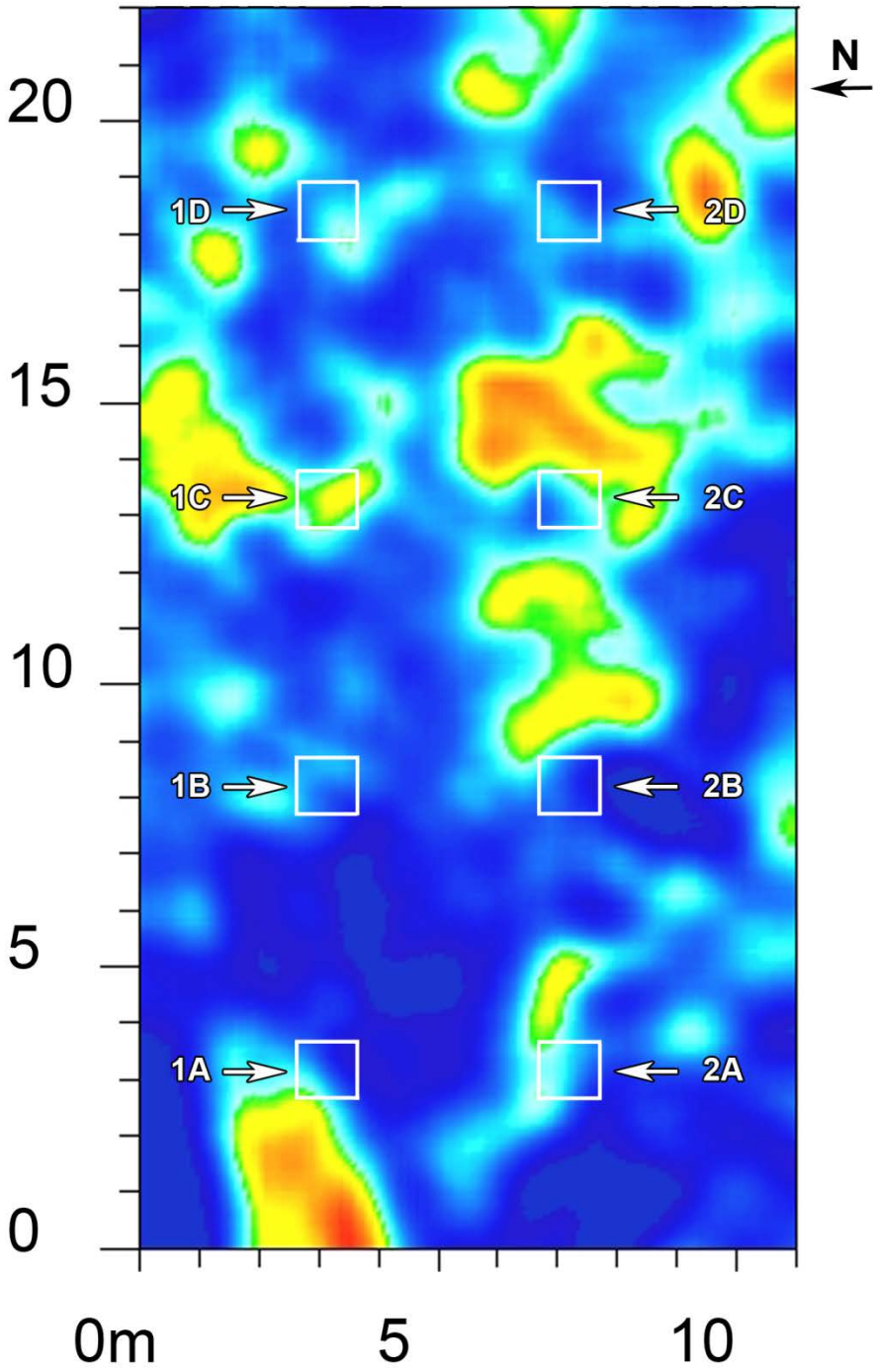

Figure E33: GPR horizontal slice using the 250-MHz antenna at 30 months. The horizontal slice is between 0.85 and 1.0 m in depth.